San Jose State University
**SJSU ScholarWorks**

Master's Theses | Master's Theses and Graduate Research

1999

# Design and analysis of typical micro pressure sensors for automotive application

Volker Schulze
*San Jose State University*

Follow this and additional works at: https://scholarworks.sjsu.edu/etd_theses

Recommended Citation
Schulze, Volker, "Design and analysis of typical micro pressure sensors for automotive application" (1999). *Master's Theses*. 1841.
DOI: https://doi.org/10.31979/etd.x42k-w4p4
https://scholarworks.sjsu.edu/etd_theses/1841

This Thesis is brought to you for free and open access by the Master's Theses and Graduate Research at SJSU ScholarWorks. It has been accepted for inclusion in Master's Theses by an authorized administrator of SJSU ScholarWorks. For more information, please contact scholarworks@sjsu.edu.

# INFORMATION TO USERS

This manuscript has been reproduced from the microfilm master. UMI films the text directly from the original or copy submitted. Thus, some thesis and dissertation copies are in typewriter face, while others may be from any type of computer printer.

**The quality of this reproduction is dependent upon the quality of the copy submitted.** Broken or indistinct print, colored or poor quality illustrations and photographs, print bleedthrough, substandard margins, and improper alignment can adversely affect reproduction.

In the unlikely event that the author did not send UMI a complete manuscript and there are missing pages, these will be noted. Also, if unauthorized copyright material had to be removed, a note will indicate the deletion.

Oversize materials (e.g., maps, drawings, charts) are reproduced by sectioning the original, beginning at the upper left-hand corner and continuing from left to right in equal sections with small overlaps. Each original is also photographed in one exposure and is included in reduced form at the back of the book.

Photographs included in the original manuscript have been reproduced xerographically in this copy. Higher quality 6" x 9" black and white photographic prints are available for any photographs or illustrations appearing in this copy for an additional charge. Contact UMI directly to order.

UMI

A Bell & Howell Information Company
300 North Zeeb Road, Ann Arbor MI 48106-1346 USA
313/761-4700 800/521-0600

# DESIGN AND ANALYSIS OF TYPICAL MICRO PRESSURE SENSORS FOR AUTOMOTIVE APPLICATION

A Thesis

Presented to

The Faculty of the Department of Mechanical and Aerospace Engineering

San Jose State University

In Partial Fulfillment

of the Requirements for the Degree

Master of Science

by

**Volker Schulze**

May 1999

UMI Number: 1394553

UMI Microform 1394553
Copyright 1999, by UMI Company. All rights reserved.

This microform edition is protected against unauthorized
copying under Title 17, United States Code.

UMI
300 North Zeeb Road
Ann Arbor, MI 48103

© 1998

Volker Schulze

ALL RIGHTS RESERVED

APPROVED FOR THE DEPARTMENT

OF MECHANICAL AND AEROSPACE

ENGINEERING

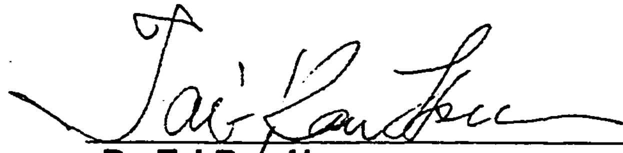

Dr. Tai-Ran Hsu

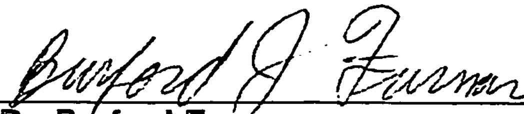

Dr. Burford Furman

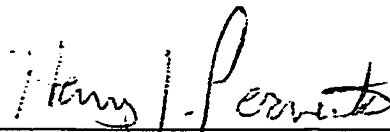

Dr. Henry Pernicka

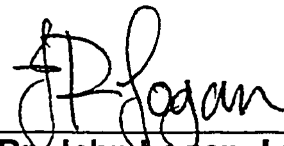

Dr. John Logan, Lucas NovaSensor

APPROVED FOR THE UNIVERSITY

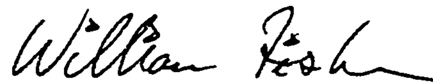

Dr. William Fisher

# Abstract

## DESIGN AND ANALYSIS OF TYPICAL MICRO PRESSURE SENSORS FOR AUTOMOTIVE APPLICATION

by Volker Schulze

This thesis addresses the topic of the design and analysis of silicon based micromachined pressure sensors. An overview over the main fabrication techniques, surface micromachining, bulk micromachining, and LIGA is given. The design considerations with respect to mechanical, electrical, chemical, and thermal influences are pointed out. Typical packaging options for automotive sensors are reviewed in detail.

A case study examines the influence of the packaging on the output of the sensor at different temperatures. A finite element calculation compares the results for an RTV, a solder, and an epoxy that are used as the bonding material with the output characteristic of a floating die. It demonstrated the feasibility of a direct die attach to an alumina substrate with the RTV without increases in the nonlinearity. The two other materials increase the nonlinearity and result in a mechanical failure due to the thermal coefficient of expansion mismatch.

# Acknowledgements

This thesis would have been impossible to complete without the substantial aid of specific people. I am especially grateful for the help and support of my advisory committee and the research and development team at Lucas NovaSensor, who created a friendly atmosphere, where I could work with pleasure. I wish to express my sincere appreciation for their help in supporting the development of my efforts.

I want to give special thanks to the following people:

Professor Dr. Tai Ran Hsu for giving continuous guidance, encouragement and support throughout the course of this study.

Dr. John Logan for providing advice on my research project as well as insightful proofing of my thesis for the sake of technical accuracy and clarity.

Mr. Gertjan van Sprakelaar for his advice and expertise in the modeling process and support in different phases of this project.

Dr. Bert van Drieenhuitzen for his support and patience when there were problems with the computer network.

Dr. Kirt Williams for organizing a second ANSYS license that saved me a lot of time.

# Contents


| | |
|---|---|
| List of Figures | viii |
| List of Tables | xi |
| 1. Introduction | 1 |
| 1.1 Evolution of Micro Pressure Sensors | 3 |
| 1.2 Applications | 8 |
| 1.3 Future Trends of Micro Sensors and Devices | 12 |
| 1.4 Current and Future Marketing | 14 |
| 2. Pressure Sensors | 18 |
| 2.1 Types | 18 |
| 2.2 Working Principles | 20 |
| 3. Overview of Micro Fabrication Processes | 28 |
| 3.1 Surface Micromachining | 28 |
| 3.2 Bulk Micromachining | 35 |
| 3.3 LIGA | 41 |
| 4. Design of Pressure Sensors | 47 |
| 4.1 General Considerations | 47 |
| 4.1.1 Physical and Environmental Constrains | 48 |
| 4.1.2 Operating Pressure | 53 |
| 4.1.3 Operating Temperatures | 56 |
| 4.1.4 Material Selection | 58 |
| 4.1.5 Strength | 63 |
| 4.2 Design Methodology | 65 |
| 4.2.1 Fabrication Processes | 66 |
| 4.2.2 Mechanics | 76 |
| 4.2.3 Electrical and Electronics | 81 |
| 4.2.4 Signal Generation and Condition | 87 |
| 4.2.5 Example Calculation | 94 |
| 4.3 Packaging | 100 |
| 4.3.1 Die Level Packaging | 102 |
| 4.3.2 Sensor Level Packaging | 105 |
| 4.3.2.1 Substrate | 106 |
| 4.3.2.2 Die Attach | 107 |
| 4.3.2.3 Wirebond | 109 |
| 4.3.2.4 Outer Package | 111 |
| 4.3.3 System Level Packaging | 117 |
| 4.4 Cost | 118 |
| 5. Packaging Design Case Study | 121 |
| 5.1 Objectives | 121 |
| 5.2 Configuration | 122 |

5.3 Material Selection and Properties 123
5.4 Mechanical Properties of the Die Attach Material 125
5.5 Geometry 136
5.6 Modeling Using Finite Element Method 137
5.7 Computational Results 142
5.8 Discussion of the Case Study 174
6. Recommendation for Future Research 181
References 183
Appendix 189
Appendix A - Technical Data Sheets A-1
Datasheet Ablebond 789-3 A-2
Datasheet Dow Corning 730 A-4
Appendix B - Material Test Results B-1
Tension Test Results 60Sn40Pb B-2
Tension Test Results Ablebond 789-3 B-3
Tension Test Results Dow Corning 730 B-4
Appendix C - Finite Element Analysis C-1
ANSYS Code: Control Modul C-2
ANSYS Code: Model (60Sn40Pb) C-4
Changes in the ANSYS Code for the Epoxy C-28
Changes in the ANSYS Code for the RTV C-29
Appendix D - Results D-1
Results of the Floating Die D-2
Results of the Epoxy D-4
Results of the RTV D-6

# List of Figures


| | | |
|---|---|---|
| Figure 1-1: | Metal Diaphragm Pressure Sensor with Bonded Strain Gages | 3 |
| Figure 1-2: | Silicon Diaphragm with Diffused Piezoresistors on Metal Constraint | 4 |
| Figure 1-3: | Isotropically etched Pressure Sensor | 4 |
| Figure 1-4: | Anisotropically etched Pressure Sensor | 5 |
| Figure 1-5: | Modem Pressure Sensors | 7 |
| Figure 1-6: | Automotive Applications of Microsensors | 8 |
| Figure 1-7: | Expected Unit Shipment | 14 |
| Figure 1-8: | World System Demand for Automotive Electronics | 15 |
| Figure 1-9: | Worldwide Unit Shipment and Revenues Forecasts | 15 |
| Figure 1-10: | MEMS Revenue Development | 16 |
| Figure 2-1: | Pressure Sensor Layout | 19 |
| Figure 2-2: | Absolute Pressure Sensor | 20 |
| Figure 2-3: | Plate with Coordinates | 21 |
| Figure 2-4: | Capacitive Pressure Sensor | 26 |
| Figure 2-5: | Vibrating Beam Pressure Sensor | 27 |
| Figure 3-1: | Thermal Evaporation | 29 |
| Figure 3-2: | Chemical Vapor Deposition | 31 |
| Figure 3-3: | Wet Etching | 36 |
| Figure 3-4: | Comer Compensation Schemes | 37 |
| Figure 3-5: | Electrochemical Etch Stop | 39 |
| Figure 3-6: | Deep Reactive Ion Etching | 39 |
| Figure 3-7: | DRIE-lag | 40 |
| Figure 3-8: | Notching | 40 |
| Figure 3-9: | LIGA-Process | 41 |
| Figure 3-10: | LIGA Process (Part2) | 42 |
| Figure 3-11: | Electroplating | 43 |
| Figure 3-12: | Integrated Micro Epicyclic Gear | 45 |
| Figure 3-13: | Optic Fiber Switch | 45 |
| Figure 4-1: | Bossed Diaphragms | 54 |
| Figure 4-2: | Typical Sensor Configuration | 56 |
| Figure 4-3: | Shear Strength over Temperature | 56 |
| Figure 4-4: | Young's Moduls over Temperature | 57 |
| Figure 4-5: | Effect of Mobile Ions | 58 |
| Figure 4-6: | Overview over the Fabrication Process | 65 |
| Figure 4-7: | Czochralski Techique | 66 |
| Figure 4-8: | Float Zone Process | 67 |
| Figure 4-9: | Electrical Layers in Die Surface | 71 |

| | | |
|---|---|---|
| Figure 4-10: | Contacts on Die Surface | 72 |
| Figure 4-11: | Silicon Fusion Bonding | 75 |
| Figure 4-12: | Piezoresistive Constans Depending on the Crystallographic Orientation | 82 |
| Figure 4-13: | Typical Resistor Placements | 84 |
| Figure 4-14: | Wheatstone Bridge | 88 |
| Figure 4-15: | Basic Compensation Circuit | 89 |
| Figure 4-16: | Piezoresistive Constants over Temperature | 95 |
| Figure 4-17: | Example Circuit for Temperature Compensation | 98 |
| Figure 4-18: | TO8 Header | 101 |
| Figure 4-19: | Stress Isolation with Spacing Element | 103 |
| Figure 4-20: | Plastic Substrate | 107 |
| Figure 4-21: | Wirebonds | 109 |
| Figure 4-22: | Wirebond | 110 |
| Figure 4-23: | Oil isolated Pressure Sensors | 113 |
| Figure 4 -24: | Oil isolated Pressure Sensor (Typical Cross Section) | 113 |
| Figure 4-25: | Stainless Steel Assembly | 114 |
| Figure 4-26: | TO8-Headers | 115 |
| Figure 4-27: | Plastic Packages | 116 |
| Figure 4-28: | Plastic Package System | 116 |
| Figure 4-29: | Integrated Package 1 | 117 |
| Figure 4-30: | Integrated Package 2 | 118 |
| Figure 5-1: | Sensor Configuration | 122 |
| Figure 5-2: | Engineering Stress-Strain Curve for 60Sn40Pb at -40°C | 126 |
| Figure 5-3: | Engineering Stress-Strain Curve for 60Sn40Pb at 25°C | 127 |
| Figure 5-4: | Engineering Stress-Strain Curve for 60Sn40Pb at 125°C | 128 |
| Figure 5-5: | Multilinear Fit at Different Temperatures for 60Sn40Pb | 129 |
| Figure 5-6: | Engineering Stress-Strain Curve for Ablebond 789-3 at -40°C | 130 |
| Figure 5-7: | Engineering Stress-Strain Curve Ablebond 789-3 at 25°C | 130 |
| Figure 5-8: | Engineering Stress-Strain Curve for Ablebond 789-3 at 115°C | 131 |
| Figure 5-9: | Multilinear Fit at Different Temperatures for Ablebond 789-3 | 132 |
| Figure 5-10: | Engineering Stress-Strain Curve for Dow Corning 730 at -40°C | 133 |
| Figure 5-11: | Engineering Stress-Strain Curve for Dow Corning 730 at 25°C | 134 |
| Figure 5-12: | Offset compensated Engineering Stress-Strain Curve for Dow Corning 730 | 135 |
| Figure 5-13: | Geometry of the Structure | 136 |
| Figure 5-14: | Finite Element Model | 138 |

| | | |
|---|---|---|
| Figure 5-15: | $\sigma_x$ for Pressurized Floating Die, T=25°C, p=35kPa | 142 |
| Figure 5-16: | Stresses in the Piezoresistive Region for the Floating Die | 143 |
| Figure 5-17: | Displacement in y-Direction of the Floating Die, T=25°C, p=35kPa | 144 |
| Figure 5-18: | Output of the Floating Die | 145 |
| Figure 5-19: | Maximum Membrane Displacement in y-Direction for 60Sn40Pb | 146 |
| Figure 5-20: | Displacement in y-Direction for 60Sn40Pb | 147 |
| Figure 5-21: | Displacement in x-Direction for 60Sn40Pb and Ablebond 789-3 | 148 |
| Figure 5-22: | $\sigma_x$ Stress for 60Sn40Pb | 149 |
| Figure 5-23: | Stresses in the Piezoresistive Region for 60Sn40Pb | 151 |
| Figure 5-24: | Output of the Die with 60Sn40Pb | 151 |
| Figure 5-25: | Von Mises Stress in the 60Sn40Pb Layer | 153 |
| Figure 5-26: | Von Mises Stress in the Die Attach for p=0, T= -40°C | 154 |
| Figure 5-27: | Influence of the Thickness of the Solder on the Output Characteristics | 155 |
| Figure 5-28: | Maximum Membrane Displacement in y-Direction for Ablebond 789-3 | 156 |
| Figure 5-29: | Displacement in y-Direction for Ablebond 789-3 | 157 |
| Figure 5-30: | $\sigma_x$ Stress for Ablebond 789-3 | 158 |
| Figure 5-31: | Stresses in the Piezoresistive Region for the Epoxy | 160 |
| Figure 5-32: | Output of the Die with the Epoxy | 161 |
| Figure 5-33: | Von Mises Stress in the Ablebond 789-3 Layer | 162 |
| Figure 5-34: | Influence of the Thickness of the Epoxy Layer on the Output Characteristics | 163 |
| Figure 5-35: | Membrane Displacement in y-Direction for Dow Coming 730 | 164 |
| Figure 5-36: | Displacement in y-Direction for Dow Coming 730 | 165 |
| Figure 5-37: | Displacement in x-Direction for Dow Coming 730, p=0 | 166 |
| Figure 5-38: | $\sigma_x$ Stress for Dow Coming 730 | 167 |
| Figure 5-39: | Stresses in the Piezoresistive Region for the RTV | 168 |
| Figure 5-40: | Output of the Die with the RTV | 169 |
| Figure 5-41: | Von Mises Stress in the Dow Coming 730 Layer | 170 |
| Figure 5-42: | Influence of the Thickness of the RTV Layer on the Output Characteristics | 171 |
| Figure 5-43: | Influence of the Die Attach on the Offset | 171 |
| Figure 5-44: | Influence of the Die Attach on the Full-Scale Output | 173 |
| Figure 5-45: | Influence of the Die Attach on the Span | 174 |
| Figure 5-46: | Deformation of the Die with the Solder at -40°C | 176 |
| Figure 5-47: | Deformation of the Die with the RTV at -40°C | 176 |

# List of Tables


| | | |
|---|---|---|
| Table 3-1: | Typical Etch Rates | 36 |
| Table 3-2: | Typical Selectivity Ratios | 37 |
| Table 4-1: | Piezoresistive Coefficients of Silicon at Room Temperature in (100) Orientation | 82 |
| Table 4-2: | Stresses in the Piezoresistive Region | 95 |
| Table 5-1: | Stiffness Modulii of Silicon | 124 |
| Table 5-2: | Material Properties | 125 |
| Table 5-3: | Mechanical Properties of the Solder | 128 |
| Table 5-4: | Yield Strength of 60Sn40Pb | 129 |
| Table 5-5: | Mechanical Properties of the Epoxy | 131 |
| Table 5-6: | Failure Stress of Ablebond 789-3 | 132 |
| Table A-1: | Tension Test Results 60Sn40Pb | |
| Table A-2: | Tension Test Results Ablebond 789-3 | |
| Table A-3: | Tension Test Results Dow Coming 730 | |
| Table A-4: | Stresses in the Floating Die | |
| Table A-5: | Uncompensated Output and Relative Nonlinearity of the Floating Die at Different Temperatures | |
| Table A-6: | Stresses in the Die with Solder | |
| Table A-7: | Uncompensated Output and Relative Nonlinearity of the Die with Solder at Different Temperatures | |
| Table A-8: | Stresses in the Die with Epoxy | |
| Table A-9: | Uncompensated Output and Relative Nonlinearity of the Die with Epoxy at Different Temperatures | |
| Table A-10: | Stresses in the Die with RTV | |
| Table A-11: | Uncompensated Output and Relative Nonlinearity of the Die with RTV at Different Temperatures | |

# 1 Introduction

Silicon has revolutionized modern electronics and enabled the development of high performance computers. It also allowed the introduction of microprocessors into many aspects of everyday life. Now silicon is on the way to revolutionize the possibilities of miniaturized mechanical systems. The nearly perfect mechanical properties were combined with manufacturing techniques that were derived from integrated circuit fabrication to produce micro-sensors and micro-actuators. In the course of this development, new manufacturing technologies such as LIGA were developed and existing techniques were modified to fit the special requirements of microstructures.

This development began about fifty years ago as a result of the development of semiconductors and the related research efforts to determine the properties of the materials. Whereas the development of integrated circuits was comparably fast, the diversity and the interdisciplinarity of micro-electro-mechanical systems (MEMS) progressed slowly. It took nearly thirty years to place the first products in larger numbers in the market.

The automotive market was, not surprisingly, the first large-scale application of micromachined sensors. Driven by legislation, it became necessary to monitor the combustion process to reduce the gas consumption and the pollution of the environment. The number of low-cost sensors needed for such an application pushed the existing sensor technology to the limits.

The emerging new technique of micromachining allowed the large-scale production of sensors in a comparably inexpensive way. After the successful introduction into the automotive market, the number of applications for micromachined systems increased. Pressure sensors were introduced into the medical and industrial market. New applications such as accelerometers, video chips, inkjet print heads, pressure valves, micro-motors, and turbines have been developed.

The design and development of MEMS is still a difficult process. Whereas the silicon itself was studied extensively, the packaging of MEMS remains a crucial part of the design process that accounts for the major part of the cost of a product. New problems are imposed with decreasing feature sizes by the scaling laws that change the behavior of miniaturized structures. The interdisciplinary character of these developments is also a major obstacle for the development of MEMS.

The automotive application exposes sensors and actuators to one of the most hostile environments. Temperatures are ranging from -40°C to 125°C and even higher for combustion measurements. Additionally, the system is subjected to aggressive media such as exhaust gases and fuel. A study of the matured design of micromachined pressure sensors for this application will give an insight into typical design considerations and manufacturing procedures.

## 1.1 Evolution of Micro Pressure Sensors

Although MEMS became important within the last two decades, the development of these devices was a long process that began about fifty years ago. This chapter reviews the development of MEMS using the example of pressure sensors.

The evolution of micro-electro-mechanical systems began with the invention of transistors in 1947. It initiated a fast development of microelectronic devices starting with this simple device and leading towards the first production of integrated circuits within the next ten years. During this period, the properties of Silicon and Germanium were investigated extensively. As a result of this effort, the piezoresistive effect in these materials was discovered by Smith in the Bell Laboratories in 1954. The first commercial application utilizing this effect was available four years later. Kulite, Honeywell, and Microsystems produced discrete silicon strain gages, which revolutionized the strain measurement. [1,2, 3]

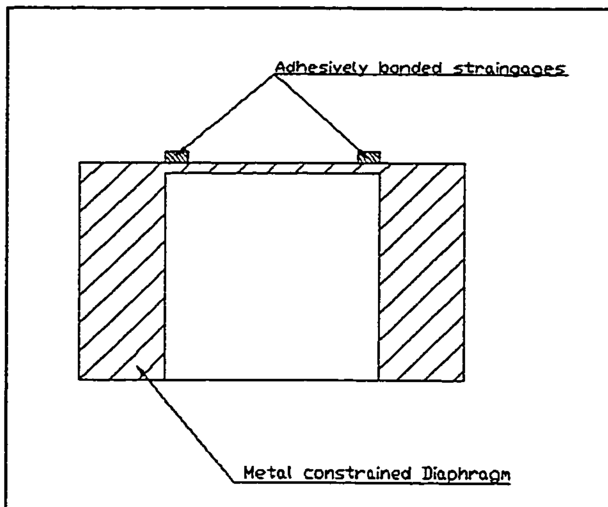


Figure 1-1: Metal Diaphragm Pressure Sensor with Bonded Strain Gages

One of the first practical applications of micromachining technology was to apply silicon strain gages in conventional pressure sensors (Figure (1-1)). The

conventional way to measure strain in a membrane was to use a strain gage adhesively bonded to a metal diaphragm. However, the bond introduced serious problems like high temperature errors due to thermal mismatch and poor stability that degraded the performance of the sensor. This problem was solved in 1961 when Kulite integrated the strain gages by diffusion into the silicon membrane (Figure (1-2)). The diaphragm was then bonded to a metal constraint. A sensor produced in this manner avoided the problems mentioned above, however the size and the cost of this product were still too high. [1, 2]

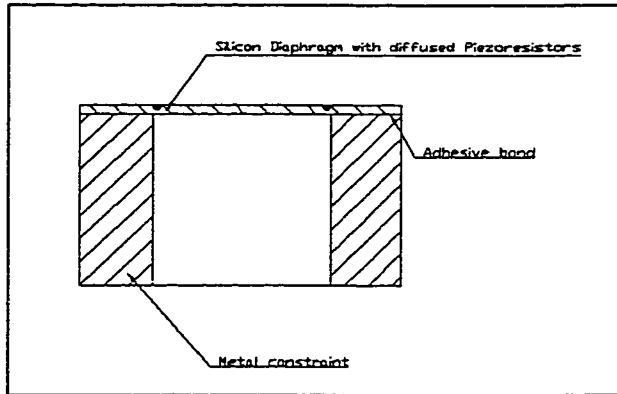


Figure 1-2: Silicon Diaphragm with Diffused Piezoresistors on a Metal Constraint

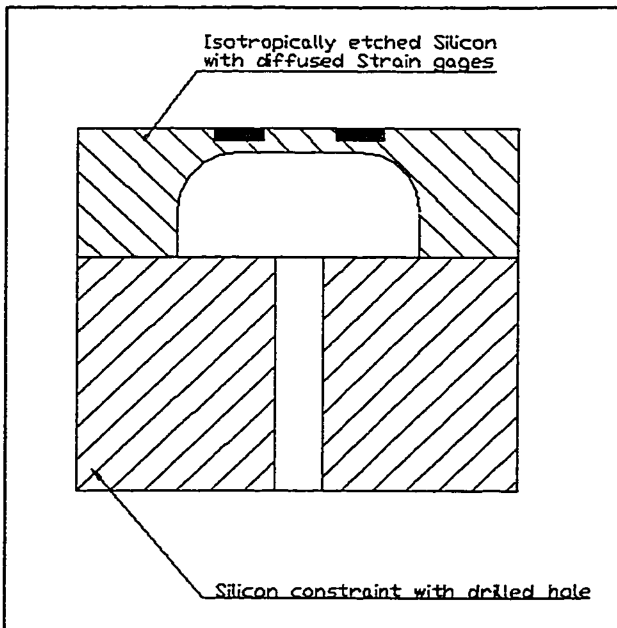


Figure 1-3: Isotropically etched Pressure Sensor

In 1966, Honeywell introduced mechanically milled cavities into the silicon to form the diaphragm. This was a great improvement because it enabled smaller die sizes. The disadvantage was that batch fabrication was impossible using this method. The milling and the bonding

were performed with single sensor dies. Consequently, the price of the transducers was still too high for most commercial applications. [1, 2]

Microfabrication technology at wafer scale became possible with the introduction of isotropic etching in 1970 by Kulite (Figure (1-3)). The process was similar to that used in IC processes. The disadvantage of this method was the rounded corners that made it difficult to place the piezoresistors at the location of the highest stress concentration. The etching process was time-controlled and allowed for better precision than the mechanical process. Anisotropic etching, the main technology of modern bulk micromachining was implemented in 1976 by the same company (Figure (1-4)). With this technique, it was possible to define sharp corners at the atomic level, which led to smaller sizes. Parallel to this, glass was introduced as the constraint of the diaphragm. The glass constraint was anodically bonded to the wafer (see Chapter (4.2.1)), a method developed in the previous decade. Both improvements enabled the fabrication of multiple sensors on one wafer simultaneously. The introduction of the electrochemical etch stop technique

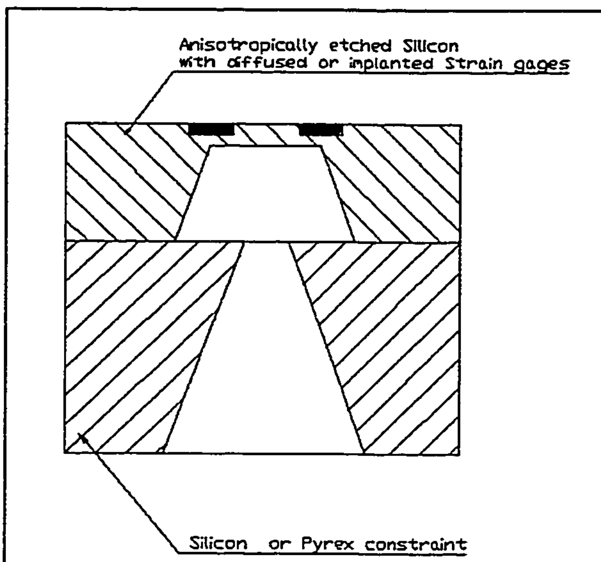


Figure 1-4: Anisotropically etched Pressure Sensor

allowed a better definition of the diaphragm thickness than the previous timing method that relied on the wafer quality. [1, 2, 4, 5]

The first monolithic integrated pressure sensor with a digital output was tested in 1971 at Case Western Reserve University (CWRU). This sensor was the first step toward the so-called smart sensors that can adjust themselves to the environmental constrains. [2]

The first automotive application of a micromachined pressure sensor was an adapted aerospace pressure sensor. General Motors Delco electronics division introduced this pressure sensor in the engine control in the Cadillac Seville in 1973. One year later, National Semiconductors Corporation produced the first high volume hybrid pressure sensor with a temperature controller. [1, 2, 6]

In 1977, researchers at Stanford University and later at the CWRU demonstrated the feasibility of capacitive pressure sensing. This type of sensor showed the ability for higher sensitivity and stability. [1, 2]

The subsequent development of pressure sensors involved the introduction of the bossed silicon diaphragm in 1978 by Endevco, the ion implanted strain gages by Honeywell and Kulite's passive on-chip temperature compensation. Both these devices were made in 1979. [1]

By this time, the silicon sensor became the de facto standard of pressure sensors. The application of this type of sensor had extended from aerospace to automotive and medical applications. Figure (1-5) shows various types of

Figure 1-5: Modern Pressure Sensors (Copyright of Lucas NovaSensor, with Permission)

modern pressure sensors. Companies like Delco, Ford, and Motorola built sensors for automotive environments whereas the first disposable medical transducers were introduced by Foxboro/ICT and Honeywell. Further developments improved the sensor performance such as active on-chip conditioning in 1982 by Honeywell and the introduction of SenStable process/design in 1990 by NovaSensor. With the help of the silicon fusion bonding technology, it was possible to reduce the die size further and therefore the price of the transducer itself. [1, 6-8]

A new manufacturing concept, surface micromachining, was developed at the beginning of 1980's at the University of California at Berkeley. The roots of this method went back to the early development in the Bell Laboratories. In 1984, Guckel et al showed the feasibility of pressure sensing based on this technology. This technology bears the possibility to further decrease the real estate of silicon needed to produce sensors. [2, 9]

The principle of using resonant structures for pressure sensing was also discussed at this time. NovaSensor demonstrated such a resonant beam pressure sensor in 1991. This sensing principle reduces the influence of the

electronics on the measurement because it is mainly effected by the mechanical characteristics of the structure. [10-12]

## 1.2 Applications

Modern cars and trucks have a variety of sensors and actuators that are vital for the normal operation as well as the safety of the passengers. Many of these devices are already micromachined or are potential applications for MEMS. This chapter focuses on the applications of pressure sensors in this sector.

Pressure sensors are the most common micromachined sensors for automotive applications. They are used in three main areas as shown below:

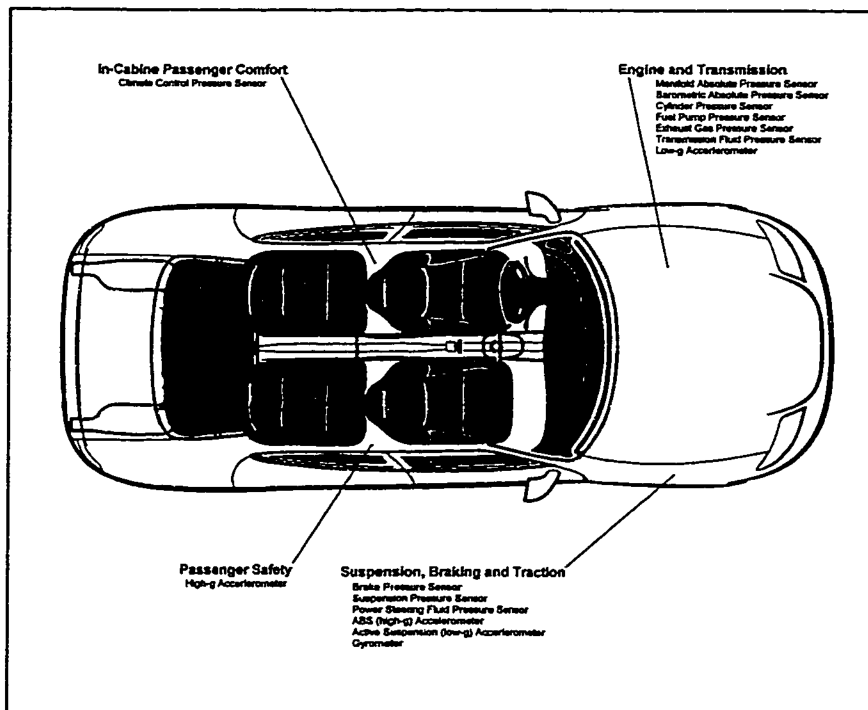


Figure 1-6: Automotive Applications of Microsensors

Group 1: Engine and transmission management

Group 2: Suspension, braking and traction control

Group 3: In-cabin passenger comfort

The first group of applications includes sensors used in every modern car. This development is driven by legislation with laws to minimize the emission of cars. The manifold absolute pressure sensor (MAP) with a pressure range of 100 to 500 kPa monitors the air intake to optimize the fuel to air ratio. This reduces the fuel consumption of the engine and therefore also the emission. This sensor might be replaced by a mass flow sensor in the future to further improve engine performance. With this trend, the number of MAP's will decrease. This does not mean that the importance of pressure sensors in this part of engine management is decreasing, because the mass flow sensors use one barometric pressure sensor within the system. This type of sensor is used presently to adjust the engine cycle in response to varying ambient pressures. [1, 6,13-20]

The most challenging application of pressure transducers is the monitoring of the cylinder pressure. The harsh environment of highly pressurized oxidizing gases made this sensing impossible in the past. With this information, a number of problems can be solved: Misfires can be detected and corrected to improve the engine performance. The information of the fuel to air ratio in conjunction with an oxygen sensor in the exhaust system enables better control

of the burning of fuel, and thus limits the exhaust emission during the warm up of the catalytic converter. [6, 13-15, 21-23]

Other typical applications in this field are fuel pump pressure sensors. These sensors are subject to up to 100 MPa dynamic pressure in Diesel injection pumps. There are also sensors employed to monitor the exhaust gas recirculation, turbo boost pressure, and the engine oil pressure. [1, 6, 14, 17]

With the introduction of continuous variable transmission, the necessity of a measurement of the fluid pressure arose. This is also an application for micromachined transducers. [1, 6, 14]

The second group includes sensors in the braking system of the automobile. These sensors are crucial for passenger safety and are consequently intended to meet the highest safety standards. Typical applications include the measurement of brake pressure in the master and wheel cylinders. The pressure range is from 1 MPa for electro-pneumatic brakes to 20 MPa for hydraulic brakes. This system plays a vital role in anti-brake lock and automatic slide control in conjunction with acceleration and angular rate sensors to stabilize a car in critical situations. [1, 6, 14, 24]

Power steering, a common function in modern cars, is also influenced by MEMS sensors. The pressure of the fluid for the steering system has to be monitored to insure safety of the system. [14]

The active suspension systems of modern luxury cars are in the third group of application of sensors. The hydraulic pressure can reach peak values of

± 20 MPa in the shock absorbers. This value is much smaller for pneumatic suspensions (1.6 MPa) due to the compressibility of the medium. These cars also feature automatic tire pressure monitoring carried out by microsensors. [6, 14]

In the area of passenger comfort, the pressure of the climate control system is controlled using two sensors. These sensors are exposed to the refrigerant at relatively low pressures (50-105 kPa). The seat support pressure system is also an application of silicon micromachined sensors. [1, 6, 14]

Beside pressure sensors, there are many other applications of microsensors in a modern car. The low price of micromachined accelerometers enabled the wide application of the airbag systems, seatbelt tighteners, the anti-lock brake, and the active suspension system. Level sensors with different working principles monitor gas, oil, and other fluids. The emission standards can only be met with the use of chemical sensors, like the lambda probe. [1, 6-8, 13-15, 21, 25-28]

Micromachined sensors are vital for the operation of a modern car. The number of applications is increasing steadily due to increasing demands from legislation to reduce the emission. Cheaper sensors enable the implementation of new safety and comfort features even in cars in the lower price section. [1,6, 15, 29]

## 1.3 Future Trends of Micro Sensors and Devices

The development of MEMS shows that the diversity of principles and applications introduces major development obstacles. Although much research has been done in the last decade, the design process of micro-electro-mechanical systems is far from the standards of conventional design processes. This section analyzes the recent trends and developments in the field of microdevices.

The future development of pressure sensors is characterized by the need for further miniaturization of the devices and with the demand for decreasing costs. This need can only be met when major improvements in the understanding of the device behavior are made. The lack of knowledge and experience in design, fabrication, and packaging in this field are the main obstacles to develop next generations of MEMS. Therefore, it is necessary to improve the database about the used materials and processes. Parallel to this development, it is important to introduce simulation programs to shorten the design cycle from the consumer demands to the available product in order to be successful in the market. As in other fields of engineering, CAD and the finite element method will play a key role in the simulators. It can provide the user with valuable data about the mechanical behavior as well as the piezoelectric and thermal behavior. Due to the complexity of the systems, this has to be combined with solid state device simulators that are common in the IC industry for the prediction of the electrical properties of the system as well as other simulators for

the fields of interest. The challenge is the multidisciplinarity of the systems. It is therefore necessary to create interdisciplinary design tools and teams. [5, 6, 30-35]

With the introduction of cheaper and smaller sensors, systems can be designed redundant and as arrays in order to minimize the influence of the failure of a single sensor. The integration of sensors with electronics enables better accuracy and stability and enables faster measurements. This function should include on chip offset balancing, temperature compensation, signal normalizing, and amplification. The means of signal and energy transfer have to be improved to simplify the operation of sensor arrays and remote sensor locations. Smart sensors will incorporate all these functions. They will also provide failure detection. [1, 6, 16, 20, 30, 31, 36]

Besides the electronic integration, the mechanical behavior of future sensors has to be improved. Features like overrange protection that are already feasible will become common. The packaging technology is of major importance to achieve cheaper devices and broader application in different environmental conditions. The first goal can be achieved with a transition towards IC like packages for large-scale production. The second problem is a typical transducer problem, because the sensor has to be in contact with the medium but also be protected from it. The current packaging technology is too expensive, introduces error sources, and has to be substantially improved. [1, 30, 31, 36-38]

The introduction of new sensing principles for pressure will also have an impact on the products. The resonant beam technology has been successfully demonstrated and showed major improvements in stability and accuracy. It has not entered large-scale application because the current manufacturing costs are too high to be competitive in the market. This may change with improvements in the manufacturing processes. Fiberoptic pressure sensors will become of interest with the introduction of optical wiring in cars. The newest technique is the use of the Hall effect connected with a normal diaphragm, which is in a prototype stage. [6, 14, 39, 15]

## 1.4 Current and Future Marketing

Although it took nearly thirty years to bring MEMS into the commercial market, the advantages of batch fabrication resulted in an explosion of applications. The market forecasts for the future are bright and promise further growth (Figure (1-7)). This section shows the market growth in the last years and the prognosis for the near future.

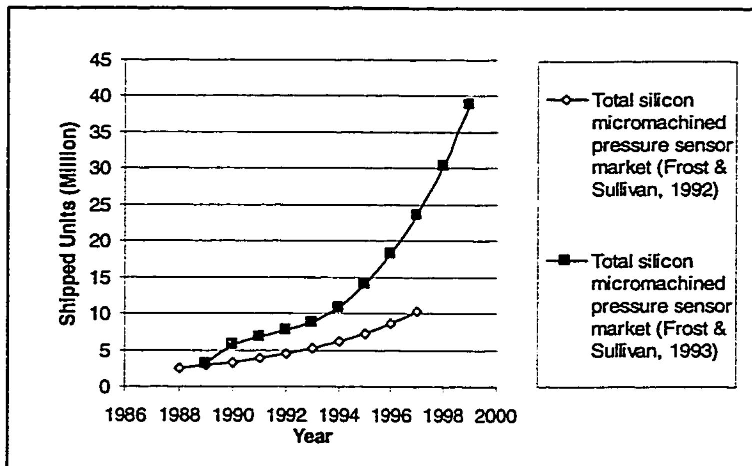


Figure 1-7: Expected Unit Shipment

The current markets for micromachined devices are dominated by three sensors that are applied in the automotive field. These sensors are pressure sensors, accelerometers, and flow sensors. In the past, micromachined pressure sensors produced virtually all the revenues for silicon based MEMS. This is about to change, and the other two sensor types have already established a strong market share. According to Frost & Sullivan, the market share of pressure sensors will drop from 80% in 1990 to about 72% in 1999. This development will be supported by the introduction of cheaper Air-Bag systems that rely on accelerometers and the change from MAP sensors to flow sensors in engine management. [39]

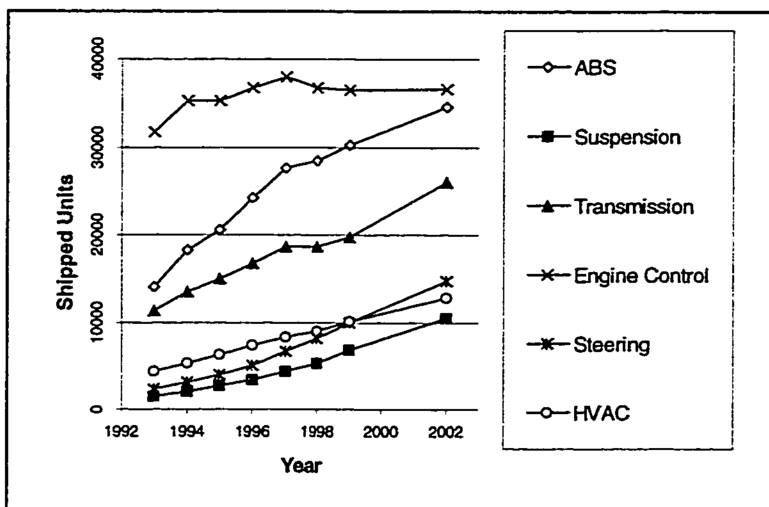


Figure 1-8: World System Demand for Automotive Electronics (BIS Strategic Decisions 1995)

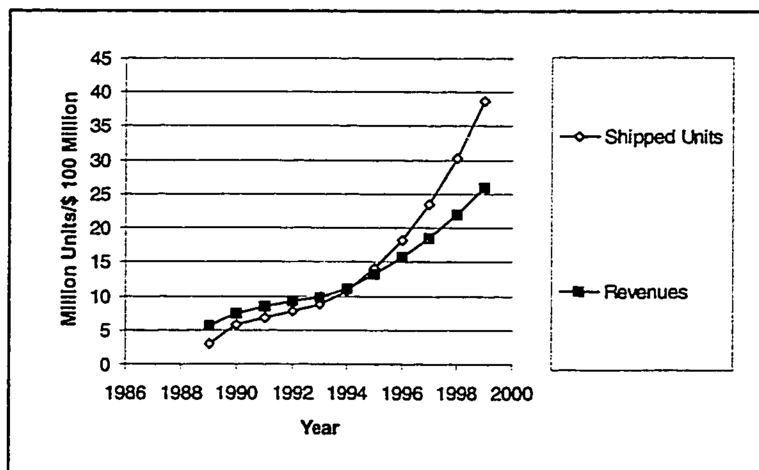


Figure 1-9: Worldwide Unit Shipment and Revenues Forecasts (Frost & Sullivan, 1993)

A market study of

electronic systems in the automotive field shows the fast growth of these applications. Figure (1-8) shows the increase of shipped units in electronical applications in which pressure sensors are commonly used. The engine control market is virtually saturated and the growth is limited by the relatively slow

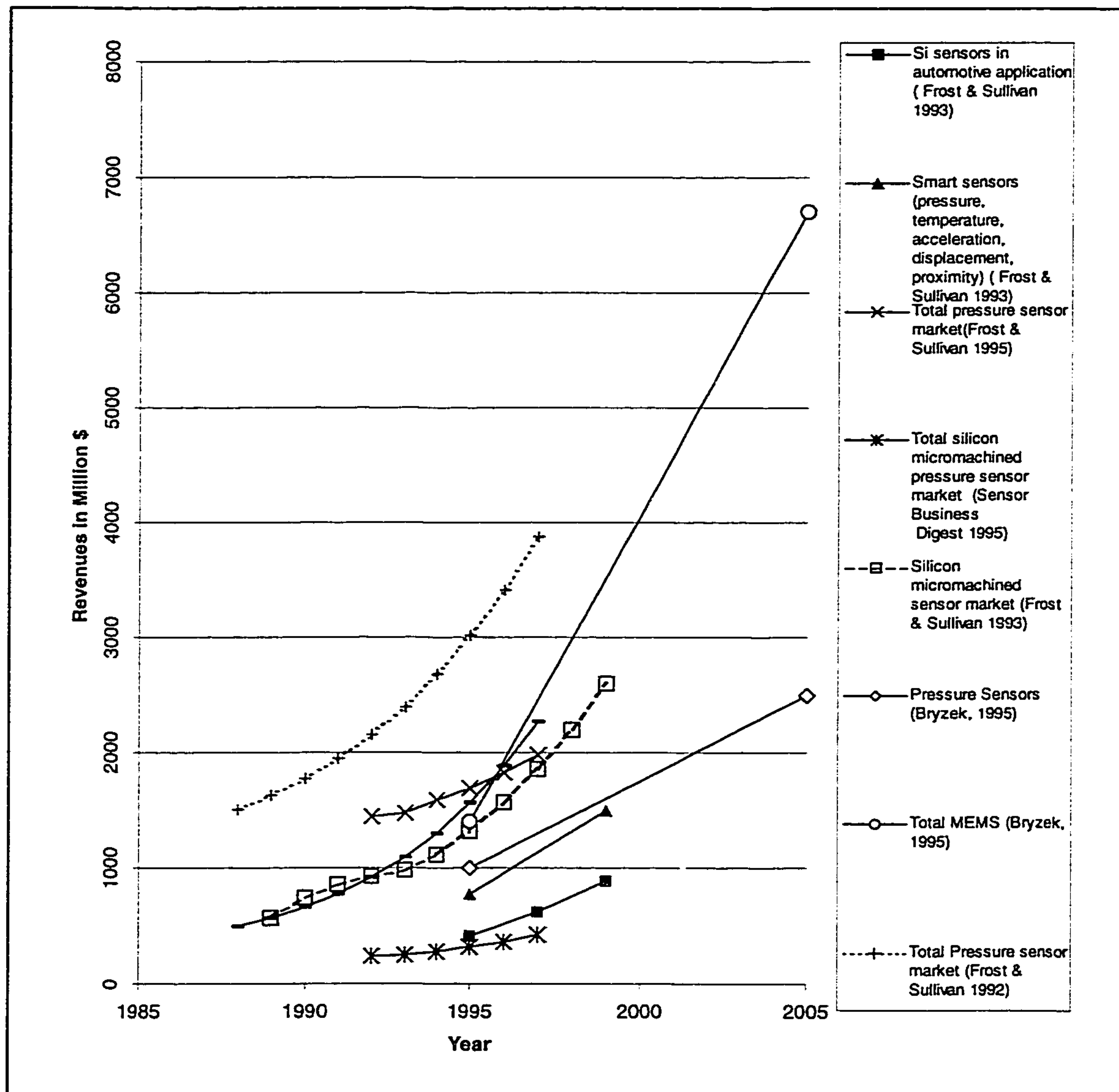


Figure 1-10: MEMS Revenue Development

growth of the automotive market. The real potential of MEMS can be seen in the newer applications that are not already standard features in a modern car. This increase is mainly supported by the low price potential of MEMS. This effect can be seen in Figure (1-9). The number of shipped units is increasing much faster than the revenues. The reason for this development is the so-called semiconductor learning curve that is heavily used by customers. According to this, the price per unit is dropping with time and output. [6, 39 - 45]

Although the number of the different market forecasts are varying, the general trend for automotive pressure sensors is clear. Figure (1-10) shows this tendency. The average growth rate of MEMS in this field is above 10% per year. Although certain markets are already saturated, the growth of the new emerging applications is pushing the development. Even with the currently developed sensors, this growth rate is expected to continue for the next years.

# 2 Pressure Sensors

Pressure sensors are the most important applications of silicon micromachined sensors. They are applied in various fields such as automotive, industrial, aerospace, medical, and consumer applications. The most important market within this field is the automotive industry. Although the range of applications is wide, there are only three basic types of sensors. Only a few sensing principles are used to measure the pressure. This chapter will first review the different types of sensors. In the second part, the different principles are studied.

## 2.1 Types

There are three different types of pressure sensors available:

- Relative pressure sensors
- Gage or vacuum pressure sensors
- Absolute pressure sensors

All of these sensors use the effect that different pressures on the two sides of a diaphragm cause a deformation proportional to the difference of the two pressures. This section shows that the distinction between the types is the used reference for the measurement.

In a relative pressure sensor, two measurement pressures are applied on both sides of the diaphragm, as shown in Figure (2-1). Since both pressures can be significantly higher than the ambient pressure, the measurement is not only

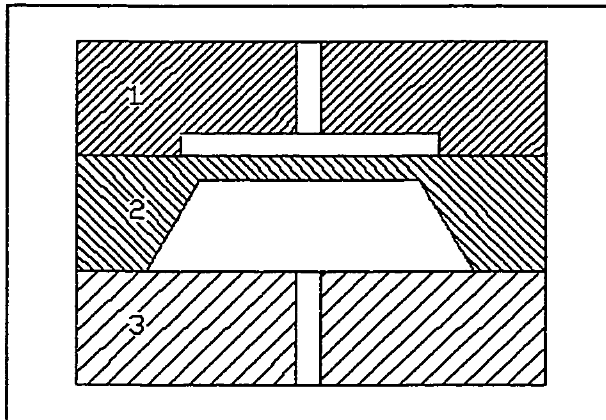


Figure 2-1: Pressure Sensor Layout
1,3 Package
2 Sensing Die

influenced by the difference of these pressures but also by the static pressure $(p_1+p_2)/2$. This unwanted effect is called static pressure sensivity. [1, 6]

The sensor in Figure (2-1) can also be used as a gage pressure sensor. The difference between this type and the previous is that the reference pressure is the atmospheric pressure. [1, 6]

A variant of this type is the vacuum sensor. In this sensor, the output terminals are reversed in a way that an increasing vacuum causes an increasing signal. [1]

The absolute pressure sensor has an evacuated cavity on one side of the diaphragm. Since this vacuum is used as the reference pressure for the measurement, the output is only depending on the absolute value of the applied pressure. The problem of this type of transducer is to maintain the vacuum for longer periods to assure an accurate measurement. A typical application of this sensor are measurements of barometric pressures. Figure (2-2) shows examples of such a sensor. [1, 6]

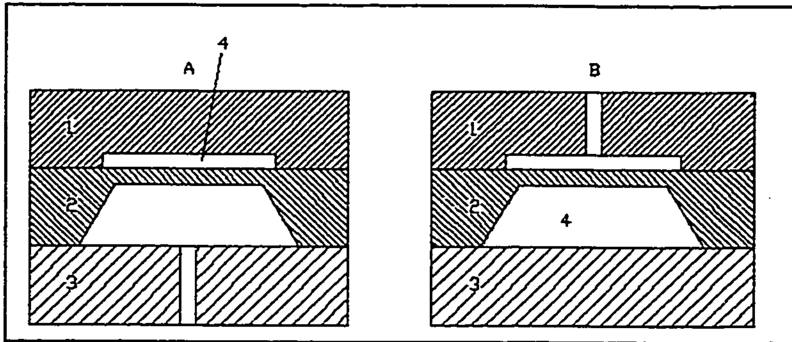


Figure 2-2: Absolute Pressure Sensor
A Backside pressurized
B Frontside pressurized
1,3 Packaging Material
2 Sensing Die
4 Reference Vacuum

There are two different ways to apply the pressure to the membrane. The Figure (2-2) illustrates these possibilities. Both ways have certain advantages and disadvantages. If the backside of the diaphragm is pressurized, the circuit side of the sensor is not influenced by the media. However, the die and the die attach are subject to tensile stress. If the pressure is applied from the outside, the structure is subject to compression if the applied pressure is higher than the reference pressure. [1, 6]

## 2.2 Working principles

Although the number of applications for pressure sensors is high, the principles that are used to convert the pressure into an electrical signal are limited. The most common principles are illustrated in this part.

The basic principle of every sensor is to convert a value of a system variable into a measurable signal. Common pressure transducers change the applied mechanical pressure into an electrical output signal. This is achieved by

applying the pressure to a thin membrane that is clamped at all edges. The resulting deformation can be described using the differential equation for plates:

$$\frac{Eh^3}{12(1-\upsilon^2)}\Delta\Delta w(x,y) = p - (1+\upsilon)\frac{\alpha}{h}\Delta T \qquad (2\text{-}1)$$

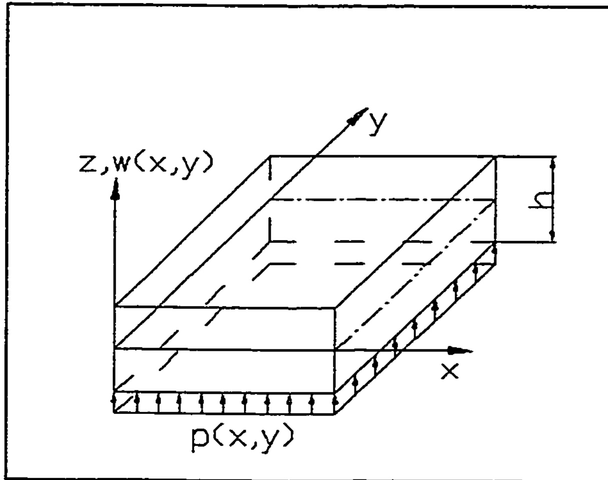


Figure 2-3: Plate with Coordinates

where w is the displacement of the plate as a function of the spatial coordinates x and y (see Figure (2-3)), h is the plate thickness, E is Young's Modulus, v is Poison's Ratio, p is the applied pressure, $\alpha$ is the coefficient of thermal expansion, and $\Delta T$ is temperature difference.

For assumed planar stresses, the strain can be calculated

$$\varepsilon_x = -zw_{,xx} \qquad (2\text{-}2)$$

$$\varepsilon_y = -zw_{,yy} \qquad (2\text{-}3)$$

$$\gamma_{xy} = \gamma_{yx} = -2zw_{,xy} \qquad (2\text{-}4)$$

where z is the coordinate that is normal to the plate surface with its origin at the center of the plate, $\varepsilon_x$, $\varepsilon_y$, and $\gamma_{xy}$ are strains, and $w_{,xy}$ are the partial derivatives with respect to the indices designating the coordinates. [46]

This differential equation can be solved by pseudo analytical and numerical methods. The pseudo analytical methods use infinite Fourier series:

$$w(x,y)=\sum_{m=1}^{\infty}\sum_{n=1}^{\infty} f_{mn}\sin(\alpha_m x)\sin(\beta_n y) \tag{2-5}$$

$$\alpha_m = \frac{m\pi}{L_x} \tag{2-6}$$

$$\beta_n = \frac{n\pi}{L_y} \tag{2-7}$$

The deflection can be determined:

$$w(x,y)=\frac{1}{K}\sum_{m=1}^{\infty}\sum_{n=1}^{\infty}\frac{p_{mn}}{\left(\alpha_m^2+\beta_n^2\right)^2}\sin(\alpha_m x)\sin(\beta_n y) \tag{2-8}$$

$$p_{mn}=\frac{4}{L_x L_y}\int_{x=0}^{L_x}\int_{y=0}^{L_y} p(x,y)\sin(\alpha_x x)\sin(\beta_n y)\,dy\,dx \tag{2-9}$$

$$K=\frac{Eh^3}{12\left(1-v^2\right)} \tag{2-10}$$

where w is the deflection, p is the applied pressure depending on the spatial coordinates, h is the thickness of the plate, E is Young's Modulus, and v is Poisson's Ratio. However, the pseudo-analytic method is very difficult and is only applicable for relative simple geometries. A more practical approach is the finite element method. This standard tool of engineering analysis enables a relatively simple calculation of the deflection even for complicated geometries such as bossed diaphragms.

Having converted the applied pressure into deflection, the stress or the strain of the deflected plate is then measured using electro-mechanical transducers like:

- Piezoelectricity
- Piezoresistivity
- Change of capacitance
- Change of natural frequency

The piezoelectric effect connects the elastic stress to a change of charge that can be detected by electrodes. This output has a high impedance and can be sensed as voltage or charge. In order to enable the measurement, the signal has to be amplified using a charge amplifier. Due to its character, it is considered as a self-generating sensor. It can only sense changes of strain and is therefore unsuitable for usual pressure sensing. This principle is more suited for the use in micro-accelerometers. [2, 47, 48]

The second type of transducers involves the piezoresistivity of silicon. Piezoresistive materials change the electrical resistance when subjected to strain. Since this is the most common sensing principle, it should be reviewed in more detail. The resistance can be calculated using:

$$R = \frac{\rho L}{wd} \qquad (2\text{-}11)$$

The dependency of this value from geometry changes(L - length, w - width, d - depth) of the resistor as well as the resistivity $\rho$ can be written as:

$$\frac{\Delta R}{R}=\frac{\Delta \rho}{\rho}+\frac{\Delta L}{L}-\frac{\Delta w}{w}-\frac{\Delta d}{d} \qquad (2\text{-}12)$$

For silicon, the change of the resistance is the dominating factor, whereas in conventional strain gages the main effect is the change of the geometry. Considering small changes of the resistance, the variation of the resistance is proportional to the strain:

$$\frac{\Delta R}{R}=K\Delta\varepsilon \qquad (2\text{-}13)$$

where R is the resistance, $\varepsilon$ is the strain, and K is the gage factor. This constant can be up to 200 for silicon resistors compared to approximately 2 for conventional devices.

The relationship between this change and the applied stress can be written as:

$$\Delta\underline{\rho}=\underline{\pi}\,\underline{\sigma} \qquad (2\text{-}14)$$

where $\Delta\underline{\rho}$ is the matrix of resistivity change, $\underline{\pi}$ is the piezoresistivity matrix, and $\underline{\sigma}$ is the stress matrix. For the cubic structure of silicon, the $\underline{\pi}$ matrix has the structure that is shown in Equation (2-15):

$$\underline{\pi}=\begin{bmatrix} \pi_{11} & \pi_{12} & \pi_{12} & 0 & 0 & 0 \\ \pi_{12} & \pi_{11} & \pi_{12} & 0 & 0 & 0 \\ \pi_{12} & \pi_{11} & \pi_{11} & 0 & 0 & 0 \\ 0 & 0 & 0 & \pi_{44} & 0 & 0 \\ 0 & 0 & 0 & 0 & \pi_{44} & 0 \\ 0 & 0 & 0 & 0 & 0 & \pi_{44} \end{bmatrix} \qquad (2\text{-}15)$$

Since the change in resistance is dominated by the change of the resistivity and this is dominated by the influence of the plane stresses, the Equation (2-12) can be rewritten as:

$$\frac{\Delta R}{R} = \pi_L \sigma_L + \pi_T \sigma_T \qquad (2\text{-}16)$$

The indices L (longitudinal) and T (tangential) refer to the direction with respect to the resistor orientation. The values of the $\pi$'s are functions of the crystallographic orientation.

In most applications there are four piezoresistors diffused into the diaphragm. They form a full Wheatstone bridge. This enables a voltage output and yields a first order compensation for temperature influences. Further passive elimination of this effect as well as for offset can be achieved with the addition of four passive resistors. This circuit is connected to a constant voltage compensation circuit for normalization of the sensivity and the compensation of the temperature coefficient of sensivity. [1, 2, 32, 49, 50]

The third method for pressure sensors uses the displacement of the diaphragm to change the capacitance of a plate capacitor (Figure (2-4)). The capacitance of this can be determined by:

$$C = \frac{\varepsilon A}{d} \qquad (2\text{-}17)$$

where A is the area of the plates, d is the plate separation ($d=d_0 \pm w$, $d_0$ is the initial gap, w is the diaphragm displacement), and $\varepsilon$ is the dielectric constant. It

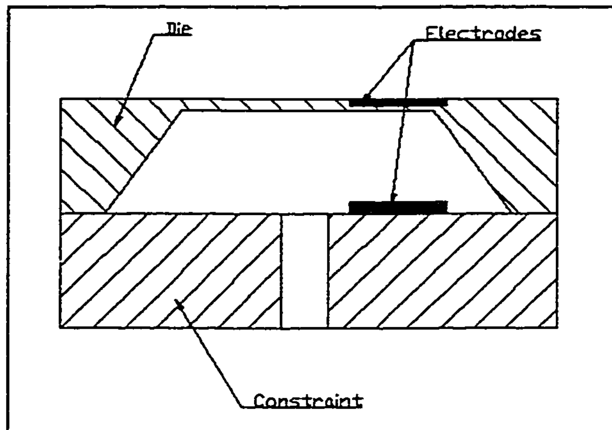


Figure 2-4: Capacitive Pressure Sensor

can be seen, that the capacitance is inversely proportional to the distance of the plates. If the second order effects are neglected, the plate spacing is proportional to the applied pressure and therefore the change of the capacitance is inversely proportional to the applied pressure. This results in a highly nonlinear response of the unit if the capacitance is the output. This problem can be addressed with the use of the impedance for the measurement. The lower temperature dependence, noise, zero drift, and power consumption combined with higher sensitivity are the main advantages of this technique. [1, 2, 6, 47, 51]

The last principle is based on a mechanical principle. The natural frequency of a vibrating beam is dependent on the tension within the beam. These frequencies are depending on the stiffness to mass ratio. Tensile stress in the beam stiffens the structure that causes a frequency increase. The strings of musical instruments are tuned using this effect. When such a structure is excited to resonant vibration, the change of the frequency of the maintainer circuit can be used to measure the applied pressure. The resulting frequency change is proportional to the applied pressure. The geometry of such a sensor is illustrated in Figure (2-5). [6, 10]

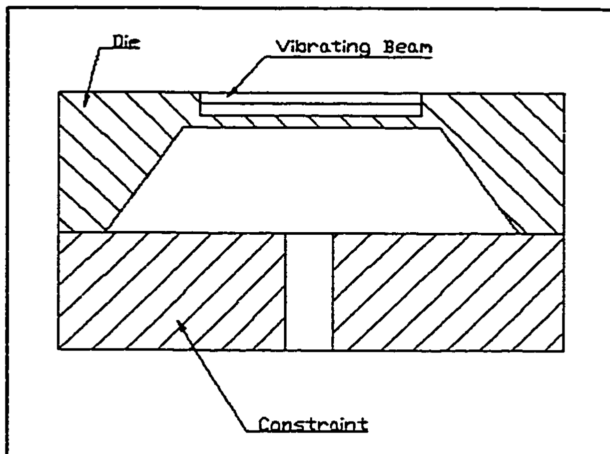


Figure 2-5: Vibrating Beam Pressure Sensor

There are certain advantages and disadvantages of sensors designed on these four working principles. The capacitive transducer is relatively insensitive to temperature changes. It has a lower zero drift, a lower power consumption, and achieves a high grade of stability for air data applications. The die size for these sensors is limited since the capacitance is depending on the size of the electrodes and the signal conditioning is very complex. Piezoresistive sensors show a better manufacturability and a slightly better signal to noise ratio than the capacitive sensors. The resonating beam technique offers higher accuracy since the influence of electrical noise and drift has only secondary effects on this method, which is primarily determined by the mechanical characteristics of the vibrating structure. However, the problem of this technology is the fabrication process that involves time consuming steps to shape this complex structure. [1, 6, 51]

# 3. Overview of Micro Fabrication Processes

The sensing element of the transducer is fabricated by micromachining techniques. There are three technologies available:

- Surface Micromachining
- Bulk Micromachining
- LIGA

The first two techniques are derived from technologies used in the integrated circuit industry and used extensively in commercial applications. LIGA is a relatively new technique that is unique to MEMS with great promises for the future.

## 3.1 Surface Micromachining

Surface micromachining is a manufacturing technique that adds and subtracts material from the surface of a carrier. The substrate itself is not shaped in this process. The process involves several steps of thin film deposition, followed by selective wet or dry etching. Common film materials are silicon, silicon oxide, silicon nitride, and metals. The structure is built by consecutive patterning of single layers each on top of the previous shape. In this way structural and sensing elements as well as electrical connections and sacrificial layers are formed. This chapter gives an overview of typical deposition and removal techniques.

Sacrificial layers are the key technique for movable parts in surface micromachining. These layers consist of a material, in most of the cases $SiO_2$, that can be etched selectively. After growing and patterning of this layer, other films are deposited and shaped on top. The final step to free the structure from the handling wafer is to etch the sacrificial layer away, usually by means of chemical etching. This process is the enabling technique to allow the fabrication of mechanical thin film sensors and actuators. [2, 3, 16]

The deposition techniques can be categorized into three groups:

Group 1: Physical vapor deposition (PVD)

Group 2: Chemical vapor deposition (CVD)

Group 3: Electrochemical deposition

The first group uses physical phenomena to build a layer on the handling wafer. The basic working principle is to evaporate a material in vacuum and to deposit the atoms or molecules onto the surface of the substrate. The process employs different methods, which result in different deposition speeds, layer qualities, and other effects. [1, 2, 6, 52]

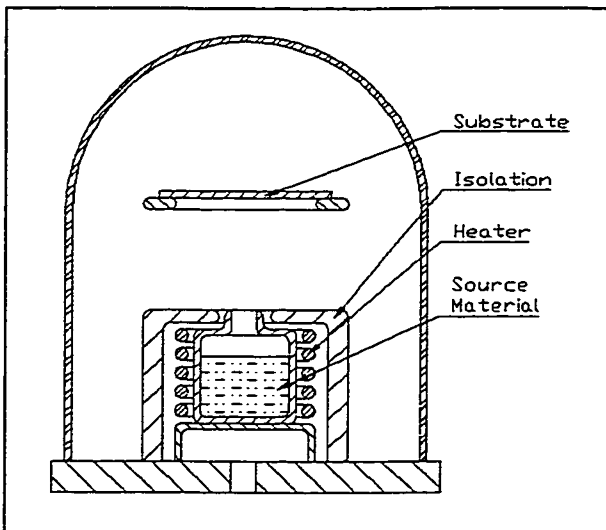


Figure 3-1: Thermal Evaporation

The oldest method is thermal evaporation using a high electric current to heat up the material

(Figure (3-1)). This procedure does not cause radiation, but the film is contaminated with atoms from the resistor that are also evaporated during the process. Radio frequencies also can be used with similar results. Purer films can be achieved by employing an electron beam to heat the material source. The disadvantage is the resulting radiation. This can cause x-ray or ion damage to the substrate. This problem can be addressed by the use of laser light. This method is fast and comparatively simple and has a relative low energy influence on the substrate. However, it is difficult to provide a large area with a uniform film thickness and the materials are limited due to decomposition effects. [1, 2, 6]

Sputtering expands the choice of deposition materials. It allows the deposition of metal, semiconductor, isolator, and composite films. In this process, the source is subjected to an ion beam which provides the material with the necessary energy. The substrate is placed on the anode and the atoms condense there. This process is very complex and the deposition rate is low. Substrate heating is necessary if a uniform step coverage is an important issue. [1, 2, 6, 53]

Laser sputtering deposition uses the energy of laser light to erode the source. This avoids the damage due to radiation that is connected with the conventional sputtering process. This process is extremely useful, when complex materials have to be deposited, because the atomic ratios of the deposited substance are replicated with high reliability in the coating film. The technique is not useful for large areas because the laser is focused on a small point. This

makes the source for material very small and consequently slows down the process. The small size of the material source creates a strong angular dependency of the deposition process, which makes the coating of high aspect ratio structures with sufficient precision difficult. [6]

Molecular beam epitaxy offers a possibility to grow atoms in a single crystal manner. The substrate is heated and subjected to a stream of atoms in an ultra-high vacuum. The deposition rate is extremely low, but the process allows control of the film thickness on atomic scale and provides ultra-pure films. [6, 53]

The cluster-beam technique deposits atom clusters that are evaporated and subsequently ionized onto the substrate. It allows the use of low temperatures to produce thin films of excellent purity and adhesion. [6, 53, 54]

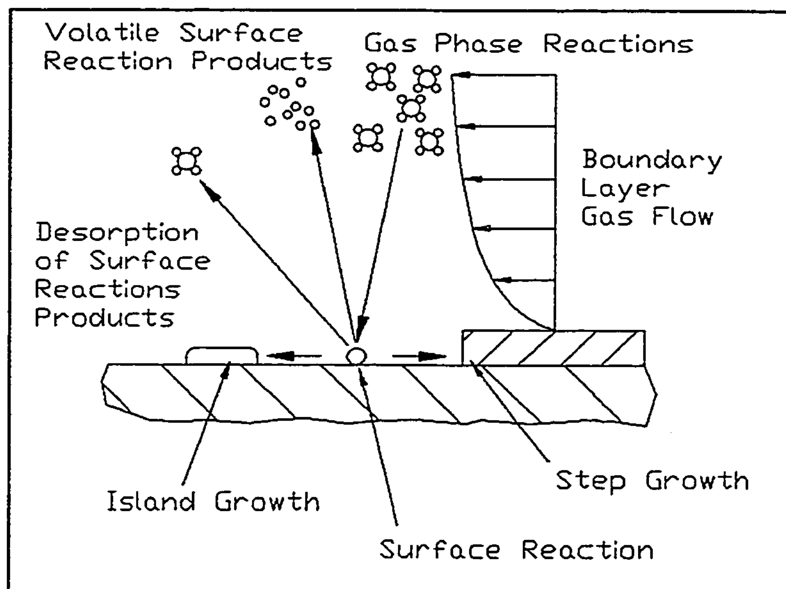


Figure 3-2: Chemical Vapor Deposition

The second group, chemical vapor deposition processes, are more complex than the procedures described above. They use chemical reactions to form a surface layer. This involves mass as well as heat transfer

problems. Figure (3-2) illustrates this process. The gaseous reactants have to be moved to the deposition area. While this happens, gas-phase reactions can lead to undesired film precursors and by-products that are then deposited onto the substrate. Surface reaction occurs on the substrate to form the new layer, and by-products of this reaction have to be removed. The added atoms migrate within this layer and finally form the film. Depending on the conditions of the overall reaction, the process can be mass transport limited or reaction limited. The first situation enables relative independence from the environmental conditions for a uniform film growth as long as the transport conditions are kept constant. Since the reaction rate is often dependent on temperature as a relatively easily controllable variable, the second situation is often desirable to increase the throughput of the process. The method allows the deposition of very pure layers with high controllability and economy. This method of thin film deposition is predominantly used. [2, 6, 52, 53]

Plasma-enhanced chemical vapor deposition employs a plasma to transfer the energy to the reactant that enables lower substrate temperatures. Since the method is surface-reaction limited, a uniform layer thickness can be achieved by a uniform substrate temperature. The reaction conditions such as the pressure and the temperature of the reactants and the substrate, have a major impact on the material and mechanical properties of the resulting layer. For good results, the pressure has to be low, the deposition should be slow, and

a high substrate temperature should be used. The plasma has to be heated at a low radio frequency. [2, 6, 52, 53, 55]

Atmospheric pressure chemical vapor deposition is mainly used to grow epitaxial layers of semiconductors and fast growing of $SiO_2$. This method works at pressures slightly below atmospheric pressure under mass transport limitation. [6, 52]

Low pressure chemical vapor deposition works at pressures below 10 Pa and deposits uniform layers on large scale due to the reaction limitation of this process. The process is temperature sensitive. It is used to grow structural and sacrificial layers. The limitations are the slow deposition rate and the high reaction temperature. With very low pressure CVD, it is possible to work at relatively low temperatures. [5, 6, 52, 53, 56]

Metalorganic chemical vapor deposition employs the gas flow for the deposition process. It is the principal technique for epitaxial layers and very economical. [6, 53]

The reaction can also be laser or electron beam enhanced. This enables the process to be performed at low temperatures and minimizes contamination. [53]

The last group is electrochemical deposition. It enables the application of thick layers of metals. The growth rate is high compared with the other groups. The method can be divided into electroplating and electroless plating. In the first case, an external bias is applied to enable the reaction. The latter technique

uses chemical reactions to reduce the metal ions in the deposition process. This group of deposition processes is especially interesting in combination with LIGA and will be discussed later. [2, 6, 53]

The deposited layers are patterned by subsequent etching techniques in lithographic processes. A photoresist is applied to the film, exposed through a patterned mask and developed. After this, the remaining photoresist is a mask for the etching process. The etching can be done with dry or wet techniques. The dry etching techniques are based on plasmas or electrical discharges, whereas the wet etching utilizes chemical reactions of acids and alkaline bases. [1, 2, 5, 6]

Sputtering is a dry physical etching technique. The ion beam is used to erode the target by momentum transfer. This results in relatively equal etching rates for different materials and a directional anisotropy. The nonselectivity introduces masking problems for this technique. The etch rates are very slow and there are problems with the redeposition of the sputtered material. [6, 53]

Another means of dry physical etching is the so-called ion-beam etching. In this case, the plasma source is decoupled from the substrate. Noble gases are used to improve the yield and avoid chemical reactions. The etch rates are significantly higher than the etch rates of sputtering. It is possible to achieve high resolutions. [6]

Dry chemical etching uses chemical reactive neutral species produced in a plasma to execute the etching process. These products react on the surface

with the substrate and form new ones that are removed. The reaction into new volatile products is the major difference between this technique and sputtering in which the sputtered material is deposited nearby. [6]

Wet chemical etching uses the reactions of bases and acids with the films. This technique is inherently selective. Whereas isotropic etching attacks the structure independently of its crystallographic orientation, anisotropic etching reacts with different crystallographic orientations of the same material at different rates. The latter etchants are frequently employed in bulk micromachining, whereas the isotropic etchants are used with surface micromachining. [1, 2, 6]

## 3.2 Bulk Micromachining

Bulk micromachining is the most utilized manufacturing technique for micromechanic devices at the present time. It was introduced in the 1960's, and it was further developed in the 1970's to enable the forming of three-dimensional structures. In contrast to surface micromachining, the shaping is done by selective etching of the wafer. [2, 4]

The wafer is usually covered with a layer of silicon oxide, silicon nitride or metals (e.g. Au, Ag, Al). This layer is shaped in a lithographic step and serves as a mask for the following etching. Depending on the desired structural geometry, the etching uses isotropic or anisotropic etchants. [2, 3, 5, 6, 16, 56]

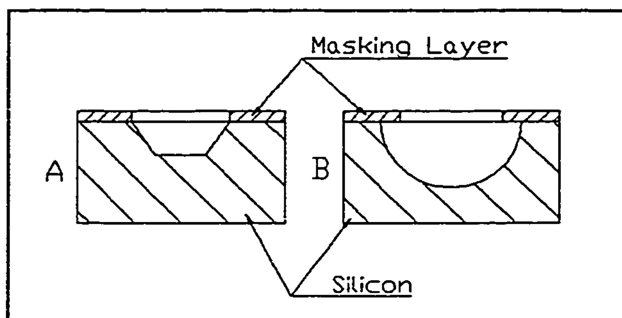


Figure 3-3: Wet Etching
A Anisotropic
B Isortopic

The dominant wet etching techniques use electrochemical reactions to dissolve parts of the wafer (Figure (3-3)). This process can be reaction or transport limited. [2]

Wet isotropic etching is used to remove damaged surfaces, to create structures in single crystalline silicon, and to pattern semiconductor films. A common etchant is the HNA system, consisting of hydrofluoric (HF), nitric acid ($HNO_3$) in water or acetic acid ($CH_3COOH$). This system has been studied extensively, and etching curves are available. [2, 5, 6]

Table 3-1: Typical Etch Rates [5, 58]

| Material | Etchant | Etch Rate |
|---|---|---|
| Si (100) | KOH | 0.25-1.4µm/min |
| Si (100) | EDP | 0.75 µm/min |
| $SiO_2$ | KOH | 40-80 nm/h |
| $SiO_2$ | EDP | 12 nm/h |
| $Si_3N_4$ | KOH | 5 nm/h |
| $Si_3N_4$ | EDP | 6 nm/h |

In contrast to isotropic etching, anisotropic etchants dissolve the wafer at different rates depending on its crystallographic orientation. It is possible to reach etch ratios of up to 400:1 for silicon with respect to the (100) to (111) orientation. The ratios are smaller for the other orientation combinations. Typical examples for this class of etchants are potassium hydroxide (KOH), ethylene-diamine, and

Table 3-2: Typical Selectivity Ratios (Compared with (100)-Silicon) [58]

| Mask Material | Etchant | Selectivity Ratio |
|---|---|---|
| $SiO_2$ | KOH | $10^3$ |
| $SiO_2$ | TMAH | $10^3$-$10^4$ |
| $SiO_2$ | EDP | $10^3$-$10^4$ |
| $Si_3N_4$ | KOH | $10^4$ |
| $Si_3N_4$ | TMAH | $10^3$-$10^4$ |
| $Si_3N_4$ | EDP | $10^4$ |

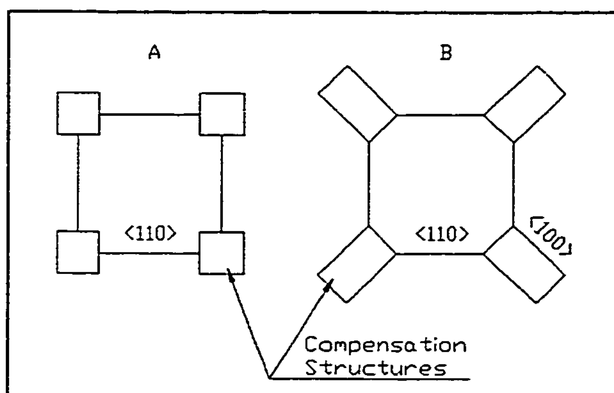


Figure 3-4: Corner Compensation Schemes
A Squares (KOH, EDP)
B Rechtangle (KOH)

pyrocatecol (EDP), tetramethyl ammonium hydroxide (TMAH), and hydrazine. The typical ranges for the etch rates are given in Table (3-1) [2, 5, 6]

The geometric shape is determined by masking layers. Typical materials for etch masks are silicon oxide and silicon nitride. These layers are shaped in lithographic processes. Since the masks are not inert to the etchants (Table (3-1)), the film has to be thick enough to provide sufficient coverage of the silicon. The selectivity ratio that is defined by the ratio of the etching rate of silicon to the etching rate of the masking material is one parameter that determines the mask thickness. Table (3-2) shows the range of typical selectivity ratios. Beside this, the porosity of the material defines a minimum thickness for the deposited layer. [5, 58]

A problem with wet etching are the effects of underetching and undercutting. In the case of underetching, the substrate that is covered with a masking layer is attacked by the etchant. For non-convex corners, this is mainly initiated by mask misalignment. For masks that feature convex corners, this effect is usually larger since the etchant attacks the substrate that only the [111] planes are remaining. This undercutting can be compensated by corner compensation structures that have to be added to the mask layout. Examples for such arrangements for typical etchants are shown in Figure (3-4). [6]

A powerful tool to determine the shape of the structure is the etch stop technique. It utilizes the fact that the etching as an oxidation-reduction process depends on a charge transfer. There are two common methods for etch stop:

- Dopant dependent etch stop
- Electrochemical etch stop

The first technique uses the fact, that different doping levels are attacked at different rates. This either amplifies the etch rate or slows it down. For the isotropic HNA system, the p or n doped areas are dissolved significantly faster than the undoped regions. The main application of this technique is to define stops for anisotropic etching. This is accomplished by heavy boron doping. The problem of this method is the fact, that the dopant has to be diffused into the wafer, which limits the maximum thickness of the features. The high doping level also introduces stress in the lattice and does not allow the fabrication of electronic devices in these areas. [2, 5, 6, 56]

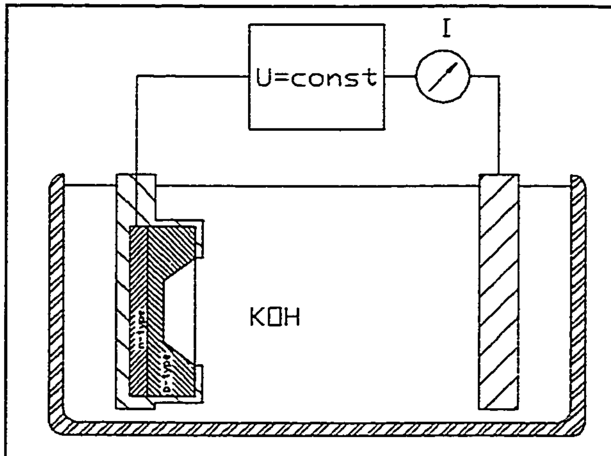


Figure 3-5: Electrochemical Etch Stop

Electrochemical etch stop does not rely on heavy doping levels and can therefore be used to create thicker structures and allows also electronic devices to be integrated. Due to the fact that the passivation potential is different for the two differently doped regions, the process can be stopped when the layer with the higher passivation energy is reached. This enables the removal of higher doped and therefore higher conductive regions with isotropic etchants. More commonly used is this technique to shape thin membranes with anisotropic etching and the effect of a p-n junction (Figure (3-5)). Since the passivation potential is also dependent on temperature and etchant concentration, it is very important to monitor the reaction conditions. [2, 5, 6, 57]

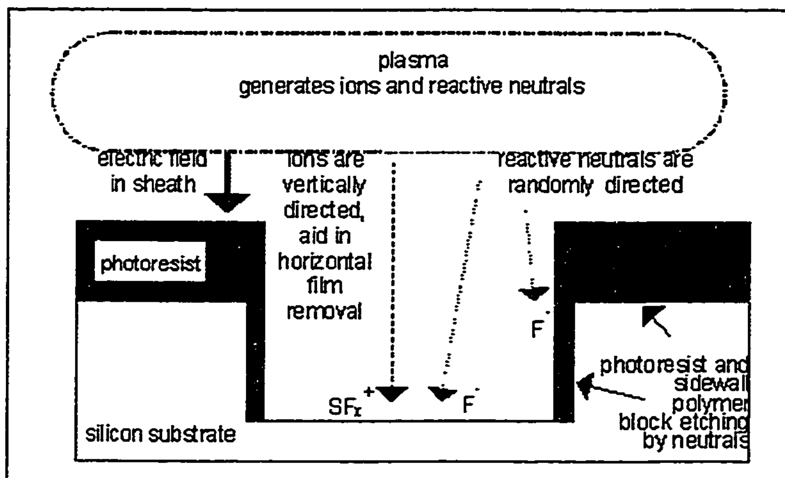


Figure 3-6: Deep Reactive Ion Etching

Dry etching is also possible in bulk micromachining. Due to difficulties in

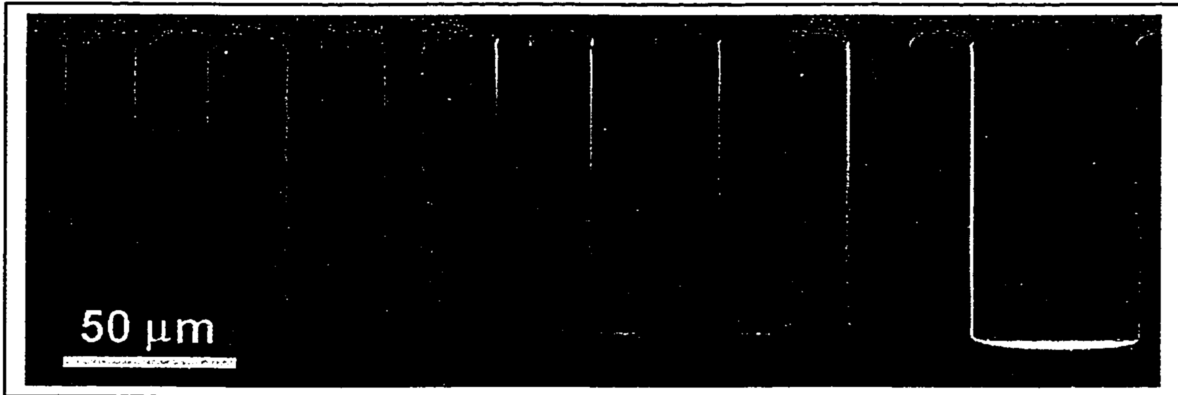


Figure 3-7: DRIE-Lag (Copyright of Lucas NovaSensor, with Permission)

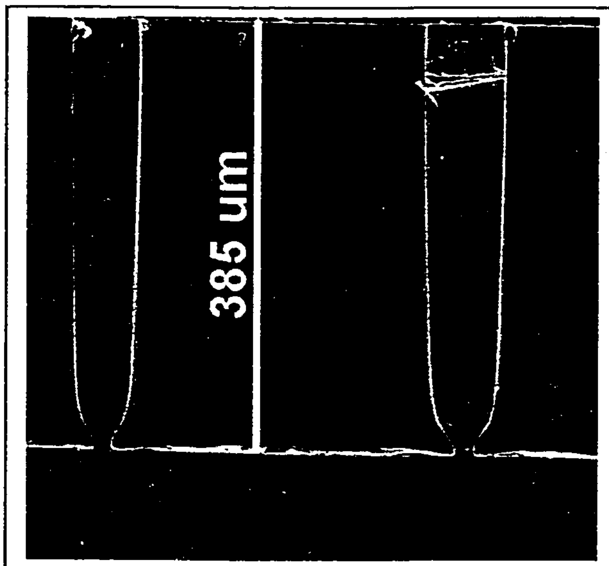


Figure 3-8: Notching (Copyright of Lucas NovaSensor, with Permission)

reproducibility and long etch times for high aspect ratio features it is not commonly used in micromachining. [2, 6]

A new development that is promising in dry etching is deep reactive ion etching (DRIE, see Figure (3-6)). It is an alternating process of etching and deposition of protective layers. The etching process utilizes radicals such as fluorine or chlorine. The polymer layer is formed by polymers such as fluoropolymers ($nCF_2$). It is possible to achieve sidewall angles of 90±2°. The etch rate is in the order of 2 to 3 μm/min which is higher than for common wet etching techniques. The selectivity ratio of up to 100 for photoresists and of up to 200 for silicon dioxide is also higher than the selectivity

of the wet etchants. A problem of this technique is the fact that wider trenches are etched at a higher rate than narrow channels (Figure (3-7)). This problem can be solved with etch stop techniques such as oxide layers. However, extensive over-etching results in notching at the sides of the trenches as shown in Figure (3-8). [58, 59]

## 3.3 LIGA

This German acronym represents the three steps of this technique:

Step 1: X-ray lithography

((Röntgen-)Lithographie)

Step 2: Electrodeposition

(Galvanoformung)

Step 3: Molding

(Abformung)

LIGA is a micromachining method that was developed by Ehrfeld at the Kernforschungszentrum Karlsruhe (Germany). It is a process that is especially useful in the fabrication of structures with high-aspect-ratios at potentially low costs.

Figure (3-9 and 10) show the generic

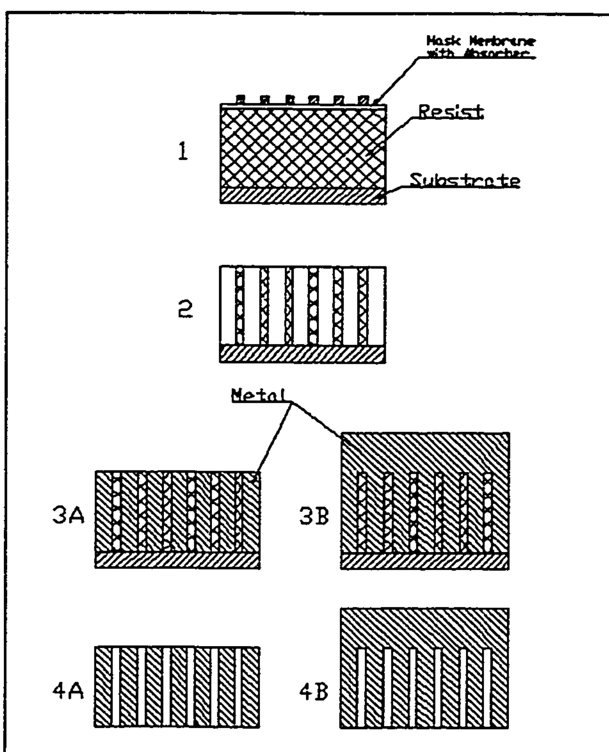


Figure 3-9: LIGA-Process
1 Irradiation
2 Shaped Resists
3 Electroplating
4 Product
A Metal Product
B Metal Mold

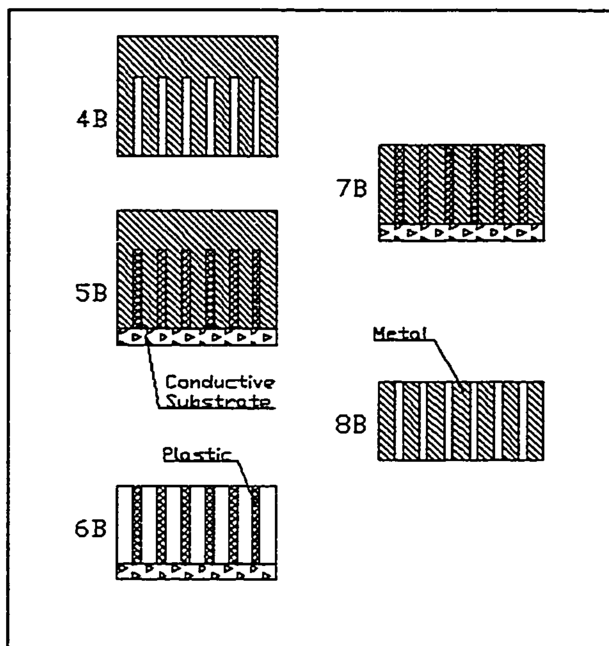


Figure 3-10: LIGA Process (Part2)
4B Metal Mold
5B Mold Filling
6B Plastic Structure (Final Product or Mold)
7B Electroplating
8B Metal Product

process that is described in this section.

In the first step, lithography is used to pattern a thick film resist. Since the resolution and possible aspect ratio increase with decreasing wavelength of the light used for the projection, x-rays are used. This enables linewidths of 0.2 µm and aspect ratios of more than 100 can be achieved. The source of the x-rays is preferably a synchrotron. It allows a high throughput because the high flux of collimated rays that shortens the exposure time. This is also the major drawback of the method because of the costs for a synchrotron. The use of high x-ray doses also introduces masking problems. [2, 6, 16, 56, 60-63]

The resist is applied to a primary substrate, that has to be conductive to enable the electrodeposition in the subsequent step. This plate has to provide good adhesion, which is usually achieved by mechanical or chemical means. The applied resist should have a high sensitivity to x-rays, high resolution and contrast, resistance to etching if unexposed, and good thermal stability up to

140°C. A typical resist for LIGA is polymethylmethacrylate (PMMA). It meets most of these requirements. However, it has a low sensivity and problems with cracking due to internal stresses. The resist can be placed on the substrate by multiple spin coating, casting, plasma polymerization or the application of commercial PMMA sheets. The irradiation lowers the average molecular weight of the PMMA. After the exposure, the resist is developed by a wet chemical etching process that is sensitive to this change. [6, 16, 56, 60, 61]

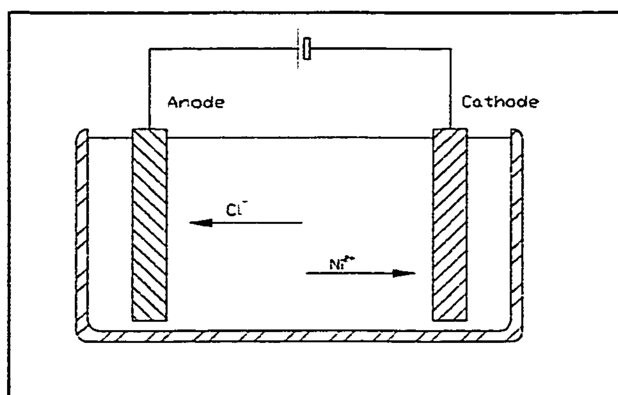


Figure 3-11: Electroplating (Nickel with $NiCl_2$)

In the second step, the resist pattern is used to form a metal. This metal is grown by electrodeposition onto the substrate (Figure (3-11)). Typical problems of this process are to get the electrolyte in contact with the substrate and to remove hydrogen, which is a byproduct of the plating. These are the two difficult problems that are especially critical with small features and high aspect ratios. The first problem can be addressed with the use of wetting agents. A close control of the pH-value, the temperature, and the current density minimizes the evolution of hydrogen. The internal stress of the deposited material is also dependent on these three variables as well as on the solution agitation and the final layer thickness. [2, 6, 16, 62]

It is also possible to deposit the metal by an electroless method. This principle is simpler and the induced internal stress is lower than in the above method. However, the adhesion of these layers is not as good. [2, 6]

The resulting structure is attached to the substrate but can also be removed. This removal is supported by chemical or electrochemical preparation of the substrate to reduce the adhesion between the deposited layer and the support. The product is polished to even out variations in the height and the remaining PMMA is stripped. The metal part is the final product or can be used as a mold for plastics. [6]

The third step, the molding, is the one that makes LIGA economically attractive. The metal mold that is formed in the previous two steps can be used to shape a large number of microstructures. The molding process can be done by reaction injection, thermoplastic injection, and impression. In the first case, the components of a polymer are mixed and the reaction takes place in the mold itself. If thermoplastic injection is used, the plastic material is heated above its glass transition temperature and then injected. The same happens in impression molding, only a vacuum is applied to pattern the material. The demolding process is also complicated by the desired high-aspect-ratios of the final product. [6, 62]

Even though the technique was developed without considering a combination with the fabrication of integrated circuits, it is possible to combine the plastic molds with silicon wafers. [62]

The plastic parts themselves can also be used as mold inserts to form metal structures in mass production. [63]

Figure 3-12: Integrated Micro Epicyclic Gear (Copyright of Institut of Mikrotechnik Mainz GmbH, with Permission)

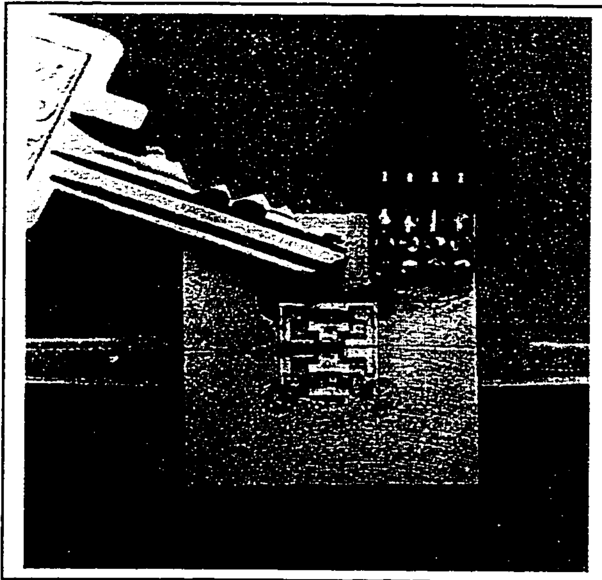

Figure 3-13: Optic Fiber Switch (Copyright of Institut of Mikrotechnik Mainz GmbH, with Permission)

LIGA offers a variety of applications in the field of MEMS. The original LIGA allowed only the production of parts that were fixed to a substrate. The introduction of SLIGA, which is a LIGA process with the use of the sacrificial layer technique enabled the fabrication of released parts. In this variant, the sacrificial layer is applied and patterned before the thick resist is placed on the substrate. [16, 56, 61-63]

Several devices like accelerometers, valves, pumps, and turbines have been successfully produced by this process. Figures (3-12,13) show structures that were produced with LIGA.

A drawback of this process is

the low compatibility to the standard integrated circuit techniques. This makes the integration of electronic circuits into the structures difficult. However, it is also a development problem because of the major differences of this new technology to the dominating ones. The main obstacle for new developments in this field is the use of synchrotron radiation that makes extremely high initial investments necessary. [6, 16, 56, 60-64]

# 4. Design of Pressure Sensors

The design of a sensor is a very complex process, beginning with the analysis of the application. As a result of this analysis, the environmental constrains are defined. This leads to special considerations for the special pressure and temperature range as well as the necessary packaging effort that is needed to ensure the function of the sensor. The integrity of the structure has to be guaranteed over the desired life span of the transducer. The fabrication limits impose also a number design constrains that the engineer has to obey. This chapter should give an overview over the different design considerations.

## 4.1 General Considerations

A pressure sensor in automotive applications has to withstand one of the harshest environments. It is subjected to aggressive chemicals, high and low temperatures. The transducer has to endure mechanical vibrations and shocks while maintaining its structural integrity. The different pressure ranges of the application demand different sensor designs for an optimum output. The materials and the design have to ensure the function of the sensor. The objective of this section is to point out the general design considerations that are imposed by this environment.

### 4.1.1 Physical and Environmental Constrains

This part analyzes the different constrains that are imposed by the exposure of the pressure sensor to the medium. There are also some general physical limits that the designer has to take in consideration for the successful development.

The contact between the sensing element and the medium to be measured introduces one of the major challenges for a sensor. Since the fluid is usually not inert, the contact to the diaphragm or the electrical connections can alter the mechanical and electrical properties of the material. In most cases, some kind of media isolation has to be considered.

The environment associated with automotive application is very hostile to sensors. Many different chemicals are likely to get in contact. These include exhaust gas, fuel, oil, hydraulic liquids, water, salt water, acidic, and alkaloid aqueous solutions. [65]

The hydrocarbon fluids damage the sensor by dissolving applied adhesives. Some of these materials absorb organic fluids and swell consequently, resulting in an output distortion. In some cases these fluids might also be caustic and attack other materials of the sensor as well. [66]

The aqueous solutions corrode the sensor by initiating electrolytic reactions. The materials that are used to build the sensor have different electrochemical potentials. The conductive connection between these triggers the reaction. This is especially dangerous for the electrical connections. Since

the spacing of the conductive paths is tight, even a small conductivity distorts the output of the sensor immediately and destroys the connections over time, leading to a failure of the sensor.

In some automotive applications, the sensor is in contact with toxic fluids. In these cases, special precautions have to be taken to prevent leakage, even in the case of extreme overpressures.

The diaphragm as a suspended mass is also prone to failure due to mechanical vibrations. This is especially dangerous for bossed diaphragms because of the mass concentration. The diapragm has to be designed so that the lowest natural frequency is higher than the expected excitation frequencies. For automotive applications, standard test procedures are prescribed in the frequency band from 100 Hz to 2 kHz. [65]

Another problem is mechanical shocks due to handling and mounting. A typical shock specification for automotive application is a 1 m drop onto concrete. This can result in an acceleration of up to 2000g. The structural integrity has to be guaranteed. This limits the diameter to thickness ratio of the membrane unless it is protected, e.g. by limiting surfaces.

Thermal shocks induce temperature gradients and resulting thermal stresses due to the thermal expansion of the materials.

The size of the die is also a major design criterion. The cost of the die is proportional to the occupied area. Therefore, it is desirable to decrease the dimensions of the structure. However, there are limits to this development. If the

membrane size is decreased, the membrane thickness has to decrease too. The Equations (4-1,2) describe the maximum stress and deflection for a square plate with fixed edges under a uniform pressure:

$$\sigma_{max} = C_1 p \left(\frac{a}{t}\right)^2 \qquad (4\text{-}1)$$

$$\delta_{max} = C_2 p \frac{a^4}{t^3} \qquad (4\text{-}2)$$

$\sigma_{max}$ is the maximum bending stress at ½ a, a the length of the square, t the thickness of the membrane, p the applied pressure, $\delta_{max}$ the maximum deflection in the middle of the diaphragm. [67]

The stress that is used for the conversion of the mechanical signal into the electrical signal scales inversely proportional to the square of the membrane thickness (Equation (4-1)). Equation (4-2) shows that the deflection scales with the inverse cube of the thickness. Consequently, the deflection is increasing with decreasing thickness for a defined stress. This introduces undesired nonlinear membrane stresses. [1, 67]

The die has to be attached to a header. This is usually done by adhesives that are applied to the bottom of the silicon, which limits the minimum footprint of the die. The area has to be large enough, that the stresses in the die attach are below the yield stress for the desired pressure range. This is especially important with backside pressurization, e.g. differential pressure sensors. The die attach material has to be applied without blocking the pressure port. The die

miniaturization is therefore limited for these sensors by the development of precision die attach methods.

The piezoresistors that are diffused into the diaphragm have also an influence to the die size. The value of the resistance is determined by:

$$R = \frac{\rho L}{A} \tag{4-3}$$

where $\rho$ is the specific resistance, L the length, and A the cross section of the resistor.

The cross section is limited by the diaphragm thickness and the doping process that also influences the specific resistance and other major parameters like the thermal behavior. Therefore, the length of the resistor is the parameter to be optimized to achieve the desired output characteristics. Ideally, the resistor has to be placed in the location of the maximum stress. Since in reality, the occupied area is finite, the stresses are averaged over a certain area. This works well only if the surface occupied by the resistor is significantly smaller than the diaphragm size itself. [1]

The same problem appears with capacitive pressure sensors. The capacitance is proportional to the area:

$$C = \frac{\varepsilon A}{d} \tag{4-4}$$

where C is the capacitance, $\varepsilon$ the permeability, A the area of the electrode and d the distance in between.

The capacitor plates have to be much smaller than the membrane to avoid secondary effects due to bending. At the same time, they have to be as large as possible to maximized the measurement effect. These two constrains limit the minimum die size. [1]

The character of pressure as an integral value presents another physical limitation to the membrane size. It has to be large enough to measure the macro-scale property. Since this is the result of micro-scale processes, namely the impact and reflection of atoms or molecules on the system boundary, the membrane has to ensure a sufficient integration over the interactions with the medium. If the size is to small, Brownian noise gets important in the signal. For a circular membrane, the pressure noise $p_n$ due to Brownian motion for low frequencies is

$$\overline{p_n^2} = \alpha \sqrt{\frac{32kT}{\pi}} \frac{\left(\sqrt{m_1}p_1 + \sqrt{m_2}p_2\right)}{a^2} BW \qquad (4\text{-}5)$$

where $\alpha$ is a numerical factor (1.7 for piezoresistive sensors, 1.2 for capacitive sensors), k is Boltzmann's constant, T is the absolute temperature, $m_1$, $m_2$ are the masses of the gas molecules, $p_1$, $p_2$ are the mean pressures of the gases on the two sides of the diaphragm, respectively, BW is the bandwidth, and a is the radius of the diaphragm. [67] For typical dimensions of automotive pressure sensors ($a \approx 1\mu m$, a pressure range of 35 kPa, a bandwidth of 1kHz, and standard conditions for the ambient pressure and temperature, the pressure

noise is less than 30 mPa. For diaphragm sizes much smaller than 1 μm, this noise gains importance. [68]

### 4.1.2 Operating Pressure

The different automotive applications require sensors for different pressure ranges. These differences in the pressure range make it necessary to develop specialized sensor geometries. This section shows typical designs and reviews the considerations for different pressures.

Typically MAP, exhaust gas, and fuel pressure sensors have to work within 0 to 105 kPa. Sensors for the air-conditioning and barometric pressure have the same upper limit but require 50 kPa as the lower measurement limit. Applications in the field of the transmission and pneumatic suspension as well as tire pressure monitoring demand sensing capabilities within the low MPa range. The highest pressures in automotive applications are cylinder (10 MPa), brake fluid (20 MPa), active hydraulic suspension (20 MPa), and diesel pump pressure (100 MPa). [6, 14, 20, 39]

For the middle pressure range from about 35 kPa to 3.5 MPa the flat diaphragm is a suitable design. In this range, linear bending stresses are dominant and enable the measurement. Beyond these limits, stresses and deflections become highly nonlinear. This makes special designs for these pressures necessary. [1]

The displacement of a thin diaphragm is linear only for cases where the deflection is much smaller than the thickness of the diaphragm. If this restriction is violated, nonlinear membrane stresses are superimposed to the linear bending stresses. In the case of low pressures, the diaphragm has to be very thin or the area has to be very large to provide the necessary stresses. Since the die price is depending on the real estate occupied by the sensor, the membrane has to be thinned. Unfortunately, the stress is inversely proportional to the square of the membrane thickness (Equation (4-1)) whereas the deflection scales with the cube (Equation (4-2)). Therefore the deflection is increasing and the output becomes highly nonlinear. A method to minimize these mechanical nonlinearities is the introduction of bossed diaphragms (Figure (4-1)). The boss stiffens the membrane and limits the deflection to a linear range. The piezoresistors are

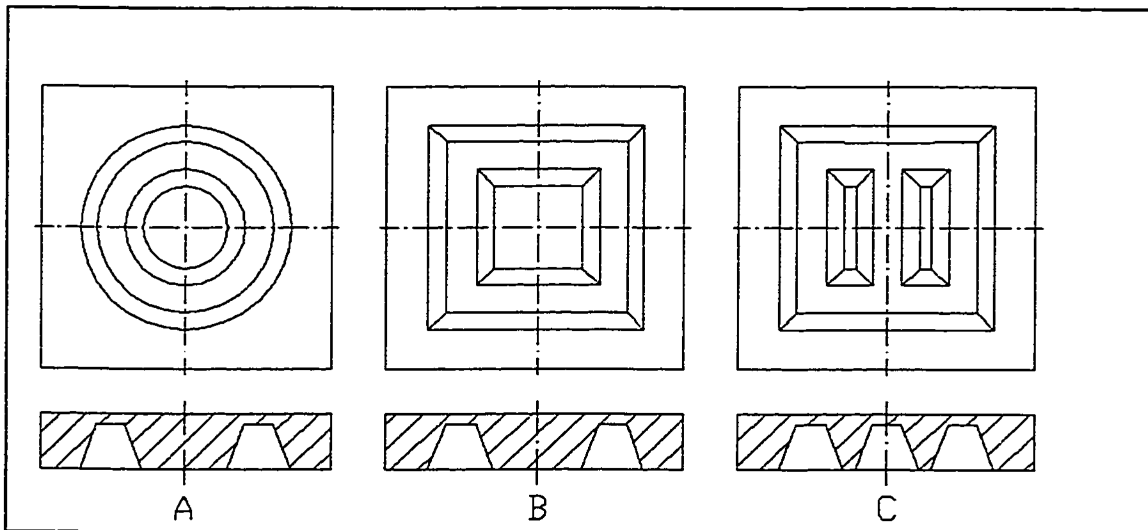


Figure 4-1: Bossed Diaphragms
A Circular Boss in Circular Diaphragm
B Square Boss in Square Diaphragm
C Double Boss in Square Diaphragm

arranged in the thin areas. However, the mass concentration in parts of the membrane makes the device sensitive to its orientation. [1, 67, 69]

Since the minimum area of the membrane is limited by the fabrication of the resistors, the diaphragm has to be thick with respect to its size for higher pressures. With this membrane thickness the nonlinear shear stresses become important. By proper design optimization that usually involves finite element analysis, the resistors can be placed in a way that minimizes the nonlinearities in the output. [1]

It is also necessary to provide a suitable overrange protection for the sensor. A typical device is dimensioned in a way that it fails only if pressures of about 10 to 30 times the full scale pressure are applied. [70]

The simplest way to ensure this protection is to use thicker diaphragms. The implementation of this protection into the normal production is easy. However, a thicker diaphragm is not desirable since it lowers the sensivity of the device.

A better way is to implement an overpressure protection into the design. A typical way is to provide a deflection limitation. For this reason, the package provides contact to the membrane if a certain pressure is exceeded. The protection can be achieved by etching a cavity into the supporting substrate or the use of bosses to limit the distance between the membrane and the support. This increases the stiffness of the diaphragm and lowers the resulting stresses. With this technique, overrange factors of up to 500 are possible. [69, 70]

### 4.1.3 Operating Temperatures

The typical operating temperature range for automotive applications is from -40°C to +125°C. This large range introduces mechanical as well as electrical problems as this chapter will point out.

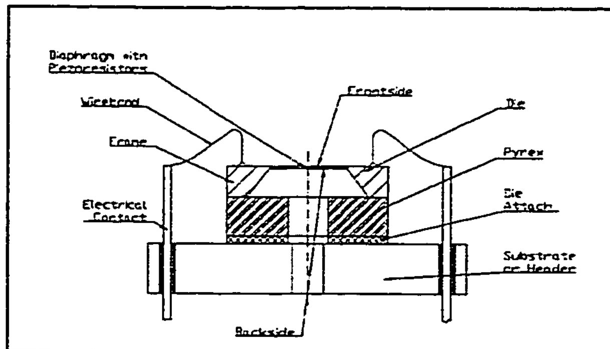


Figure 4-2: Typical Sensor Configuration

The die is mounted on a substrate made of a different material, e.g. ceramic or stainless steel, as shown in Figure (4-2). The mismatch of the coefficients of thermal expansion of the materials induces stresses if the temperature deviates from the manufacturing temperature. Stresses induced by this mechanism will be detected by the strain gages like pressure changes causing a temperature dependent error signal to be imposed on the output. [1, 71-73]

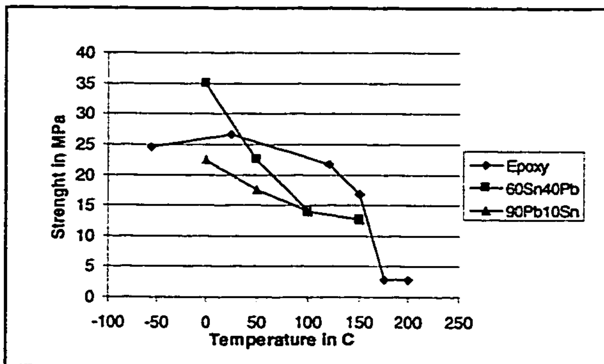


Figure 4–3: Shear Strength over Temperature

The strength of the die attach and the die itself are decreasing with increasing temperature (Figure (4-3)). Materials like epoxies change their mechanical properties drastically if a critical temperature, in this case the glass

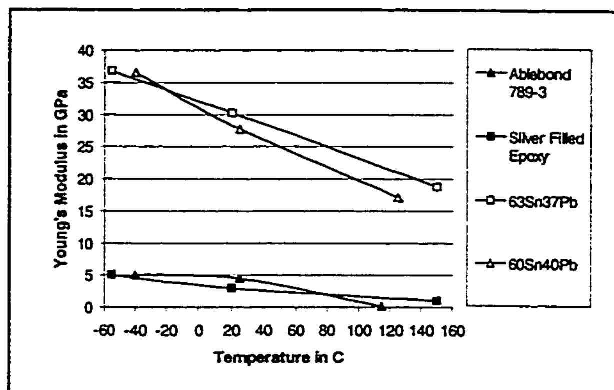


Figure 4-4: Young's Modulus over Temperature

transition temperature, is exceeded. For this reason, the design has to consider the properties at the highest expected temperature. [37, 74-78]

Since Young's Modulus decreases with rising temperature (Figure (4-4)), the deflection for an applied pressure increases. This can add nonlinear effects to the output of the sensor as described above. On the other hand, the flexibility of materials decreases with falling temperatures, which diminishes the stress isolation and makes the structure prone to failure due to mechanical shocks. [6, 37]

High temperature applications have also major problems with long term stability. Internal stresses due to the manufacturing process can relax over a long time. This changing stress is seen as a drift in output over time. [73]

There are also influences of temperature changes on the electrical side of the sensor. Since the piezoresistors exhibit high temperature dependence, it is impossible to use piezoresistors for the measurement without temperature compensation. [79-82]

In typical piesoresistive pressure sensors, the resistors are diffused p-regions into the n-type surface of the diaphragm. The isolation is done by means of back-biased diodes, formed by the p-n-junction. At temperatures above 120°C, the leakage current through this junction doubles every 10°C. The

leakage is no longer negligible, and this isolation is not longer sufficient. For temperatures above 150°C, the silicon on isolator technique (SOI) provides the necessary isolation. [83]

The higher mobility of impurity ions in the dielectric layer also imposes a problem. The electrical field that is applied to the resistors induces electrostatic forces to the ions. The concentration of these charges decreases the effective resistor cross section and alters therefore the resistance (Figure (4-5)). [1]

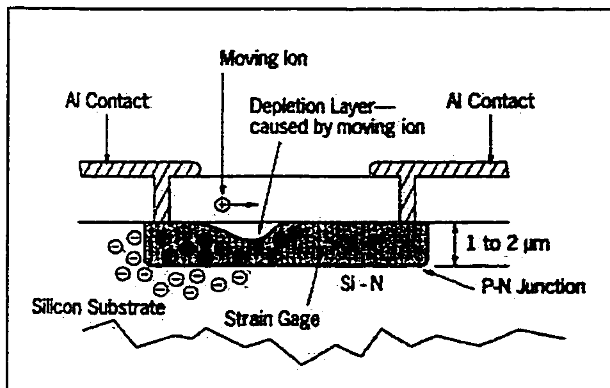


Figure 4-5: Effect of Mobile Ions

Capacitive devices have a much lower thermal influence on the electrical part of the sensor. The influence of temperature to the dielectric constant is marginal for the commonly used dielectrics such as air or vacuum. [1]

### 4.1.4 Material Selection

The behavior of the sensor is strongly influenced by the materials used for its production. This part shows the different considerations that are important for the materials that are used for different functions within the transducer.

The material for the sensor die is usually silicon. Single crystalline silicon is one of the most extensively examined materials. It is a nearly ideal material for structural and electronical purposes. It combines the same elastic modulus as

steel (210 GPa), higher hardness (850 MPa), and strength (1260 - 2100 MPa) than steel with a density (2300 $kgm^{-3}$) that is lower than aluminum. It has nearly no mechanical hysteresis. The low thermal expansion coefficient and the high thermal diffusivity make the material relatively insensitive to thermal shocks. On the electrical side is the high band gap of 1.12 eV. This allows high temperature applications. Beside these properties, silicon has a high melting point, an excellent chemical resistivity, and a low dislocation density. Since silicon is the basis of modem microelectronics, the material is readily available and manufacturing methods could be adapted from integrated circuit processes. All these facts make silicon the perfect material for the production of micromachined pressure sensors. [4]

Young's Modulus and Poisson's Ratio determine the deformation of the structure under an applied load. A high modulus results in less deformation, which is desirable for structural parts of the sensor. On the other side, an elastic material with low modulus can provide a mechanical isolation. For example a rubberlike material behavior can better compensate for thermo-mechanical distorsions.

The sensing element should be made of a material that has nearly no mechanical hysteresis. This ideal elastic behavior is substantial for the measurement. Any mechanical nonlinearity would directly influence and degrade the sensor performance.

High yield strength is also a demanded property. This provides the possibility of lightweight and small structural designs even for high-pressure applications.

The change of these mechanical properties over the given temperature range can be drastic. Materials that perform excellently in their tasks at room temperature can fail at low or high temperatures. It is therefore necessary to determine the material properties over the whole design temperature range and evaluate the suitability of the material for the assigned duty.

A major challenge in the field of MEMS is the change of material characteristics with size. Whereas on a macro scale the continuum theory is sufficient to describe the material, this method becomes increasingly inadequate for smaller structural dimensions and an atomistic description becomes necessary. The current MEMS technology lies in-between these limits. The influence of lattice imperfections becomes more important than on the macro scale. Deposited films possess different properties than the bulk materials. Therefore, it is important to develop new testing schemes that enable testing at a meso scale to provide the vital data needed for numerical simulations. [33, 35, 84]

The thermal properties of automotive sensors are also of interest. The most important factor in this temperature range is the thermal expansion coefficient. It is important to use materials that have closely matched coefficients. The thermal mismatch induces internal stresses, whenever the temperature

deviates significantly from the temperature at which the parts were bonded together. These stresses distort the output of the sensor. However, this matching is not always possible. Typical packaging materials like stainless steel have an expansion coefficient about eight times higher than that of silicon. This makes stress isolation layers or electronic compensation necessary. This additional effort makes sensors more expensive.

The thermal diffusivity for all materials used in the sensor package should be high. This property e.g., minimizes stresses due to thermal gradients within the sensor. With high thermal diffusivity, the temperature gradients decrease within the package and a thermal equilibrium is reached faster.

While the melting point of materials is usually not a serious concern within the automotive operating temperature range, it becomes important for manufacturing reasons. High manufacturing temperatures can degrade the on chip circuitry or can render such sensor functions impossible. However, low melting points for materials that are used to connect the sensor parts may cause failure as well. This can be the case, if higher temperatures are applied in subsequent manufacturing steps, e.g. if the packaged sensor is welded to a pressure vessel. The solder would melt and destroy the connection. The curing temperature of plastic or elastic materials shows the same problems for high temperatures. Drastic change of material properties beyond the glass transition temperature limits the use of these materials.[37, 38]

For electronic reasons, it is desirable to use a material for the transducer that has little or no temperature dependency on the sensing effect. An example for this principle is the capacitive pressure sensors that have outstanding primary temperature independence. However, the piezoresistive effect in silicon is highly temperature dependent and additional circuitry is needed for compensation. [37]

The choice of the type of silicon that is used for the sensing element is of great importance. The crystallographic orientation results in different stress and angular dependencies of the piezoresistive coefficients. [5]

Low ionic impurities are essential for materials that are in contact with conductors. Mobile ions are a major threat for high temperature applications. Therefore, the material selection should avoid any pollution of conductive parts. This limits the choice of possible coatings and adhesives that are in direct contact with the sensing die. [37]

Impurity atoms that are migrating at higher temperatures from contact points into the silicon can also degrade the sensor performance. To avoid this, it is necessary to plate additional layers as diffusion barriers onto the bonding areas.

The chemical resistance of the used materials is also of high importance. The automotive environment is one that features a large variety of aggressive chemicals. The material choice has to make sure that the sensor withstands the attack in the desired lifetime. [38, 85]

In absolute pressure sensing applications, the leakage rate of the packaging materials is of high interest. The long-term stability of the sensor depends heavily on this factor. It is also important in the cases in which the measured fluid is highly hazardous to the environment. [38, 86]

The cost of the used materials should be kept low. The variation between different shipment has to be small to keep the calibration process at low costs. For manufacturing processes it is important to choose materials with a high availability and exchangeability between different suppliers. Certain applications may make it necessary to employ special materials, but in general, off the shelf materials should be considered first. [4]

Finally, the lifetime of material components that are used for manufacturing is of high interest for the manufacturing process. Since the amount of applied adhesives is small, even for large volume production, the shelf lifetime and the lifetime in the production should be considerably high.

### 4.1.5 Strength

The sensor has to withstand many different mechanical loads. Therefore, the strength of the package materials is important to ensure the desired lifetime for the sensor.

The applied pressure induces stresses in the membrane. The maximum stresses are located at the middle of the edge of a square membrane or at the edge of a circular membrane. These stresses have to be significantly lower than

the yield stress of the sensor material. This has also to be true for the bonding material that attaches the die to the substrate. However, since the footprint of the die has to be relatively large to ensure adhesion, this criterion is less important.

In most applications, the sensor is subject to pressure changes. Therefore, the stresses in the die vary with changing loads. This may result in fatigue problems. Since silicon is a single crystalline material with low dislocation density, fatigue is a minor problem for the die itself. However, the die attach and the substrate are prone to this kind of failure. The cyclic pressure changes can result in cracks, especially when the die attach is not ideally applied.

The sensor has to be designed to withstand mechanical vibrations. In the field of automotive applications, the main source of cyclic excitations is the engine. The maximum speed for typical applications is below 10,000 rpm. This means that the main excitation, resulting from the combustion process is below 350 Hz. Automotive testing schemes prescribe tests in a frequency range up to 2 kHz to ensure that the sensor survives the designed life cycle. The lowest natural frequency of the sensor has to be well above this expected actual frequency range. The critical part is the diaphragm as a suspended structure. The design has to maximize the resonant frequency by stiffening the membrane or lowering the attached mass. Silicon with its high elastic modulus and low specific density is an ideal material to reach this requirement.

Another strength problem is mechanical shock survivability. The sensor is subjected to mechanical shocks during handling and application, e.g. dropping of

the sensor or rough road conditions. The design has to ensure that cantilevered elements like the diaphragm are protected from shocks or be strong enough to withstand these influences.

## 4.2 Design Methodology

The design of the sensor is oriented on the possibilities of the fabrication process. A good understanding of these processes is therefore essential. The mechanical design has to ensure the integrity of the stucture. The finite element method is an important tool for the designer. The last part of this chapter shows the aspects of the signal generation and signal conditioning.

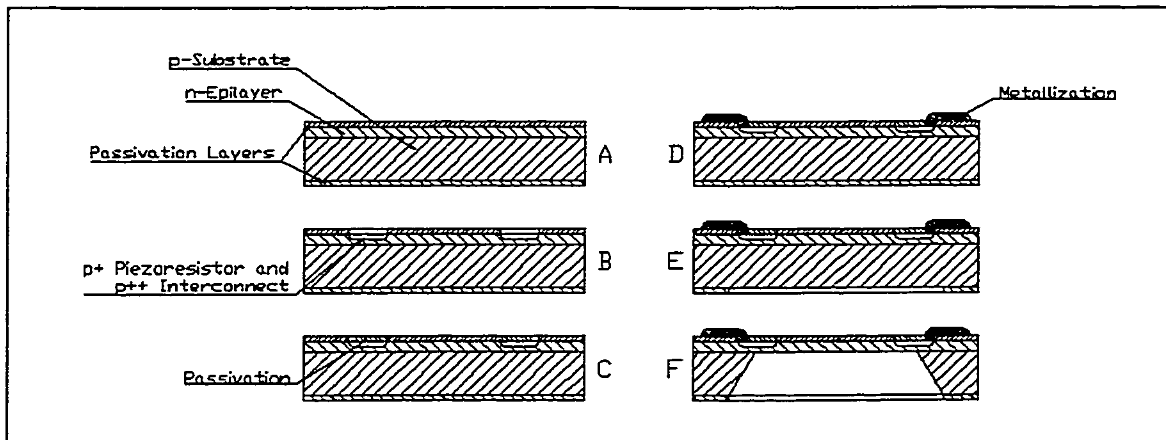


Figure 4-6: Overview over the Fabrication Process
A Wafer with Epitaxial Layer and Passivation Layers
B Shaping of the Passivation Layer and Implantation of the Piezoresistors and Contact Strips
C Passivation of the Electrical Components and Opening of a Contact Window for Metal Contact
D Metal Deposition and Shaping
E Shaping of the Backside Passivation
F Anisotropic Etching of the Cavity

### 4.2.1 Fabrication Processes

This chapter describes the fabrication of a typical silicon based micromachined pressure sensor die. Figure (4-6) gives an illustration of the generic processes.

The fabrication of silicon based MEMS starts with the production of the silicon wafer. Single crystal silicon is made from silicon oxide, which exists in the natural state in the form of pure sand. Two different processes are available for the production of single crystal silicon:

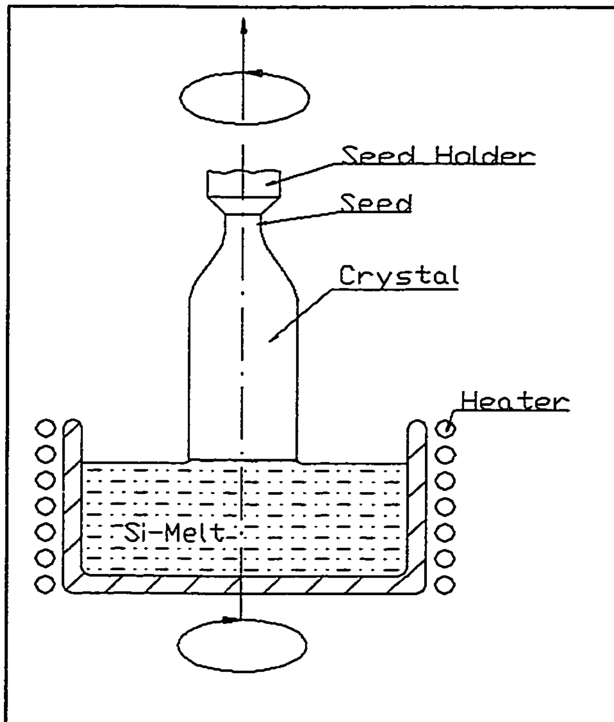


Figure 4-7: Czochralski Techique

The Czochralski technique uses a furnace to melt the silicon. The seed crystal is inserted in the melt and then slowly withdrawn as illustrated in Figure (4-7). The seedholder and the crucible rotate in opposite directions. A noble gas such as Argon is used to protect the growth from environmental influences. The typical growth rate is a few millimeters per second. It is possible to dope the silicon in this process. Typically, the concentration of the dopant in the melt rises during the formation of the crystal. The reason for this phenomenon is the different

concentration of the dopant in the melt and in the crystal, which is expressed for a material by the equilibrium segregation coefficient $k_0$:

$$k_0 = \frac{C_S}{C_L} \tag{4-6}$$

where $C_S$ and $C_L$ are respectively the equilibrium concentrations of the dopant in the respective solid and liquid states. Since $k_0$ is usually smaller than 1, the dopant is rejected during the growth, therefore concentrating in the melt. As a result, the dopant concentration in the crystal changes during the process. Another problem of this process is the possibility of the incorporation of impurities from the wall of the furnace. [6, 87]

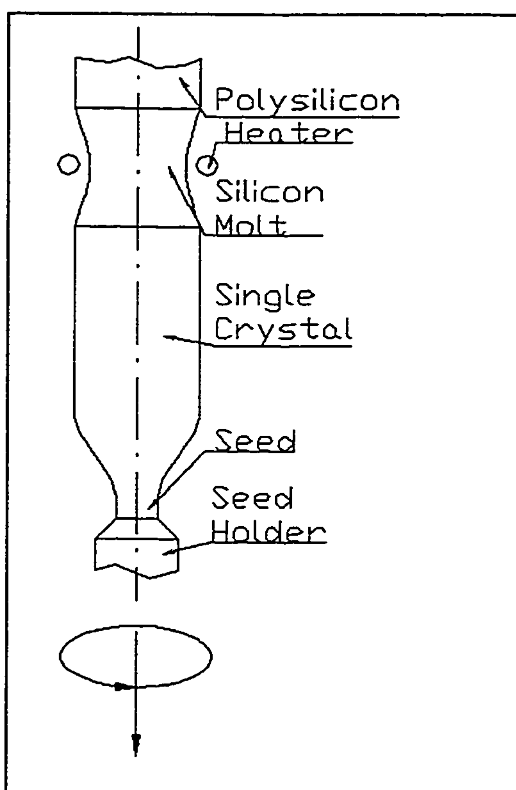


Figure 4-8: Float Zone Process

The float zone process (Figure (4-8)) uses solid polysilicon as a material source. It is formed to a rod covered by quartz and heated by radio frequency coils in a noble gas (Argon). A zone of molten material forms and is contacted with a seed crystal. The rod is moving through the melting zone, converting itself into the single crystal. This process enables higher purity levels because of no contact with the heater. The dopant concentrates in the course of the process in the molten zone as described

above. As a result, the doping concentration rises with increasing length of the crystal during the process. [6, 87]

Subsequently the crystal orientation is determined by x-ray or electron beam diffractions. The orientation is marked by grinding one or more flats on the crystal. The largest or primary flat serves mainly as a positioning reference. The smaller secondary flat identifies the orientation and the doping type. A diamond saw is used to slice the crystal into wafers. The standardized surface flatness is achieved by polishing of the surface with aluminum oxide powder in glycerin. The edges of the wafers are rounded to remove micro cracks to reduce the sources for wafer fracture. [6]

For a typical bulk micromachined pressure sensor, the standard wafer thickness accuracy is not sufficient to enable the production of uniform membranes. Since the growth of an epitaxial layer on top of a wafer can be controlled very precisely, this technique is utilized to deposit a layer with an opposite doping, usually an n-type layer onto a p-type substrate. This enables the use of p-type piezoresistors, which have superior properties over n-type resistors. The exptaxial layer is usually grown in a CVD process as described before. [6]

Subsequently a silicon oxide layer is grown on the wafer. The layer is utilized as a mask for subsequent etching and as a surface passivation. The

oxidation can be done in a dry or wet process. The dry process uses oxygen, which results in :

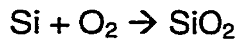

$$Si + O_2 \rightarrow SiO_2$$

whereas the wet process needs the addition of water in the process as shown below:

$$Si + 2H_2O \rightarrow SiO_2 + 2H_2$$

The silicon oxide that is formed from the silicon has a volume more than double of the consumed silicon. It also has a lower thermal expansion coefficient than the silicon substrate. Therefore, the silicon oxide layer is compressive at room temperature. [6]

Another masking and passivation material is silicon nitride. This material can be deposited at high temperatures by LPCVD or at low temperatures with PECVD. The low temperature process is preferred to decrease the residual stresses in the material. The PECVD process allows also better control over the properties of the deposited film. Typical reactions are:

$$SiH_4 + NH_3 \rightarrow SiNH + 3H_2$$

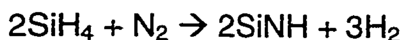

$$2SiH_4 + N_2 \rightarrow 2SiNH + 3H_2$$

The silicon nitride films have a low tensile stress. The use of radio frequency enhanced PECVD enables the deposition of layers with tensile and compressive stresses. [6]

The residual stresses result in nonlinearities in the output of the sensor. It is therefore important to minimize this influence. One method is to use the

opposite character of the layers of silicon oxide and silicon nitride to cancel the stresses within the surface layer. However, the stress relaxation at the interface of the layers can degrade the long-term stability of the sensor. The use of silicon nitride, deposited by RFPECVD, enables the deposition of one virtually stress free layer. [6]

At this stage, alignment marks are patterned on both sides of the wafer. These marks allow the correct positioning of the piezoresistors on the front side of the wafer with respect to the cavity in the backside. In the next step, the piezoresistors are diffused into the epitaxial layer. These are usually boron-doped $p^-$-type regions. The doping profile influences the piezoresistive constants, the resistivity, and piezoresistive temperature coefficient. It is desirable to create shallow piezoresistive regions to minimize the stress averaging effect of the resistor. The doping process is used to minimize the temperature dependence of the system. This is possible, because the temperature coefficients of the piezoresistivity and the resistivity are dependent of the dopant concentration. Ideally, the temperature coefficient of the resistivity and the coefficient of the piezoresistivity are matched. As a result, the bridge resistance would increase over temperature whereas the piesoresistive effect would decrease. This decrease results in a decreasing sensitivity. The increase of the bridge resistance is used to increase the output voltage with temperature. The combination of both processes would cancel the temperature effect on the output. However, the manufacturing precision does not allow an exact

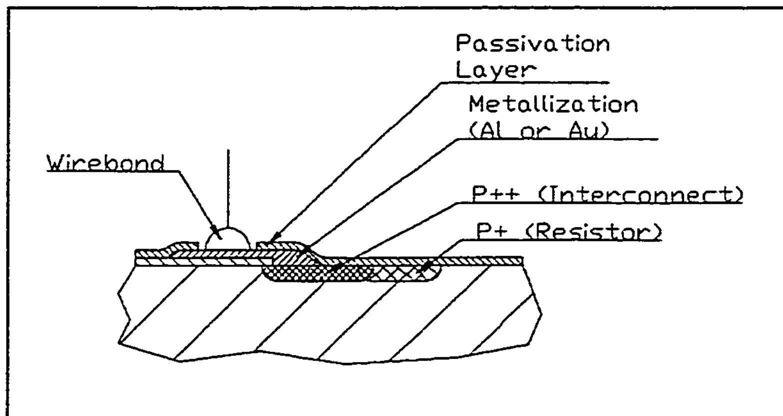


Figure 4-9: Electrical Layers in Die Surface

compensation. In typical applications, it is desired to have a higher increase of resistivity than the decrease of sensitivity. This enables the compensation with additional circuitry. The combination can be achieved at two doping concentrations: the lightly doped regions ($p^+$) and the highly doped regions ($p^{++}$). Since the piesoresistive effect is decreasing with increasing doping level, the piezoresistors are created with light doping. The heavily doped region is utilized for contacts. The higher doping level results in lower resistivity as well as lower stress and temperature sensitivity. [1]

Heavily doped $p^{++}$-type regions contact the piezoresistors. These intermediate contacts are important to ensure a low ohmic resistivity to the aluminum pads (Figure (4-9)). It is crucial to align these intermediate contacts precisely to the piezoresistors. Any unsymmetry adds an imbalance and therefore an offset to the output of the sensor. [1]

The doped regions are activated by a heating process that brings the wafer to a temperature of 1000°C. This means that the crystallographic dislocations that result from the ion implantation are minimized and the boron atoms are integrated into the lattice.

The subsequent step prepares the metallization with the removal of the coating to enable the contact to the $p^+$-region and the n-type substrate. This is done in a photolithographic step. The metal, usually aluminum or gold, is deposited and patterned in another lithographic process (Figure (4-10)). In addition to the wiring contacts, a metal grid is laid over the wafer to contact the substrate for the electrochemical etch stop. The design should avoid metal depositions onto the diaphragm area. These deposits degrade the sensor performance because of the high thermal coefficient of expansion and mechanical hysteresis. Conductive strips to contact the resistors are formed by the $p^{++}$-regions that are not prone to these problems. [1]

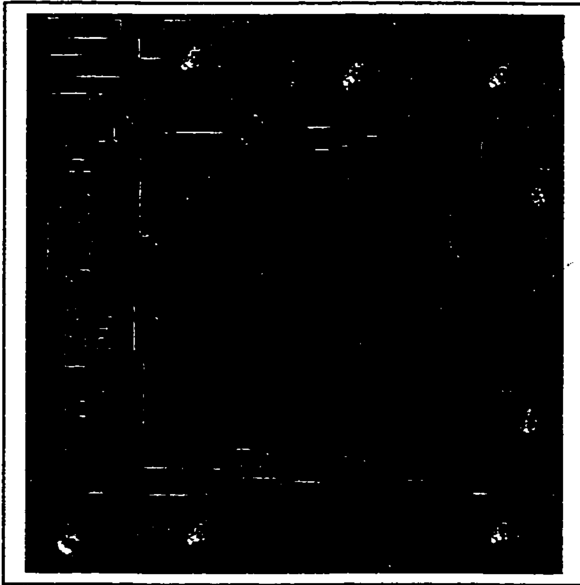

Figure 4-10: Contacts on Die Surface (Copyright of Lucas NovaSensor, with Permission)

The processing of the front side is finished by an alloy step. This heating enables aluminum atoms to diffuse into the silicon and vice versa. The diffusion process improves the contact and reduces the electrical resistance. This is of high importance since the output is proportional to the relative change of the resistance. Consequently, the design has to ensure that the contact strips have the lowest possible contribution to the bridge resistance.

The backside of the wafer is passivated and the front side is protected from the anisotropic etchant by special fixtures. The passivation layer is shaped by a lithographic step followed by wet etching. The correct mask alignment is very important, because the dislocation of the mask results in an incorrect placement of the piezoresistors. The uniformity of the wafer is also very important for this step. Since the diaphragm size is determined by the mask size on the backside of the wafer, a thickness variation results in the variation of the membrane dimensions. The commonly used KOH etching system that is extensively investigated and enables fast processes makes it necessary to use silicon nitride or thick silicon oxide layers as a masks. Other possibilities are EDP (ethylene diamine pyrocatechol) and TMAH (tetramethyl ammonium hydroxine). This allows the use of silicon oxide, that is easily grown as a masking layer or can be utilized as an etch stop in special wafers. These SIMOX wafers contain a layer of silicon oxide between two silicon layers. The compatibility of the TMAH system to IC processes reduces the necessary effort to isolate the front side of the wafer during the ansiotropic etch step. Deep reactive ion etching can also be used to shape the diaphragm. This highly anisotropic process allows the formation of vertical sidewalls, which minimizes the real estate needed for the sensor. It can also be utilized to thin the front side of the diaphragm, which is impossible with the above methods because of the ionic impurities that would be introduced. However, this method has one major shortcoming, the lack of an etch stop. [6, 1]

The electrochemical etch stop is usually preferred over the dopant dependent etch stop, because it allows the integration of electronic circuits in the same region. This technique utilizes the effect of a biased p-n junction. Since the passivation potential for these two types of layers is different, the chemical reaction is virtually stopped when it reaches the n-type epitaxial layer. The diaphragm thickness is therefore determined by the precision of the epitaxial layer deposition. [1]

After the wafer is etched at the backside to form the cavity, the packaging process determines the following procedures. Depending on the application of the sensor, the wafer is mounted on a die attach and diced by mechanical means. This dicing limits the outer shape of the die to a rectangle or square. The introduction of nonmechanical dicing techniques would allow different structures such as honeycomb dies. This change in the die shape would support other possible diaphragm shapes, e.g. circular diaphragms that are currently not very popular. [1]

The wafer can be mounted on Pyrex. This material was developed to match the thermal coefficient of expansion of silicon. The anodic bonding technique that is used for this purpose ensures an excellent sealing of the structure. Voids can be detected by the fringes that result of the optical discontinuities caused by imperfect bonds. The bonding process takes place at temperatures of about 180 to 500°C and a bias of 200 to 1000 V. Under these conditions, the glass softens and the mobile sodium ions in the Pyrex move

towards the cathode creating a space charge in the interface region. The resulting electrostatic force enables the bond. [6, 1]

Glass frits use the same bonding principle to connect two silicon wafers. However, the fact that the Pyrex paste is applied between two nontransparent wafers makes failure detection more difficult.

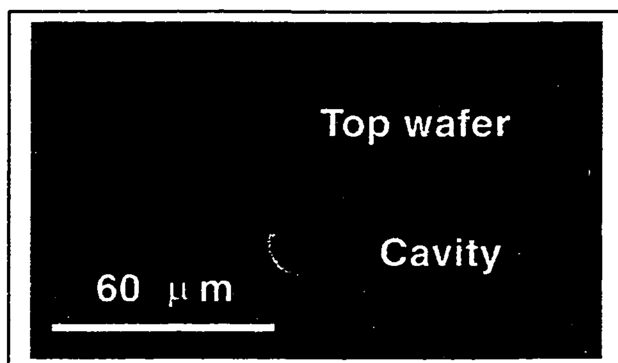


Figure 4-11: Silicon Fusion Bonding (Copyright of Lucas NovaSensor, with Permission)

Silicon fusion bonding (SFB) is method to mate single crystalline silicon wafers to each other (Figure (4-11)). The wafers are hydrated beforehand to create a hydrophilic layer. The contact between these layers creates an instant bond, the silanol bond. A chemical reaction at furnace temperatures of 900 to 1200°C dehydrates the bond, creating the siloxane network that forms the final bond between the wafers. This process is nearly ideal because the resulting structure consists of only one material, eliminating thermal mismatch problems. Since each of the wafers can be machined before the mating process, silicon fusion bonding enables the formation of very complex structures. With this technique it is possible to reduce the real estate per die dramatically. In conjunction with isotropic etching it allows the precise manufacturing of circular shaped membranes. [6]

### 4.2.2 Mechanics

The mechanical design is a very important step in the overall sensor design. The correct prediction of the mechanical behavior of the transducer decreases the necessary number of prototypes and therefore the development cycle time. The mechanical modeling involves usually the use of the finite element method. However, for design purposes it is important to use simple formulas for “back-of-the-envelop” calculations to determine conceptual dimensions of the sensor.

The desired pressure range determines the proportions of the used diaphragm. The highest applicable pressure is the one at which the yield stress of any part of the structure, usually the edge of the membrane, is reached. Another criterion is the contact of the membrane to other parts of the sensor. This is especially interesting for capacitive sensors that feature a small gap between the two electrodes. Usually a high safety factor, in the range of 5 to 20 is used to give enough overpressure capability. [68]

The two parameters for the design process are the size of the diaphragm and its thickness. Ideally the deflection of the diaphragm at full-scale pressure should be small compared to the thickness of the membrane. This keeps nonlinearities at a minimum. This imposes problems at the low and high pressure range. Special designs for these ranges are necessary. For low-pressure sensors, the designer has to consider the use of bossed or convoluted diaphragms. The bosses result in a local stiffening of the structures. This

decreases the deflection of the diaphragm and therefore the nonlinear membrane stresses and concentrates the linear bending stresses in the thinner regions where the resistors are located. In general, the output of these sensors is of higher linearity than the output of sensors that use a simple diaphragm. Whereas the bossed diaphragm can be manufactured using the traditional technology, the convoluted geometry relies on etching on both sides of the wafer. This introduces major problems since the common wet etching techniques are not compatible to electronic structures and other processes such as deep reactive ion etching (DRIE) have to be employed. [68, 88]

Beside these mechanical constrains there are fabrication constrains as well. Since the doping process is highly sensitive, it is a common practice to use the same doping profile for all sensors produced. This constrains the minimum thickness and diaphragm size. Piezoresistors that are large with respect to these parameters cause large averaging effects over regions with decreasing stresses, which results in a lower sensitivity of the die. The maximum stress is determined by the available solutions of the differential equation of the deflection of plates. The diaphragm size and the needed bonding area for the die determine the initial die size. The footprint of the sensor has to maintain a certain area for a specific adhesive to ensure the integrity of the bond. This size is usually not determined by the bulk properties of the adhesive, but by the adhesion properties and the manufacturing process. These data define the initial geometry of the sensor.

In a first analytical step, the initial die geometry is used to build a finite

element model. The model includes not only the initial geometry but also surface layers that are deposited in standardized processes during fabrication. The regions in which the piezoresistors should be placed are usually modeled using the submodeling technique. This process allows high mesh density and fast geometry variations in small regions of interest without reaching the computational limits. The die is subjected to the expected pressures and temperatures of the specific application. These tests can verify the initial design and predict the behavior of the actual sensor. The data can be used to place the piezoresistors in the regions of the maximum stresses for maximum sensitivity and linearity of the device. Vital information such as the burst pressure can be determined with this method. [32]

For high accuracy models, the deposition processes can be simulated. Special elements have to be used that can be added and subtracted by the change of element parameters at certain stages of calculation. The ANSYS® program provides such elements as birth and death elements. These elements can be used to model the respective surface micromachining and bulk fabrication processes. The model is created with all elements that are needed at certain stages of the simulation. Depending on the process, the elements are activated or deactivated, simulating additive or subtractive processes. Results of this type of modeling often include the residual stresses resulting from the fabrication process. This enables the analysis of the residual stresses resulting from the fabrication process. This can alter the sensivity of the device. However,

in comparison analysis that involve the same ultra-thin surface coating, this effect is often neglected for computational reasons, if the influence of other design elements is the focus of interest. [32, 68, 89]

It is important to keep the internal stresses at a minimum. They alter not only the output of the sensor but degrade the long-term stability because of creep and cracking especially of polycrystalline materials. For this reason, the thickness of deposited layers should be minimized with respect to the function of the layer. The deposition parameters have to be optimized to lower the stresses due to the coating process. These two considerations limit the influence of internal stresses on the sensor output. [72, 88]

In the submodeling technique, the die is meshed with a relatively coarse mesh to cover the overall behavior. The area of interest is modeled separately and the results of the coarse model are interpolated and used as the boundary conditions for the submodel. In this way a more accurate solution is obtained in the region of interest. However, it is crucial to verify that the boundary of the submodel are not too close to a singularity that would disturb the coarse solution. [32]

In the case of special membrane geometries for high and low pressures the use of FEM for the positioning of the piezoresistors and the optimization of the geometric elements such as bosses or corrugations is imperative. The simple analytical solutions are not applicable for nonuniform geometries. For thick diaphragms that are needed for high pressure ranges, the analytical solution is

only a rough estimation since the assumed boundary conditions, i.e. clamped at the edges, are not longer valid. The deformation of the supporting material cannot be neglected. [32, 88]

The modal analysis has to insure that the natural frequency of the structure is sufficiently higher than the highest expected excitation frequency. This is especially critical for bossed membranes because of the mass concentration towards the center and the relative high flexibility of the thin regions.

The use of FEM also allows a thermal analysis of the structure. The following different cases are of interest:

- Thermal equilibrium with the ambient temperature
- Thermal shock
- Local gradients due to power dissipation of electronic parts

The first case is of interest because of influence of the package on the overall performance of the sensor. The thermal mismatch between the different materials of the package results in changing thermal stresses in the die. Ideally, the die should be isolated from these stresses. The traditional solution for this problem is the use of spacers. FEM is used to optimize the size of these elements. Complex models that include the die, the die attach, and the headers are necessary for this process. However, mechanical spacers cause additional packaging cost. It is therefore of high interest to examine the influence of the die attach materials for dies that are directly bonded to the header. [32]

Thermal shock is another case that has to be considered. The sudden change of temperature causes internal stresses in the material due to thermal gradients and the resulting differences in the expansion of the structure. It also influences the electronic components.

Local thermal gradients are important during warm up periods. This is especially interesting, if two resistors are spaced closely whereas the other two are at the edge of the diaphragm. The local heating can distort the bridge balance and cause an undesired output.

Another advantage of the use of FEM to test the die prior production is that the overpressure protection elements can be included into the model. The use of contact elements allows the correct simulation of the behavior of the die, if the membrane gets into contact with these protection surfaces. These elements can also be used to simulate the behavior of capacitive pressure sensors that use the touch mode for the measurement. [70]

### 4.2.3 Electrical and Electronics

The electrical design process has to optimize the signal conversion from mechanical stresses into an electrical signal. This section is focused on the considerations for the signal generation of piezoresistive sensors.

The piezoresistive principle utilizes the influence of stress to change the resistivity of a material. This effect can be observed in most materials, but is especially strong in semiconductors such as silicon. In general, the

piezoresistivity is described by a second order tensor $\underline{\pi}$. For a cubic crystal as silicon, the tensor can be written as a 6x6 matrix that is aligned with the symmetry axes of the crystal. A set of only six coefficients is needed to describe the electrical behavior of silicon when stress is applied. The piezoresistive constants of silicon at room temperature are shown in Table 4-1. [6, 50, 81, 90, 91]

Table 4-1: Piezoresistive Coefficients of Silicon at Room Temperature in (100) Orientation (Typical Values)

| | $\pi_{11}$ in $10^{-11}$ Pa$^{-1}$ | $\pi_{12}$ in $10^{-11}$ Pa$^{-1}$ | $\pi_{44}$ in $10^{-11}$ Pa$^{-1}$ |
|---|---|---|---|
| p-type Silicon | +6.6 | -1.1 | +138.1 |
| n-type Silicon | -102.2 | +53.4 | -13.6 |

The resistance change can be calculated from

$$\frac{\Delta R}{R} = \sigma_L \pi_L + \sigma_T \pi_T \tag{4-7}$$

where $\sigma_L$ is the longitudinal stress component parallel to the direction of the current, $\sigma_T$ is the transversal stress component, perpendicular to the direction of the current, $\pi_L$ and $\pi_T$ are the respective longitudinal

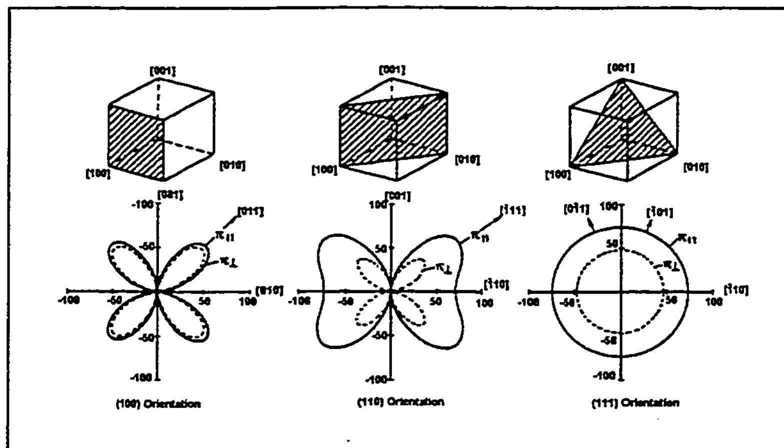

Figure 4-12: Piezoresistive Constants Depending on the Crystallographic Orientation

and transversal piezoresistive coefficients. These coefficients are mapped for different crystallographic orientations. The actual values are depending on the angle of the piezoresistor with respect to the crystal as shown in Figure (4-12). [6, 91]

Common designs have piezoresistors in the [110] direction. This has two reasons. The first reason is that the wafers used in the mainstream integrated circuit industry are in the (100) plane that are therefore easily available for micromachining purposes. The second reason is that the longitudinal and transversal coefficients of piezoresistivity have nearly the same value but opposite sign for this orientation in p-type silicon (Figure (4-11)).

However, the sensivity is higher for (110) wafers with the resistors in the [111] direction. The limitation of this optimization is the manufacturability. The common anisotropic etchants are unsuitable to form the sensing elements. New techniques such as MPE and DRIE are necessary to form the diaphragm. The problem with these processes is that no etch stop techniques are available. This degrades the tolerances of the membrane thickness to the relative low precision of the wafer flatness. [92]

For <111> wafers, the coefficients of piezoresistivity are independent of the orientation of the resistors. This eliminates resistance variations due to misalignment of the resistors. [91]

For the [110] orientation of a (100) the values can be obtained from

$$\pi_L = \frac{1}{2}\left(\pi_{11} + \pi_{12} + \pi_{44}\right) \qquad (4\text{-}8)$$

$$\pi_T = \frac{1}{2}(\pi_{11} + \pi_{12} - \pi_{44}) \quad (4\text{-}9)$$

A commonly used approximation for the change of the resistivity can be derived from the Equations (4-8,9) and the dominance of $\pi_{44}$ in p-silicon:

$$\frac{\Delta R}{R} = \frac{\pi_{44}}{2}(\sigma_L - \sigma_T) \quad (4\text{-}10)$$

where $\sigma_L$ is the longitudinal stress component parallel to the direction of the current, $\sigma_T$ is the transversal stress component.

Using the dominance of the other two coefficients for n-silicon, an approximation formula for the <110> direction is:

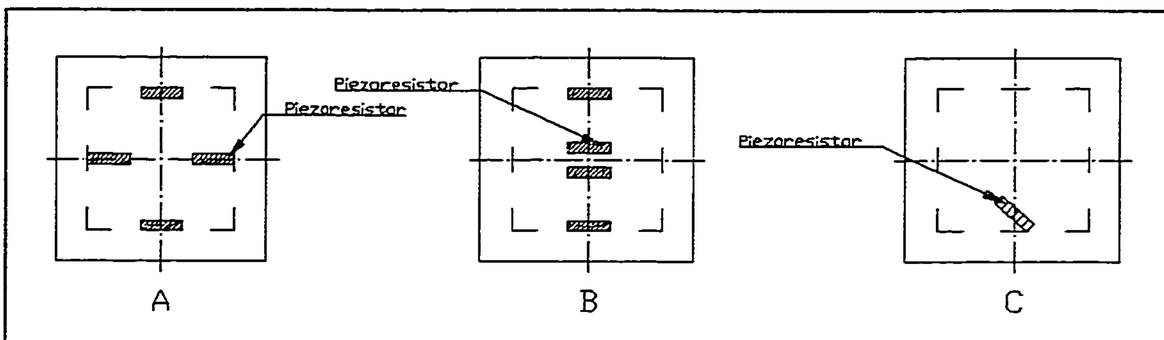


Figure 4-13: Typical Resistor Placements
A Four Resistors at the Edges
B Two Resistors at the Edges, two Resistors in the Center
C One Resistor at the Edge under 45°

$$\frac{\Delta R}{R} = \frac{\pi_{11} + \pi_{12}}{2}(\sigma_L + \sigma_T) \quad (4\text{-}11)$$

These approximations are only valid, if the resistor size is small compared with the diaphragm or a uniform stress field is applied. [6,91]

The resistors are usually positioned at the places where the highest stresses are expected (Figure (4-13)). For thin square diaphragms, this is the center of the edge. Commonly two resistors are placed parallel to the edge and two perpendicular to it. As a result of this placement, two resistors will increase their resistance whereas the other two will lower the resistance. This design ensures maximum symmetry and minimizes therefore common mode influences such as the thermal dependence of the piezoresistive coefficients. This design is also compatible to the use of a center boss. [6,91]

Another typical placement locates all four resistors in one line at the middle of the membrane. Two resistors are located at the edge and the others in the middle of the diaphragm. In conjunction with a rectangular membrane, this increases the sensitivity if the resistors are orientated along the <100> direction of a (100) wafer. This placement of the resistors allows the use of a single center boss or double bosses to concentrate the stresses and minimize the nonlinearity of the output. However, this design has a lower symmetry and the power dissipation of the resistors that are closely positioned at the midpoint of the membrane causes nonlinear temperature effects. [6]

The third resistor placement that is commercially used utilizes the shear stress. A single resistor is placed on the membrane under a 45° angle. This single resistor is employed to measure the stresses. The use of the single resistor minimizes the necessary wiring. It has also the lowest symmetry and is

highly prone to thermal influences. Higher compensation efforts are therefore needed. [50, 92, 93]

Typically, a gage factor is determined for the device that couples the change in resistance to the applied strain:

$$G = \frac{\frac{\Delta R}{R}}{\varepsilon} \tag{4-12}$$

where G is the gage factor, R is the resistance, and ε is the strain in the membrane. [6, 81]

The capacitive sensing principle measures the resulting deflection of the diaphragm as a change of capacitance. A plate capacitor is formed by parts of the membrane and the substrate. From the equation for the capacitance

$$C = \frac{\varepsilon A}{d} \tag{4-13}$$

where C is the capacitance, ε is the dielectric coefficient, A is the area of the plate, and d the spacing. For small deflections, the change in capacitance can be determined to:

$$\frac{\Delta C}{C} = \frac{\Delta d}{d - \Delta d} \tag{4-14}$$

where C and ΔC are the capacitance and its change, respectively, d and Δd the spacing of the two plates and its change.

Equation (4-14) shows that the capacitve change is highly nonlinear with respect to the change of the gap between the two electrodes. For a higher

sensivity, the gap between the two capacitor plates has to be minimized in order to maximize the change in capacitance. Ideally, the area of the conductive regions should be kept small to minimize second order effects on the measurement. [51]

As mentioned before, it is desirable to design the sensor as symmetrically as possible to minimize the temperature influence on the measurement. As a part of this effort, it is important, to create the electrical connections with respect to this rule. In the case of a piezoresistive sensor, the diffused conductor strips in the diaphragm should ideally contact the resistors so that the effective length is the same for both sides of the Wheatstone Bridge. In order to minimize the effect of the piezoresistance in these conductors, the angle has to be optimized. Silicon wafers with a <100> orientation offer the advantage over all other orientations that the effect deceases at 45° to the <110> orientation under which the resistors are implanted. It is also important to minimize the resistance in these electrical connections for a maximum sensivity. [91]

### 4.2.4 Signal Generation and Condition

The output signal of a piezoresistive pressure sensor is usually generated in a Wheatstone Bridge. This technique is used to amplify the effect of the resistance change and to minimize the temperature effect on the piezoresistors themselves. However, this first conditioning is usually not sufficient and additional circuitry is necessary to generate the desired output signal. This

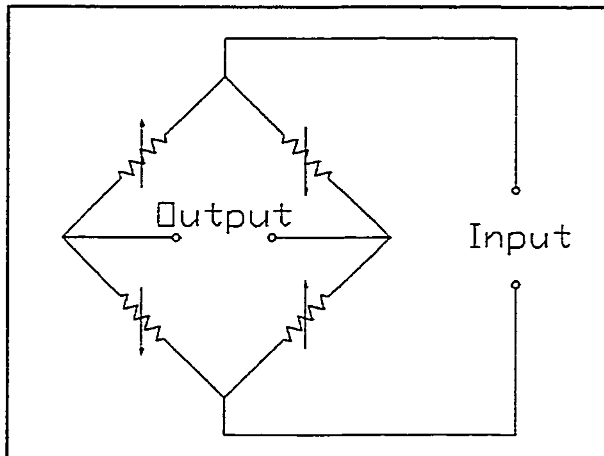

Figure 4-14: Wheatstone Bridge

chapter covers general aspects of the common compensation and signal conditioning techniques.

The fundamental elements of the Wheatstone Bridge are four resistors (Figure (4-14)). It is not necessary that all four elements change their value, however a full bridge circuit has the highest output and the best temperature compensation. For this reason, most commercial sensors employ the full bridge. [94]

Typically, the bridge is used in a voltage-sensitive mode. This means that the output is connected with a high-impedance device that amplifies the signal for further processing. In this case, the output voltage can be determined by:

$$U_O = U_i\left(\frac{R_2}{R_1+R_2} - \frac{R_4}{R_3+R_4}\right) \qquad (4\text{-}15)$$

where $U_O$ is the output voltage, $U_i$ is the input voltage, $R_n$ are the resistivities of the resistors (n=1,2,3,4).

Ideally, the resistance change of neighboring resistors should be of the same magnitude but opposite sign. This can be achieved by the placement of the resistors in zones with opposite stresses or by the choice of the orientation of the resistors. Assuming this, the output voltage for a bridge that has initially a zero output is:

$$U_O = U_I\left(\frac{R_2+\Delta R}{R_1+R_2}-\frac{R_4-\Delta R}{R_3+R_4}\right) \tag{4-16}$$

For the case of equal resistors, the change is:

$$U_O = U_I\frac{\Delta R}{R} \tag{4-17}$$

It can be seen that it is desirable to keep the overall resistance small with respect to the expected resistance change. [94]

The signal generated by this type of Wheatstone Bridge has to be conditioned. The typical functions of the signal conditioning process are:

- Offset balancing and temperature compensation
- Sensitivity normalization, linearization, and temperature compensation
- Special conditioning (e.g. static pressure effect, temperature output)

These effects result from the manufacturing precision and the physical properties of the used materials. [1]

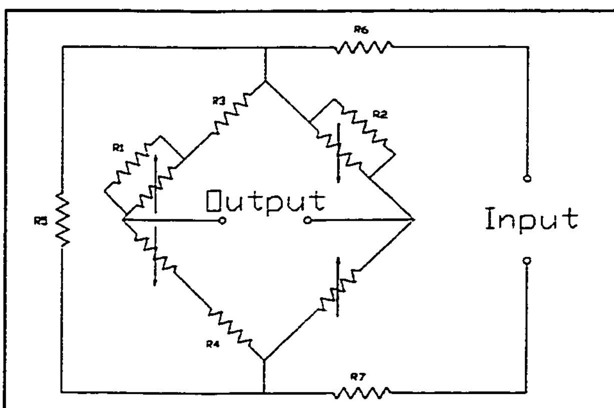


Figure 4-15: Basic Compensation Circuit

The offset voltage results from a mismatch of the resistors in the bridge or residual stresses. The bridge circuit is unbalanced and the output is nonzero without any pressure applied. The typical requirement of 1% full-scale output makes additional circuitry either on or off the chip necessary (Figure (4-15)). The offset is also temperature dependent

since residual stresses and the resistance of the strain gages change with temperature. [1]

High and low pressure sensors are especially prone to mechanical nonlinearities. Special designs can minimize this problem, but for high precision applications, the nonlinearities have to be compensated. Ideally, the sensor has to maintain a specified sensivity over the whole pressure and temperature range. [1]

For special applications other conditioning processes become important. For high-precision differential pressure sensors, the dependence of the output on the applied static pressure level becomes important. In other cases, the temperature of the sensor has to be measured for further data processing. [1]

The bridge circuit can be utilized in a constant current and constant voltage mode. In the constant voltage mode, the output is directly proportional to the sensivity:

$$U_{FS}=SU_B \qquad (4\text{-}18)$$

where $U_{FS}$ is the full scale output voltage, $U_B$ is the bridge voltage, and S is the sensivity. The sensivity is temperature dependent and decreases with increase of the temperature due to the fact that the piezoresistivity of the silicon decreases with increasing temperature. [1, 95]

In the constant current mode, the output is also depending on the bridge resistance $R_B$:

$$U_{FS} = SR_B I \qquad (4\text{-}19)$$

where I is the input current. This additional dependency offers the possibility to utilize the change of the bridge resistance with temperature to compensate the output voltage on a simple basis. This is also the disadvantage of this mode with respect to the previous, because it introduces additional variables that effect the output and can lower the accuracy of the compensation. [1, 95]

The compensation process can be based on iterative active processes or modeled test data. The first process is very time consuming and is only suitable for smaller production volumes. The latter method allows for a higher throughput while maintaining a good compensation. For this method, an analog model of the sensor is needed to evaluate the necessary adjustments from a small number of tests. In these models, certain resistances represent the effect of different sources of errors. The values of these parameters are determined by a testing procedure. With this data, the necessary compensation resistance values can be determined. [1]

In the constant current mode, the offset voltage can be compensated by the addition of a single resistor in series with one arm of the bridge. The compensation of the temperature dependency of this parameter can be achieved by shunting a resistor that is stable with respect to temperature across one arm of the bridge. This alters the temperature coefficient of this arm with respect to the others. The compensation of the full-scale output is achieved by a resistor that is parallel to the bridge and the compensation circuitry discussed above. [1, 95]

The compensation in the constant voltage mode changes the bridge voltage or the gain of the subsequent amplifier. This can be achieved with temperature insensitive resistors, thermistors or diodes in series to the sensor bridge. The resistor compensation results in a significant loss of full-scale output (up to 80%), which is not desirable. Thermistors have a large thermal change of resistivity but this is extremely nonlinear. The use of these devices in conjunction with resistors allows not only the compensation of this linearity but also for the internal full scale nonlinearity of the sensor. The third possible method, the use of diodes, offers a simple temperature compensation scheme. Since the bias and the temperature coefficient do not scale with the current, this compensation scheme is sensitive to the applied voltage. [1, 95]

For the applications in which resistors are used to compensate the output, laser trimming is often utilized to adjust the value of the resistance. This process is relatively slow because of its sequential character, newer approaches use electronic memory to compensate actively using the data stored in a batch mode. This electronic trimming becomes more and more popular. [49, 94, 96]

Even after this compensation the output voltage of the bridge circuit needs to be conditioned further. Since the voltage is relatively small (about 100mV), the signal has to be amplified. The raw output signal is usually applied to a circuit that includes operational amplifiers. These amplifiers have very high input impedances in the Megaohm range and have an extremely high gain (up to $10^6$).

The response of these devices is very fast. A problem is the offset that has to be adjusted by additional circuitry. [94]

Depending on the application, different filters are applied to minimize the environmental influences on the measurement. Filters are also important for the signal conditioning prior the digitalization of a signal. The input frequency range of has to be limited to avoid signal distortion in the sampling process. Since computers are more frequently used for control purposes, these applications become more important. [94]

It is common to use a standard voltage span such as 0-5 V for the signal processing. In some cases, it is useful to transmit the signal on a carrier frequency. This minimizes the necessary wiring because one channel can be used to transmit several measurements. [49]

Another standard output for sensors is the 4-20 mA signal, which is especially common in industrial applications. The signal conditioning circuitry that is integrated in the sensor is used to transform the voltage signal from the Wheatstone Bridge of the die into a current signal. The current is transmitted to a receiver. At the receiver, the signal is converted back into the voltage domain by a voltage divider. The receiver usually includes the constant voltage source (e.g. 24 V) that is used to feed the sensor. This type of signal condtioning is often preferred over voltage signals because it is relatively uneffected by long wire length. It also reduces the wiring effort since only two wires are needed for the power supply and the signal transmission. Consequently, the supply current of

this circuitry must be less than 4 mA for zero pressure which is the life zero for this signal type. [97]

### 4.2.5 Example Calculation

This chapter shows an example calculation of the output of a sensor at different temperatures. The stress values are taken from the FEM calculation of a floating die (see Chapter 5). A compensation example, using the adjustment of the input voltage is given and the determination of the resistor value is demonstrated.

The floating die is the ideal case of a sensor because no stresses are imposed by the mounting of the die. The following temperature values are used in the calculation:

$T_1$= 25°C

$T_2$= 125°C

It is further assumed that the full-scale pressure of p= 35kPa is applied. The piezoresistive constants are taken from Table (4-1):

$\pi_{11}$= 0.066 $GPa^{-1}$ (at 25°C)

$\pi_{12}$=-0.011 $GPa^{-1}$ (at 25°C)

$\pi_{44}$= 1.381 $GPa^{-1}$ (at 25°C)

The change of these values can be described with a linear model (Figure (4-16)):

$\pi(T) = \pi(1-TCP(T-T_{ref}))$ (4-20)

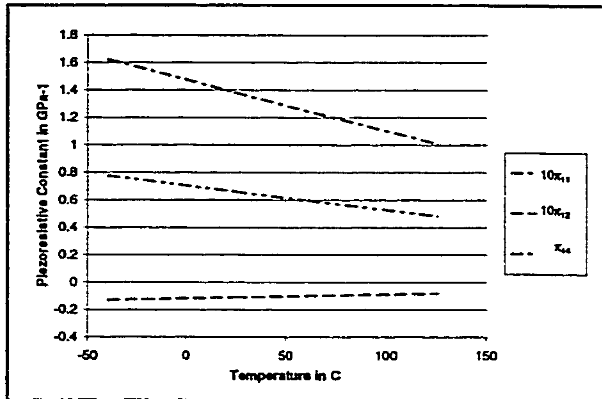


Figure 4-16: Piezoresistive Constants over Temperature

where $\pi(T)$ and $\pi$ are the piezoresistive coefficients at the temperature T and at reference temperature $T_{Ref}$, respectively, and TCP is the thermal coefficient of piezoresistivity ($0.0027K^{-1}$). [98]

The FEM calculation of the floating die yields the following average stresses in the piezoresistive region:

Table 4-2: Stresses in the Piezoresistive Region

| Stress Component | Region 1 (Resistor 1) | Region 2 (Resistor 2) |
|---|---|---|
| $\sigma_X$ in MPa | -49 | -15 |
| $\sigma_Z$ in MPa | -15 | -49 |

The piezoresistive constants have already the correct value for the first temperature. The resulting constants $\pi_L$ and $\pi_T$ can be determined using Equations (4-8, 9):

$$\pi_L = \frac{1}{2}(\pi_{11} + \pi_{12} + \pi_{44}) = \frac{10^{-11}}{2}(6.6 - 1.1 + 138.1)Pa = \underline{0.72nPa}$$

$$\pi_T = \frac{1}{2}(\pi_{11} + \pi_{12} - \pi_{44}) = \frac{10^{-11}}{2}(6.6 - 1.1 - 138.1)Pa = \underline{-0.66nPa}$$

Assuming that the Resistor 1 is oriented along the x-direction in the first region, then $\sigma_L$ is equal to $\sigma_{1x}$ and $\sigma_T$ is equal to $\sigma_{1z}$. With these values, the Equation (4-7) is used to calculated the relative change of the resistance:

$$a = \frac{\Delta R}{R} = \sigma_{1x}\pi_L + \sigma_{1z}\pi_T = -49\text{MPa} \cdot 0.72\text{GPa}^{-1} + 15\text{MPa} \cdot 0.66\text{GPa}^{-1} = \underline{-0.025}$$

Resistor 2 is also oriented along the x-direction, but is located in the second region. Consequently, the stresses in the longitudinal and transverse direction of the resistor have the same configuration:

$\sigma_L = \sigma_{2x}$

$\sigma_T = \sigma_{2z}$

and Equation (4-7) yields the value of the relative change in resistance:

$$b = \frac{\Delta R}{R} = \sigma_{2x}\pi_L + \sigma_{2z}\pi_T = -15\text{MPa} \cdot 0.72\text{GPa}^{-1} + 49\text{MPa} \cdot 0.66\text{GPa}^{-1} = \underline{0.022}$$

The use of a Wheatstone Bridge results in the following output $\Delta U$ that is normalized with the input voltage U:

$$\frac{\Delta U}{U} = \frac{a - b}{2 + a + b} \qquad (4\text{-}21)$$

$$\frac{\Delta U}{U}(25^{\circ}C) = \frac{-0.025 - 0.022}{2 - 0.025 + 0.022} = \underline{\underline{-24\text{mV}/\text{V}}}$$

The second temperature $T_2$ is different from room temperature. Therefore, the change in the piezoresistance has to be included into the model. This study utilizes a linear approximation of this change, as shown in Equation (4.2.5-1).

Since the stresses in the floating die are practically equal for the two different temperatures, only the piezoresistive constants have to be reevaluated:

$\pi_{11}$(T=125°C)= 0.066 GPa$^{-1}$(1-0.0027(125-25))= $\underline{0.0473\ \text{GPa}^{-1}}$

$\pi_{12}$(T=125°C)=-0.011 GPa$^{-1}$(1-0.0027(125-25))= $\underline{0.0079\ \text{GPa}^{-1}}$

$\pi_{44}$(T=125°C)= 1.381 GPa$^{-1}$(1-0.0027(125-25))= $\underline{0.989\ \text{GPa}^{-1}}$

Using these results, the piezoresistive constants along the resistor and in the perpendicular direction can be determined using Equations (4-8, 9):

$$\pi_L = \frac{1}{2}(\pi_{11} + \pi_{12} + \pi_{44}) = \frac{10^{-11}}{2}(4.73 - 0.79 + 98.9)\text{Pa} = \underline{0.51\text{GPa}^{-1}}$$

$$\pi_T = \frac{1}{2}(\pi_{11} + \pi_{12} - \pi_{44}) = \frac{10^{-11}}{2}(4.73 - 0.79 - 98.9)\text{Pa} = \underline{0.48\text{GPa}^{-1}}$$

The relative change of resistance can be determined with Equation (4-7):

$$a = \frac{\Delta R}{R} = \sigma_{1x}\pi_L + \sigma_{1z}\pi_T = -49\text{MPa} \cdot 0.51\text{GPa}^{-1} + 15\text{MPa} \cdot 0.48\text{GPa}^{-1} = \underline{-0.018}$$

$$b = \frac{\Delta R}{R} = \sigma_{1x}\pi_L + \sigma_{1z}\pi_T = -15\text{MPa} \cdot 0.51\text{GPa}^{-1} + 49\text{MPa} \cdot 0.48\text{GPa}^{-1} = \underline{0.016}$$

Consequently, the normalized output of the Wheatstone Bridge can be evaluated with Equation (4-21). This output is independent of the change in the value of the resistors:

$$\frac{\Delta U}{U}(125^\circ\text{C}) = \frac{-0.018 - 0.016}{2 - 0.018 + 0.016} = \underline{\underline{-17\text{mV/V}}}$$

This shows that the temperature influence on the output of the sensor is not negligible. This change has to be compensated. One possibility is to adjust the input voltage of the bridge. Assuming an input voltage of 5V at 25°C, the

output voltage at this temperature is 125mV. In order to maintain this output for 125°C, the input voltage has to be increased to:

$$U_B(T) = U_B(T_{ref}) \frac{\frac{\Delta U}{U}(T_{ref})}{\frac{\Delta U}{U}(T)} \tag{4-22}$$

$$U_B(125^{\circ}C) = 5V \frac{24mV/V}{17mV/V} = \underline{\underline{7.1V}}$$

where $U_B$ is the bridge voltage and $\frac{\Delta U}{U}$ is the relative output voltage at the different temperatures.

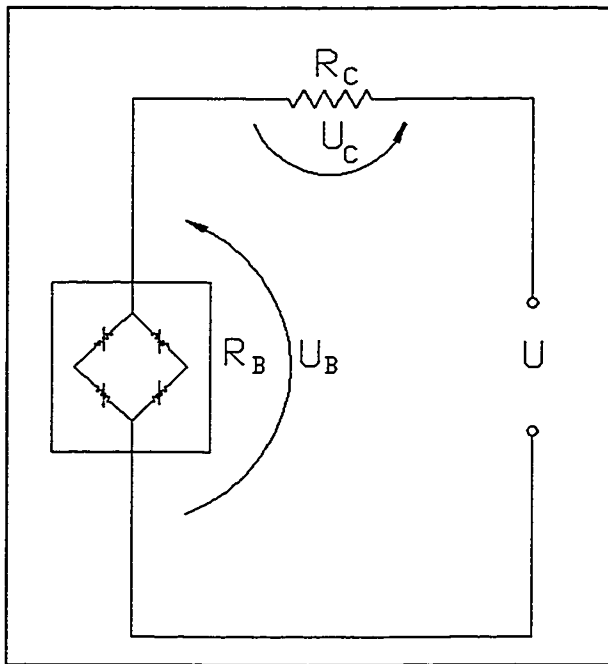


Figure 4-17: Example Circuit for Temperature Compensation

With this change in the input voltage, the output maintains the same full-scale value. This change can be achieved, using the methods described in Chapter (4.2.4). For the compensation, the thermal change of the bridge resistance has to be taken into account.

Using a constant voltage approach, the value of the compensating resistor can be determined. The voltage divider formula for the circuit in Figure (4-17) yields the following equation for the bridge voltage:

$$U_B = U\frac{R_B(T)}{R_B(T)+R_C(T)} \tag{4-23}$$

$$U_B(T) = U\frac{R_B(1+\delta_B\Delta T)}{R_B(1+\delta_B\Delta T)+R_C(1+\delta_C\Delta T)} \tag{4-24}$$

where $U_B$ is the bridge voltage, U is the constant input voltage, $R_B$ and $R_C$ are the bridge resistance and the compensation resistance at reference temperature, respectively, $\Delta T$ is the temperature change $T\text{-}T_{Ref}$, $\delta_B$ and $\delta_C$ are the thermal coefficients of resistivity for the bridge and the compensation resistor, respectively.

Using this equation for the reference temperature $T_1$ and the second temperature $T_2$, the input voltage U can be expressed in terms of $U_B$, $R_B$, and $R_C$:

$$U = U_B(T_{Ref})\frac{R_B}{R_B+R_C} \tag{4-25}$$

The use of Equation (4-24) in Equation (4-25) allows the determination of the value of the compensation resistor:

$$R_C = R_B\frac{(1+\delta_B\Delta T)[U_B(T_{Ref})-U_B(T)]}{U_B(T)(1+\delta_C\Delta T)-U_B(T_{Ref})(1+\delta_B\Delta T)} \tag{4-26}$$

The assumption of typical values for the bridge and the compensation resistor

$R_B$= 5kΩ [95]

$\alpha_B$= 2500ppm$K^{-1}$ [95]

$\alpha_C$= 3000ppm$K^{-1}$ (epitaxial resistors) [99]

results in a compensator resistance of 4.4 kΩ for the compensation of the above

calculated sensitivity change. The input voltage can be determined with the Equation (4-22). With the values above, the voltage is determined to be 9.4 V.

## 4.3 Packaging

The packaging process is one of the most important processes in sensor manufacturing. It defines primarily the possible applications and the price of the sensor.

Micro pressure sensor packages can be divided into three levels:

1st level: Die level

2nd level: Sensor level

3rd level: System level

The general purpose of packaging is to protect the sensing element from the hostile environment while enabling the interaction with it. A major threat to the sensor is corrosion. This would destroy the electrical connections such as aluminum wires or strips.

Typical sensors involve the following functions:

- Mechanical functions
- Thermal functions
- Electrical functions
- Chemical functions

These are often incorporated in the aforementioned packaging levels (e.g. chemical protection at the die level as well as at the sensor level) and some

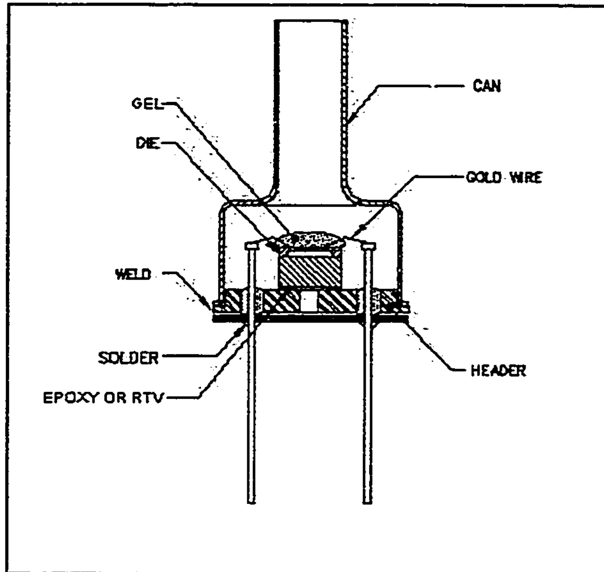


Figure 4-18: TO8 Header (Copyrigth of Lucas NovaSenso, with Permission)

elements serving in different functions simultaneously (e.g. silicon nitride layers as electrical and chemical isolators). Different packaging methods are building blocks that have to be arranged according to the special needs of the application. A typical package is shown in Figure (4-18).

Some general considerations have to be made up front. The sensor has to be designed to prevent pressure leakage. Possible weaknesses of the package are the electrical feedthroughs, the adhesive bonds of the dies and cracks in the diaphragm. The number of potential failure points has to be reduced to a minimum. For this reason, the number of bonds and feedthroughs has to be minimized and sufficient overpressure capability of the membrane has to be ensured. [86]

The environmental performance and price constrains have to be defined according to the targeted sensor application. These restrictions narrow down the possible choices of materials and processes for the package.

#### 4.3.1 Die Level Packaging

The first packaging level begins with the die. Different material layers can be applied to protect the active circuitry. This packaging step also provides stress isolation for the sensing elements. It is also possible to include structures that provide overrange protection to allow the die to survive overload conditions.

The packaging process starts during the fabrication of the die. For example, the sensing elements, the piezoresistors on the diaphragm, have to be contacted electrically. These connections have to be electrically and chemically isolated to prevent short-circuits and corrosion. Layers of silicon oxide and silicon nitride commonly do this. However, it is impossible to passivate the die completely by this method. The contact pads must be unprotected to enable the wirebond. These areas are prone to corrosion. A way to avoid this is to use inert materials such as gold for the metallic conductors and for the bonding pads. [6,1]

Although, these layers provide good isolation, they also introduce the problem of thermal mismatch and residual stresses directly at the sensing elements. When silicon oxide is grown on silicon, the resulting layer is compressive. The deposition of silicon nitride by conventional CVD methods results in a tensile coating of the wafer. This inverse behavior can be utilized to minimize the influence of the residual stresses on the measurement. The measurement error will decrease, if the thickness of the layers is chosen that the compressive and tensile stresses are of the same magnitude. A problem of this technique is the introduction of another material layer, resulting in possible long-

term stability problems due to creep and relaxation at the interface. The use of radio frequency enhanced CVD offers the possibility to deposit silicon nitride in compressive and tensile layers, depending on the used frequency. Because of this dependency it is possible to control the process in a way that allows the deposition of a practically stress free layer. [6]

For high-temperature applications, it becomes necessary to isolate the circuitry by other means than by reverse biased p-n-junctions. In this case, the silicon on isolator technique has to be applied. The isolation layer is made from silicon oxide, glass or saphire. The two latter materials have some manufacturing shortcomings such as insufficient thickness control and complex fixturing. The deposition of polysilicon on a silicon oxide layer is possible, however, the piezoresistive properties of this material are inferior to single crystal silicon. Silicon fusion bonding can be used to produce high temperature sensors with a silicon oxide isolation layer. [37, 83]

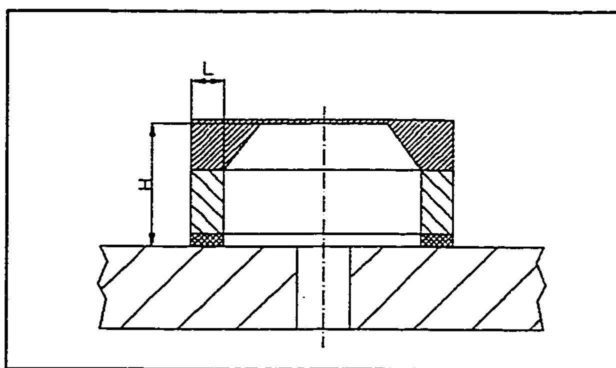


Figure 4-19: Stress Isolation with Spacing Element

The die has to be isolated from stresses in the substrate. This isolation is achieved by the addition of an ideally soft spring-like packaging material between the die and the substrate. The stresses can be reduced due to the geometry by a factor of 100. This can be achieved if

the ratio of the distance membrane-substrate (H) to the contact thickness of the spacing element (L) is larger than 1:1 (Figure (4-19)). The wafer thickness itself provides some isolation of the diaphragm, but this is not sufficient for most applications. Additional spacers are needed. Further improvements can be made, if compliant materials are used to connect the components. [1]

A common way is to bond the silicon wafer on a Pyrex constrain base by anodic bonding. This process forms a reliable, hermetic seal between the two materials. With this technique, aspect ratios of up to 3:1 are feasible. However, the thermal mismatch of Pyrex and silicon induces undesired thermal stresses. [1, 6]

One way to prevent this from happening is the use of silicon as a mounting material. Different processes can attach a wafer to another one. Although the glass frit technique is commonly used, it has some flaws that make it not a better alternative to the Pyrex mounting. The thermal mismatch between the materials is not overcome. Additionally, it is an expensive process that is prone to imperfections.

The silicon fusion bonding process is probably the best-suited technology that is available. It allows the formation of a hermetic seal without any additional materials. The resulting wafer is practically single-crystalline. This minimizes fatigue problems that are inherent with multi-layered sensors. It is also possible to decrease the die size with this technique because each of the wafers can be premanufactured. Recent sensors have only one spacing wafer because of

manufacturing limitations, since tools are mainly derived from mainstream IC technology. This limits current applications to aspect ratios of about 1:1. However, this limitation is not process inherent. Specialized manufacturing tools allow the bonding of more than two wafers and subsequent processing. The commercial application of this process is only limited by the higher price for this process. [1, 6]

Another way to minimize thermal stress would be the incorporation of stress relief structures in the spacer. Especially the silicon fusion bonding process has the potential for an extension of the stress isolation with this method. However, common commercial applications do not use this technique. [38]

This process can also be used to implement the overrange protection of the sensor. Integrated stopping surfaces are shaped in the spacer. This is not only limited to silicon spacers but is also possible for Pyrex. However, the manufacturing precision for these surfaces is much higher for silicon. [70]

### 4.3.2 Sensor Level Packaging

The sensor level packaging gives the sensor its final shape. After the wafer is tested and sawn, the dies are attached to the substrate. Subsequently the electrical connections are established. The assembly is finished by the outer package.

#### 4.3.2.1 Substrate

The substrate has to support the die mechanically. It provides the electrical and mechanical connections to the environment. At the same time, it has to ensure the structural integrity of the sensing die. Different materials can be used in this function.

This mechanical connection is crucial for the sensor. It connects the sensing element with the handling part and the electrical leads of the sensor. The substrate material has to be chosen carefully. There are three main choices for substrates:

- Metal headers
- Ceramic carriers
- Plastic molded lead frames

The traditional substrates are made of metal, which has a significantly higher thermal expansion coefficient than silicon. This results in thermo-mechanical stresses. It also has a mechanical hysteresis. These two effects will influence the output, if the die is not sufficiently stress isolated.

Ceramics with low expansion coefficients such as aluminum oxide are better suited for this purpose. However, the manufacturing of these substrates is extremely expensive since sealed vias for the electrical connections have to be formed.

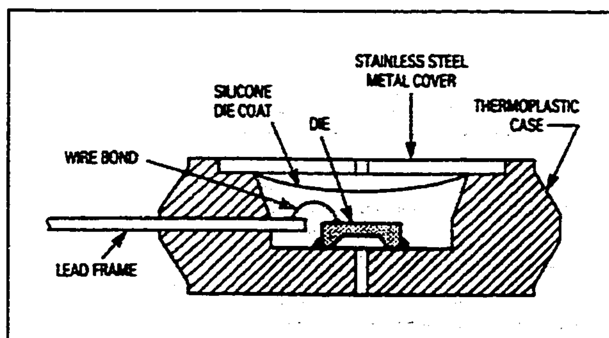


Figure 4-20: Plastic Substrate (Copyright of Motorola, with Permission)

The most cost effective material is plastic (Figure (4-20)). Major problems of these materials are the mechanical hysteresis and the thermal instability. Plastic substrates are best suited when cost is an important factor and the performance degradation can be acceptable. [1]

#### 4.3.2.2 Die Attach

The die attach fixes the die to the substrate. It has to provide sufficient strength to withstand the interfacial stresses. The different materials have distinct influences on the sensor performance and fabrication, which are discussed.

The die can be attached to the substrate by the gold-silicon eutectic bond. This is the traditional technology that was used in the IC industry. It results in a good mechanical and thermal connection. However, the high bonding temperature above 370°C induces significant residual stresses in the structure. Another problem of this method is the high cost of the gold preforms. [1]

The use of epoxies with curing temperatures between 60 and 200°C is a good alternative. In addition, these materials are inherently more flexible than the gold-silicon eutectic bond. The properties of these materials can be controlled by the control of the cross-link density of the thermoset. Epoxies have to be used

below the glass transition temperature. Above this temperature, the properties of the material degrade rapidly. The leakage rate of epoxies is very low. Thermal cycling results in an increase of this rate, especially if the highest temperature is close to the glass transition temperature. [1, 37,86]

The softest die attach in commercial use is RTV. This is a silicon rubber that cures at room temperature. This minimizes the residual stress problem and maximizes the stress isolation of the die. However, the chemical resistance of this material is not as good and it also skins immediately when it gets in contact to air, making the die attach process difficult. The material is also not suitable for high-pressure applications.

A problem of the organic die attach materials is the outgassing at high temperatures. This process goes along with loss of a mass that results in a shrinking of the material. Another problem is the susceptibility of these materials to swelling in organic solutions such as fuel and oil or in moist environments. These dimensional changes result in significant output changes (experimental data shows induced stresses of up to 12 kPa). [66,100-102]

Solders are comparably chemically inert materials for the die attach. The use of soft solders with a melting point below 300°C allows the fabrication of low stress connections. Nevertheless, the shortcoming of this connection is the creep and fatigue of solders, if they are used above 50%of their homologous melting temperature, which is typically the case for automotive applications. Several models are used to predict the lifetime of solder joints. The general influence

factors are the applied loads and temperature. The frequency and hold time of the load and temperature changes are also of importance. Especially the mechanical load-hold time has a negative impact on the fatigue life at elevated temperatures. The expected lifetime of these connections decreases with the increase of the temperature and decrease of the load frequency. [37, 103, 104]

#### 4.3.2.3 Wirebond

After the die is attached, the electrical connections to the sensing elements are established. The wires are bonded by thermosonic, thermocompression or wedge-wedge ultrasonic bonding (Figure (4-21 and 22)). Different wire materials can be used.

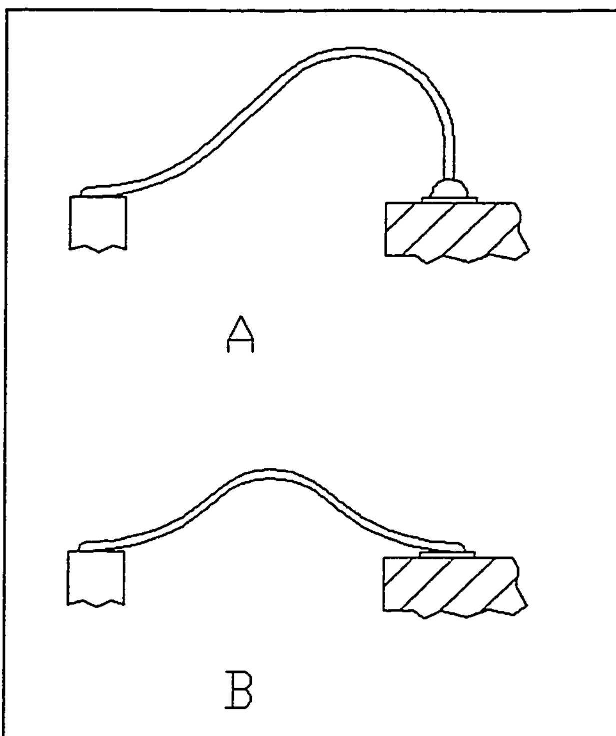


Figure 4-21: Wirebonds
A Ball-Wedge Bond
B Wedge-Wedge Bond

The first two processes are used to form the ball-wedge (or stitch) bond, commonly in conjunction with a gold wire. Usually the first processes are preferred because of the higher speed. [105]

The wedge-wedge bond has the lower loop. This minimizes the

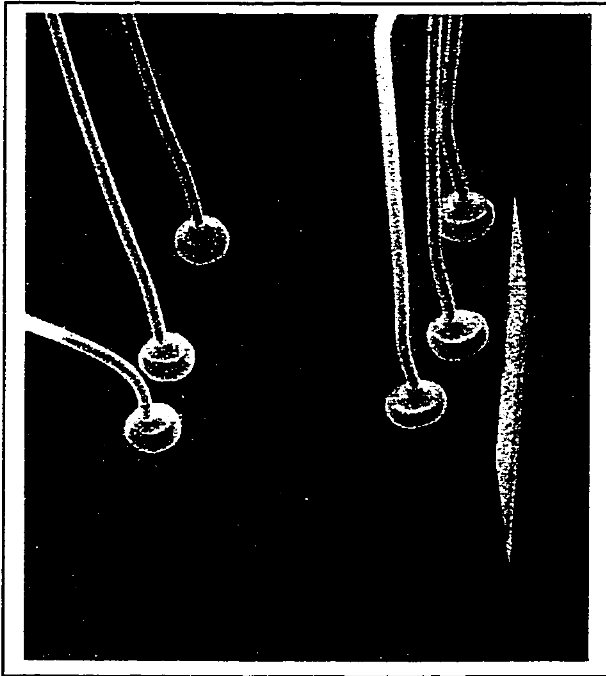

Figure 4-22: Wirebond (Copyright of Lucas NovaSensor, with Permission)

sensivity of the wire to break under mechanical shocks or vibrations. It also decreases the potential for short-circuits due to contacting wire loops. [105]

Gold bonding wire is a very soft material. Therefore very small concentrations of impurity atoms (Be or Cu in the ppm range) are used to strengthen the material. The Be doped wire has better mechanical properties, but the wire has to be annealed after the bonding. The inertness of gold is of interest for many applications. It minimizes the necessary chemical isolation effort. On the other side is the high density of gold. In conjuction with its softness it decreases the natural frequency of the wire, making it prone to failure.[105]

Pure aluminum like gold is too soft to be used for wire bonds. It is alloyed with small percentages of other materials such as silicon or magnesium.

The 99Al1Si alloy is advantageous because the alloy material silicon neutralizes the problem of semiconductor poisoning. It is also a perfect match to the die metallization that usually also contains about 1% silicon. The problem with this alloy is the tendency to form silicon as a second phase due to the

limited solubility at the bonding temperature. This can degrade the bond integrity. [37, 105]

The aluminum alloy with 0.5 to 1% magnesium shows superior mechanical behavior. The fatigue life and the break-strength are higher. There is no tendency of the material towards segregation. [37, 105]

The lower density and the increasing hardness during the bonding process makes these wires less prone to short-circuiting and mechanical failure.

#### 4.3.2.4 Outer Package

The next step is the final protection of the die. The outer package provides the necessary mechanical protection as well as mechanical and electrical connections. At the same time, the chemical passivation has to be finished.

As mentioned before, the coating of the interconnects by silicon nitride or oxide contributes to this passivation process. The application of this process to the wired die would be sufficient for most applications. However, practical purposes do not allow the application of this technique. Other methods have to be added to complete the chemical passivation. [1]

The attached die can be coated by a silicone gel. The gel consists of one or two parts of siloxanes. After dispensing the gel as a thick film in the mm-range, it has to be cured. The low modulus of the gel minimizes the effects of the coating on the measurement. [1, 106]

A relatively new method is the use of Parylene, a conformal coating, to protect the die surface after wiring. This material adds a uniform layer of passivation material in a vacuum deposition process near room temperature. After deposition, the film has to be annealed. The minimum thickness is determined by the need to avoid layer imperfections. The thermal drift that is induced by the coating limits the maximum thickness. Experimental results show that for temperatures up to 105°C, the coating has to be thinner than 3.5 μm [107]. The coating has a negative impact on the performance of the device. The coating stiffens the diaphragm, therefore the sensivity decreases with the increasing layer thickness. At the same time, the magnitude of the zero offset increases due to the thermal mismatch that is close to the sensing elements. The temperature coefficient of sensivity and the linearity of the device are also influenced since the material exhibits a thermo-mechanical hysteresis. This effects the accuracy and repeatability of the measurement, especially if the diaphragm size is of the same order of magnitude as the coating. [1, 107-109]

Experiments show that these two processes can be combined [106,107]. The result is not only an addition of protection but also an enhancement of the predicted lifetime due to synergy effects. The addition of the two layers naturally reduces the amount of corrosive agents that reach the diaphragm at steady state. It also reduces the delamination of the lower layer, a common failure mode for Parylene coatings. The low Young's Modulus of the gel enables it to fill macro defects of the lower layer that would otherwise cause the contact with the

corrosive medium. This enhances the survivability of the sensor by a factor of more than four. [106,107]

Backside pressurization capitalizes the good chemical inertness of silicon. The medium is not in contact with the circuitry on the front side of the membrane. In this case, the adhesive has to be chosen to withstand the pressurized media. From a mechanical point, this load case is disadvantageous. The bond and the possible glass constraint will be under tensile stress. This is undesirable because most bonding materials have a higher compressive strength. [106]

Figure 4-23: Oil isolated Pressure Sensors (Copyright of Lucas NovaSensor, with Permission)

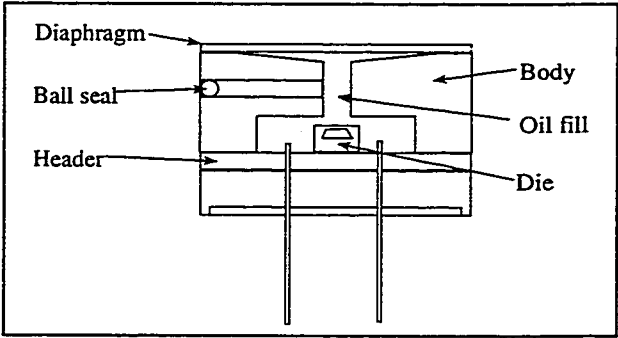


Figure 4 -24: Oil isolated Pressure Sensor (Typical Cross Section) (Copyright of Lucas NovaSensor, with Permission)

For severe environments, when the media to be measured is corrosive or aggressive such as sea water, complete isolation of the die becomes necessary. Such a protection is the oil isolated sensor package as shown in Figures (4-23 and 24). In this case, the sensing die itself is not in contact with measurant. The pressure is applied to an inert membrane. This membrane is

manufactured from stainless steel or special materials suited to the medium that is measured. It has to be extremely compliant, about 100 times more than the silicon diaphragm. This ensures that the thermal expansion of the oil (about $0.001K^{-1}$) inside the package is of minor effect on the die. However, a temperature dependent zero pressure offset will still result from this packaging process. The thermal expansion of the oil can also stress the diaphragm beyond the elastic limit, resulting in a output hysteresis. It is therefore crucial to minimize the volume of oil used in the sensor. For this reason, the chamber volume has to be reduced to the absolute minimum. Special volume compensators, made of low expansion material such as ceramic, are inserted into the package to fill the spaces between the die and the contact pins. The oil used to transmit the pressure has to be baked out and outgassed before injected into the package, the otherwise resulting gas bubbles inside the sensor would degrade the sensor performance. The major problem of this packaging method is

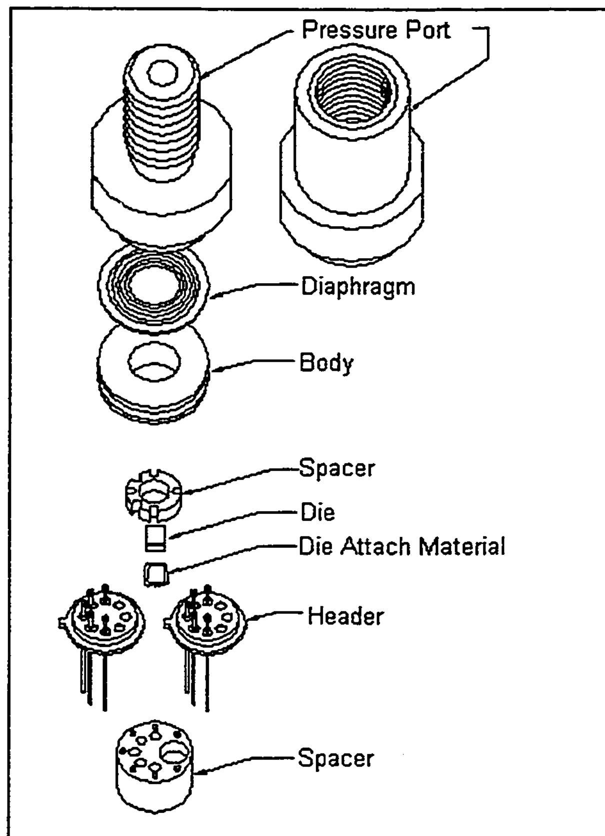


Figure 4-25: Stainless Steel Assembly (Copyright of Lucas NovaSensor, with Permission)

the high price and its unsuitability to high volume production. [1]

The metal diaphragm oil isolated all media package as described above is very flexible, but also extremely expensive. To keep the costs down, it is desirable to minimize the layout differences between different packages to customized pressure ports. Figure (4-25) illustrates such a assembly system. This minimizes the necessary number of testing devices, the price per header and enhances the production flexibility. The pressure ranges from 0 to 70 MPa. Usually other packages are considered unless the application makes this extreme isolation unavoidable. [1]

A common, very cost effective possibility for a robust housing are the TO-series packages as shown in Figure (4-26). These packages are derived from military IC's and provide excellent mechanical and electrical integrity. The die is usually protected by gel or Parylene, that can also cover the wire bonds, which gives additional shock survivability. This kind is not suited for applications with combustible or explosive media, because the circuit side of the die is pressurized. It is also not suitable for conductive media for the same reason unless the wire bonds are completely covered. This method allows for high volume production at low costs. [1]

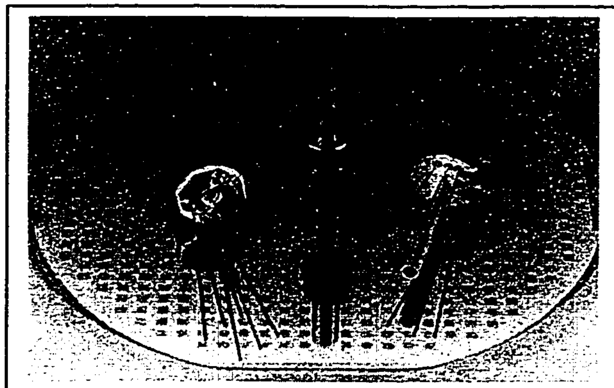

Figure 4-26: TO8-Headers (Copyright of Lucas NovaSensor, with Permission)

Hybrid substrate packages use alumina that has a low thermal expansion coefficient and a high modulus as the base material. This minimizes thermal mismatch compared with metal headers and ensures structural integrity, even if outside forces are applied. It allows automated high volume batch production of sensors. Thick film resistors can be placed on the material and these can be used for temperature and pressure calibration in a laser trimming process. [1]

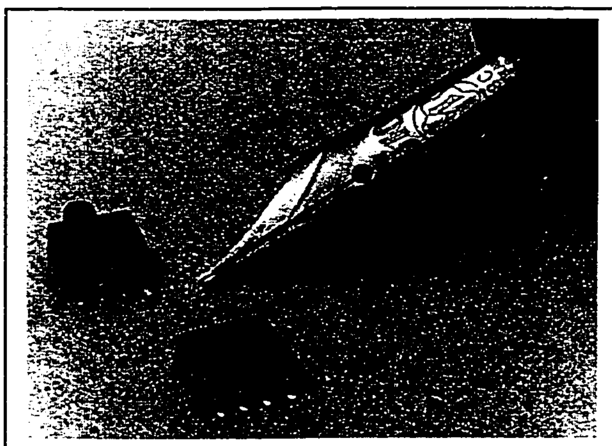

Figure 4-27: Plastic Packages (Copyright of Lucas NovaSensor, with Permission)

Plastic lead frame based packages offer the ultra-low cost possibility of packaging (Figure (4-27 and 28)). The die is covered by gel or Parylene and a plastic cap is molded over the leadframe. In many cases, the pressure connection is provided by a barbed hose fitting. The pressure range of this type is limited by the hydrostatic strength of the plastic and the strength of the pressure connection. Pressure sensors with a range up to 0.7 MPa have been manufactured with this

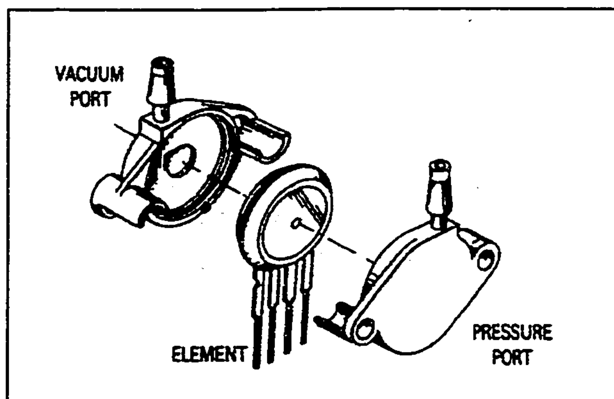


Figure 4-28: Plastic Package System (Copyright of Motorola, with Permission)

housing technique. The seal between the plastic and the lead frame is not hermetic, therefore, the gel has not only a protecting function but also seals the sensor. It is also not suited for low volume production due to the high initial tool costs. [1, 37]

### 4.3.3 System Level Packaging

In many cases, the sensors are shipped as described above. The customer normally includes the sensor and the conditioning electronics into a new package. Although this is a common practice, it is not economically feasible, since this package is usually built around the existing package. A better way is to include the primary signal conditioning circuitry into the package of the sensor. For this case, the package has to provide the mechanical and thermal isolation as well as electromagnetic shielding of the circuitry. Most circuits are very sensitive to these influences. If the protection is insufficient, the accuracy and repeatability of the measurement degrades.

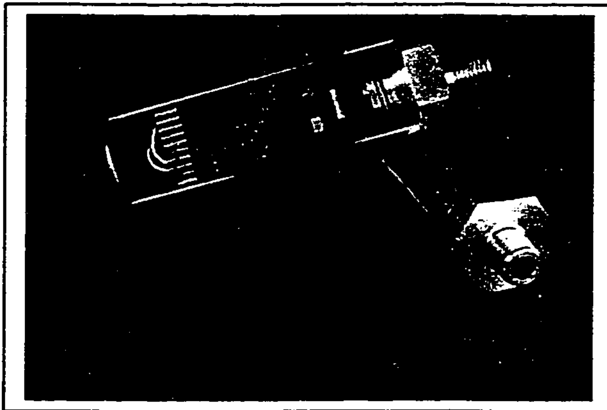

Figure 4-29: Integrated Package 1 (Copyright of Lucas NovaSensor, with Permission)

A metal housing (Figure (4-29 and 30)) gives an excellent protection for mechanical and electromagnetic influences. The good thermal conductivity makes isolating layers for high temperature applications

necessary. As mentioned above, the major problem of these packages is the unsuitability for large-scale production at low cost.

The plastic encapsulation of the sensor and the conditioning circuitry is better suited for large-scale production. It provides sufficient mechanical and thermal protection. Thin metal layers can provide the necessary electromagnetic shielding.

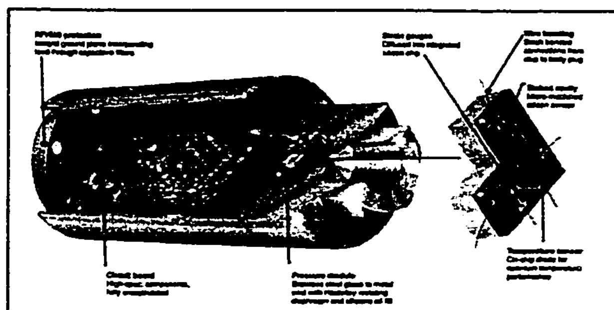

Figure 4-30: Integrated Package 2 (Copyright of Druck, with Permisssion)

## 4.4 Cost

The manufacturing costs are an important concern. The decrease of the prize of sensors enables new applications that were previously impossible. Consequently, this fabrication aspect is decisive for the future development of micromachined pressure sensors. An analysis of the cost structure of a product is useful to optimize development efforts.

The price range of pressure sensors reaches from about $3 for consumer applications such as tire pressure gages to $900 for special industrial applications. The average price of fully integrated automotive pressure sensors, e.g. MAP sensors, is at about $10. [1, 16]

The cost per die came down from about $1000 in the 1960 to the recent figure of approximately $0.5. This means that improvements in the die itself are not longer sufficient to reduce the manufacturing costs. [6]

The packaging determines between 50 to 99% of the costs of the final product. This means that improvements in the packaging process can make a major contribution to reduce the expenses for production. For this reason, it is useful, to standardize the packages. This enables the sufficient use of test and calibration devices and increases the throughput. The special tailoring of the sensor has to be minimized to meet this goal. In most cases, it is sufficient to customize the pressure port and the electrical connectors after the testing of the standard device.

Ideally, the product mix of a company should be based on a modular principle. Sensors for different pressure ranges have to fit into the same housings. This decreases the purchase price and minimizes the number of fixtures needed for production. At the same time, the flexibility to react fast on the customer's demand is improved, since fewer stock parts are needed. [1]

Low-quantity special designs that are unavoidable to meet certain specifications have to fit into the normal production process without major arrangements of the used tools.

In many applications, a low-price sensor with reasonable performance is preferable over a high-performance product. This limits the affordable calibration

processes. For large-scale low-price sensors, statistical calibration methods are reasonable.

# 5. Packaging Design Case Study

The understanding of the influence of the packaging effects on the performance of a sensor is critical to the development of accurate, repeatable, and stable sensors. In the field of micromachined pressure sensors, the finite element method has been used extensively to analyze and predict the thermal and mechanical behavior of the sensing die. This type of analysis allows the optimization of a design for a particular application. This chapter will describe a case study where different die attach materials were modeled and the resulting effect on the sensor output characteristics was predicted.

## 5.1 Objectives

The objective of this study was to determine the effect of packaging stress on the performance of a typical micromachined sensor die.

The finite element method has previously been used in the design of the micromachined sensor die but has usually only considered the effect of pressure on the silicon membrane. In real world applications the sensing element has to be attached to a substrate in a package.

The methods of attachment and the material chosen for this process can have a significant effect on the performance of the sensor. An improvement in understanding these effects could help reduce the design and development time for this type of sensor.

There has been much work published about modeling of packaging effects on integrated circuits. This information is of limited use for micromachined sensor design, because a pressure sensor needs to come in contact with the medium whereas in the IC package the package is specifically designed to prevent this from happening. This means that the die and the packaging material are not only subjected to temperature changes but also to pressure changes and chemical reactions with the medium.

## 5.2 Configuration

Figure (5-1) shows a cross section of the model used in this study. The square die is a typical piezoresistive pressure sensor used in automotive applications. The front side of the silicon accommodates the electronic circuitry with four piezoresistors that are diffused into the diaphragm at the middle of the edges and connected to form a Wheatstone Bridge. The cavity in the backside of the die is formed by anisotropic wet etching with electrochemical etch stop. The die is directly bonded to the substrate (Figure (5-1)) that is made of aluminum oxide ($Al_2O_3$).

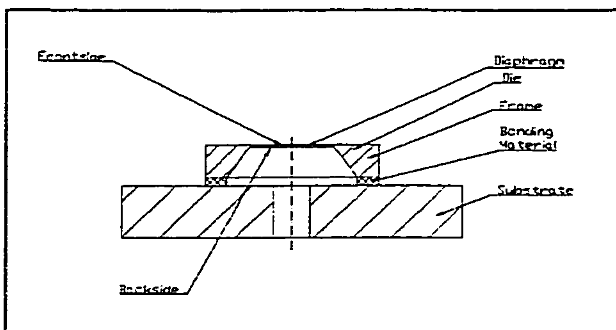


Figure 5-1: Sensor Configuration

The direct die attach can reduce the packaging effort, because the bonding to a intermediate material (e.g. Pyrex) is eliminated. However, it increases the thermo-mechanical stresses due to thermal expansion coefficient mismatch at the interface die-substrate. This makes the choice of the adhesive very important. It has to provide enough elasticity to compensate for this mismatch. At the same time, it also has to withstand the applied pressure and stresses and has to provide sufficient chemical resistance.

The pressure is applied from the backside of the membrane to minimize the environmental influences on the electronic circuitry. This causes the diaphragm to bend upwards. The bending stresses change the resistance of the piezoresistors, thus changing the output of the Wheatstone Bridge.

## 5.3 Material Selection and Properties

The silicon die is mounted on an aluminum oxide substrate. Aluminum oxide has a relatively low thermal expansion coefficient compared with other typical materials such as stainless steel or plastic.

Three bonding materials for the attach of the sensor die to the substrate have been studied. These materials represent the three typical die attach materials: RTV's, Epoxies, and Solders. The choice of the materials was determined by their use for recent products at Lucas NovaSensor. The mechanical properties of the materials are listed in Table (5-2).

The RTV Dow Corning 730 is a soft silicon rubber. It cures at room temperature at 50% humidity. Its low modulus makes it very interesting for a direct die attach as an isolation material. The material has good chemical properties. It withstands the contact to fuels, oils, and solvents, which is important in the automotive environment. (See also Appendix A)

Epoxies are generally harder than the RTV's and more chemically inert. The studied epoxy (Ablebond 789-3) is an excellent adhesive that is widely used for harsh environments. It is cured at 150°C, resulting in residual stresses at room temperature. It provides good moisture resistance. (Appendix A)

The solder studied is 60Sn40Pb. It is a near eutectic material with a solidus temperature of 183°C. The high modulus makes it problematic for the application because of the lack of compliance. However, the chemical inertness to the automotive environment is of great interest. The use of solders makes additional metal plating of the sensor die necessary to enable sufficient wetting of the surfaces.

The Tables below show the mechanical properties of the modeled materials as given in literature.

Table 5-1: Stiffness Modulii of Silicon [110,111]

| T / °C | $E_{11}$ / GPa | $E_{12}$ / GPa | $E_{44}$ / GPa |
|---|---|---|---|
| -40 | 166.4 | 64.28 | 79.77 |
| 0 | 165.9 | 64.05 | 79.63 |
| 40 | 165.5 | 63.81 | 79.50 |
| 80 | 165.1 | 63.57 | 79.37 |
| 125 | 164.7 | 63.30 | 79.22 |

Table 5-2: Material Properties

| Material | E/MPa | v | $\alpha/10^{-6}K^{-1}$ | Source |
|---|---|---|---|---|
| RTV Dow Corning 730 | 1.2 | 0.49 | 370 | [77] |
| Epoxy Ablebond 789-3 | 4,100 | - | 63 below 126°C<br>140 above 126°C | [76] |
| Solder 60Sn40Pb | 31,000 | 0.44 | 26 | [112] |
| $Al_2O_3$ | 344,830-408,990 (20°C)<br>344,830-395,010 (500°C) | 0.21-<br>0.27 | 6.0-7.0 (25-300°C) | [112] |
| Silicon | 190,000 | 0.29 | 2.33 | [6] |

The available properties for the silicon and the aluminum oxide are sufficient to describe the thermal change in a temperature dependent finite element model. However, the available data for the adhesives and the solder are not enough. Therefore, material tests are needed to determine the values of Young's Modulus and Poisson's Ratio for the intended modeling.

## 5.4 Mechanical Properties of the Die Attach Material

As shown in Chapter (5.3), the mechanical properties of the die attach materials over temperature were not available in the literature nor could be provided by the suppliers. This chapter describes the evaluation of the material test results and the determination of the input data for the finite element model.

The tests were executed by the Integrated Technology Inc. (Bothell, Washington). Standard tensile tests were used to determine the stress-strain

curve of the materials at three different temperatures. For each temperature and material, three samples were tested. The resulting curves were interpolated to determine the mechanical properties that are needed for the finite element model.

The solder 60Sn40Pb is a relative ductile material. The engineering stress-strain curve shows a large plastic deformation before failure. The Figures (5-2, 3 and 4) show the engineering stress-strain curves, which are the raw data. The engineering stress is calculated using the initial size of the cross section of the sample. However, with increasing strain, the specimen cross-section is contracting, resulting in an increase of the stress. The true stresses in the structure are determined with the consideration of this contraction. The

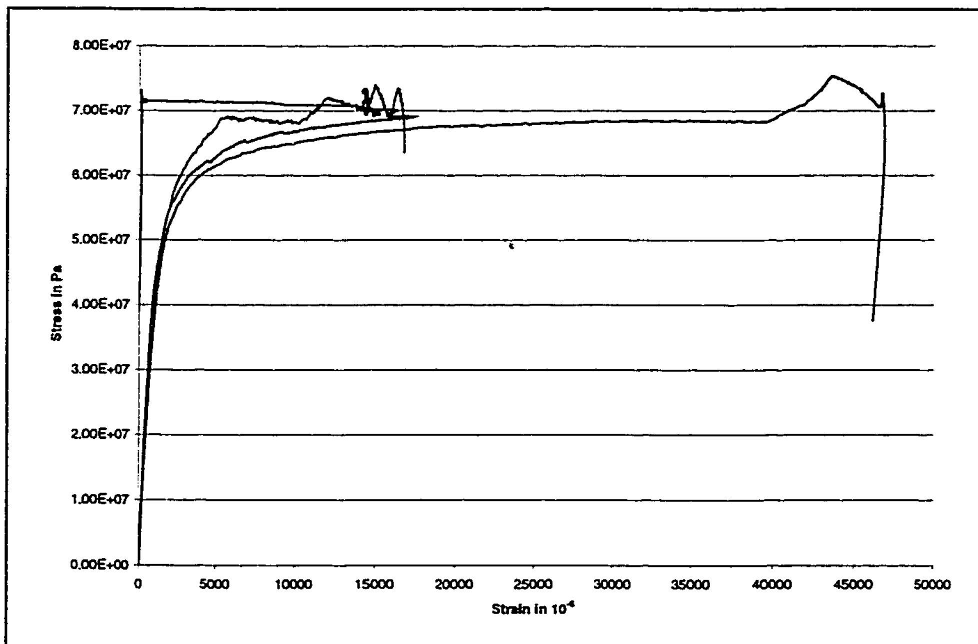


Figure 5-2: Engineering Stress-Strain Curve for 60Sn40Pb at -40°C

transverse strain is used to calculate these values, assuming that both dimensions of the specimen change uniformly:

$$\sigma_{True} = \frac{\sigma_{Eng}}{(1+\varepsilon_T)^2} \tag{5-1}$$

where $\sigma_{True}$ is the true stress, $\sigma_{Eng}$ is the engineering stress, and $\varepsilon_T$ is the transverse strain.

The problem with the assumption above is that non-uniform changes of the specimen cross section results in the deviation of the calculated true stresses from the actual stresses in the sample.

After the determination of the true stress-strain curve, the curves for the three specimens per temperature were used to fit a multilinear curve. Straight

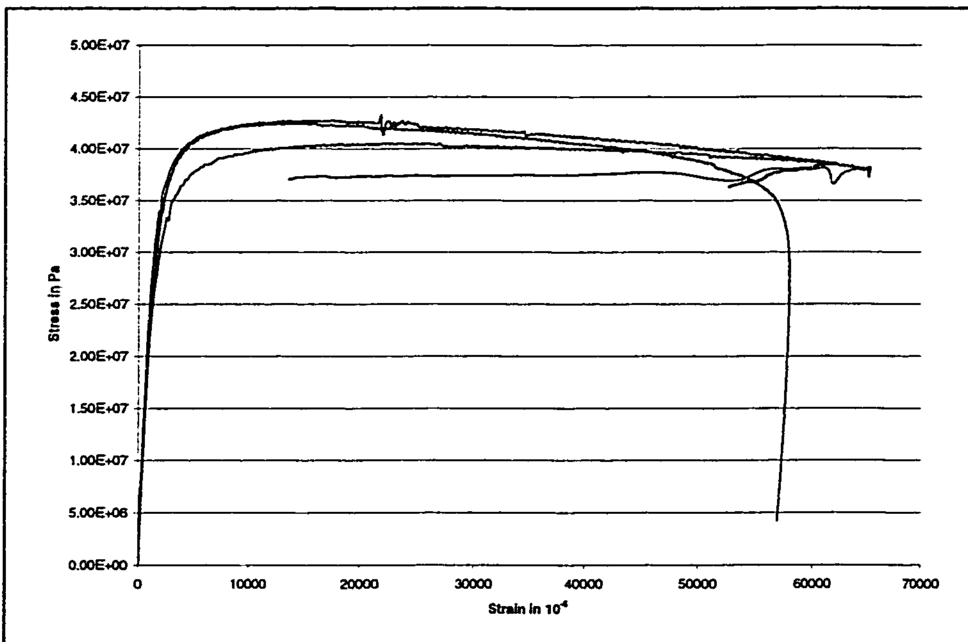


Figure 5-3: Engineering Stress-Strain Curve for 60Sn40Pb at 25°C

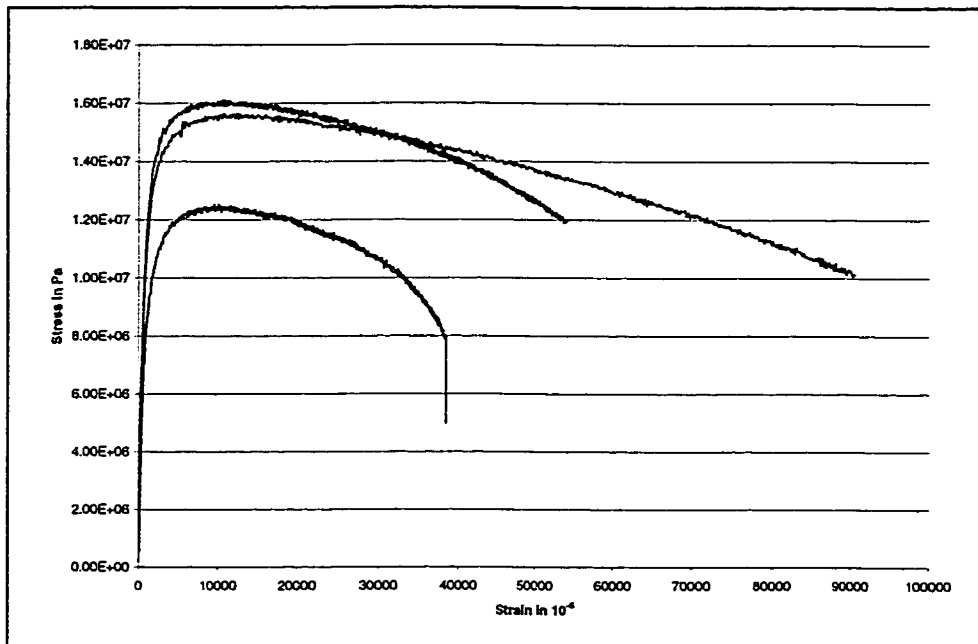


Figure 5-4: Engineering Stress-Strain Curve for 60Sn40Pb at 125°C

lines are used to approximate the stresses in the certain strain ranges. The input format of ANSYS® requires the strain ranges at each temperature to be the same. Therefore, the curve fit is a compromise between the different temperatures. Figure (5-5) shows the least square multilinear curve fit for the solder. The gradients E are listed in Table (5-3).

Table 5-3: Mechanical Properties of the Solder

| $\varepsilon$ in $10^{-6}$ Range | | E in MPa | | | ν | | |
|---|---|---|---|---|---|---|---|
| From | To | -40°C | 25°C | 125°C | -40°C | 25°C | 125°C |
| 0 | 500 | 46100 | 27700 | 17000 | 0.32 | 0.43 | 0.43 |
| 500 | 1500 | 27800 | 16200 | 4670 | 0.32 | 0.43 | 0.43 |
| 1500 | 3000 | 5600 | 5290 | 1140 | 0.32 | 0.43 | 0.43 |
| 3000 | 10000 | 1490 | 700 | 210 | 0.32 | 0.43 | 0.43 |

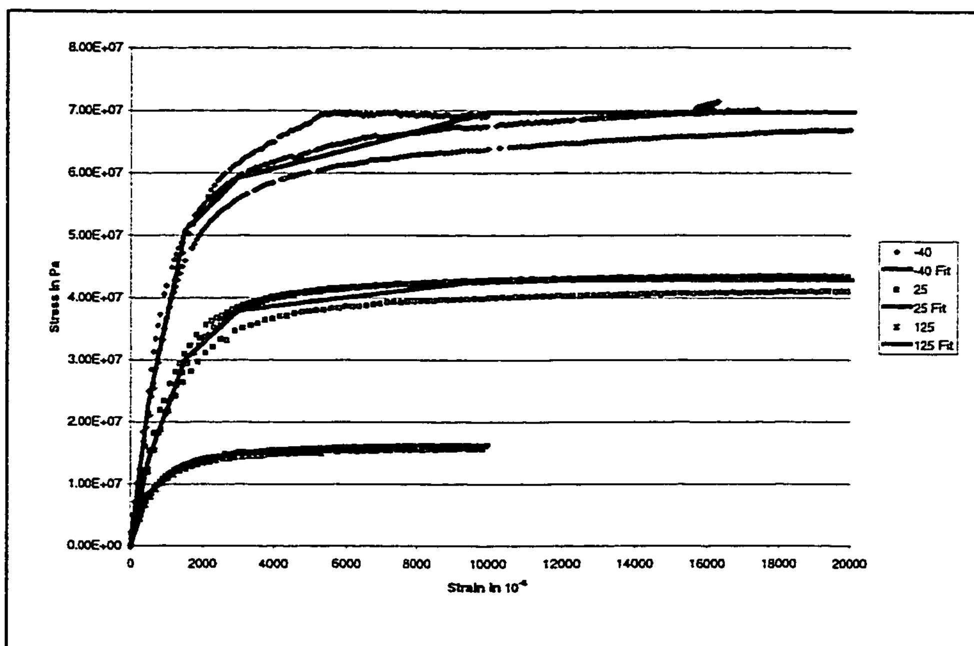


Figure 5-5: Multilinear Fit at Different Temperatures for 60Sn40Pb

Table 5-4: Yield Strength of 60Sn40Pb

| T in °C | $\sigma_{Yield}$ in MPa |
|---|---|
| -40 | 60 |
| 25 | 38 |
| 125 | 14 |

Since the solder is prone to failure by fatigue, plastic deformation has to be avoided. Consequently, the 0.2% yield strength can be used as a failure criterion. Table (5-4) lists the yield strength of the material at the three temperatures.

The Epoxy Ablebond 789-3 is the second material in this study. This can be seen in the test data that are shown in the Figures (5-6,7 and 8).

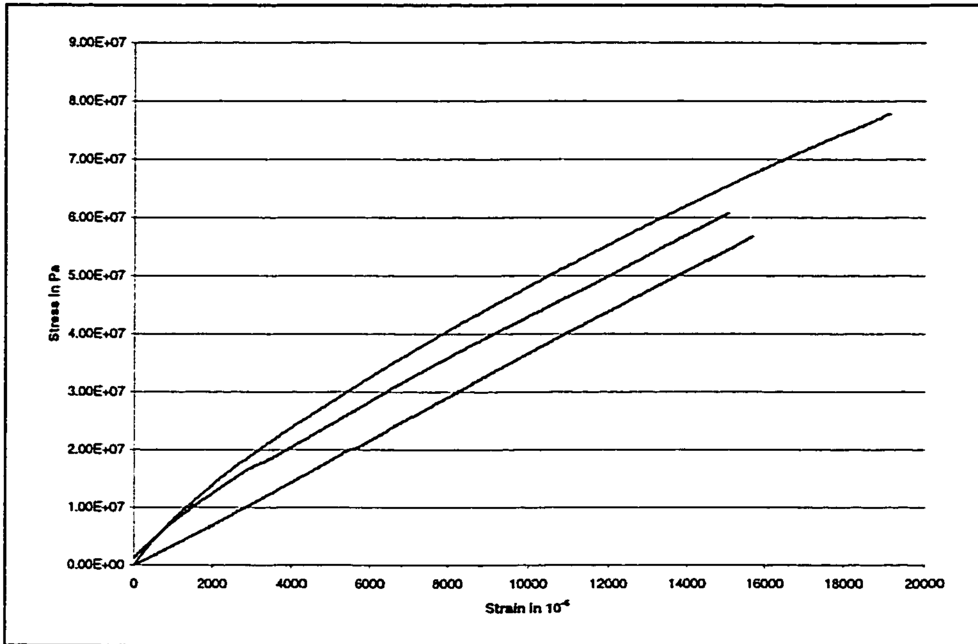


Figure 5-6: Engineering Stress-Strain Curve for Ablebond 789-3 at -40°C

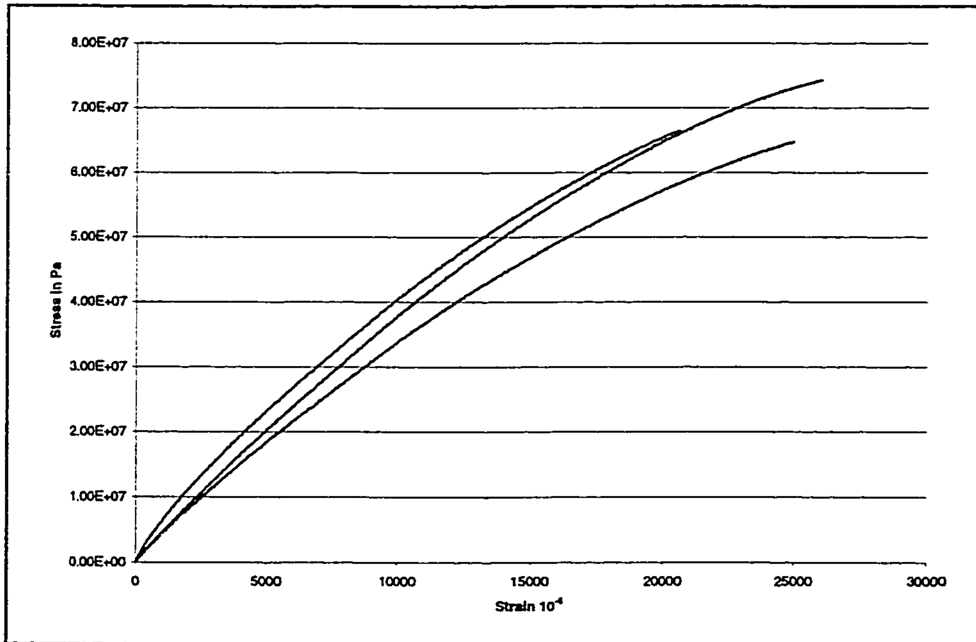


Figure 5-7: Engineering Stress-Strain Curve Ablebond 789-3 at 25°C

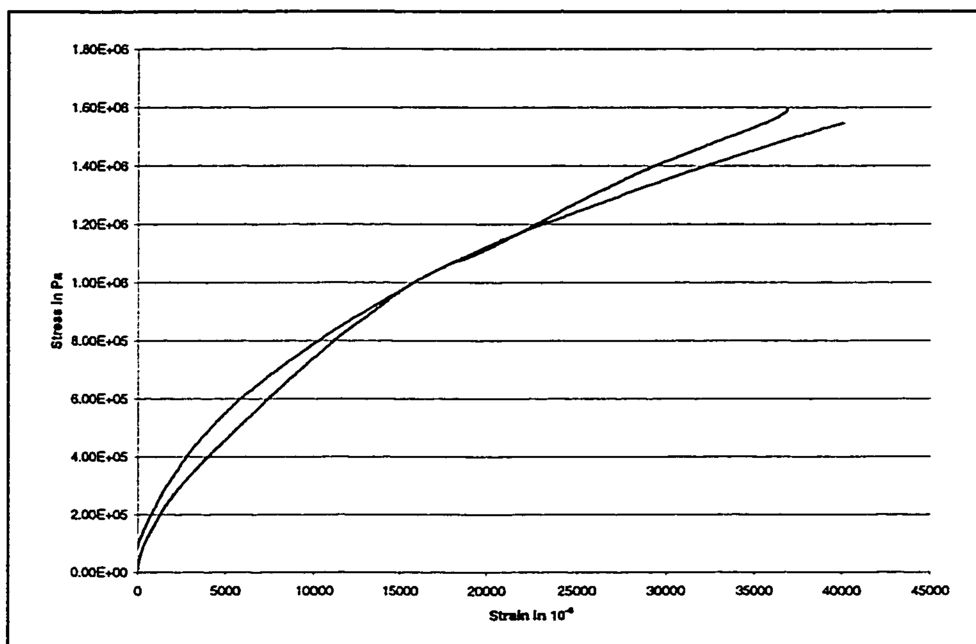


Figure 5-8: Engineering Stress-Strain Curve for Ablebond 789-3 at 115°C (only two specimens successfully tested)

The material deforms with little plastic deformation before the failure at -40°C. The change in the slope becomes significant at room temperature, and the highest temperature shows plastic deformation.

The evaluation of these curves with the procedure described above, gives the data listed in Table (5-5). Figure (5-9) shows the test data and the multilinear curve fitting.

Table 5-5: Mechanical Properties of the Epoxy

| $\varepsilon$ in $10^{-6}$ Range | | E in MPa | | | $\nu$ | | |
|---|---|---|---|---|---|---|---|
| From | To | -40°C | 25°C | 115°C | -40°C | 25°C | 125°C |
| 0 | 500 | 7990 | 5930 | 200 | 0.42 | 0.42 | 0.49 |
| 500 | 2000 | 4680 | 4360 | 110 | 0.42 | 0.42 | 0.49 |
| 2000 | 10000 | 3830 | 3620 | 60 | 0.42 | 0.42 | 0.49 |
| 10000 | 20000 | 3610 | 2650 | 40 | 0.42 | 0.42 | 0.49 |
| 20000 | 30000 | | 1790 | 30 | | 0.42 | 0.49 |

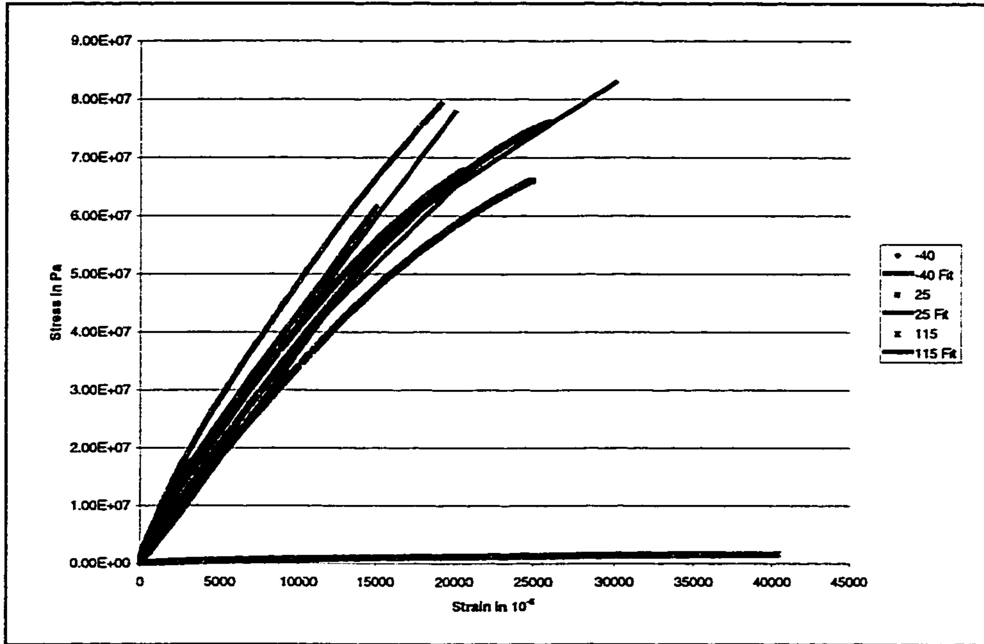


Figure 5-9: Multilinear Fit at Different Temperatures for Ablebond 789-3

Table 5-6: Failure Stress of Ablebond 789-3

| T in °C | $\sigma_{Failure}$ in MPa |
|---|---|
| -40 | 55 |
| 25 | 60 |
| 115 | 1.5 |

The failure criterion is established by the failure stress. The Table (5-6) shows the strength of the material. The brittle character at -40°C results in a lower failure stress than at room temperature. The failure stress at 115°C is one order of magnitude smaller. The reason for the drastic change in the material properties is the glass transition temperature of 126°C.

The RTV Dow Corning 730 is a silicon rubber. The FEM model uses a hyperelastic element to simulate the behavior of this adhesive. The tensile tests

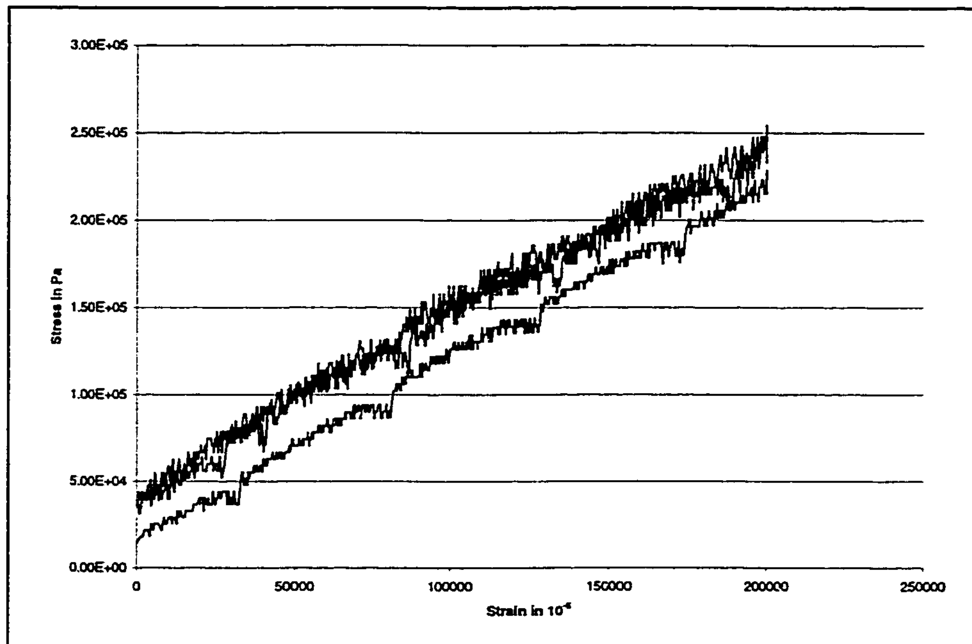


Figure 5-10: Engineering Stress-Strain Curve for Dow Corning 730 at -40°C

at room temperature and low temperature resulted in similar behaviors of the material. The test at 125°C resulted in unusable data. The FEM calculation was done with the assumption of constant material properties over the studied temperature range. The data taken have relative high noises and large offsets. The repeating changes in the slope for -40°C are the result of the influence of the cooling system on the measurement. However, the slope of the measurement is very repeatable as shown in the Figures (5-10 and 11).

A careful evaluation of the available data resulted in a modulus of 0.9 MPa for the material at both temperatures. The Poisson's Ratio for this rubber like material was assumed to be $\nu$=0.49. The input parameters for the Mooney-Rivlin hyperelastic model are determined by these values. These

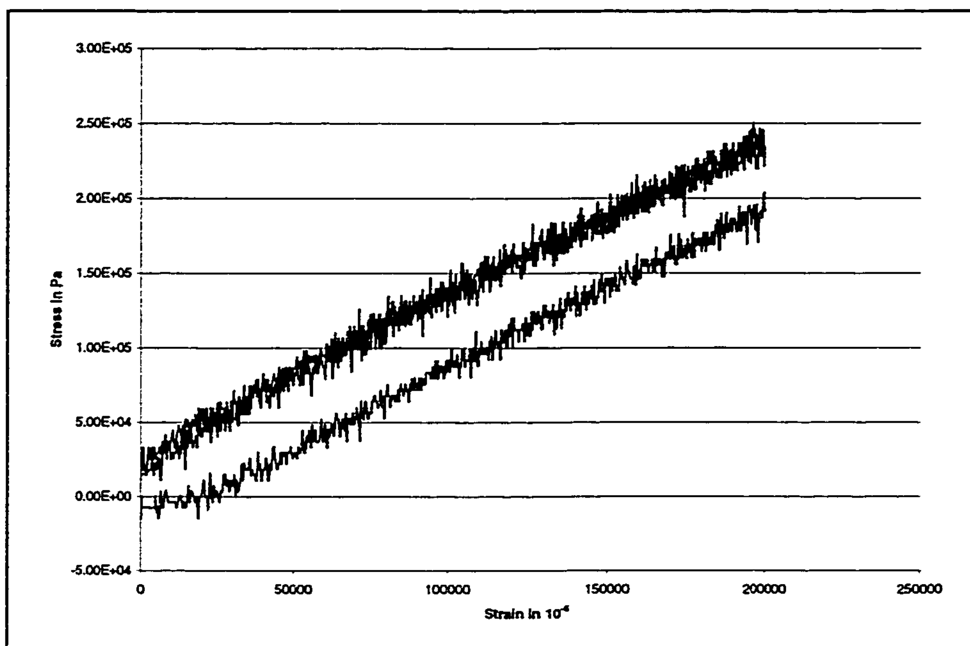


Figure 5-11: Engineering Stress-Strain Curve for Dow Corning 730 at 25°C

values of these measurements were used to create a finite element model of the test specimen and the load conditions. The behavior of the model was in good correlation to the results of the tensile test.

Figure (5-12) shows the results of the two measurements in one diagram. The large offsets have been shifted towards zero by linear least square fits to the individual curves. The resulting offset has been subtracted from the measurement values. It can be seen from this figure that the slope of the stress

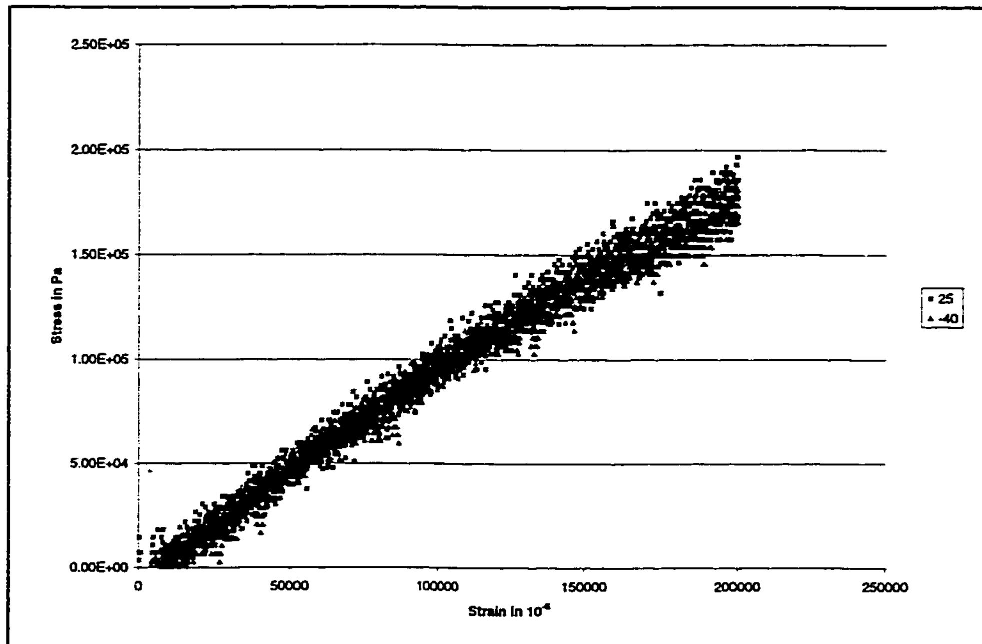


Figure 5-12: Offset compensated Engineering Stress-Strain Curve for Dow Corning 730

strain curve is very repeatable for the two temperatures and varies only within the measurement accuracy. Therefore, the assumption of constant values is valid for this temperature range.

Due to the test limitations for the maximum strain that can be applied to the specimen, the samples were not taken to failure. Consequently, a tensile stress of 0.2 MPa can be considered to be safe and is used as the strength of the material for the calculation.

## 5.5 Geometry

The dimensions of the sensor are schematically shown in Figure (5-13). These are the characteristic dimensions for a typical pressure sensor. The height (H) is determined by the typical wafer size and the length of the die is in the range of 1 to 3 mm. The diaphragm thickness is between a few microns and about 50 µm for high-pressure applications.

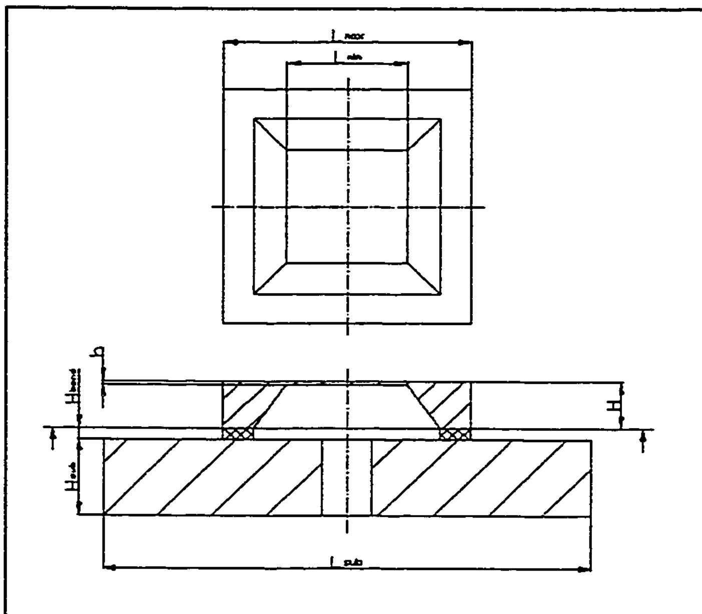

Figure 5-13: Geometry of the Structure

The model is for a low pressure range (35kPa) die without bosses. The length of the die ($L_{max}$) is 2000 µm. The diaphragm has a size ($L_{min}$) of about 1500 µm x 1500 µm. The height of the membrane (h) is less than 10 µm. The height of the whole die is assumed to be 385 µm.

The die is mounted on a substrate. Typically the height of the ceramic is between 0.5 and 2 mm. For the model, it is assumed to be 625 µm. The length of the substrate is 4 mm. It is assumed that the substrate can expand freely at the bottom side.

## 5.6 Modeling Using Finite Element Method

The structure is modeled using the commercial finite element code ANSYS ®. The model includes only the major materials and parts. The coating layers of silicon oxide and silicon nitride are neglected. It is assumed that the influence of these layers will be the same for all bonding materials. The inclusion of these layers would increase the computational effort by magnitudes, since the thickness is very small in comparison to the other dimensions of the film. Unless the element size is decreased dramatically, the numerical problems due to the high aspect ratio of the elements would decrease the accuracy of the model. Likewise, the metal plating that is necessary for the solder is neglected.

Since the main goal of this study is to determine the influence of the bonding material on the output of the sensor, residual stresses resulting from the production of the sensing element are presumed to be zero. Consequently, the structure is assumed to be stress free at the bonding temperature. For the solder, this temperature is the solidus temperature of 183°C. In this study, the glass transition temperature of 126°C takes this place for the epoxy and room temperature (25°C) is the equivalent for the RTV.

It is further assumed that the alumina substrate is fixed to a support that allows free expansion with temperature but constrains the basis in the vertical direction. Consequently, the model is constrained only in the y-direction.

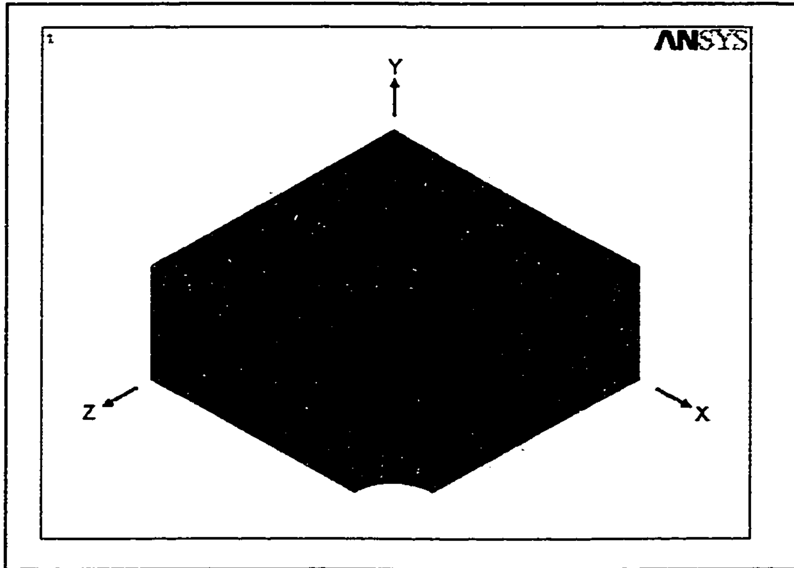


Figure 5-14: Finite Element Model

In order to reduce the computation time, only a quarter of the structure is modeled. The finite element mesh for the substrate is comparably coarse for the same reason. Even with this, the number of elements is about 6000 (Figure (5-3))

Silicon as an ansiotropic material is modeled with the element SOLID64. It enables the temperature dependent input of the anisotropic stiffness matrix. The general stress-strain relation can be expressed as:

$$\begin{bmatrix} \sigma_x \\ \sigma_y \\ \sigma_z \\ \tau_{xy} \\ \tau_{xz} \\ \tau_{yz} \end{bmatrix} = \begin{bmatrix} E_{11} & E_{12} & E_{13} & E_{14} & E_{15} & E_{16} \\ & E_{22} & E_{23} & E_{24} & E_{25} & E_{26} \\ & & E_{33} & E_{34} & E_{35} & E_{36} \\ & & & E_{44} & E_{45} & E_{46} \\ & & & & E_{55} & E_{56} \\ \text{symm.} & & & & & E_{66} \end{bmatrix} \begin{bmatrix} \varepsilon_x \\ \varepsilon_x \\ \varepsilon_x \\ \gamma_{xy} \\ \gamma_{xz} \\ \gamma_{yz} \end{bmatrix} \tag{5-2}$$

Since silicon has a cubical crystal structure, the number of necessary elastic constants is reduced to three, resulting in the following stress-strain relation:

$$\begin{bmatrix} \sigma_x \\ \sigma_y \\ \sigma_z \\ \tau_{xy} \\ \tau_{xz} \\ \tau_{yz} \end{bmatrix} = \begin{bmatrix} E_{11} & E_{12} & E_{12} & 0 & 0 & 0 \\ & E_{11} & E_{12} & 0 & 0 & 0 \\ & & E_{11} & 0 & 0 & 0 \\ & & & E_{44} & 0 & 0 \\ & & & & E_{44} & 0 \\ \text{symm.} & & & & & E_{44} \end{bmatrix} \begin{bmatrix} \varepsilon_x \\ \varepsilon_x \\ \varepsilon_x \\ \gamma_{xy} \\ \gamma_{xz} \\ \gamma_{yz} \end{bmatrix} \quad (5\text{-}3)$$

The values for the model are taken from the literature, therefore, the silicon is assumed to be elastic. [111]

The epoxy and solder layer are included in the model with the SOLID45, an 8-node, 3-D structural solid. This model assumes an isotropic behavior of the material. The data are determined by standard tensile tests as described above. The same element is used to simulate the substrate. However, since material properties for the aluminum oxide are taken from the literature, the model considers only elastic deformations. [97]

The RTV as a rubber-like material is represented by a hyper-elastic element (HYPER86). This element relies on the Mooney-Rivlin function for the material. The necessary data is acquired by a tensile test. The resulting deformation is used as the input data to determine the material constants for the hypereleastic model.

The analysis was performed at three different temperatures (-40°C, 25°C, and 125°C). The pressure was applied in the designed range (0-35kPa) at eleven equidistant values. Geometric nonlinearities caused by the large deflection of the membrane compared with its thickness and the material nonlinearities due to plasticity make an iterative solution necessary.

The output characteristic is derived from the stresses in two elements that are located in the region in which the piezoresistors are placed. The nodal stresses of the nodes of these elements are averaged in this area, since the piezoresistor will act in the same way. Subsequently the output is determined for a constant voltage bridge using a linear model for the temperature change of the piezoresistive effect. Equation (4-20) describes this function. [97]

The output voltage change $\Delta U$ can be determined using the Equations (4.7-9) and Equation (4-21) as shown in Chapter (4.2.5).

The pressure nonlinearity $\Delta_{NL}$ of the output is determined using the terminal value approach. The value of the output at zero and full-scale pressure connected by a straight line and the difference between the actual output to this line are normalized by the full-scale output:

$$\Delta_{NL}(T,p) = \frac{\alpha(T,p) - \alpha(T,0) - \dfrac{\alpha(T,p_{max}) - \alpha(T,0)}{\alpha(T,p_{max})} p}{\alpha(T,p_{max})} \qquad (5\text{-}4)$$

The span of the sensor is determined by the difference of the output value at full-scale and zero pressure.

$$S(T) = \alpha(T,p_{max}) - \alpha(T,0) \qquad (5\text{-}5)$$

In order to determine the value of the temperature nonlinearity of the sensor the value of the output component for 25°C is linearly interpolated using

the results at –40°C and 125°C. The difference between this value and the result of the calculation for 25°C is normalized with the span at this temperature. Therefore the span nonlinerity is:

$$\Delta S = \frac{S(25^\circ C) - S(-40^\circ C) - \frac{S(125^\circ C) - S(-40^\circ C)}{165} 65}{S(25^\circ C)} \quad (5\text{-}6)$$

The offset nonlinearity is defined by:

$$\Delta\alpha_{off} = \frac{\alpha(25^\circ C,0) - \alpha(-40^\circ C,0) - \frac{\alpha(125^\circ C,0) - \alpha(-40^\circ C,0)}{165} 65}{S(25^\circ C)} \quad (5\text{-}7)$$

Finally the full-scale nonlinearity is:

$$\Delta\alpha_{FS} = \frac{\alpha(25^\circ C,p_{max}) - \alpha(-40^\circ C,p_{max}) - \frac{\alpha(125^\circ C,p_{max}) - \alpha(-40^\circ C,p_{max})}{165} 65}{S(25^\circ C)} \quad (5\text{-}8)$$

The other region of interest is the intermediate layer between the silicon and the substrate. The die attach material that connects these materials is subject to high stresses due to the thermal mismatch of the materials. The strength of the silicon and the aluminum oxide is much higher than the strength of the materials that are examined. Therefore, it is the weakest region of the structure and will fail first.

## 5.7 Computational Results

The structure was modeled as described above (Figure (5-13 and 14) and the computational results will be presented in this chapter. The floating die is used a reference model to determine the influence of the bonding material on the die performance.

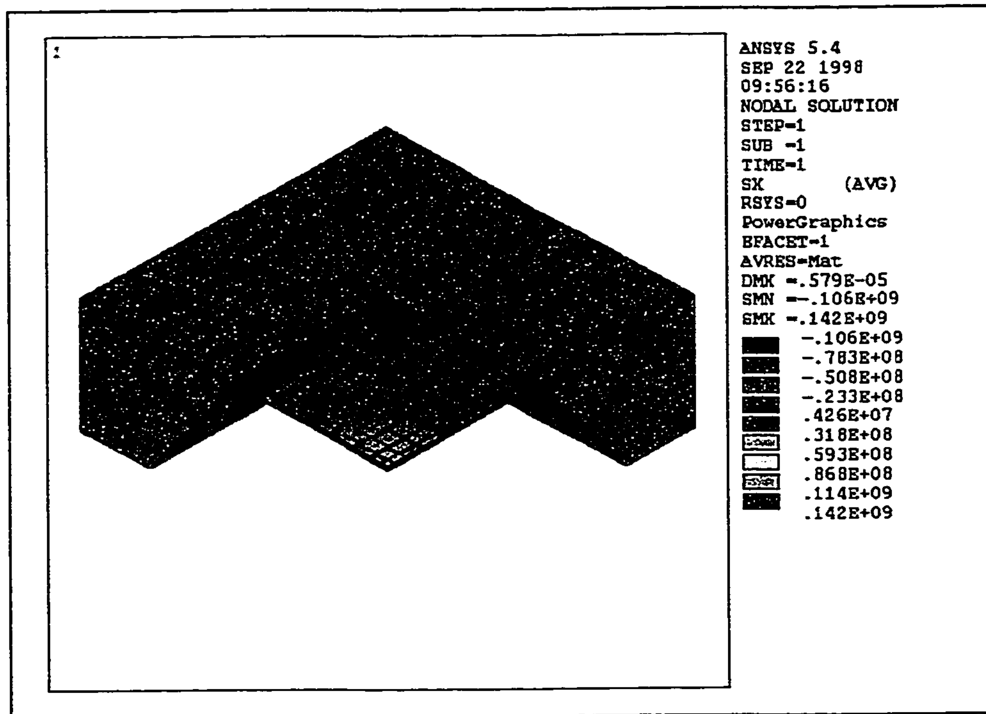


Figure 5-15: $\sigma_x$ for Pressurized Floating Die, T=25°C, p=35kPa

Figure (5-15) shows the stress distribution for the $\sigma_x$-stress. It can be seen that the stresses are concentrated at the edge of the membrane. This is the place where the piezoresistors are located. The stresses in the frame of the die are several orders of magnitude smaller than the stresses at the edge of the diaphragm. The calculation for zero pressure reveals zero stresses in the

structure due to the free thermal expansion. Due to the symmetry of the structure and the minor influence of the isotropy of the silicon, the values for $\sigma_z$ can be observed as well. The distribution and the values are the same, only mirrored at the diagonal of the membrane.

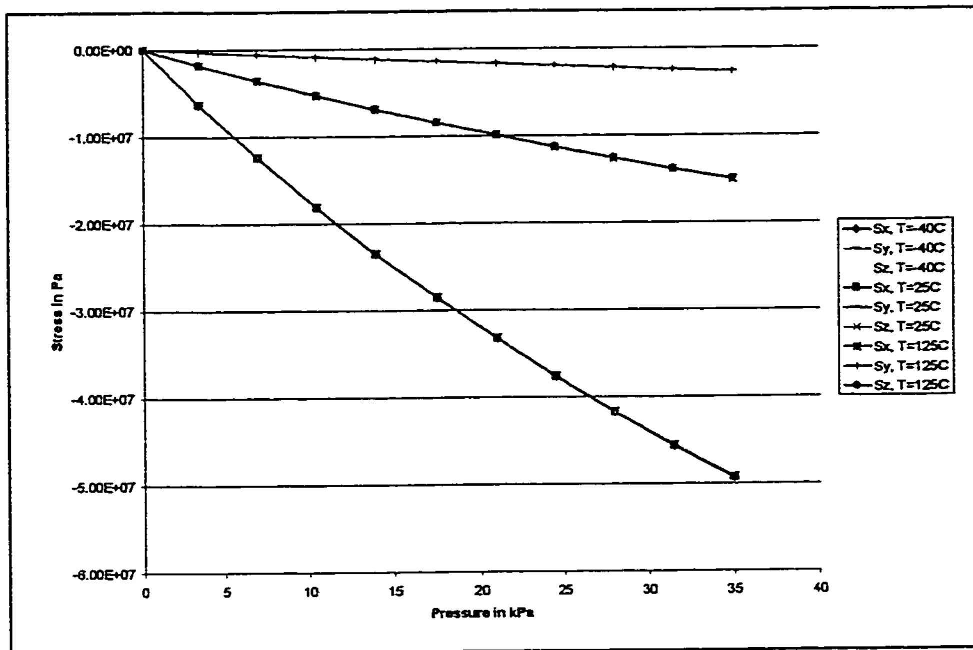


Figure 5-16: Stresses in the Piezoresistive Region for the Floating Die

Consequently, the residual stresses that are measured in the piezoresistive region are zero (Figure (5-16)). When pressure is applied, the magnitude of the stresses increases in a nonlinear manner. The pressure nonlinearity is about 8% in $\sigma_x$, 3% in $\sigma_y$, and 6% in $\sigma_z$. The stress-pressure curves for the different temperatures are exactly coinciding. The full-scale stresses are about 49 MPa for $\sigma_x$, 2.7 MPa for $\sigma_y$, and 15 MPa for $\sigma_z$. The

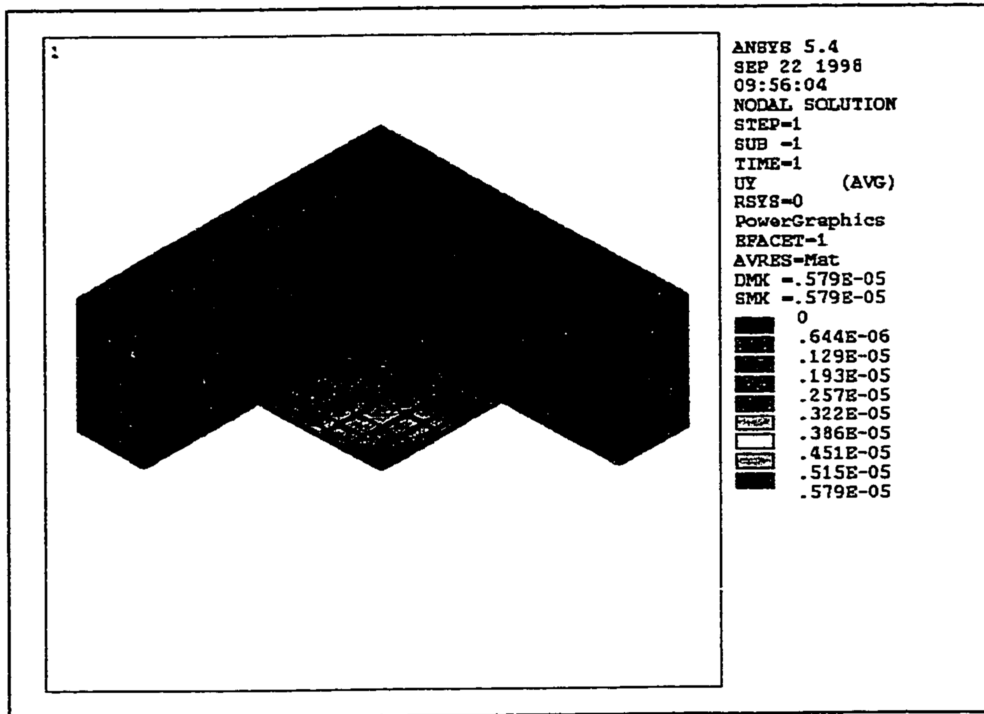


Figure 5-17: Displacement in y-Direction of the Floating Die, T=25°C, p=35kPa

nonlinearity is a result of the large displacement of about 5 μm at the center of the diaphragm compared with its thickness of less than 10 μm (Figure (5-17 and 19)). The deformation of the die is concentrated on the diaphragm. The deformation of the frame is about two orders of magnitude smaller than the deformation of the membrane.

The next step of the analysis is the signal conversion. The use of Equation (5-17) gives the prediction of the output characteristic of the sensing die. Although the stress-pressure curves are coinciding for the different temperatures, the decrease of the piezoresistive coefficients over temperature

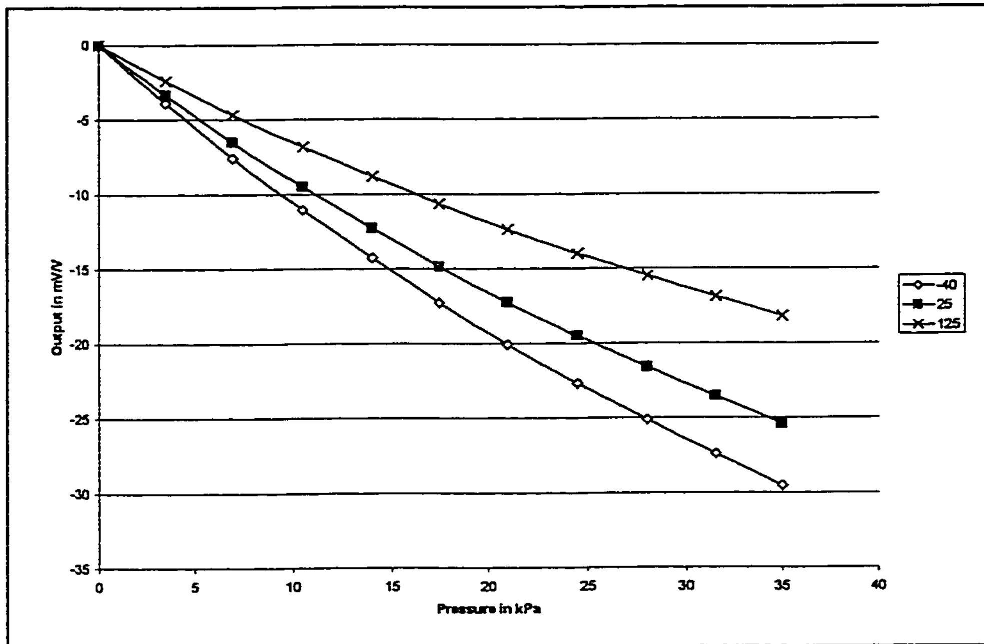


Figure 5-18: Output of the Floating Die

will effect the output. Consequently, the gradient of the output-pressure curves for different temperatures will be different. Figure (5-18) shows the computational results (Equation (4-7 and 21). The curves have the expected distribution, with the highest output values at a given pressure for the lowest temperature. The offset in the output is zero for the assumed model with balanced resistors. The full-scale output value is changing from about -30 mV/V at -40°C to -18 mV/V at 125°C, which is equivalent of a loss of 38%. Due to the zero offset, these values are equivalent to the output span. The temperature dependency of the piezoresistive coefficients results in different output characteristics. The inherent nonlinearity of the die is less than 9% of the full-scale output, using a terminal value approach. The attachment of the die to the

substrate with the solder results in a displacement of the structure. Since the materials are shrinking with decreasing temperature, the displacement is negative and increasing with decreasing temperature (Figure (5-20)). The membrane is bowed upward due to this deformation (Figure (5-19)). The displacement in the x-direction shows the same tendency to increase with decreasing temperatures (Figure (5-21)). The deflection increases along the z-direction. This gives the frame a double hourglass shape.

Figure (5-19 and 20) also shows the displacement in y-direction with full-scale pressure applied. It can be seen that the maximum displacement of the

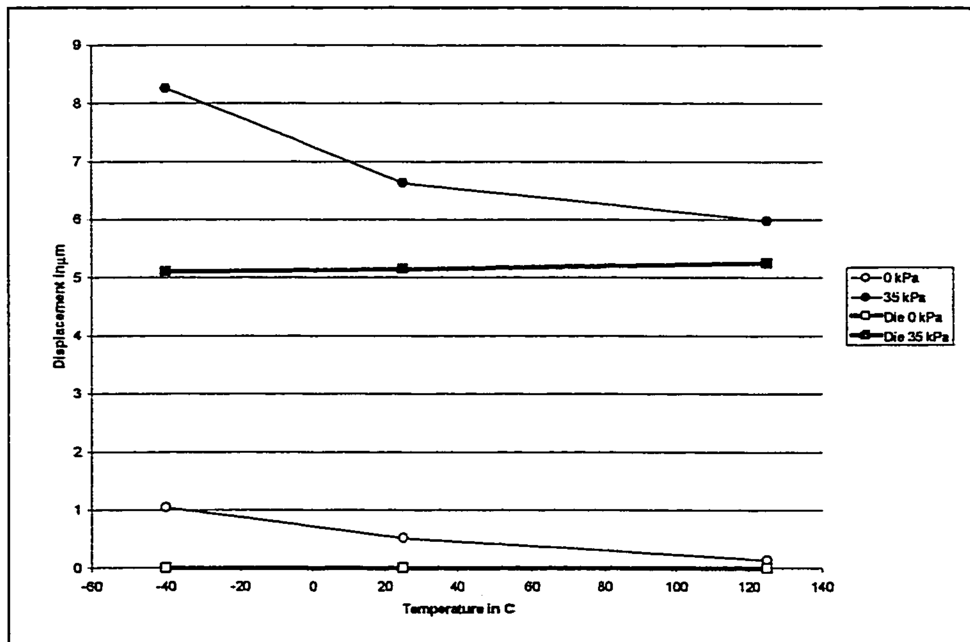


Figure 5-19: Maximum Membrane Displacement in y-Direction for 60Sn40Pb

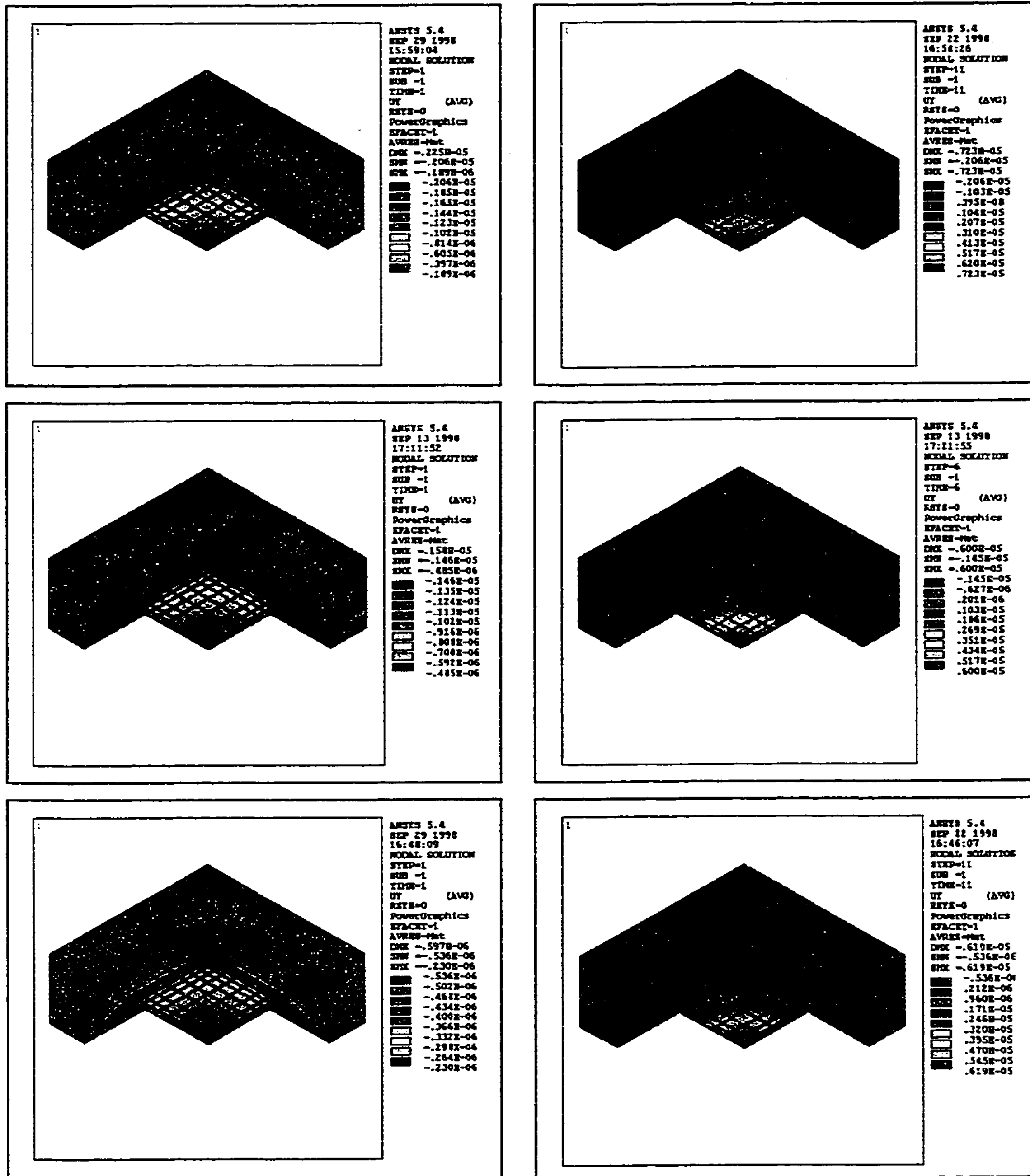

Figure 5-20: Displacement in y-Direction for 60Sn40Pb
Left Column: p=0kPa
Right Column: p=35kPa
Top Row: T=-40°C
Middle Row: T=25°C
Bottom Row: T=125°C

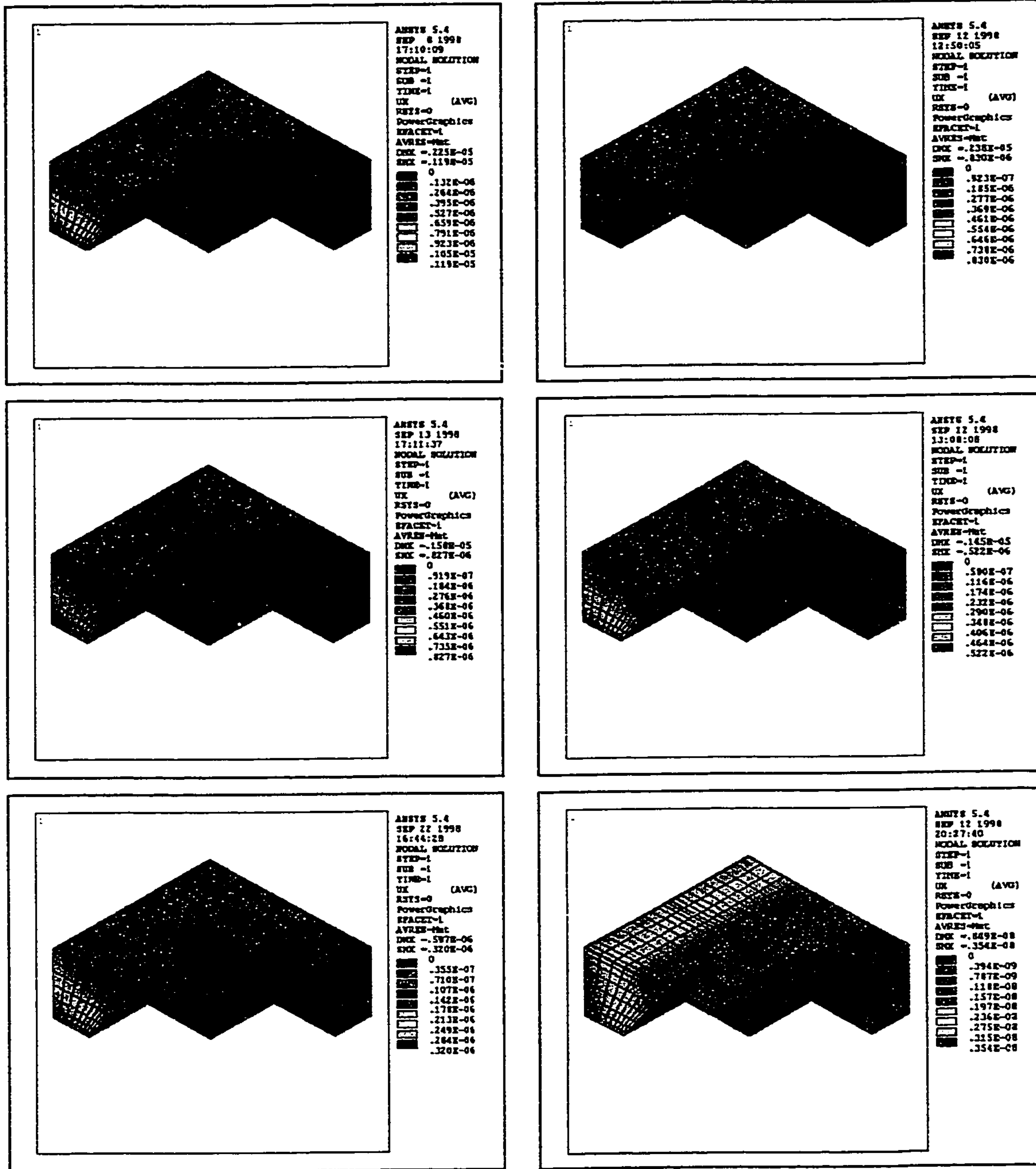

Figure 5-21: Displacement in x-Direction for 60Sn40Pb and Ablebond 789-3
Left Column: 60Sn40Pb
Right Column: Ablebond 789-3
Top Row: T=-40°C
Middle Row: T=25°C
Bottom Row: T=125°C

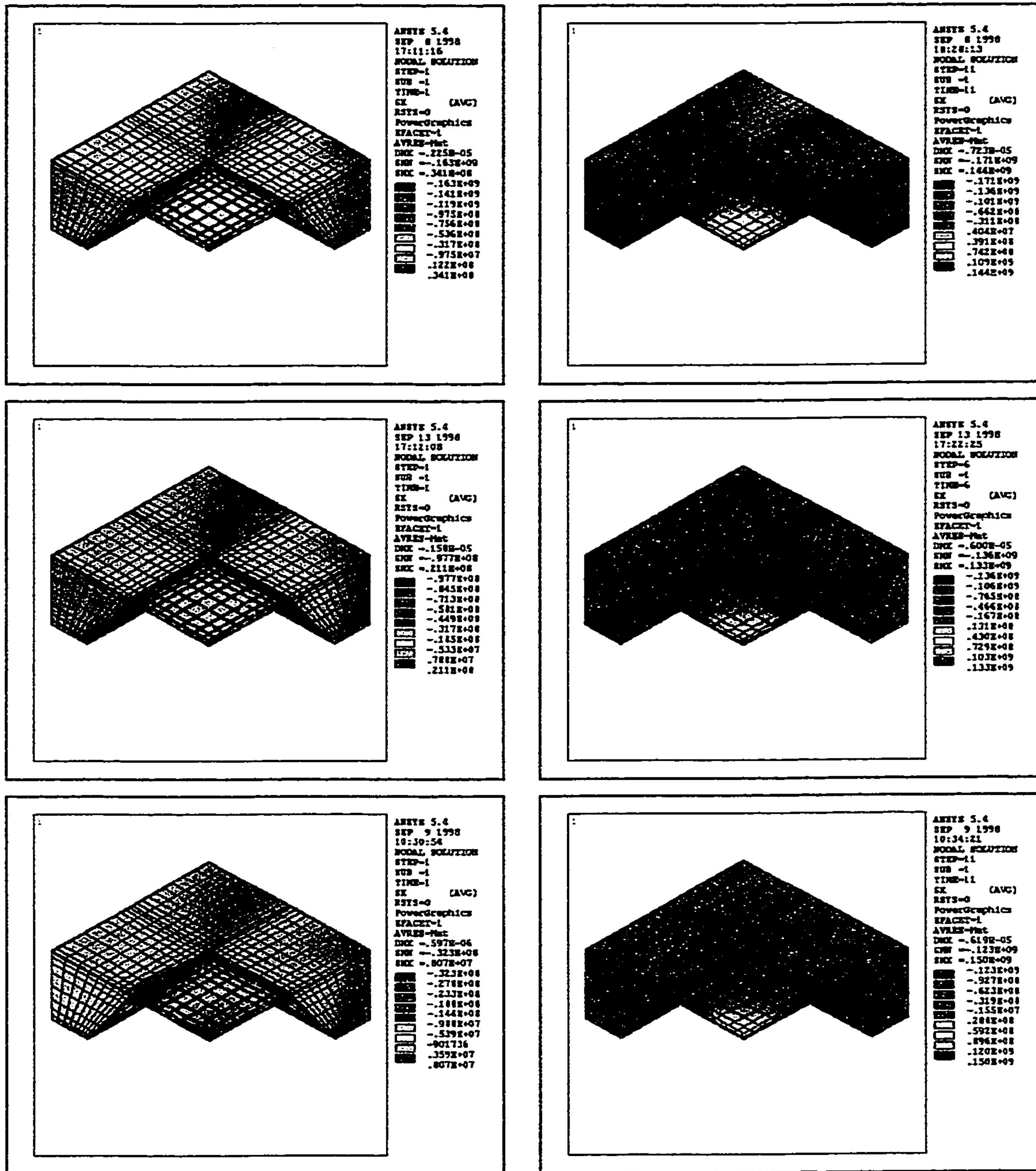

Figure 5-22: $\sigma_x$ Stress for 60Sn40Pb
Left Column: p=0kPa
Right Column: p=35kPa
Top Row: T=-40°C
Middle Row: T=25°C
Bottom Row: T=125°C

middle of the membrane due to the pressure is higher than the maximum displacement of the floating die.

The stress in the $\sigma_x$ direction at the different temperatures is shown in the Figure (5-22). It can be seen that the diaphragm is pre-stressed, due to the thermal coefficient of expansion mismatch of the different materials. These stresses reach magnitudes that are comparable to the full-scale pressure stresses in the floating die. With pressure applied, the stress pattern returns to the stress concentration at the middle of the edge of the diaphragm. The only change is the stress level that is increasing.

The residual stresses that are detected by the piezoresistors due to the mismatch reach -42 MPa for $\sigma_x$, -22 MPa for $\sigma_y$, and -10 MPa for $\sigma_z$ at -40°C (Figure (5-23)). As expected, the stresses are decreasing with increasing temperature. All normal stress components that are measured in the piezoresistive region are compressive. The stresses in the y-direction are an order of a magnitude lower than the stresses in the x and z-direction. The nonlinearity of the stresses over pressure is decreasing with increasing temperature, e.g. the nonlinearity in the $\sigma_x$ component is raising from 9% at 125°C to 14% at -40°C. The spans of the stresses have the same trend ($\sigma_x$: 380 ppm$K^{-1}$, $\sigma_y$: 730 ppm$K^{-1}$, $\sigma_z$: 640 ppm$K^{-1}$). The maximum stress spans (-40°C) are: -53 MPa for $\sigma_x$, -3.1 MPa for $\sigma_y$, and -17 MPa for $\sigma_z$.

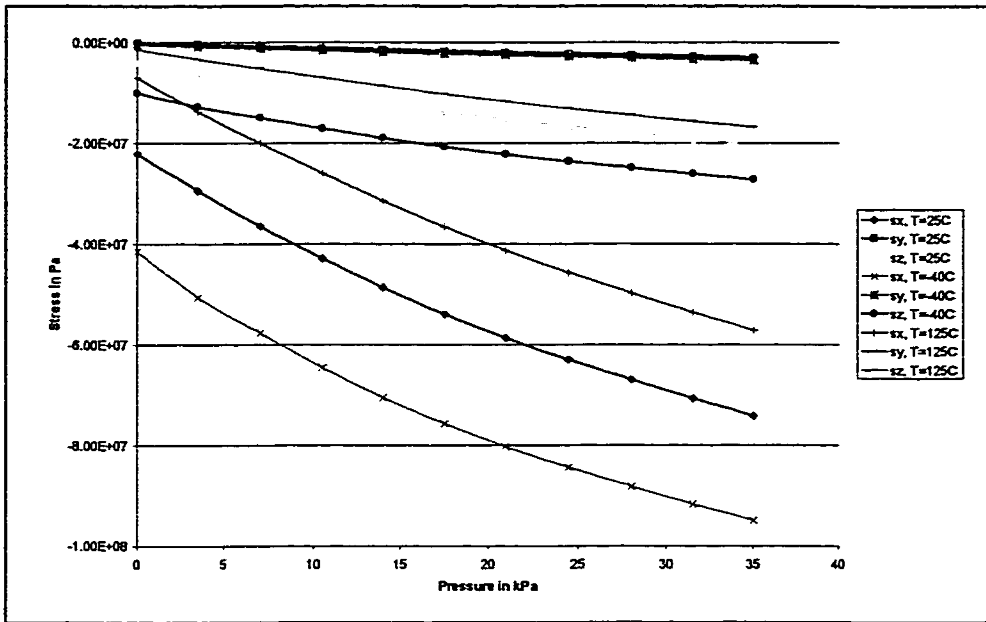


Figure 5-23: Stresses in the Piezoresistive Region for 60Sn40Pb

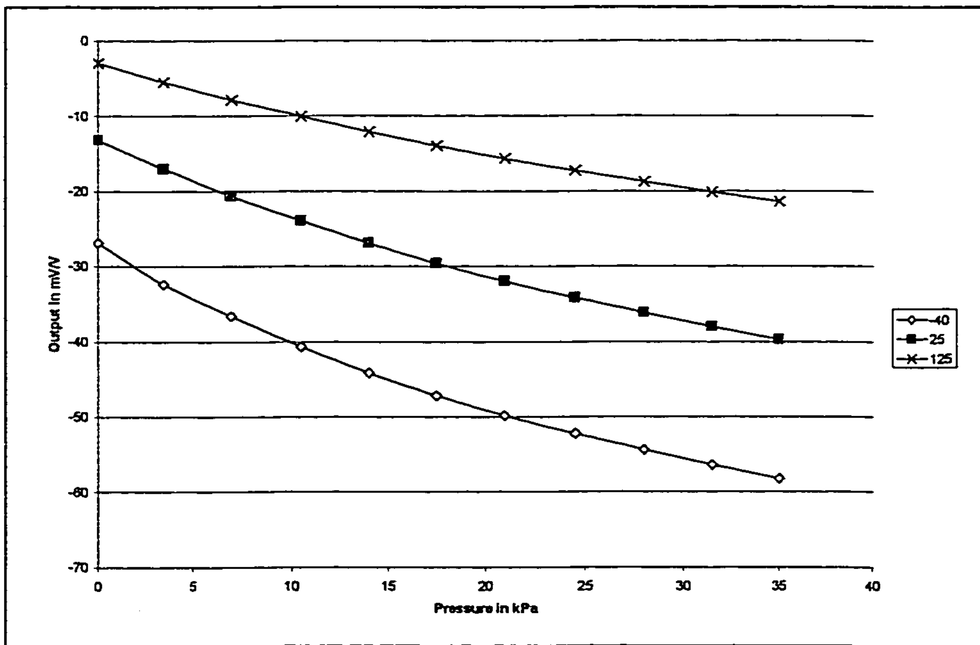


Figure 5-24: Output of the Die with 60Sn40Pb

The residual stresses result in an offset in the output (Figure (5-24)). The offset rises from a magnitude of 3 mV/V at 125°C to 29 mV/V at -40°C. The full-scale output is also varying over temperature, dropping from a magnitude of 58 mV/V to an absolute value of 21 mV/V. The curve for -40°C has the highest gradient. This is a result of the increase of the piezoresistive constants and the increase in the stress range with decreasing temperature. The increasing pressure nonlinearity of the stresses at lower temperatures causes an increase of the output nonlinearity. Whereas the maximum deviation at 125°C is equivalent to the floating die, the value reaches up to 15% deviation at -40°C.

Figure (5-25) shows the stresses in the solder layer at the different temperatures. The stresses are extremely high for this material. The von Mises stress exceeds the yield strength (0.2% criterion) of 60 MPa at -40°C. As expected the magnitude of the stress at the interface is decreasing with increasing temperatures. Since the yield strength is also decreasing with temperature, the stresses remain critical to the structure. They are dominated by the stresses due the thermal mismatch between the materials. The influence of the applied pressure on the interface stresses is negligible.

The result of a thickness increase from 50 μm to 150 μm for the lowest temperature shows a decrease of the stresses in the bulk of the layer. However, the peak value of the stress remains unchanged. The peak values for all cases are located at the interface between the solder and the silicon (Figure (5-26)). Figure (5-27) shows the effect of the increase of the solder layer thickness on

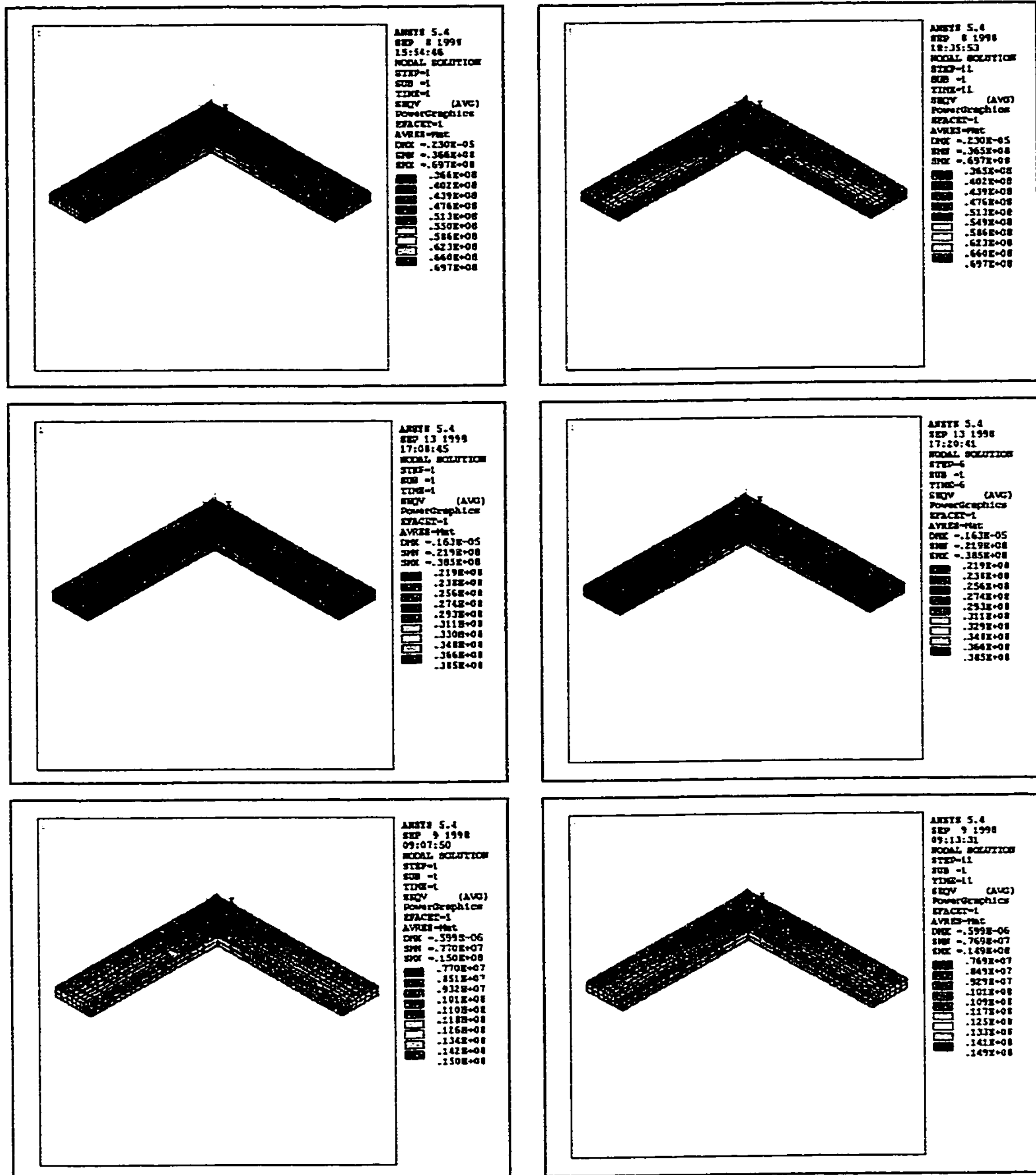

Figure 5-25: Von Mises Stress in the 60Sn40Pb Layer
Left Column: p=0kPa
Right Column: p=35kPa
Top Row: T=-40°C
Middle Row: T=25°C
Bottom Row: T=125°C

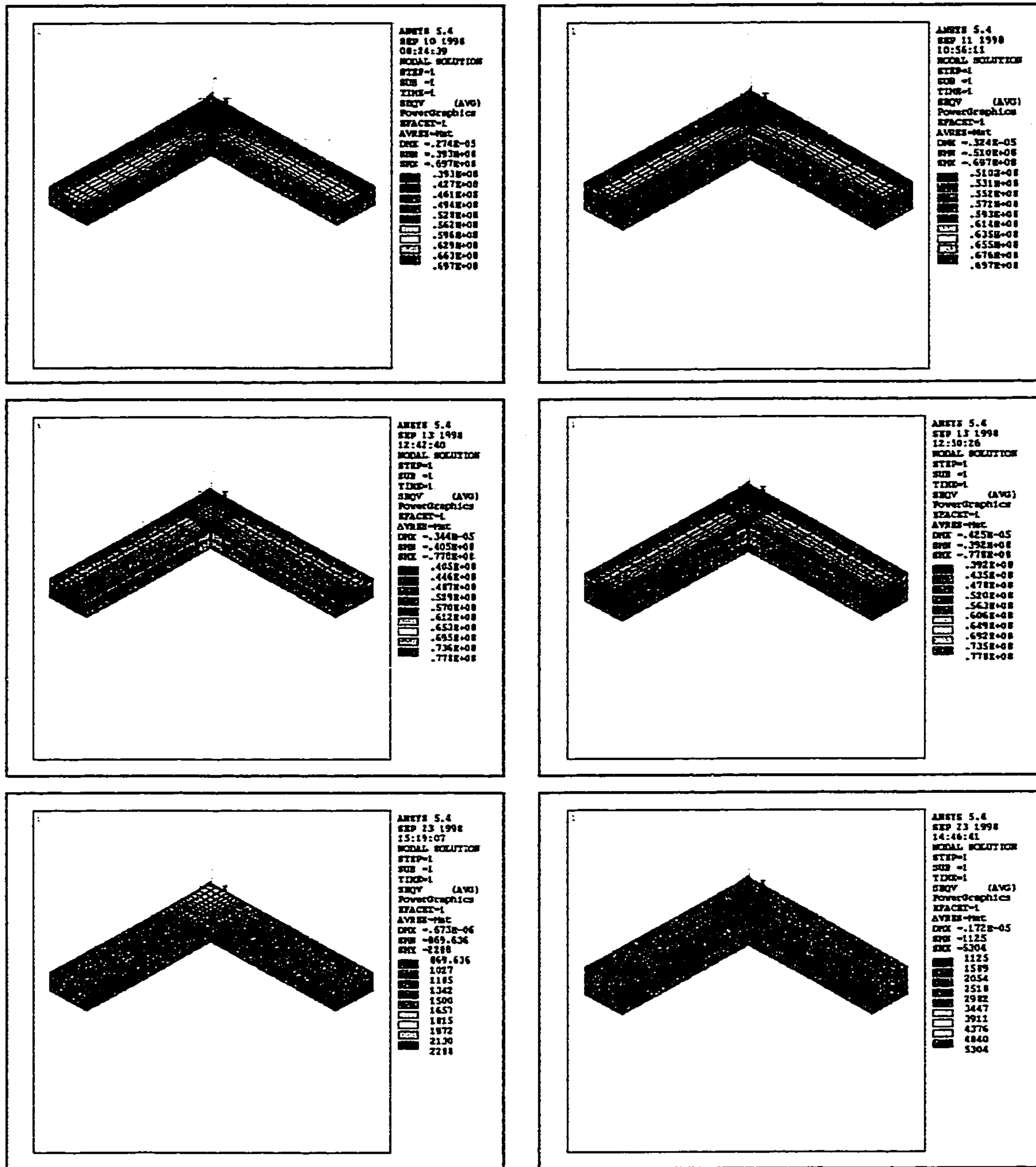

Figure 5-26: Von Mises Stress in the Die Attach for p=0, T= -40°C
Left Column: h=100 μm
Right Column: h=150 μm
Top Row: 60Sn40Pb
Middle Row: Ablebond 789-3
Bottom Row: Dow Corning 730

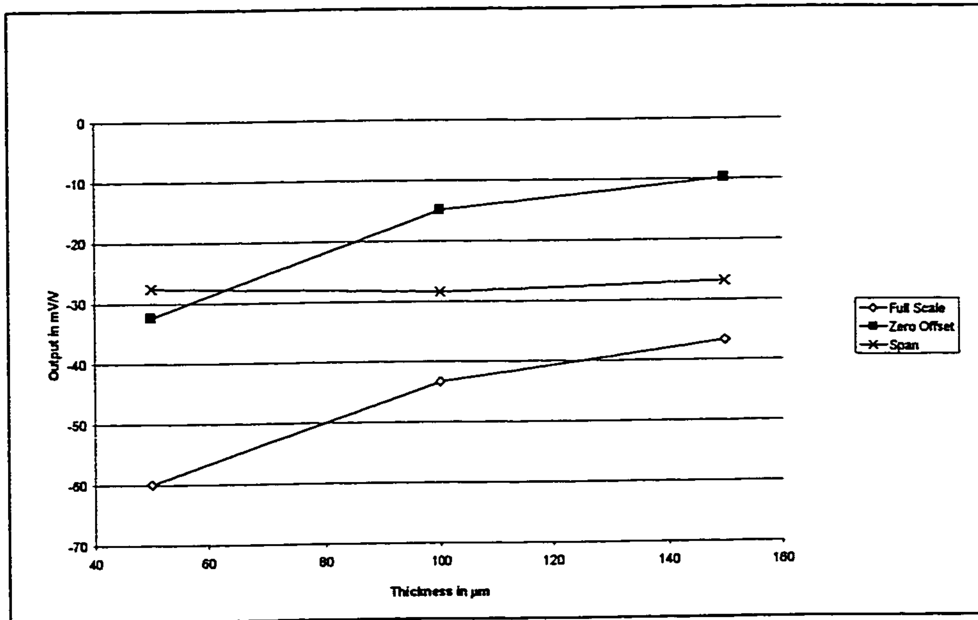


Figure 5-27: Influence of the Thickness of the Solder on the Output Characteristics

the output of the sensor. The offset and the full-scale output are decreasing with virtually the same rate. Consequently, the span shows no sensitivity to the thickness change.

The application of the Epoxy Ablebond 789-3 reduces the deformation in the unpressurized state. The Figures (5-21 and 29) show the deformation of the die at different temperatures. As seen above, the deformation is decreasing with increasing temperatures. The membrane is also bowed upward. The deformation in x-direction is similar to the one of the solder. The sides of the die are moved inwards, with the maximum at the middle of frame edge. The magnitude of the displacement is higher than the one of the solder because of the higher thermal expansion coefficient. In contrast to the larger uniform displacement, the

resulting deformation of the die is smaller than with the solder as the die attach material.

The right column of Figure (5-29) shows the y-deflection of the structure under full pressure. The membrane moves further upward. The frame is not effected by the pressurization and remains in the deformation mode that is determined by the thermal coefficient of expansion mismatch. The maximum displacement of the membrane is higher than the one of the floating die but lower than with the solder as the die attach material.

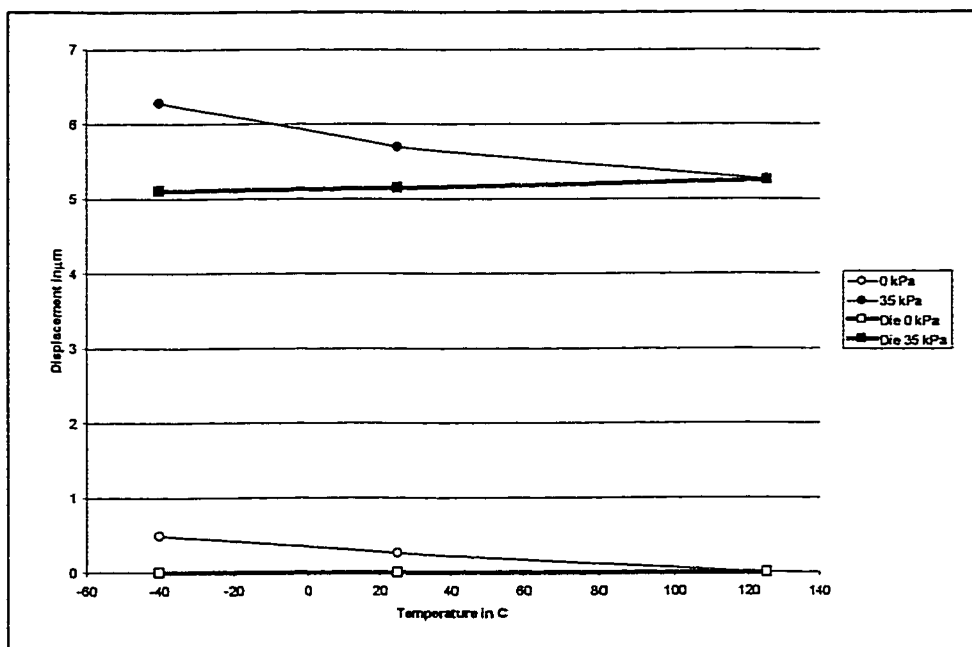


Figure 5-28: Maximum Membrane Displacement in y-Direction for Ablebond 789-3

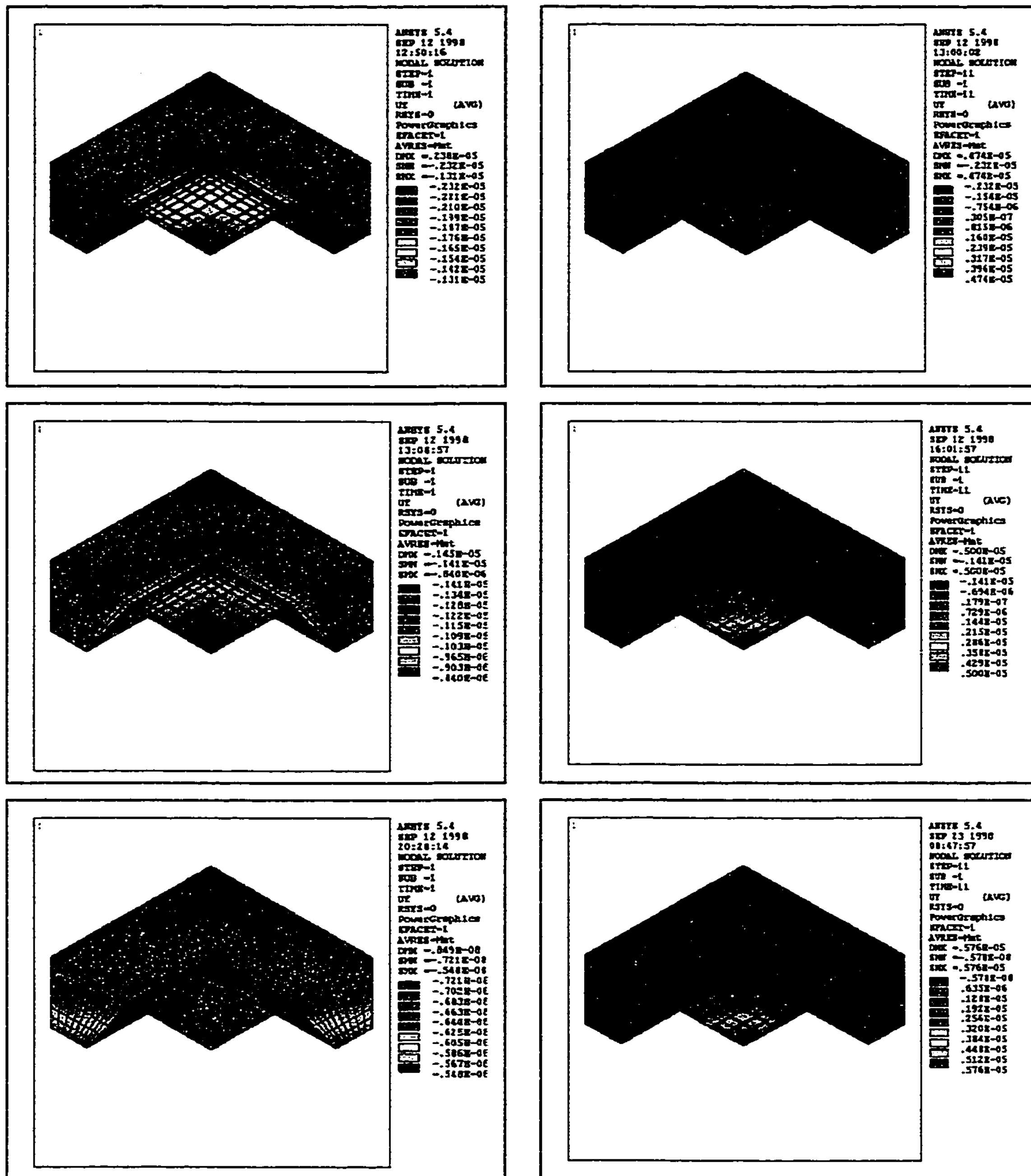

Figure 5-29: Displacement in y-Direction for Ablebond 789-3
Left Column: p=0kPa
Right Column: p=35kPa
Top Row: T=-40°C
Middle Row: T=25°C
Bottom Row: T=125°C

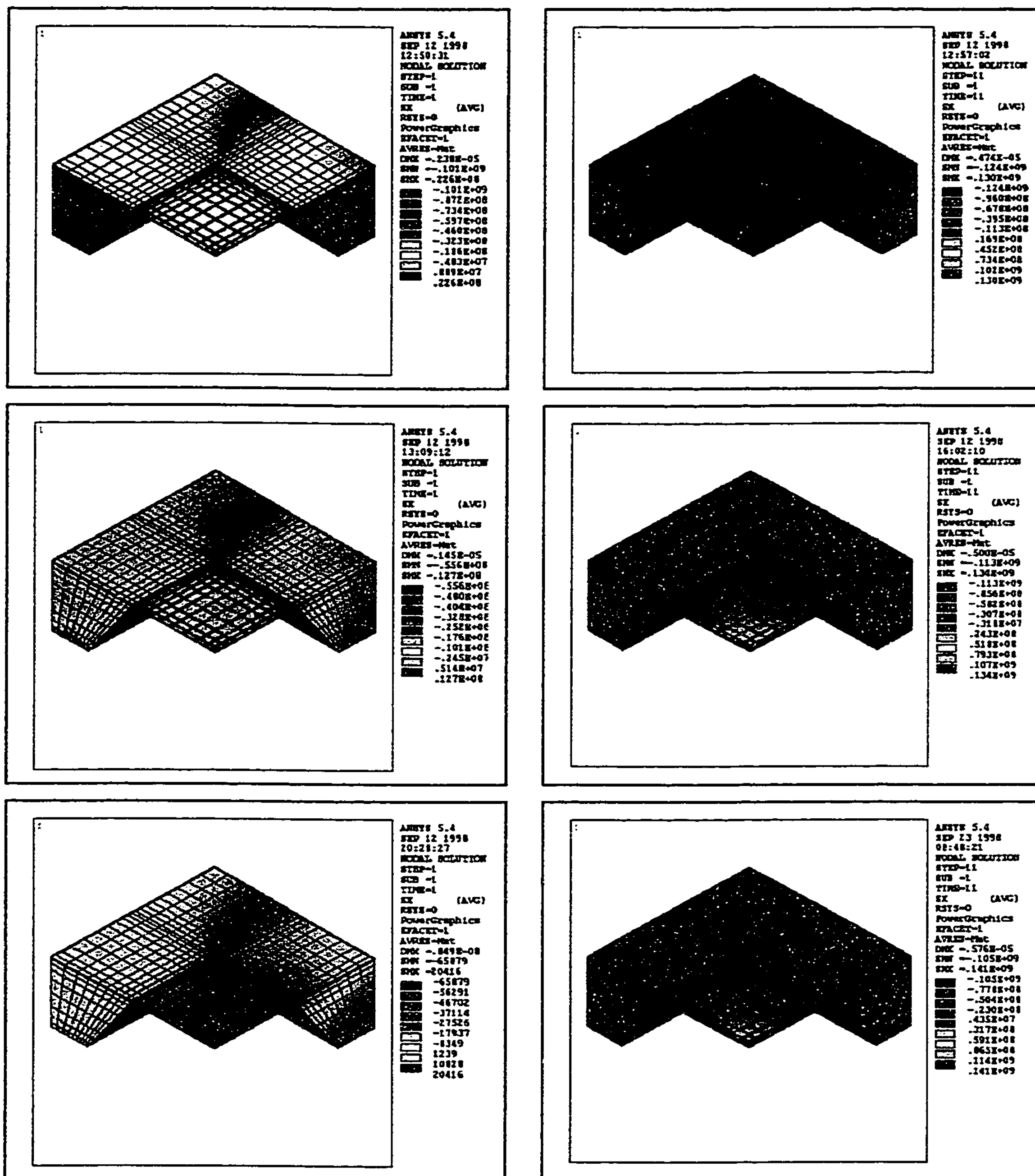

Figure 5-30: $\sigma_x$ Stress for Ablebond 789-3
Left Column: p=0kPa
Right Column: p=35kPa
Top Row: T=-40°C
Middle Row: T=25°C
Bottom Row: T=125°C

The magnitude of the residual stresses in the die also decreases, when the epoxy is used as the die attach material. Figure (5-30) show the $\sigma_x$ distribution in the die before pressure is applied in the right column. The magnitude of the residual stresses is smaller than before, but the distribution is similar.

The distribution of the stress in the pressurized die shows the known stress concentration at the middle of the diaphragm edge. The left side of Figure (5-30) shows the distribution of this component for full-scale pressure. Because of the residual stresses and the initial deformation, the stresses at full-scale pressure are increasing with decreasing temperature.

Figure (5-31) shows the calculation results in the piezoresitive region of the die. The maximal magnitude of the residual stresses in this area is about 16 MPa for $\sigma_x$, 0.1 MPa for $\sigma_y$, and 1 MPa for $\sigma_z$ (-40°C). An interesting aspect of the result is the fact that the $\sigma_z$ has a positive value for zero pressure. This component is rising in the temperature range of -40 to 25°C. A further increase in temperature results in the decrease of the stress component. This effect disappears for thicker layers of the adhesive (100 μm instead of 50 μm). The pressure nonlinearity of the stresses is also increasing for lower temperatures. The stress span is slightly decreasing with increasing temperatures ($\sigma_x$: 120 ppmK$^{-1}$, $\sigma_y$: 240 ppmK$^{-1}$, $\sigma_z$: 250 ppmK$^{-1}$). The maximum stress spans (-40°C) are: -50 MPa for $\sigma_x$, -2.8 MPa for $\sigma_y$, and -16 MPa for $\sigma_z$.

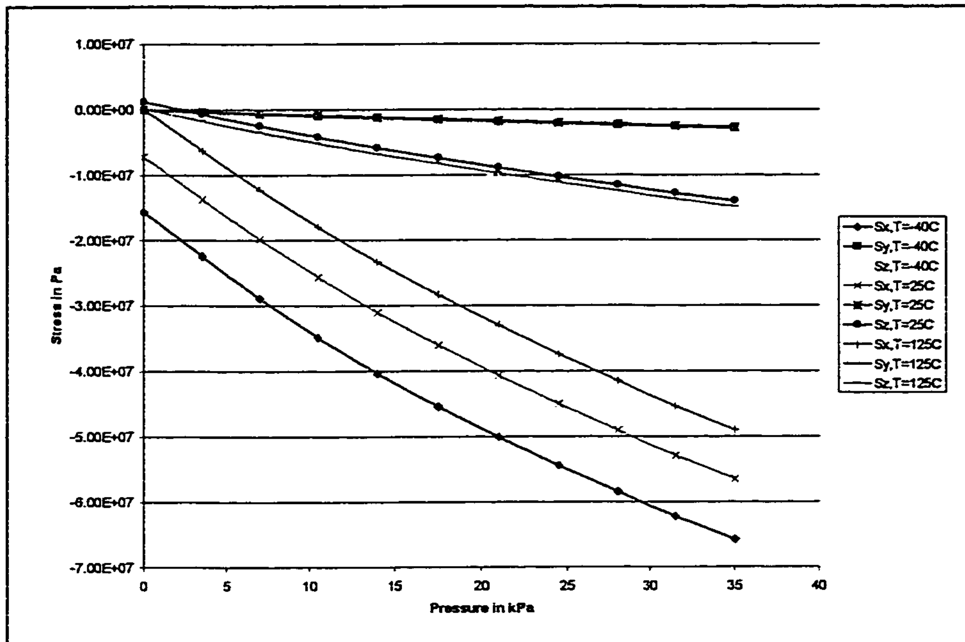


Figure 5-31: Stresses in the Piezoresistive Region for the Epoxy

The effect on the output is a lower offset with the maximal absolute value of 13 mV/V at -40°C dropping to 0 mV/V at 125°C as shown in Figure (5-32). The full-scale output ranges from -43 mV/V at -40°C to -18 mV/V at 125°C. Consequently the span is changing from -30 mV/V to -18 mV/V, which corresponds to the floating die. The pressure linearity of the output deviates from the ideal output between 8.5% (125°C), and 10% (-40°C).

The epoxy layer is also subject to extreme stresses (Figure (5-33)). The von Mises stress exceeds 75 MPa at -40°C, which is higher than the strength of the epoxy (70 MPa) and can result in a brittle failure. These stresses are decreasing with temperature. This decrease is much faster than the loss of strength of the material. Consequently, the structure is less likely to fail at higher

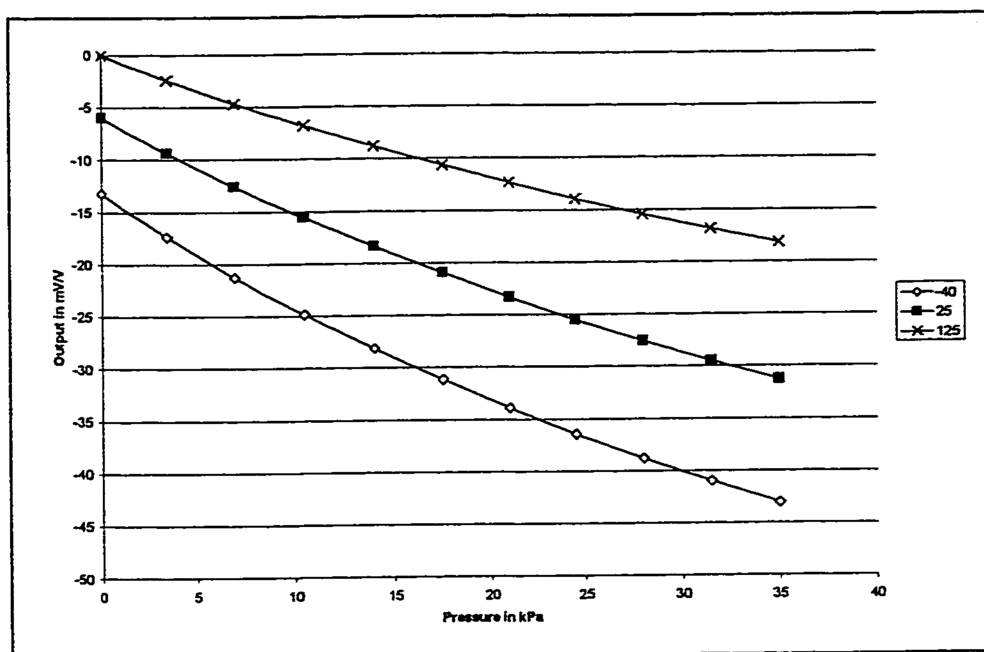


Figure 5-32: Output of the Die with the Epoxy

temperatures. The influence of the pressure on the stress in the epoxy layer is negligible for the lower temperatures. At 125°C it is the dominating factor and the stress pattern is changing.

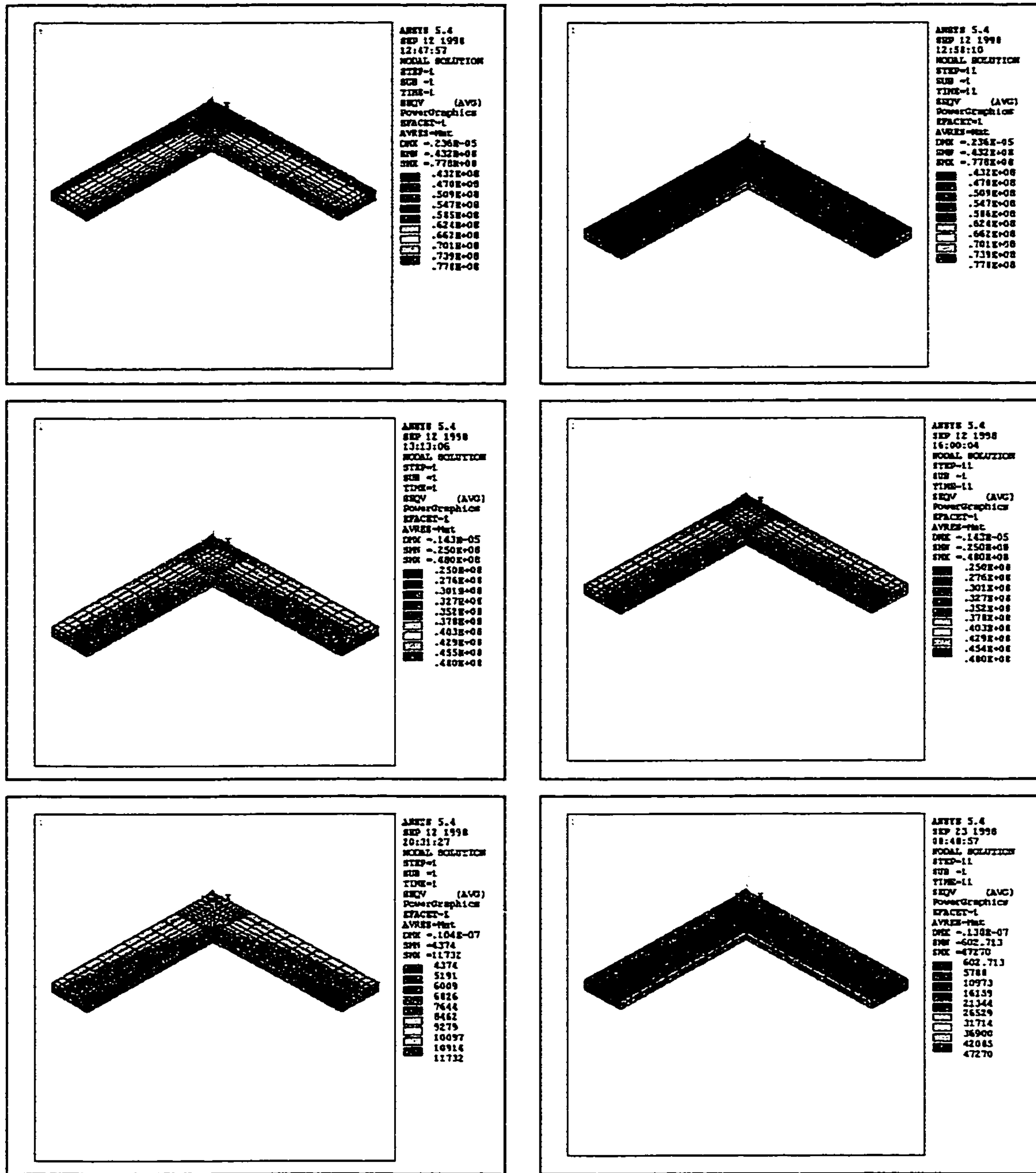

Figure 5-33: Von Mises Stress in the Ablebond 789-3 Layer
Left Column: p=0kPa
Right Column: p=35kPa
Top Row: T=-40°C
Middle Row: T=25°C
Bottom Row: T=125°C

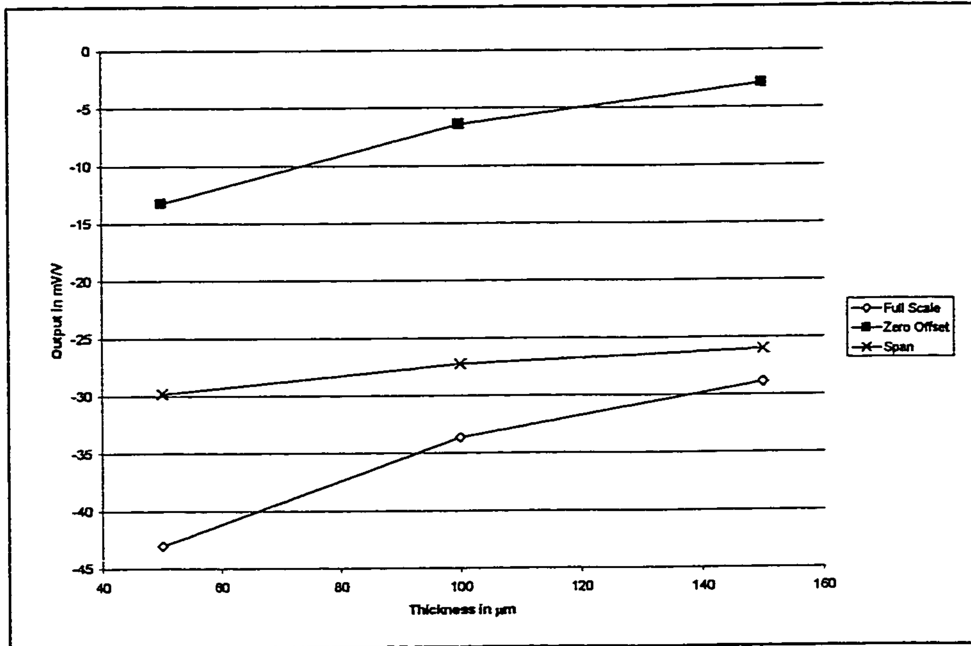


Figure 5-34: Influence of the Thickness of the Epoxy Layer on the Output Characteristics

The thickness increase has similar effects like with the solder. The stresses in the bulk of the layer are decreasing while the peaks at the interface to the silicon are remaining (Figure (5-26)). The stress isolation is increased and the offset is decreasing. The increase in flexibility of the structure results in a faster change in the full-scale output than in the offset. The span changes from -30 mV/V with a 50 µm layer to -26 mV/V for a 150 µm film as shown in Figure (5-34)

The last bonding material is a silicon rubber. The flexibility of the RTV should give the die sufficient stress isolation. Consequently, the deformations at zero pressure are very small for all temperatures Figure (5-35). At the bonding temperature of 25°C, the material is completely deformation and stress free at

this particular temperature. Another result of the bonding temperature is the opposite signs for the displacements at -40°C and 125°C (Figure (5-36 and 37)).

The left column of Figure (A-9) shows the y-displacement at full-scale pressure. The results show that the whole die is moved upward when pressure is applied. This is a result of the flexibility of the RTV. The deflection of the membrane corresponds to the deflection of the unbonded die.

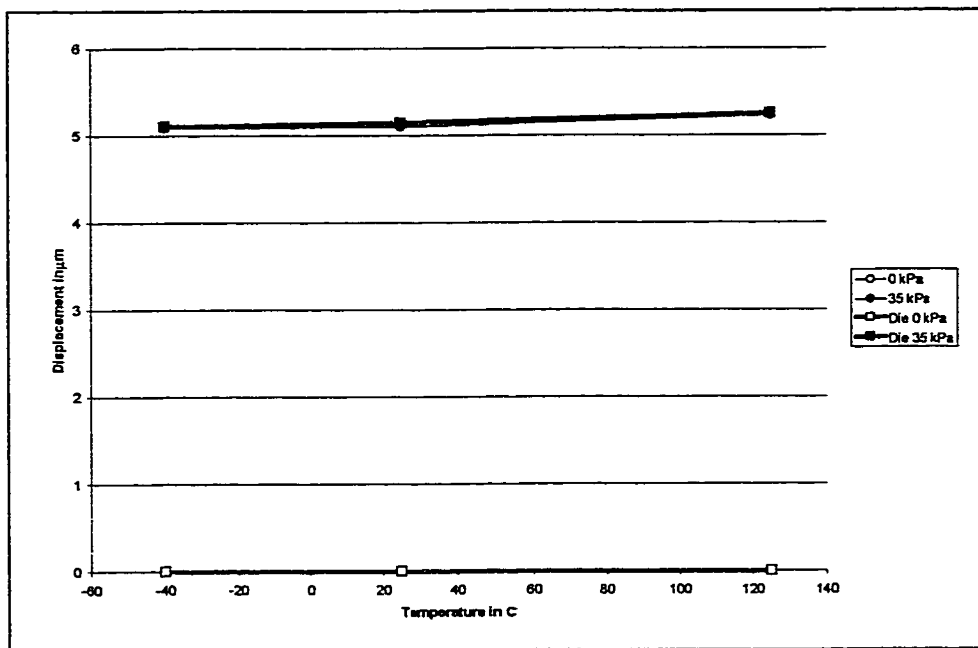


Figure 5-35: Maximum Membrane Displacement in y-Direction for Dow Corning 730

The $\sigma_x$ stress in the unpressurized die is shown in right side of Figure (5-38). It can be seen that the stress level in the die is very low compared with the previous results. An interesting aspect of the result is the fact that $\sigma_x$ in the membrane is tensile for -40°C and compressive for 125°C.

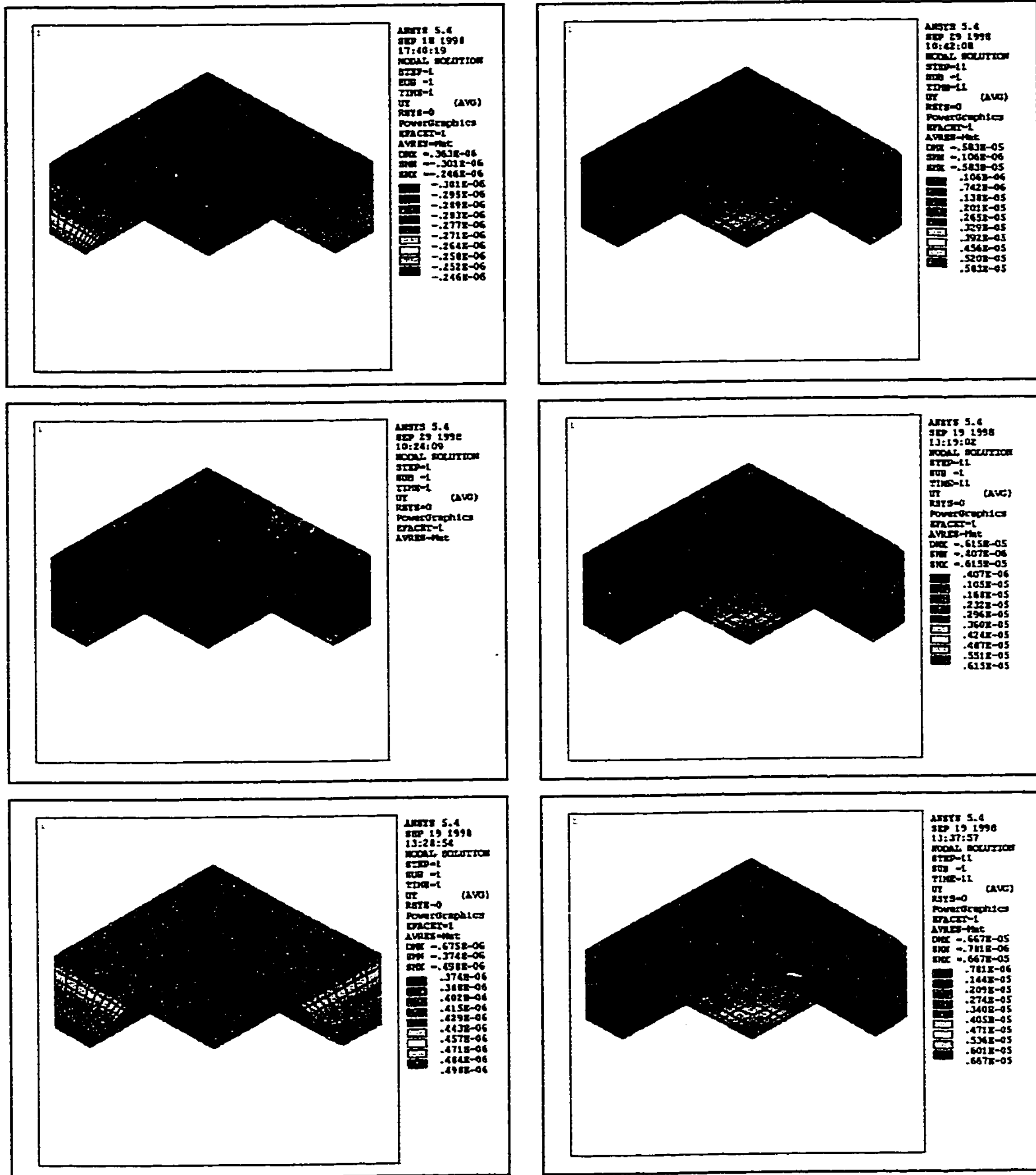

Figure 5-36: Displacement in y-Direction for Dow Corning 730
Left Column: p=0kPa
Right Column: p=35kPa
Top Row: T=-40°C
Middle Row: T=25°C
Bottom Row: T=125°C

Figure 5-37: Displacement in x-Direction for Dow Corning 730, p=0
Top Row: T=-40°C
Middle Row: T=25°C
Bottom Row: T=125°C

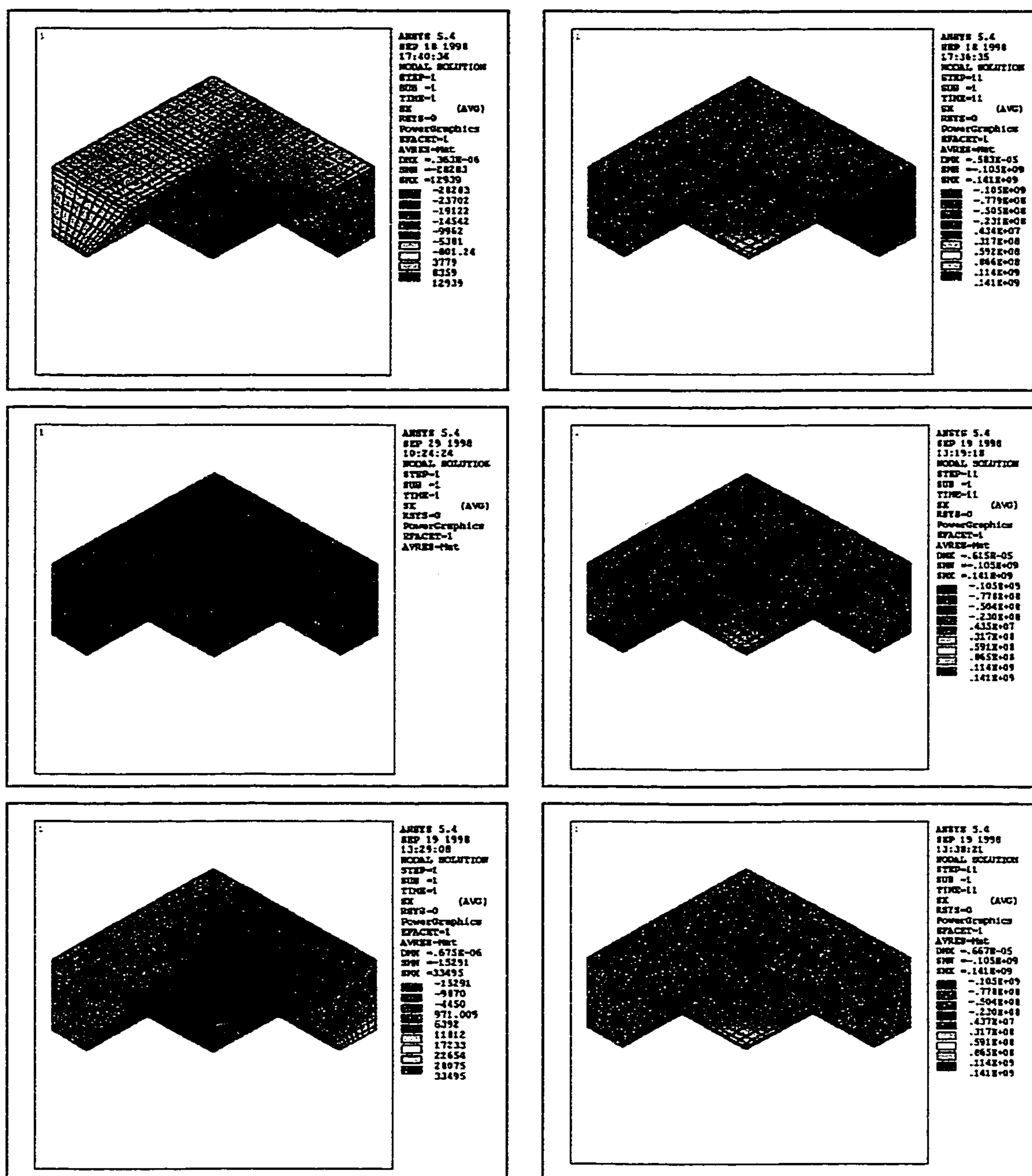

Figure 5-38: $\sigma_x$ Stress for Dow Corning 730
Left Column: p=0kPa
Right Column: p=35kPa
Top Row: T=-40°C
Middle Row: T=25°C
Bottom Row: T=125°C

The results for the $\sigma_x$-component in the pressurized die is illustrated in the left column of Figure (5-38). The stress shows the same pattern and magnitudes for all three temperatures that correspond to the floating die.

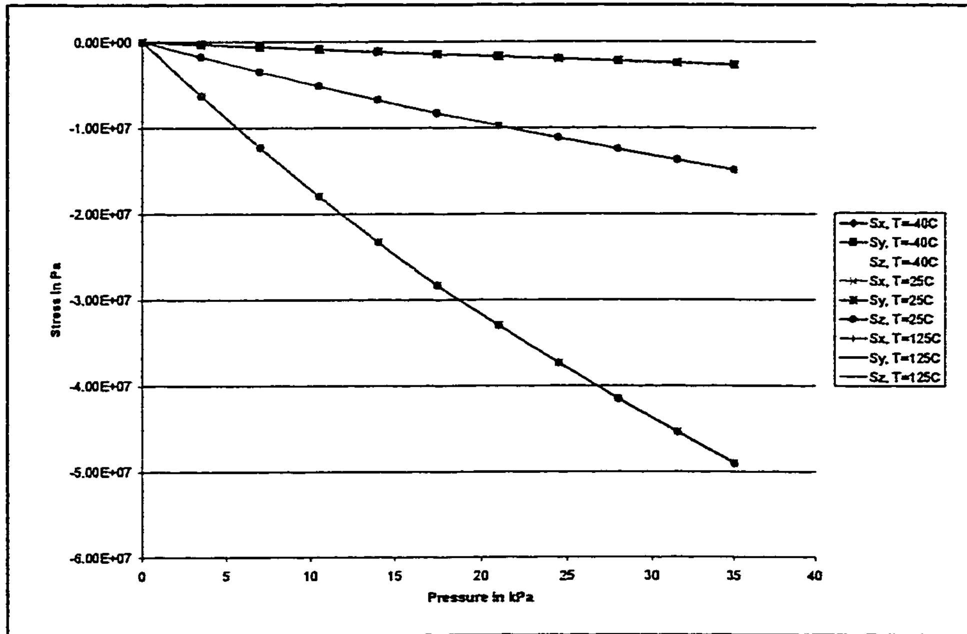


Figure 5-39: Stresses in the Piezoresistive Region for the RTV

The magnitude of the residual stresses in the region of the piezoresistors are with less than 15 kPa in $\sigma_x$, 60 Pa in $\sigma_y$, and 10 kPa in $\sigma_z$ negligible, compared with the full-scale stresses of 15 or 50 MPa in these components as shown in Figure (5-39). The residual stresses are tensile in the low temperature case and compressive for high temperatures. The stress span at all three temperatures is coinciding with the stress span of the floating die, since the change of the stress span is minor ($\sigma_x$: 11 ppmK$^{-1}$, $\sigma_y$: 42 ppmK$^{-1}$, $\sigma_z$: 24 ppmK$^{-1}$).

The small residual stresses cause an offset, that is also negligible (absolute value less than 5 μV/V). The full scale offset and therefore the span is ranging from -30 mV/V at -40°C to -18 mV/V at 125°C. The pressure nonlinearity for all three temperatures is less than 9%, which is the value that is determined by the die (Figure (5-40).

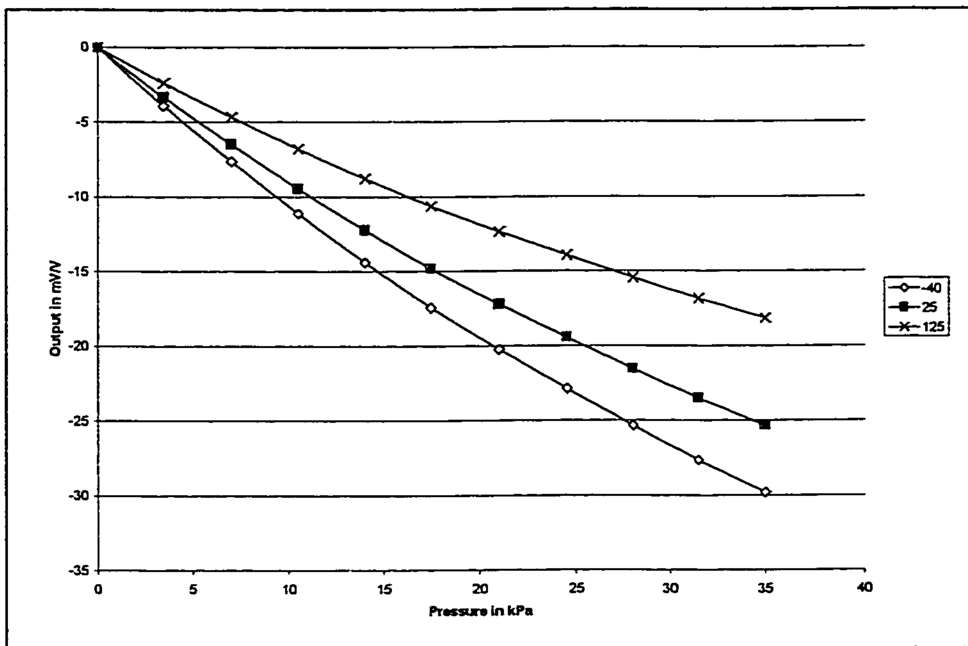


Figure 5-40: Output of the Die with the RTV

The stresses in the RTV layer are much smaller than the stresses in the bonding materials tested above (Figure (5-41)). The von Mises stress due to the thermal mismatch is less than 5 kPa. The applied pressure has a large influence on these stresses. At full scale, the stress rises to about 40 kPa (125°C). The thickness of the layer (50 μm) is already sufficient to provide the desired stress

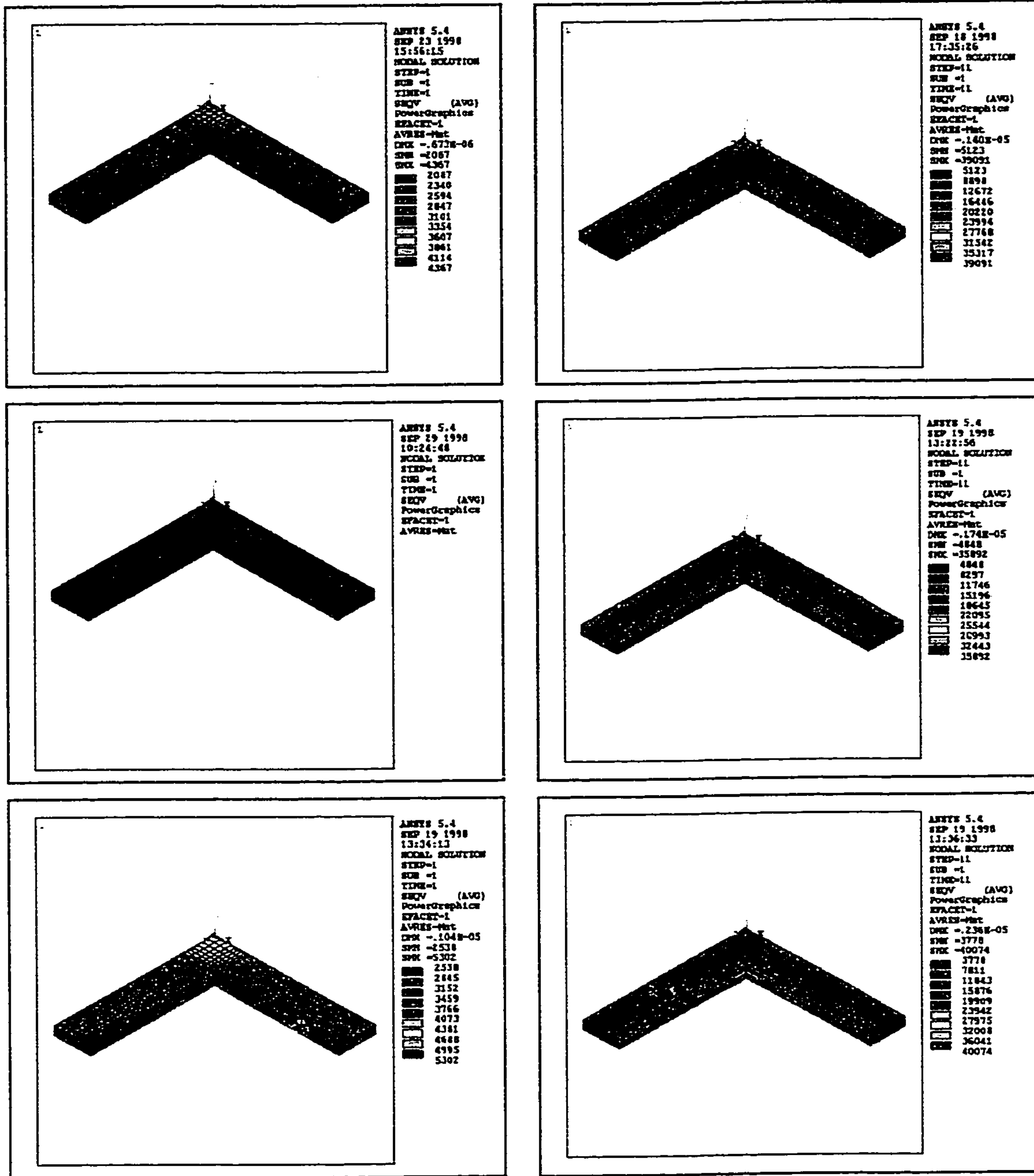

Figure 5-41: Von Mises Stress in the Dow Corning 730 Layer
Left Column: p=0kPa
Right Column: p=35kPa
Top Row: T=-40°C
Middle Row: T=25°C
Bottom Row: T=125°C

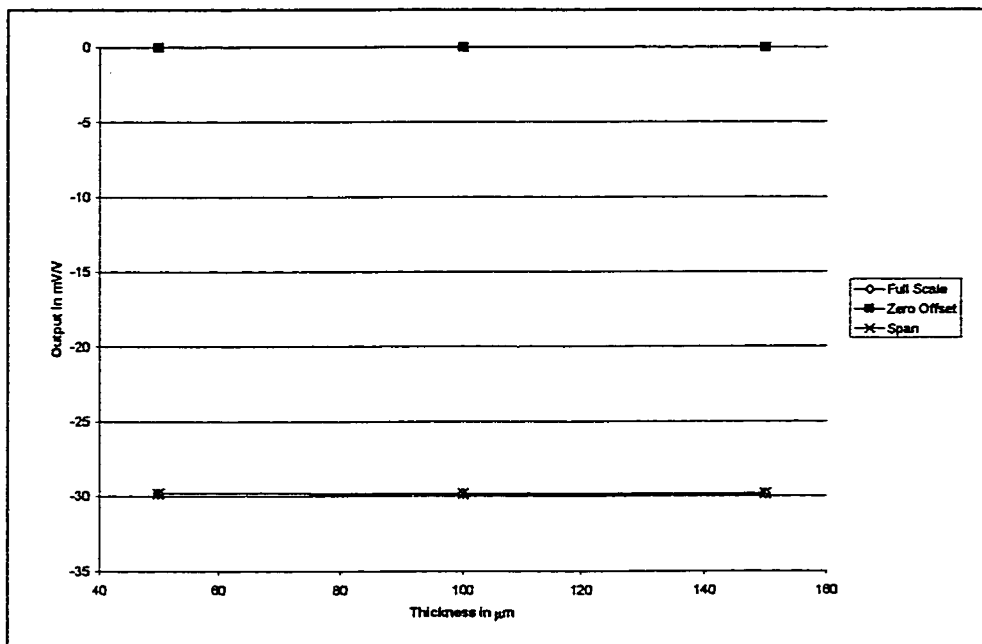


Figure 5-42: Influence of the Thickness of the RTV Layer on the Output Characteristics

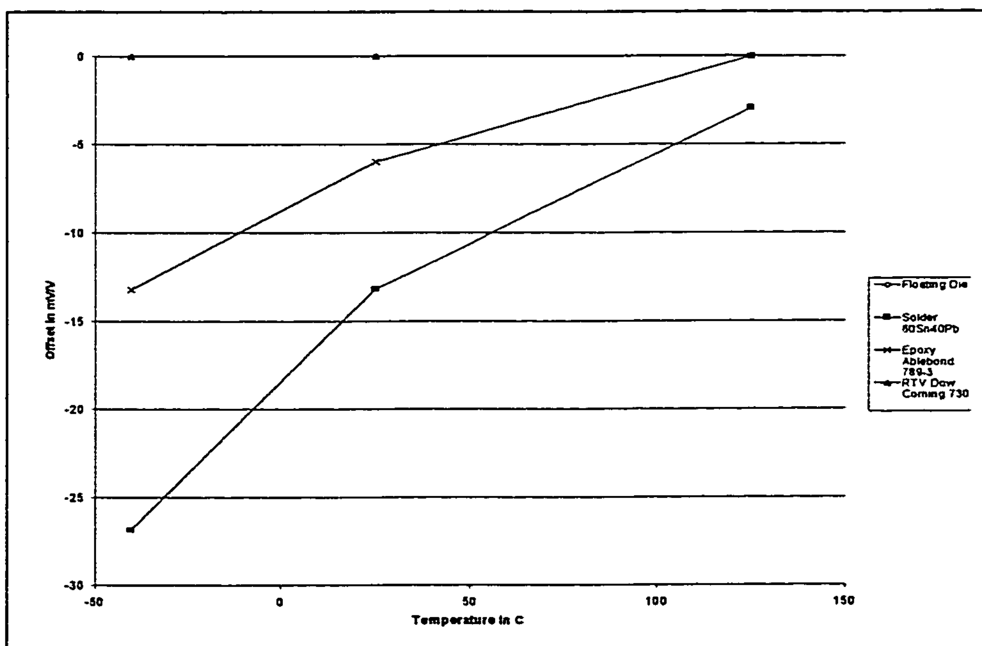


Figure 5-43: Influence of the Die Attach on the Offset

isolation. An increase in the thickness has no influence on the die performance (Figure (5-42)) or on the stresses in the layer (Figure (5-26)).

Figure (5-43) indicates the influence of the different die attach materials on the offset of the die. The offset of the ideally balanced floating die is zero for all temperatures. The use of the RTV as the die attach material allows a mounting of the die that virtually does not influence the offset of the die. The low residual stresses result in extremely low offsets with a linearity deviation of less than 0.5% (normalized with the span at 25°C). The epoxy has practically no offset at 125°C. It shows an increase in the offset magnitude with decreasing temperatures, reaching an offset of -13 mV/V at -40°C. This change is nonlinear and the gradient is increasing at lower temperatures. The nonlinearity of the offset-temperature curve is about 7%. The solder with the highest Young's Modulus results in the highest offset magnitudes. Due to the higher bonding temperature of 183°C, there is an offset for all measured temperatures. The change of this offset over temperature is higher than with the epoxy as the die attach material. It can also be seen that there is the same trend of an increasing gradient at lower temperatures. The offset of the solder is changing from -3 mV/V at 125°C to -27 mV/V at -40°C. The nonlinearity of the solder is the highest with 16% of the span at 25°C.

The full-scale output is also influenced by the die attach. This influence is shown in Figure (5-44). The output change over temperature for the floating die is determined by the decrease of the piezoresistive coefficients. With the

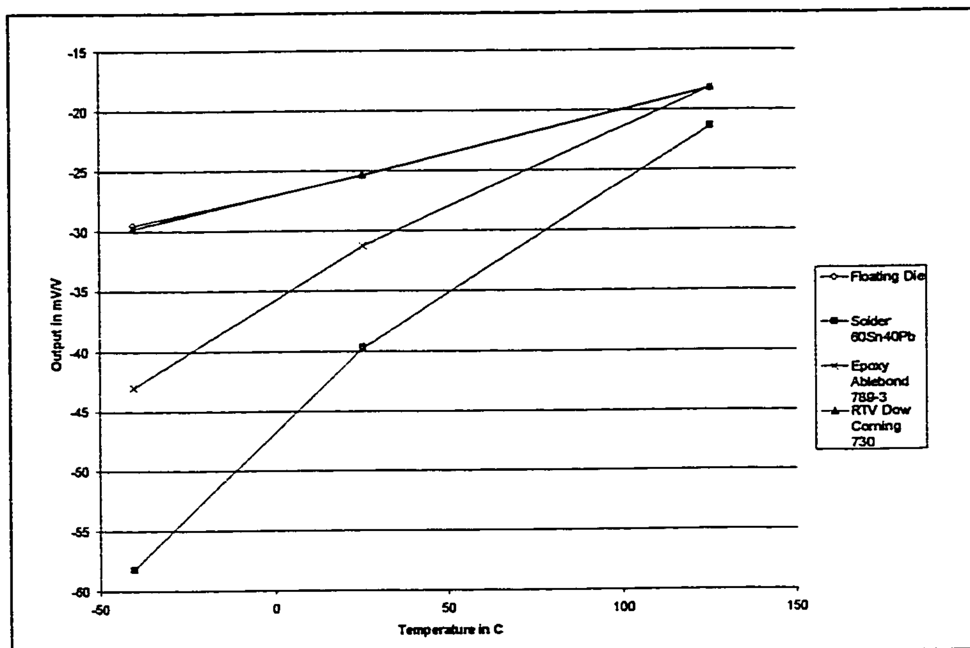


Figure 5-44: Influence of the Die Attach on the Full-Scale Output

assumption of a linear change in this parameter, the full-scale output is also changing linearly from -30mV/V at -40°C to -18 mV/V at 125°C. The application of the RTV results in minor changes of this behavior and the magnitude of the output is slightly larger. The nonlinearity is also minor with less than 0.5% of the span at 25°C. The use of the epoxy or the solder as the die attach material results in a change that is characteristic. The nonlinearity of the full-scale output is about 7% for the epoxy and 14% for the solder. However, this change is primarily a superposition of the linear change of the piezoresistive coefficients and the offset described above. Consequently , the epoxy changes the output from -43 mV/V (-40°C) to -18 mV/V (125°C). Only the solder exhibits a change

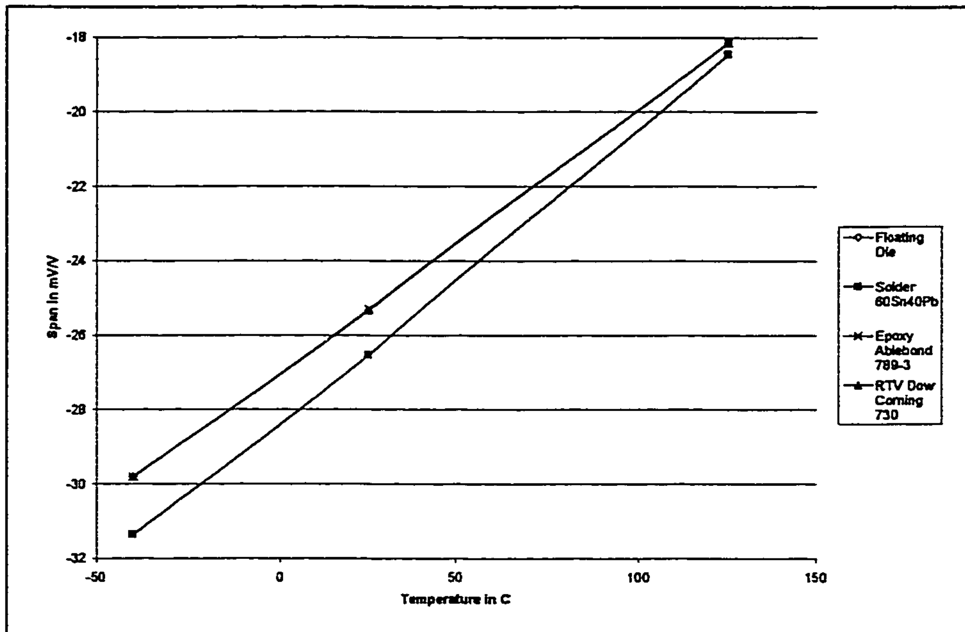


Figure 5-45: Influence of the Die Attach on the Span

that is exceeding these effects with a change from -58 mV/V to -21m/V over the studied temperature range.

The span that is shown in Figure (5-45) is the difference between the full-scale output and the offset for a particular temperature. The span for the floating die, the RTV, and the epoxy is changing at the same rate of about 0.07 mV/VK. The output for the solder differs from this span. It has higher magnitude and is steeper (0.08 mV/VK) than the other span-temperature curves.

## 5.8 Discussion of the Case Study

The finite element analysis showed that the die attach material has an important influence on the output of the sensor

The results of the calculation of the floating die show the effects that are cause by the structure of the die itself and the inherent changes of the piezoresistivity with temperatures. Although this model shows a nonlinear pressure dependency, the temperature performance is ideal.

The application of the die to a substrate results in a thermal mismatch at the interface of the materials. The intermediate layer can be utilized to buffer this mismatch. It is therefore desirable to use a material with a low elastic modulus and a good linearity in this layer.

The solder has a low modulus compared to the silicon and the aluminum oxide. However, it has the highest modulus of the bonding materials tested. Consequently, the residual stresses are the highest in the test. The value for the $\sigma_x$ at -40°C is more than double the value of the epoxy (42 MPa vs. 16 MPa). Both materials show a decrease of linearity of the stresses over pressure as well as a decrease of the stress span with increasing temperature. The reason for this behavior is the effect of pre-stressing and pre-deformation. Figure (5-46) shows an exaggerated picture of the die deformation at -40°C for the solder. The frame of the die is pushed inward, causing compressive stresses in the membrane and an upward displacement. This pre-deformation stiffens the membrane and causes the stresses span to rise.

Figure (5-47) shows the result for the die that is attached with the RTV. The deformation mode is different. The frame is twisted outward, stretching the

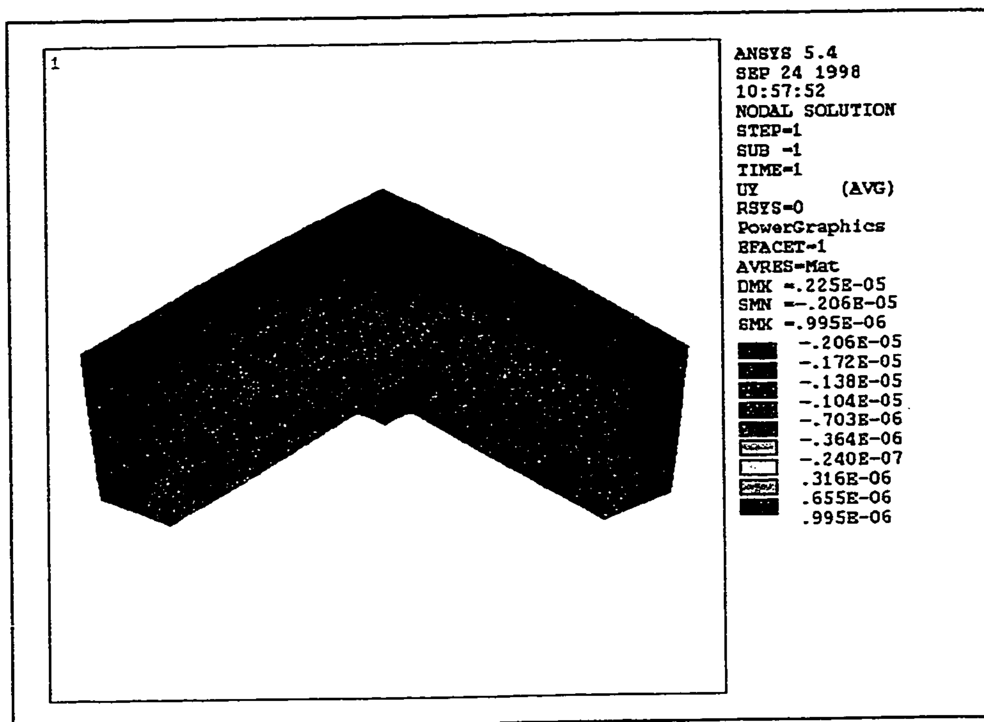


Figure 5-46: Deformation of the Die with the Solder at -40°C

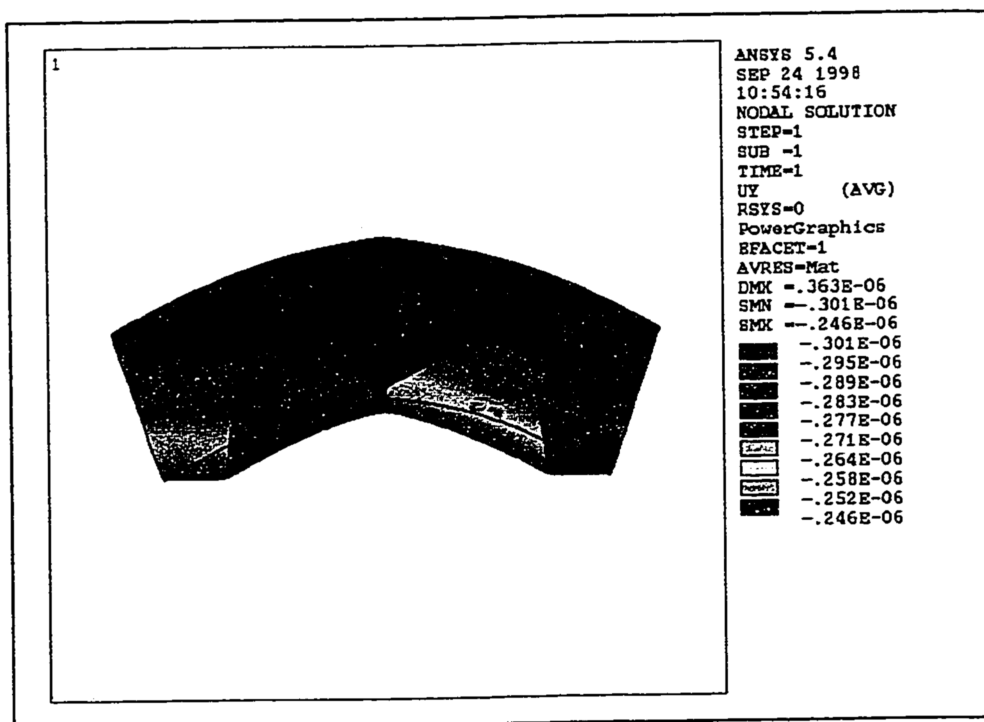


Figure 5-47: Deformation of the Die with the RTV at -40°C

diaphragm. This is the reason for the slight tensile stresses that are predicted in the piezoresistive region.

These two results are caused by the difference of the die attach. The high modulus of the solder is not sufficient to isolate the die from the displacement of the substrate. Therefore, the thermal shrinkage of the alumina is dominating the deformation in this case. The RTV has a modulus that is several orders of magnitude smaller than the solder. Consequently, the adhesive complies to the dimensional changes of the aluminum oxide. This shearing of the RTV layer causes a twisting of the frame rather than a bending.

The epoxy has a modulus that is closer to that of the solder. Therefore, the displacement isolation is only sufficient for small displacements or with thicker layers of the adhesive. This can be seen in the behavior of the $\sigma_z$ offset in the piezoresistive region. The tensile stresses are decreasing in the higher temperature span, where the epoxy provides a reasonable displacement isolation. With increasing dimensional change of the alumina, this isolation becomes insufficient and the compressive stresses caused by this change are taking over. The tensile stress is therefore decreasing. The doubling of the thickness of the adhesive layer provides the needed compliance to compensate for this development. Consequently, this effect disappears and the tensile stress is increasing with decreasing temperatures.

The pressure and temperature nonlinearities of the output of the sensor are increasing with increasing Young's Modulus of the bonding material. This is

a result of the above-described pre-deformation of the die. The overall deformation of the diaphragm is increasing. This causes an increase in the nonlinear stress component that influences the output of the sensor.

The bonding material is the weak point of the structure. The high stresses exceed the yield stress of the solder at -40°C and stay close to this value at the other evaluated temperatures. The expected plastic deformation causes an undesired hysteresis in the output of the sensor. Thermal cycling will also result in failure due to fatigue, which is a major problem of solders. Consequently, cyclic plastic deformation caused by thermal or pressure cycling has to be avoided.

A similar problem exists for the epoxy. The failure strength is exceeded at the lowest temperature, whereas the stress level at the higher temperatures remains below the strength of the material. This can result in the immediate failure of the unit at low temperatures. The strength loss at temperatures that are close to the glass transition temperature (126°C) limits the pressure range for sensors in which the material can be used.

The stress values are completely within the elastic range for the RTV. This is not only a result of the low modulus of this material but also of the bonding temperature of 25°C. The location of the stress free temperature within the desired temperature span reduces the dimensional changes of the structure. Whereas the maximum temperature difference for the solder to the bonding temperature is 223°C, it is less than the half for the RTV. This combined with the

elastic behavior of the material makes it an interesting adhesive for low-pressure die attach applications.

An increase in the die attach thickness results in the decrease of the stress in this layer, while the peak stresses remain constant. The decrease of the bulk stress can be explained with the nature of these stresses that are caused by a prescribed deformation. The increase in the height decreases the strain in the layer. It also reduces the influence of the dimensional changes of the substrate. However, the peak strains and stresses are determined by the direct contact of the materials. They remain constant because the strain at the interface is not effected by the increase of the layer thickness.

The RTV Dow Corning 730 has the best performance of the three materials that were analyzed. The effect on the output of the sensing die is negligible and it withstands the loads due to the thermal coefficient of expansion mismatch of the materials. A problem of this material is its chemical resistance and the swelling when it is in contact with organic fluids.

The epoxy Ablebond 789-3 is insufficient for low temperature applications. The influence of the direct attach is acceptable and can be reduced by an increased thickness of the layer. The higher chemical inertness makes it interesting for automotive applications.

The application of the solder 60Sn40Pb results the highest distortion of the output signal. The stresses in the material exceed the elastic limit, causing

thermal hysteresis and the danger of fatigue failure. The studied material is not applicable for a direct die attach.

# 6. Recommendations for Future Research

Several new problems arose in the course of this study, that are worth of consideration for future research in the field of MEMS.

This study covers the influence of the die attach step on the sensor performance. The wafer-scale production steps are other important sources for residual stresses in the die. An investigation of the influence of the production steps on the die performance would be of high interest. This would lead to a procedure to determine the properties of the different material layers for a specified die application. This includes not only the deposition of surface layers such as silicon nitride, silicon oxide and metal, but also the systematization of doping profiles.

One huge field for research is the systematization of the effects of the mechanical parameters of the die attach materials. It would be interesting to analyze the individual influence of the Young's Modulus, Poisson's Ratio and the thermal coefficient of expansion. A resulting interesting aspect would be the optimization of the bond height for specific material properties.

Due to their higher chemical resistance, solders are interesting bonding materials. This study showed that the 60Sn40Pb solder is not applicable for the direct die attach. Other solders, with lower modulii should be studied to find a possibility of a direct die attach for hostile environments.

The material properties that are used in this study are taken from conventional material test techniques. The application of the material in thin

layers (50 μm) will result in changes in the properties because surface properties will gain more influence. It is therefore necessary to develop techniques that enable the measurement of specimens that have surface to volume ratios that are similar to the application. Another approach is to develop a theory that enables the recalculation of data taken at bulk specimens into the meso-scale of MEMS that is between the macro-scale of standard tests and the micro-scale of the atomistic approach.

The long-term stability of a sensor is an important design parameter. A predictive model for this criterion could reduce the product development time. The influence of stress relaxation and creep of deposited layers such as silicon oxide and silicon nitride as well as the die attach has to be studied in detail for such a model.

# References


[1] Bryzek, J., Petersen, K., Mallon, J. R. Jr., Christel, L., Pourahmadi, F.: "Silicon Sensors and Microstructures", NovaSensor, Sept 1991

[2] Mehregany, M., Walsh, S.: "MEMS Technology Tutorial", SEMI Technical Programs,1997

[3] Pottenger, M., Eyre, B., Kruglick, E., Lin, G.: "MEMS: The maturing of a new technology", Solid State Technology, Sept 1997, p 89 (5)

[4] Petersen, K.: "Silicon as a Mechanical Material", Proceedings of the IEEE, v 70, n 5, May 1982, p 420 (18)

[5] Wise, K. D.: "Micromechanical Sensors, Actuators and Systems", The American Society of Mechanical Engineering, Micromechanical Sensors, Actuators, and Systems, Ed. Cho, D., Warrington, R. Jr., Pisang, A., Bau, H., Friedrich, C., Jara-Almonte, J., Liburdy, J., 1991, p1 (14)

[6] Madou, M.: "Fundamentals of Microfabrication", CRC Press, 1997

[7] Bryzek, J., Petersen, K., Christel, L., Pourahmadi, F.: "New Technologies for Silicon Accelerometers Enable Automotive Applications", SAE Technical Paper Series, from Sensors and Actuators, 1992, p 25 (9)

[8] Abachi, R.: "An Overview of Automotive Sensors", Sensors, , v 13, n 4, Apr 1996, p 82 (4)

[9] Kovacs, G. T. A.: "Micromachined Transducers - Sourcebook", WBC McGraw-Hill, 1998

[10] Petersen, K., Pourrahmadi, F., Brown, J., Parson, P., Skinner, M., Tudor, J.: "Resonant Beam Pressure Sensor Fabricated with Silicon Fusion Bonding", Transducers 91, IEEE Electron Devices Society, 1991, p 664 (4)

[11] Smits, J. G., Tilmans, H. A. C., Lammerink, T. S. J.: "Pressure dependence of resonant diaphragm pressure sensor", Transducers 85, International conference on solid-state sensors and actuators, 1985, p 93 (4)

[12] Lammerink, T. S. J., Wlodarski, W.: "Integrated thermally excited resonant diaphragm pressure sensor", Transducers 85, International conference on solid-state sensors and actuators, 1985, p 97(4)

[13] "Trends in automotive engineering", Automotive Engineering, Sept 1997, p 31 34

[14] Adler, U.: "Automotive Handbook", Robert Bosch GmbH, 1993, 3rd edition

[15] Powell, J. D.: "Engine Control Using Cylinder Pressure: Past, Present, and Future", Journal of Dynamic Systems, Measurement, and Control, Transactions of the ASME, v 115, n 2B, June 1993, p 343 (8)

[16] Bryzek, J., Petersen, K., McCulley, W.: "Micromachines on the march", IEEE Spectrum, v 31, n 5, May 1994, p20 (12)

[17] "Motorola Sensors", Automotive Engineering, v 103, n 9, Sept 1995, p 44 (1)

[18] Tada, Y., Kishimoto, Y.: "Airflow Sensors for Automobiles", Mitsubishi electric advance, v 62, Mar 1993, p 2 (2)

[19] Baney, W., Chilcott, D., Huang, X., Long, S., Siekkinen, J., Sparks, D., Staller, S.: "A Comparison Between Micromachined Piezoresistive and Capacitive Pressure Sensors", SAE International, Electronics and Electrical Systems for Trucks and Busses, p 61 (4)

[20] Meth, C.: "Micromachining Improves Automotive Sensors", Electronic Design, Feb 5, 1996, p 67 (7)

[21] "Fiber-optic sensors for combustion monitoring and control", Automotive Engineering, v 103, n 9, Sept 1995, p 45 (1)

[22] Lee, C. E., Taylor, H. F.: "A Fiber-Optic Pressure Sensor for Internal Combustion Engines", Sensors, Mar 1998, p 20 (6)

[23] Wlodarczyk, M. T., He, G.: "A Fiber-Optic Combustion Pressure Sensor for Automotive Engine Control", Sensors, June 1994, p 35 (8)

[24] Ashley, S.: "Spin control for cars", Mechanical Engineering, v117, n 6, June 1995, p 66 (3)

[25] "Berlin conference projects bright future for automotive microsystems", Micromachine devices , Apr. 1998, n 4, p1 (6)

[26] Binder, J.: "New Generation of automotive sensors to fulfil the requirements of fuel economy and emission control", Sensors and Actuators A, v 31, n 1-3, March 1992, p 60(8)

[27] Ohlckeners, P., Jakobsen, H.: "High volume production of silicon sensor microsystems for automotive applications", IEE Colloquium, n 4, 1997, p 8/1 (7)

[28] Sasayama, T., Suzuki, S., Tsuchitani, S., Koide, A., Suzuki, M., Nakazawa, T., Ichikawa, N.: "Highly reliable silicon micro-machined physical sensors in mass production", Transducers '95, Eurosensors IX, p 687 (4)

[29] Chanko, T., Hepburn, J., Sweppy, M., Zaghati, Z., Zimlich, G., Kurihara, N., Kimura, H., Ishii, T., Takaku, Y.:"The Challenges of OBD-II", Automotive Engineering International, Feb 1998, p 14 (3)

[30] Ko, W. H.: "The future of sensor and actuator systems", Sensors and Actuators A, v 56, n 1-2, Aug 1996, p 193 (5)

[31] Allan, R.: "Silicon MEMS Technology Is Coming Of Age Commercially", Electronic Design, v 45, n 2, Jan 20, 1997, p 75 (8)

[32] Pourahmadi, F., Twerdok, J. W.: "Modeling Micromachined Sensors with finite elements", Engineering & Technology Guide, from Machine Design, July 26, 1990, 8 pages

[33] Vinci, R.P., Bravman, J. C.: "Mechanical testing of thin films", Transducers 91, IEEE Electron Devices Society, 1991, p 943 (6)

[34] Krulevitch, P., Howe, R. T., Johnson, G. C., Huang, J.: "Stress in undoped LPCVD polycristalline silicon", Transducers 91, IEEE Electron Devices Society, 1991, p 949 (4)

[35] Connally, J. A., Brown, S. B.: "Micromechanical Fatigue Testing", Transducers 91, IEEE Electron Devices Society, 1991, p 953 (4)

[36] Leonard, M.: "Micromacining Technologies promise Smarter Sensors, Actuators For A Broad Range of Applications", Electronic Design, v 43, n 25, Dec 4 1995, p 35 (5)

[37] McCluskey, P., Pecht, M.: "Pushing the Limit", Advanced Packaging, Jan/Feb 1997, p 36 (3)

[38] Ko, W. H.: "Packaging of microfabricated devices and systems", Materials Chemistry and Physics, v 42, 1995, p 169 (7)

[39] "Trends in automotive sensing", Automotive Engineering, Sept 1997, p 31 (4)

[40] "Automotive Electronics Market Study", BIS Strategic Decisions, 1995

[41] "World Pressure Sensor Markets", Frost & Sullivan, Market Intelligence, 1992

[42] "Sensor Market Sourcebook", Frost & Sullivan, Market Intelligence, 1995

[43] Walsh, S.: "Creating Competitive Advantages with MEMS Technology", Commercialization of Microsystems '96, EF, SEMI, NJIT, p 14(4)

[44] Bryzek, J.: "Starting MEMS Manufacturing Business in Silicon Valley", Commercialization of Microsystems '96, EF, SEMI, NJIT, p 251 (13)

[45] Milt, L.: "MEMS: A large Global Market", Electronic Design, Dec 1995, p 42

[46] Timoshenko, S.: "Strength of Materials", D. van Nostrand Company, Inc., 1956

[47] Ko, W. H., Wang, Q., Wang, Y.: "Touch mode capacitive pressure sensors for industrial applications", Solid State Sensors and Actuators, Hilton Head, SC, 1996, p 244 (3)

[48] "Understanding Accelerometer Technology", IC Sensors Inc., Milpitas, CA

[49] Kress, H.-J., Marek, J., Mast, W., Schatz, O., Muchow, J.: "Integrated pressure sensors with electronic trimming", Automotive Engineering, v 103, n 4, April 1995, p 65 (4)

[50] Shah, M. K., McNeil, A. C., Summers, M. D., Meyer, B. D.: Application of Finite Element Analysis to Predict the Performance of Piezo-resistive Pressure Sensor", Sensors in Electronic Packaging, ASME, v 14, 1995, p 79 (7)

[51] Catling, D. C.: "High-sensitivity silicon capacitive sensors for measuring medium-vacuum gas pressures", Sensors and Actuators A, v 64, 1998, p 157 (8)

[52] Hess, D. W, Jensen, K. F.: "Microelectronics Processing", ACS, 1989

[53] Schuegraf, K. K.: "Handbook of Thin-film deposition processes and Techniques", Noyes Publications, Park Ridge, New Jersey, 1988

[54] Takagi, T.: "Ionized-Cluster Beam Deposition and Epitaxy", Noyes Publications, 1988

[55] Mort, J., Jansen, F.: "Plasma Deposited Thin Films", CRC Press, 1986

[56] O'Conner, L.: "MEMS: Microelectromechanical Systems", Mechanical Engineering, Feb 1992, p 40 (8)

[57] Palik, E. D., Bermudez, V. M., Glembocki, O. J.: "Ellipsometric Study of Bias-Dependent Etching and The Etch-Stop Mechanism for Silicon in

Aqueous KOH", Micomachining and Micropackaging of Transducers, Ed.: Fung, C. D., Cheung, P. W., Ko, W. H., Fleming, D. G., Elsevier, 1985, p 135 (17)

[58] Kovacs, G. T. A.: "Micromachined Transducers – Sourcebook", McGraw-Hill, 1998

[59] Williams, K.: "New Technology and Applications at Lucas NovaSensor", Tribology Issues and Opportunities in MEMS, Ed.: B Bhushan, Kluwer Academic Publishers, 1998, p 121 (14)

[60] Burbaum, C., Mohr, J., Bley, P.: "Fabrication of Capacitive Acceleration Sensors by the LIGA Technique", Sensors and Actuators A, v 25-27, 1991, p 559 (5)

[61] Guckel, H., Skrobis, K. J., Christenson, T. R., Klein, J., Han, S., Choi, B., Lovell, E. G.: "Fabrication of assembled micromechanical components via deep x-ray lithography", IEEE Micro Electro Mechanical systems, 1991, p 74 (5)

[62] Menz, W., Bacher, W., Harmening, M., Michel, A.: "The LIGA Technique - a Novel Concept for Microstructures and the combination with Si-Technologies by Injection Molding", Transducers 91, 1991, p 607 (3)

[63] Bley, P., Bacher, W., Menz, W., Mohr, J.: "Description of Microstructures in LIGA-Technology", Microelectronic Engineering, v 13, 1991, p 509 (4)

[64] Cheng, Y.: "LIGA activity in Taiwan", Microsystem Technologies, v 2, 1996, p 157 (5)

[65] "Sensor Device Data", Motorola, 3rd Edition 1995

[66] Volition, A.S., Tsao, P.-H., Polak, A.J., Baker, T.L.: "Analysis of Environment Induced Stresses in Silicon Sensors", EEP-Vol. 10-1, Advances in Electronic Packaging, ASME 1995, p 489 (4)

[67] Young, W. C.: "Roark's Formulas for Strain & Stress", 6th Edition, McGraw-Hill Book Company, 1989, p 458 (24)

[68] Chau, H.-L.: "Scaling Limits in Batch-Fabricated Silicon Pressure Sensors", IEEE Trans Electron Devices, v ED-34, n 4, Apr 1987, p 850 (9)

[69] Wu, M.-P.: "A New Pressure Sensor with Innercompensation for Nonlinearity and Protection to Overpressure", Sensors and Actuators A, v 21-23, 1990, p 65 (4)

[70] Christel, L., Petersen, K., Barth, P., Pourahmadi, F., Mallon, J. JR., Bryzek, J.: "Single crystal Silicon Pressure Sensors with 500x Overpressure Protection", Sensors and Actuators A, v 21-23, 1990, p 84 (5)

[71] Schilling, F., Langheinrich, W., Weiblein, K., Arand, D.: "Simulation of thermally induced package effects with regard to piezoresistive pressure sensors", Sensors and Actuators, A 60, 1997, p 37 (3)

[72] "NovaSensor Application Note 1", Lucas NovaSensor, Fremont / CA , Dec 1992

[73] Pollak-Diener, G.: "Montagetechniken für Silizium-Sensoren", Technisches Messen, v 56, n 11, 1989, p 422 (12)

[74] "Motorola Sensor Device Data", Motorola, 1st Edition, 1993
[75] Dudek, R., Vogel, D., Michel, B.: "Mechanical Failure in COB-Technology Using Glob-Top Encapsulation", IEEE Transactions on Components, Packaging, and Manufacturing Technology, Part C, v 19, n 4, Oct 1996, p 232 (8)
[76] "Mechanical & physicalproperties of Indalloy speciality solders", Indium Corporation of America, 1993
[77] "Ablebond 783-3", Technical Data Sheet, Ablestik Electronic Materials & Adhesives, Rancho Dominguez, CA, May 1994
[78] "Dow Corning 730 solvent resistant sealant", Information about Fluorosilicone Sealants, Dow Corning, Midland, MI, 1994
[79] Paillard, B.: "Temperature Compensating an Integrated Pressure Sensor", Sensors, Jan 1998, p 36 (11)
[80] Tufte, O. N., Stelzer, E. L.: "Piezoresistive Properties of Silicon Diffused Layers", Journal of Applied Physics, Feb 1963, v 34, n 2, p 313 (6)
[81] Kanda, Y.: "Piezoresistance effect of silicon", Sensors and Actuators, A 28, 1991, p 83 (9)
[82] "SenSym -solid state pressure sensors handbook", SenSym, Milpitas / CA., 1995
[83] Petersen, K., Brown, J., Vermeulen, T., Barth, P., Mallon, J. JR., Bryzek, J.: "Ultra-stable, High-temperature Pressure Sensors Using Silicon Fusion Bonding", Sensors and Actuators, A 21-23, 1990, p 96 (5)
[84] Krulevitch, P., Howe, R.T., Johnson, G.C., Huang, J.: "Stress in undoped LPCVD polycrystalline silicon", Transducers 91, IEEE Electron Devices Society, May 1991, p 949 (4)
[85] Ryan, K., Bryzek, J.: "Packaging Technology for Low-Cost Media Isolated Pressure Sensors", Sensors 95, p 685 (6)
[86] Monk, D.J.: "Pressure leakage through material interfaces in pressure sensor packages", Sensors in Electronic Packaging, v 14, 1995, p 87 (7)
[87] Sze, S.M.: "Semiconductor Devices", John Wiley & Sons, 1985
[88] Mallon, J.R., Pourahmadi, F., Petersen, K., Barth, P., Vermeulen, T., Brysek, J.: "Low-Pressure Sensors Employing Diaphragms and Precision Etch Stop", Sensors and Actuators, A21-A23, 1990, p 89 (7)
[89] Hsu, T.-R., Sun, N.: "Residual Stresses/Strains Analysis of MEMS", MSM'98 Conference, Santa Clara, Apr 1998
[90] Matsuda, K., Kanda, Y., Yamamura, K., Suzuki, K.: "Nonlinearity of Piezoresistance Effect in p- and n- Type Silicon", Sensors and Actuators, A21-23, 1990, p 45 (4)
[91] Middelhoek, S., Audet, S.A.: "Physics of Silicon Sensors", Academic Press, 1989
[92] Kanda, Y., Yasukawa, A.: "Optimum design considerations for silicon piezoresistive pressure sensors", Sensors and Actuators, A62, 1997, p 539 (4)

[93] Wang, Y., Bao, M.-H., Yu, L.-Z.: "The effect of shear stress on the piezoresistance of silicon", Sensors and Actuators, v 18, 1989, p 221 (11)
[94] Beckwith, T.G., Marangoni, R.D., Lienhard, J.H.: "Mechanical Measurements", Addison-Wesley Publishing Company, 1993
[95] "NovaSensor Application Note 2", Lucas NovaSensor, June 1993
[96] Dunn, W., Frank, R.: "Automotive Silicon Sensor Integration", SAE Technical Paper Series, 920471
[97] Lee, R.: "NovaSensor Application Note 4", Lucas NovaSensor, Jan 1996
[98] French, P.J., Eavens, A.G.R.: "Piezoresistance in single crystal and polycrystal Si", Properties of Silicon, INSPEC, 1988, p 94 (10)
[99] Gray, P.R., Meyer, R.G.: "Analysis and Design of analog integrated circuits", John Wiley & Sons, 1984, p 119
[100] Farquhar, D.S., Steinwall, J.E.: "Elastic properties of filled epoxy encapsulants", EEP-Vol. 10-2, Advances in Electronic Packaging, ASME 1995, p 707 (5)
[101] Mix, D.E., Bar-Cohen, A.: "Hygro-Thermal Nonlinear Behavior of IC Die",INTERpack 95, part 2 (2), March 1995, v 10-2, p 751 (13)
[102] Harper, P.R., Cherkur, R.P.: "Selecting the right die attach material for the Power PC 603TM", EEP-Vol. 10-1, Advances in Electronic Packaging, ASME 1995, p 507 (6)
[103] Keer, L.M., Moran, B.: " Lifetime prediction of solders in electronic packaging", EEP-Vol. 10-2, Advances in Electronic Packaging, ASME 1995, p 651 (5)
[104] Vaynman, S., Mavoori, H., Fine, M.E.: "Comparison of isothermal fatigue of lead-free solders with lead-tin solders", EEP-Vol. 10-2, Advances in Electronic Packaging, ASME 1995, p 657 (6)
[105] van Gestel, R.: "Reliability related research on plastic IC-packages: A chip test approach", Delft University Press, 1994
[106] "Media compatible packaging and environmental testing of barrier coating encapsulated silicon pressure sensors", Solid-State Sensor and Actuator Workshop, Hilton Head Island 1996, p 36 (6)
[107] Petrovic, S., Brown, C., Ramirez, A., King, B., Maudie, T., Stanerson, D., Bitko, G., Matkin, J., Wertz, J., Monk, D.J.: "Low-cost, water compatible piezoresistive, bulk micromachined pressure sensor", EEP-Vol. 19-1, Advances in Electronic Packaging, ASME 1997, p 455 (8)
[108] "World-Class Parylene Coating Service", Speciality Coating Systems, Inc., Indianapolis/Indiana, 1997
[109] "Parylene Conformal Coating Specifications and Properties", Speciality Coating Systems, Inc., Indianapolis/Indiana, 1997
[110] McCall, F.: "Temperature Coefficients of the modulii of elasticity of Silicon", Apr 1987
[111] Nielsen, O.H.: "Stiffness of Si", Properties of Silicon, INSPEC, 1988, p 14 (3)
[112] "CRC Materials Science and Engineering Handbook", CRC Press, 1997

# Appendix

# Appendix A - Technical Data Sheets

The suppliers of the Epoxy Ablebond 789-3 and the RTV Dow Corning 730 provide general information about the adhesives. However, the mechanical properties that are included in this information are not sufficient for a temperature dependent finite element model.

Technical Data Sheet Ablebond 789-3 (2 pages)

Information About Fluorosilicone Sealant (3 pages)

TECHNICAL DATA SHEET

# ABLEBOND® 789-3

## MOISTURE RESISTANT ADHESIVE

| TYPICAL PROPERTIES | | TEST METHOD |
|---|---|---|
| Viscosity @ 25°C: | 36,500 cps | PT-42 |
| Work Life @ 25°C: | 2 weeks | PT-54 |
| Cure Condition: | 1/2 hour @ 150°C | |
| Cure Option: | 1 hour @ 125°C | |
| Lap Shear Strength | | MT-6 |
| Al to Al @ 25°C: | 5000 psi | |
| Au to Au @ 25°C | 5500 psi | |
| Volume Resistivity: | $2 \times 10^{14}$ ohm-cm | PT-47 |
| Dielectric Strength: | 800 volts/mil | PT-49 |
| Dielectric Constant: | 4.2 (@ 1 KHz) | PT-48 |
| Dissipation Factor: | 0.011 (@ 1 KHz) | PT-48 |
| Glass Transition Temperature (Tg): | 126°C | MT-9 |
| Coefficient of Thermal Expansion (TMA): | | MT-9 |
| Below Tg: | 63 x 10[illegible] in/in/°C | |
| Above Tg: | 14 x 10[illegible] in/in/°C | |
| Weight Loss (TGA) @ 250°C | 0.28% | PT-20 |
| Thermal Conductivity @ 121°C: | 0.17 BTU $ft^{-1}hr^{-1}°F^{-1}$ | PT-48 |
| Storage Life @ 5°C: | 6 months | PT-13 |
| @ -40°C: | 1 year | |

Typical properties are not intended to be used as specification limits.

5/94

### DESCRIPTION

Ablebond® 789-3 one component, high strength toughened adhesive is designed for microelectronic applications, including substrate attach and package sealing, which require good moisture resistance.

Ablebond 789-3 adhesive may be used as an alternative in applications where Ablefilm 550 adhesive film is not suitable. It exhibits strong adhesion to difficult-to-bond metals, such as gold, silver, and copper. This adhesive retains its bond strength after exposure to moisture.

## INSTRUCTIONS

Apply adhesive as required. Assemble bonds. Cure at one of the recommended cure schedule(s).

## AVAILABILITY

Ablebond® 789-3 adhesive is available in a variety of package sizes, ranging from 1cc to one pound (by weight) jars.

## STORAGE

When packaged in jars, this adhesive may be stored at refrigerated temperature (5°C maximum) for six (6) months. At -40°C, shelf life is one (1) year.

When packaged in syringes, this adhesive should be stored at 5°C or colder. Shelf life at 5°C is six (6) months.

When not in use, containers should be tightly sealed and refrigerated.

CAUTION This product may cause skin irritation in sensitive persons. Avoid skin contact. If contact does occur, wash area immediately with soap and water. Please refer to Material Safety Data Sheet (OSHA) for more details.

ABLESTIK
Electronic Materials & Adhesives
a subsidiary of National Starch and Chemical Company
20021 Susana Road, Rancho Dominguez, CA 90221
(310) 764-4600 FAX 310-764-2545 CUSTOMER SERVICE FAX 310-764-1783

DISCLAIMER: [illegible] statements, technical information [illegible] contained herein are [illegible] to be accurate, but the accuracy [illegible] thereof is not guaranteed, and the following is made in lieu of [illegible] express or implied. Seller and manufacturer's obligation shall be to replace such quantity of the product proved to be defective. Neither seller nor manufacturer shall be liable for any injury, loss or damage, direct or consequential, arising from the use or inability to use the product. Before using, user shall determine the suitability of the product for his intended use, and user assumes all risk and liability whatsoever in connection therewith. No statement or recommendation not contained herein shall have any force or effect unless in an agreement signed by officers of seller and manufacturer.

# Information About Fluorosilicone Sealants

DOW CORNING

## DESCRIPTION

DOW CORNING® 730 solvent resistant sealant is a ready-to-use, solventless, nonslumping fluorosilicone rubber paste that reacts with moisture in the air to form a tough, rubbery solid. It is a fluid-resistant material that is ideally suited for use in many applications where resistance to fumes, splash, and sometimes even total immersion in fuels, oils and solvents is needed.

DOW CORNING 730 solvent resistant sealant features good resistance to weathering, vibration, moisture, ozone, and temperature extremes. It retains its flexibility over a wide temperature range from -70 to 500 F (-57 to 260 C) and may be applied in subzero weather without loss of extrusion properties.

DOW CORNING 730 solvent resistant sealant adheres to most common industrial surfaces and can be applied overhead or on vertical surfaces without fear of sagging, slumping or running off.

## DOW CORNING® 730 SOLVENT RESISTANT SEALANT

| | |
|---|---|
| Type | One-part, general-purpose fluorosilicone rubber adhesive |
| Physical Form, | |
| as supplied | Nonslumping paste |
| as cured | Tough, rubbery solid |
| Cure | On exposure to atmospheric moisture gives off a small amount of acetic acid |
| Special Properties | Resists swelling upon exposure to fuels, oils and solvents over a wide temperature range |
| Primary Uses | Bonding, sealing and caulking applications where resistance to fuels, oils and solvents is required |

## USES

DOW CORNING 730 solvent resistant sealant is used primarily for bonding, sealing and caulking applications where resistance to the swelling effects of fuels, oils and solvents is needed. It has proved [illegible] for assembling and/or repairing the fuel lines and tanks of cars, small engines, aircraft and rockets. Other typical applications include:

- Sealing seams on various fluid storage tanks
- Sealing aerospace and automotive fuel lines and tanks
- Providing [illegible] for rubber [illegible] exposed to corrosive conditions
- Sealing pipe joints on lines carrying corrosive chemicals and solvents
- Providing formed-in-place gaskets for sealing chemical compressors
- Providing formed-in-place gaskets where irregular shapes and harsh conditions reject ordinary seals
- Bonding or sealing components exposed to moisture, vibration, shock, certain fuels, oils and solvents for long periods of time
- Providing a protective coating [illegible] from ketone [illegible]
- Providing formed-in-place gaskets for sealing insulators and entrance [illegible] in fluid-filled distribution transformers

## HOW TO USE

### Application

DOW CORNING 730 solvent resistant sealant is supplied ready to use. Under pressure, it flows readily from its container. The paste-like consistency makes it easy to work; a spatula or wooden paddle can be used for tooling the surface.

The cure of DOW CORNING 730 solvent resistant sealant progresses inward from the surface. At conditions of at least 75 F (23.9 C) and 50 percent relative humidity, the sealant forms a skin within 10 minutes. Tooling is not practical after the skin begins forming and should be completed within 4 to 8 minutes of application even though this may require alternate periods of application and tooling.

### Curing

DOW CORNING 730 solvent resistant sealant begins curing upon exposure to moisture in the air and at normal room temperature will skin over in 10 minutes or less. This period may be reduced under conditions of high temperature and humidity or lengthened at low temperature and low humidity. Beneath the skin the material continues to cure, and within 48 hours sections up to 1/8-inch (3.[illegible] mm) thick will cure to a state where they can be handled. Cure time becomes longer as the thickness of the rubber and the degree of confinement increase. Under normal conditions, full cure properties can be expected in 7 days.

It should be noted that absolute confinement can prevent cure. Therefore

[illegible]

## TYPICAL PROPERTIES

These values are not intended for use in preparing specifications.

| Property | Value |
| --- | --- |
| ***As Supplied*** | |
| Color | White |
| Specific Gravity at 77 F (25 C) | 1.40 |
| Nonvolatile Content, after 24 hrs at 158 F (70 C), percent | 95 |
| Extrusion Rate, 1/8-inch (0.318-cm) orifice at 90 psi (0.621 MPa) air, g/minute | 200 |
| Skin-Over Time, minutes | 10 |
| Tack-Free Time, minutes | 25 |
| Flow, MIL-S-8802 JIG, maximum, inch (cm) | 0.1 (0.254) |
| ***As Cured – 7 days at 77 F (25 C) and 50% RH*** | |
| Durometer Hardness, Shore A-2, points | 35 |
| Tensile Strength, psi (MPa) | 300 (2.07) |
| Elongation, percent | 175 |
| Tear Strength, ppi (kN/m) | 30 (5.25) |
| Brittle Point, °F (°C) | -81 (-63) |
| Low Temperature Flexibility, °F (°C) | -70 (-57) |
| Peel Strength, Aluminum Alloy Alclad 2024T3, with DOW CORNING® 1200 RTV prime coat, ppi (kN/m) | 15 (2.63) |
| Lap Shear, | |
| Unprimed Aluminum Alloy Alclad 2024T3, cohesive, ppi (kN/m) | 260 (45.53) |
| Aluminum Alloy Alclad 2024T3, with DOW CORNING 1200 RTV prime coat, cohesive, ppi (kN/m) | 260 (45.53) |
| Unprimed cold-rolled steel, cohesive, ppi (kN/m) | 158 (27.67) |
| Cold-rolled steel with DOW CORNING 1200 RTV prime coat, cohesive, ppi (kN/m) | 240 (42.03) |

**Specification Writers: Please obtain a copy of the Dow Corning Sales Specification for this product, and use it as a basis for your specifications. It may be obtained from any Dow Corning Sales Office, or from Dow Corning Product Information in Midland, MI. Call (517) 496-6000.**

every application that involves confinement during cure should be thoroughly tested before use. Additionally, inadequate cure can result in a softening of the sealant at elevated temperatures.

**Bonding**

DOW CORNING 730 solvent resistant sealant will bond to almost any clean, grease-free surface including glass, cured silicone rubber, cork phenolic, polyester, epoxy, silicone resin laminates, stainless steel, titanium and aluminum. It will not, however, adhere to polyethylene, certain rubbers, plastics, organic materials or concrete.

For best adhesion, a primer such as DOW CORNING® 1200 RTV prime coat is recommended for most surfaces to ensure a stronger, more uniform bond. When using a prime coat:

1. Thoroughly clean surfaces to be bonded with a solvent, and then with acetone. Caution: Some solvents leave a residue that prevents adhesion; therefore, solvent choice is critical.

*NOTE: Always provide adequate ventilation when using any volatile solvent. Follow precautionary handling*

### TABLE I: TYPICAL FLUID RESISTANCE VALUES[1]

These values are not intended for use in preparing specifications.

| Fluid | *Volume Swell, %* | *Durometer Hardness, pts change* | *Tensile Strength, % change* | *Elongation % change* |
| --- | --- | --- | --- | --- |
| Gasoline | 9.40 | -6 | -19 | -15 |
| Toluene | 16.50 | -5 | -12 | -13 |
| VM&P Naphtha | 5.30 | None | None | -10 |
| Methanol | [illegible] | -5 | -34 | -3 |
| Perchloroethylene | 4.00 | -3 | -2 | -10 |
| Methylene Chloride | 50.00 | -22 | -36 | -44 |
| Chlorothene | 47.50 | -31 | -36 | -39 |
| JP-4 | 5.50 | None | -25 | -35 |
| [illegible] | [illegible] | -8 | -14 | -3 |
| Jet Reference Fuel | [illegible] | -4 | -22 | -36 |
| JP-5 | [illegible] | -1 | -12 | -15 |
| ASTM No. 3 Oil, after 72 hours at 302 F (150 C) | [illegible] | -4 | -12 | 2 |
| MIL-H-5606, after 72 hours at 302 F (150 C) (American Oil PQ 4226) | 5.10 | -4 | -40 | -22 |
| DOW CORNING® 561 transformer fluid after 72 hours at 302 F (150 C) | -4.30 | -5 | 2 | -19 |
| GM hydramatic Fluid Type A, after 72 hours at 302 F (150 C) | -2.40 | -3 | -10 | -5 |

[1] DOW CORNING 730 solvent resistant sealant cured 7 days before immersion; properties obtained after 7 days immersion at room temperature.

Specification Writers: Please obtain a copy of the Dow Corning Sales Specification for this product, and use it as a basis for your specifications. It may be obtained from any Dow Corning Sales Office, or from Dow Corning Product Information in Midland, MI. Call (517) 496-6000.

**TABLE II: TYPICAL THERMAL STABILITY PROPERTIES**
These values are not intended for use in preparing specifications.

| *Physical Property* | Exposure Time, days: *0* | *1* | *3* | *7* | *14* |
|---|---|---|---|---|---|
| ***Tested at Room Temperature After Exposure at 300 F (149 C)*** | | | | | |
| Durometer Hardness, Shore A-2, points | 33 | - | 38 | 37 | 38 |
| Tensile Strength, | | | | | |
| psi | 380 | - | 450 | 450 | 450 |
| MPa | 2.52 | - | 3.10 | 3.10 | 3.10 |
| Elongation, percent | 210 | - | 240 | 230 | 230 |
| Tear Strength, | | | | | |
| ppi | 30 | - | 34 | 36 | 31 |
| kN/m | 5.25 | - | 5.95 | 6.30 | 5.42 |
| ***Tested at Room Temperature After Exposure at 400 F (204 C)*** | | | | | |
| Durometer Hardness, Shore A-2, points | - | 35 | 38 | - | 38 |
| Tensile Strength, | | | | | |
| psi | - | 430 | 465 | - | 260 |
| MPa | - | 2.96 | 3.2 | - | 1.79 |
| Elongation, percent | - | 220 | 240 | - | 180 |
| Tear Strength, | | | | | |
| ppi | - | 34 | 36 | - | 34 |
| kN/m | - | 5.95 | 6.30 | - | 5.95 |

**Specification Writers:** Please obtain a copy of the Dow Corning Sales Specification for this product, and use it as a basis for your specifications. It may be obtained from any Dow Corning Sales Office, or from Dow Corning Product Information in Midland, MI. Call (517) 496-6000.

*statements on solvent container and observe regulations regarding solvent usage.*

2. Apply a thin film of prime coat on the surface. (Silicone rubber surfaces should not be primed.) Allow the surface to air dry for 30 minutes minimum at room temperature. Only a thin film of prime coat is required; heavy films will not give consistent results.

3. Spread a uniform layer of DOW CORNING 730 solvent resistant sealant 20- to 40-mils (0.5- to 1.0-mm) thick on one of the surfaces to be bonded. Then join the surfaces, using just enough pressure to displace the air. Maintain at least a 20-mil (0.5-mm) thickness for best results, and let stand undisturbed at room temperature until fully vulcanized. The time required for the adhesive to vulcanize or cure depends on the thickness of the rubber and the amount of moisture in the air.

Bond strengths will continue to increase for several days after tack is complete. Where narrow sections are being bonded, full strength will be reached in about 7 days. Heavy sections will require more time.

**TABLE III: TYPICAL ELECTRICAL PROPERTIES***
These values are not intended for use in preparing specifications.

| Property | Value |
|---|---|
| Arc Resistance, seconds | 154 |
| Dielectric Strength, volts/mil | 331 |
| Dielectric Constant, 100 kHz | 3.98 |
| Dissipation Factor, 100 kHz | 0.00599 |
| Volume Resistivity, ohm cm | 1.38 x 10[illegible] |
| Repairability | Excellent |

*As cured after 7 days at 77 F (25 C) and 50% relative humidity.

**Specification Writers:** Please obtain a copy of the Dow Corning Sales Specification for this product, and use it as a basis for your specifications. It may be obtained from any Dow Corning Sales Office, or from Dow Corning Product Information in Midland, MI. Call (517) 496-6000.

**Sealing**

Using DOW CORNING 730 solvent resistant sealant in sealing applications follows approximately the same step-by-step procedures outlined for bonding applications. After preparing the surface and priming where required, the sealant is applied by forcing it into the joint or seam to obtain full contact between sealant and surface.

**STORAGE AND SHELF LIFE**

When stored at or below 90 F (32 C), DOW CORNING 730 solvent resistant sealant has a shelf life of 12 months from date of manufacture by Dow Corning.

Since moisture in the air will cause the sealant to cure, containers should always be sealed when not in use. Once a container has been opened, a plug of cured sealant may form in the nozzle or tube tip during storage. This is easily removed and does not affect the remaining material.

**HANDLING**

WARNING: DIRECT CONTACT OF UNCURED SEALANT IRRITATES

## Appendix B - Material Test Results

The tensile tests were conducted by Intec. The company also provided the following result sheets for the three materials, including the Young's Modulus and Poisson's Ratio. In addition to this information, the raw test data were provided, which was necessary to generate the multilinear curve fits.

Tension Test Results 60Sn40Pb (1 page)

Tension Test Results Epoxy Ablebond 789-3 (1 page)

Tension Test Results 60Sn40Pb (1 page)

Tension Test Results RTV Dow Corning 730 (1 page)

Table A-1: Tension Test Results 60Sn40Pb

Integrated Technologies, Inc.

# Lucas NovaSensor

506LN

Test Specification: ASTM D638, Type I
Purchase Order: 31773

† Ultimate Stress = Ultimate Load / (Average Width * Average Thickness)

| Intec ID | Group ID | Test Environ. | Average Width (in) | Average Thickness (in) | Actuator Speed (in/min) | Peak Load (lbs) | †Peak Stress (psi) | Load @ Mkr 1 (lbs) | Axial @ Mkr 1 (με) | Load @ Mkr 2 (lbs) | Axial @ Mkr 2 (με) | Initial Modulus (Msi) | Axial @ Mkr 3 (με) | Trans @ Mkr 3 (με) | Axial @ Mkr 4 (με) | Trans @ Mkr 4 (με) | Poisson Ratio | Test Temp | Relative Humidity | Test Date | Failure Location & Comments |
|---|---|---|---|---|---|---|---|---|---|---|---|---|---|---|---|---|---|---|---|---|---|
| 506-001 | 1-1 | 25°C | 0.5012 | 0.1317 | 0.05 | 340 | 5,151 | 106 | 433 | 264 | 2304 | 1.285 | 59769 | | 24814 | | N/A | 80°F | 45% | 8/14/98 | Not taken to failure |
| 506-002 | 1-2 | 25°C | 0.5020 | 0.1342 | 0.10 | 427 | 6,335 | 105 | 385 | 314 | 1862 | 2.098 | | 28101 | | 12045 | 0.46 | 80°F | 45% | 8/14/98 | Not taken to failure, axial gage failed at 73K µstrain |
| 506-003 | 1-3 | 25°C | 0.4998 | 0.1315 | 0.10 | 408 | 6,204 | 86 | 333 | 330 | 1639 | 2.846 | 0.47016 | | 0.48541 | | N/A | 80°F | 45% | 8/14/98 | Not taken to failure, axial gage failed at 50K µstrain |
| | | Averages: | 0.5010 | 0.1324 | | | 5,897 | | | | | 2.076 | | | | | 0.46 | | | | |
| | | Standard Deviation: | 0.0011 | 0.0015 | | | 649 | | | | | 0.780 | | | | | | | | | |
| | | COV: | 0.2% | 1.1% | | | 11.0% | | | | | 37.6% | | | | | | | | | |
| 506-008 | 2-1 | 25°C | 0.5035 | 0.1343 | 0.10 | 424 | 6,265 | 85 | 259 | 229 | 937 | 3.146 | 37831 | 18548 | 17787 | 8778 | 0.49 | 74°F | 47% | 8/18/98 | Not taken to failure, axial gage failed @ [illegible]K & trans gage @ 22K µstrain |
| 506-009 | 2-2 | 25°C | 0.5012 | 0.1332 | 0.10 | 412 | 6,166 | 82 | 317 | 207 | 967 | 2.872 | 38318 | 17816 | 20056 | 9855 | 0.44 | 73°F | 46% | 8/19/98 | Necking failure in gage section |
| 506-011 | 2-3 | 25°C | 0.5018 | 0.1347 | 0.10 | 397 | 5,873 | 117 | 485 | 213 | 1044 | 2.548 | 28195 | 10531 | 13065 | 4885 | 0.37 | 73°F | 46% | 8/19/98 | Not taken to failure, axial gage failed at [illegible]K µstrain |
| | | Averages: | 0.5022 | 0.1341 | | | 6,101 | | | | | 2.855 | | | | | 0.43 | | | | |
| | | Standard Deviation: | 0.0012 | 0.0008 | | | 204 | | | | | 0.299 | | | | | 0.06 | | | | |
| | | COV: | 0.2% | 0.6% | | | 3.3% | | | | | 10.5% | | | | | 13.2% | | | | |
| 506-007 | 3-1 | 125°C | 0.5012 | 0.1309 | 0.10 | 119 | 1,816 | 33 | 311 | 76 | 690 | 1.722 | 36517 | 16336 | 13641 | 7175 | 0.40 | 257°F | DRY | 8/17/98 | Slight necking in gage section |
| 506-010 | 3-2 | 125°C | 0.5020 | 0.1327 | 0.10 | 151 | 2,264 | 42 | 272 | 88 | 711 | 1.591 | 40192 | 18276 | 20056 | 9822 | 0.42 | 257°F | DRY | 8/17/98 | Not taken to failure |
| 506-012 | 3-3 | 125°C | 0.5033 | 0.1334 | 0.10 | 157 | 2,334 | 44 | 217 | 91 | 668 | 1.532 | 39868 | 19420 | 20410 | 10344 | 0.47 | 257°F | DRY | 8/17/98 | Not taken to failure |
| | | Averages: | 0.5022 | 0.1323 | | | 2,139 | | | | | 1.615 | | | | | 0.43 | | | | |
| | | Standard Deviation: | 0.0011 | 0.0013 | | | 282 | | | | | 0.097 | | | | | 0.03 | | | | |
| | | COV: | 0.2% | 1.0% | | | 13.2% | | | | | 6.0% | | | | | 7.9% | | | | |
| 506-004 | 4-1 | -40°C | 0.5048 | 0.1317 | 0.10 | 706 | 10,617 | 178 | 348 | 521 | 1898 | 3.335 | 16141 | 6135 | 10300 | 4424 | 0.29 | -40°F | DRY | 8/17/98 | Necking failure in gage section |
| 506-005 | 4-2 | -40°C | 0.5075 | 0.1334 | 0.10 | 772 | 11,400 | 93 | 290 | 468 | 1605 | 4.216 | | | | | N/A | -40°F | DRY | 8/17/98 | Necking failure in gage section |
| 506-006 | 4-3 | -40°C | 0.5065 | 0.1356 | 0.10 | 729 | 10,615 | 101 | 189 | 447 | 1419 | 4.099 | 20322 | 8551 | 10703 | 5176 | 0.35 | -40°F | DRY | 8/17/98 | Necking failure in gage section |
| | | Averages: | 0.5063 | 0.1335 | | | 10,878 | | | | | 3.883 | | | | | 0.32 | | | | |
| | | Standard Deviation: | 0.0013 | 0.0019 | | | 453 | | | | | 0.478 | | | | | 0.04 | | | | |
| | | COV: | 0.3% | 1.5% | | | 4.2% | | | | | 12.3% | | | | | 12.7% | | | | |

B-2

22310 20th Avenue SE
Bothell, WA 98021

Integrated Technologies, Inc.
e-mail: intec@intec.com

Phone (425) 487-2888
Fax: (425) 485-2911

Table A-2: Tension Test Results Epoxy Ablebond 789-3 (Joint Resin)

intec
Integrated Technologies, Inc.

Lucas NovaSensor
506LN

Test Specimen Size: ASTM D638, Type I
Purchase Order: 31773

† Peak Stress = Peak Load / (Average Width * Average Thickness)

| Intec ID | Group ID | Test Environ. | Average Width (in) | Average Thickness (in) | Actuator Speed (in/min) | Peak Load (lbs) | †Peak Stress (psi) | Load @ Mkr 1 (lbs) | Axial ε @ Mkr 1 (με) | Trans ε @ Mkr 1 (με) | Load @ Mkr 2 (lbs) | Axial ε @ Mkr 2 (με) | Trans ε @ Mkr 2 (με) | Initial Modulus (Msi) | Axial ε @ Mkr 3 (με) | Trans ε @ Mkr 3 (με) | Axial ε @ Mkr 4 (με) | Trans ε @ Mkr 4 (με) | Poisson Ratio | Test Temp | Relative Humidity | Test Date | Failure Location & Comments |
|---|---|---|---|---|---|---|---|---|---|---|---|---|---|---|---|---|---|---|---|---|---|---|---|
| 506-201 | 31-1 | 25°C | 0.502 | 0.1243 | 0.05 | 601.5 | 9,638 | 240.3 | 5,391 | 3,771 | 416.7 | 11,843 | 6,361 | 0.438 | 10,232 | 5,676 | 17,170 | 8,608 | 0.423 | 75°F | 43% | 9/8/98 | GAGE SECTION, 1" FROM CENTER |
| 506-205 | 31-2 | 25°C | 0.504 | 0.1237 | 0.05 | 604.1 | 9,686 | 204.0 | 6,047 | 3,046 | 325.7 | 10,349 | 4,879 | 0.454 | 10,314 | 4,860 | 17,579 | 7,458 | 0.413 | 73°F | 42% | 9/9/98 | GAGE SECTION, 1" FROM CENTER |
| 506-206 | 31-3 | 25°C | 0.505 | 0.1274 | 0.05 | 671.8 | 10,434 | 200.8 | 5,542 | 2,812 | 414.0 | 12,524 | 5,900 | 0.474 | 10,097 | 4,825 | 17,202 | 7,797 | 0.425 | 74°F | 41% | 9/8/98 | GAGE SECTION, 0.5" FROM CENTER |
| | | Average: | 0.504 | 0.1251 | | | 9,919 | | | | | | | 0.455 | | | | | 0.420 | | | | |
| | | Standard Deviation: | 0.002 | 0.0020 | | | 446 | | | | | | | 0.018 | | | | | 0.006 | | | | |
| | | COV: | 0.3% | 1.6% | | | 4.5% | | | | | | | 4.0% | | | | | 1.5% | | | | |
| 506-203 | 32-1 | -40°C | 0.505 | 0.1235 | 0.05 | 548.8 | 8,808 | 161.6 | 3,336 | 1,766 | 370.8 | 9,474 | 4,254 | 0.547 | 4,938 | 2,424 | 10,345 | 4,597 | 0.402 | -40°F | DRY | 9/9/98 | GAGE SECTION, 0.5" FROM CENTER |
| 506-213 | 32-2 | -40°C | 0.505 | 0.1265 | 0.05 | 525.6 | 8,225 | 212.0 | 6,367 | 1,581 | 365.4 | 10,760 | 3,407 | 0.546 | 6,367 | 1,581 | 10,760 | 3,407 | 0.416 | -40°F | DRY | 9/9/98 | GAGE SECTION, 1" FROM CENTER AT VOID |
| 506-214 | 32-3 | -40°C | 0.506 | 0.1144 | 0.05 | 652.3 | 11,278 | 202.9 | 4,062 | 2,828 | 444.5 | 11,340 | 6,053 | 0.574 | 4,318 | 2,959 | 10,792 | 5,820 | 0.442 | -40°F | DRY | 9/9/98 | GAGE SECTION, 1" FROM CENTER |
| | | Average: | 0.505 | 0.1215 | | | 9,437 | | | | | | | 0.556 | | | | | 0.420 | | | | |
| | | Standard Deviation: | 0.000 | 0.0063 | | | 1,621 | | | | | | | 0.016 | | | | | 0.020 | | | | |
| | | COV: | 0.1% | 5.2% | | | 17.2% | | | | | | | 2.8% | | | | | 4.8% | | | | |
| 506-210 | 33-1 | 125°C | 0.504 | 0.1214 | 0.05 | 16.9 | 276 | 1.2 | 326 | | 3.7 | 2,983 | | 0.015 | 16,417 | 5,785 | 29,125 | 8,747 | 0.233 | 239°F | DRY | 9/11/98 | 25 lb LOAD CELL, GAGE SECTION, 0.5" FROM CENTER |
| 506-211 | 33-2 | 115°C | 0.506 | 0.1292 | 0.05 | | | | | | | | | | | | | | | 257°F | DRY | 9/9/98 | |
| 506-212 | 33-3 | 115°C | 0.504 | 0.1177 | 0.05 | 13.8 | 233 | 0.9 | 436 | | 2.5 | 2,280 | | 0.014 | 15,692 | 2,202 | 23,410 | 3,313 | 0.144 | 239°F | DRY | 9/11/98 | 25 lb LOAD CELL, GAGE SECTION, 0.5" FROM CENTER |
| | | Average: | 0.505 | 0.1227 | | | 254 | | | | | | | 0.015 | | | | | 0.189 | | | | |
| | | Standard Deviation: | 0.001 | 0.0059 | | | 31 | | | | | | | 0.001 | | | | | 0.063 | | | | |
| | | COV: | 0.2% | 4.8% | | | 12.1% | | | | | | | 4.9% | | | | | 33.4% | | | | |

B-3

Table A-3: Tension Test Results RTV Dow Corning 730

intec
Integrated Technologies, Inc.

**Lucas NovaSensor**
**506LN**

Test Specimen Size: 2" x 6"
Purchase Order: 31773

† Peak Stress = Peak Load / (Average Width * Average Thickness)

| Intec ID | Group ID | Test Environ. | Average Width (in) | Average Thickness (in) | Actuator Speed (in/min) | Peak Load (lbs) | †Peak Stress (psi) | Load @ Mkr 1 (lbs) | Axial ε @ Mkr 1 (με) | Trans ε @ Mkr 1 (με) | Load @ Mkr 2 (lbs) | Axial ε @ Mkr 2 (με) | Trans ε @ Mkr 2 (με) | Initial Modulus (psi) | Axial ε @ Mkr 3 (με) | Trans ε @ Mkr 3 (με) | Axial ε @ Mkr 4 (με) | Trans ε @ Mkr 4 (με) | Poisson Ratio | Test Temp | Relative Humidity | Test Date | Failure Location & Comments |
|---|---|---|---|---|---|---|---|---|---|---|---|---|---|---|---|---|---|---|---|---|---|---|---|
| 506-101 | 1-1 | 25°C | 1.944 | 0.0972 | 0.05 | 7.3 | 38.7 | 2.00 | 42,969 | 12,726 | 4.70 | 148,718 | 46,729 | 135.2 | 99,237 | 30,829 | 39,594 | 11,621 | 0.322 | 79°F | 48% | 8/26/98 | Specimen not tested to failure |
| 506-102 | 1-2 | 25°C | 1.934 | 0.0978 | 0.10 | 5.8 | 30.6 | 2.00 | 88,721 | 19,019 | 4.00 | 166,547 | 43,719 | 135.8 | 159,747 | 41,547 | 99,237 | 22,217 | 0.319 | 79°F | 48% | 8/26/98 | Specimen not tested to failure |
| 506-103 | 1-3 | 25°C | 1.950 | 0.0963 | 0.10 | 6.4 | 34.1 | 2.00 | 46,515 | 12,744 | 4.00 | 122,034 | 37,726 | 141.0 | 139,252 | 43,365 | 79,425 | 23,315 | 0.335 | 79°F | 48% | 8/26/98 | Specimen not tested to failure |
| | | Average: | 1.943 | 0.0971 | | | 34.5 | | | | | | | 137.3 | | | | | 0.326 | | | | |
| | | Standard Deviation: | 0.008 | 0.0008 | | | 4.0 | | | | | | | 3.2 | | | | | 0.008 | | | | |
| | | COV: | 0.4% | 0.8% | | | 11.7% | | | | | | | 2.3% | | | | | 2.6% | | | | |
| 506-104 | 2-1 | -40°C | 1.953 | 0.0972 | 0.10 | 5.6 | 29.5 | 2.10 | 57,178 | 12,231 | 4.50 | 154,523 | 40,753 | 129.9 | 159,460 | 42,084 | 89,899 | 22,009 | 0.289 | -40°F | DRY | 8/27/98 | Specimen not tested to failure |
| 506-105 | 2-1 | -40°C | 1.957 | 0.0902 | 0.10 | 6.1 | 34.6 | 2.50 | 49,683 | 6,323 | 4.70 | 149,500 | 22,296 | 124.9 | 150,610 | 22,516 | 68,402 | 8,575 | 0.170 | -40°F | DRY | 8/27/98 | Specimen not tested to failure |
| 506-106 | 2-3 | -40°C | 1.956 | 0.0887 | 0.10 | 6.5 | 37.5 | 2.80 | 63,599 | 12,036 | 4.90 | 160,168 | 39,313 | 125.4 | 164,825 | 40,631 | 89,374 | 19,385 | 0.282 | -40°F | DRY | 8/27/98 | Specimen not tested to failure |
| | | Average: | 1.955 | 0.0920 | | | 33.9 | | | | | | | 126.7 | | | | | 0.247 | | | | |
| | | Standard Deviation: | 0.002 | 0.0045 | | | 4.0 | | | | | | | 2.8 | | | | | 0.067 | | | | |
| | | COV: | 0.1% | 4.9% | | | 11.9% | | | | | | | 2.2% | | | | | 27.1% | | | | |
| 506-107 | 3-1 | 125°C | 1.964 | 0.0913 | 0.10 | 7.4 | 41.3 | 2.49 | 50,403 | 25,604 | 4.80 | 100,378 | 43,781 | 257.7 | 80,054 | 39,569 | 50,403 | 25,604 | 0.471 | 257°F | DRY | 9/14/98 | Gage Section |
| 506-108 | 3-2 | 125°C | 1.956 | 0.0930 | 0.10 | 10.5 | 57.7 | 1.65 | 50,562 | 17,462 | 3.97 | 100,604 | 42,560 | 254.9 | 80,029 | 31,561 | 58,490 | 21,259 | 0.478 | 257°F | DRY | 9/14/98 | Inside grip |
| 506-109 | 3-3 | 125°C | 1.921 | 0.0895 | 0.10 | 11.2 | 65.1 | 2.41 | 50,012 | 22,168 | 4.82 | 100,690 | 43,958 | 276.6 | 80,231 | 35,205 | 50,012 | 22,168 | 0.431 | 257°F | DRY | 9/14/98 | Inside grip |
| | | Average: | 1.947 | 0.0913 | | | 54.7 | | | | | | | 263.1 | | | | | 0.460 | | | | |
| | | Standard Deviation: | 0.023 | 0.0018 | | | 12.2 | | | | | | | 11.8 | | | | | 0.025 | | | | |
| | | COV: | 1.2% | 1.9% | | | 22.3% | | | | | | | 4.5% | | | | | 5.5% | | | | |
| 506-103A | 1-3 | 25°C | 1.268 | 0.0963 | 0.10 | N/A | | 1.14 | 41,125 | 9,180 | 2.85 | 114,349 | 25,061 | 191.2 | 99,475 | 22,229 | 59,753 | 13,611 | 0.217 | 79°F | 48% | 9/14/98 | Retested dogbone specimen, not tested to failure |

B-4

# Appendix C - Finite Element Analysis

The finite element analysis was performed using ANSYS. The first module controls the settings of the loads whereas the second determines the geometric model. This separation of the functions avoids undesired changes in either part of the model. The body of the geometric model remained the same for all three materials, only the modifications documented here were done to change from one material to another.

Control module (2 pages)

Anisotropic temperature dependent model with multilinear solder (24 pages)

Changes in the ANSYS code for the Epoxy (1 page)

Changes in the ANSYS code for the RTV (1 page)

```
!*************************************************************
!* Control Modul                                             *
!*                                                           *
!* Parameters: offset - Load Control (see below)             *
!*          LST   - Number of Loadcases                      *
!*          p     - Pressure                                 *
!*          T     - Temperature                              *
!*          AH    - Adhesive Height                          *
!*************************************************************
/clear
! offset =-1, LST =11: 0,1,2,3,4,5,6,7,8,9,10 x p
! offset =+1, LST =9: 2,3,4,5,6,7,8,9,10 x P
offset=0
LST=1
!Full Scale Pressure
P=350000
! Uniform Temperature
T=125
!Interface layer height (Solder, RTV or Epoxy)
AH=50E-6
! floating die 28
! solder 34 - regular; 35-4 elements die attach layer; 36-4 elements, tapered
!epoxy 38 - regular; 38a-with 10ppm TCE
!header only 38b
!RTV 40 - modulus 0.9MPa for all temperatures
/input,vsps35_28.prp

FINISH
/SOLU
/STAT,SOLU
! Nonlinear Geometry, Stress Stiffening On
NLGEOM,1
NROPT,FULL, ,
LUMPM,0
EQSLV,FRONT,1e-08,0,
SSTIF,ON
TOFFST,0,
OUTRES,NSOL,LAST,
OUTRES,STRS,LAST,

LSSOLVE,1,LST,1,
FINISH
```

```
!* File Output of Stresses in Piezoresistive Region

/POST1
!*First Region
SET,FIRST
FLST,5,2,2,ORDE,2
FITEM,5,2938
FITEM,5,-2939
ESEL,S, , ,P51X
NSLE,S
/output,nsol,,dat25rtv1v2.dat,append.
*DO,I,1,LST
AVPRIN,0,0,
PRNSOL,S,COMP
SET,NEXT
*ENDDO
!*Second Region
SET,FIRST
FLST,5,2,2,ORDE,2
FITEM,5,2952
FITEM,5,2960
ESEL,S, , ,P51X
NSLE,S
*DO,I,1,LST
AVPRIN,0,0,
PRNSOL,S,COMP
SET,NEXT
*ENDDO
/output
FINISH
/EXIT,ALL
```

```
/BATCH
!*******************************************************************************
!* anisotropic temperature dependent model with multilinear solder            *
!*                        -----------------                                   *
!* Solder: 60Sn40Pn, Solidus: 183 C                                           *
!* Input: AH     - Adhesive Height                                            *
!*        p      - Pressure                                                   *
!*        T      - Uniform Temperature                                        *
!*        LST    - Number of Loadcases                                        *
!*        offset - Offset Control: Pressure=p*0.1*(i+offset) ; i=1..LST       *
!*******************************************************************************
! /COM,ANSYS RELEASE  5.4   UP19970828      09:19:11    07/06/1998
/input,start,ans     ,/ansys54/docu/,,,,,,,,,,,,,,,1
!*
!Reference Temperature (Stress free Temperature)
tref=183
!Half Length of the Die
s=1000e-6
!Hight of the Die
h=385e-6
!Diaphragm Thickness
d=8e-6
! Epitaxial Layer Thickness
e=0
! Half Window Width
w=775e-6
! Half Membrane Width
m=w-0.707*(h-d)
! Thickness of Adhesive
adthick=AH
! Hight of Header
headhig=0.625e-3
! Half Lenght of the Substrate
headsid=1.5e-3
!Radius of the Throughhole in the Substrate
holerad=250e-6
! Applied Pressure
press=P
! Mesh Concentration
c=3
n=1/c
o=-c
! Die Mesh Desity
dm=9
/PREP7
!* Element Type
!*die
ET,1,SOLID64
!*adhesive
ET,2,SOLID45
!*header
ET,3,SOLID45
!*
```

```
!* Die (Silicon, isotropic)
!Tempearturliste
MPTEMP,1,-40,25,150, , , ,
!REFERENCE TEMPERATURE
MP,REFT,1,tref
!Thermal expansion coeff
MPDATA,ALPX,1,1,2.20e-6,2.58e-6,3.22e-6, , , ,
tb,anel,1,5,21,1
tbtemp,-40,
tbdata,1,166.4e9,64.28e9,64.28e9,0,0,0
tbdata,7,166.4e9,64.28e9,0,0,0,166.4e9
tbdata,13,0,0,0,79.77e9,0,0
tbdata,19,79.77e9,0,79.77e9
tbtemp,0,
tbdata,1,165.9e9,64.05e9,64.05e9,0,0,0
tbdata,7,165.9e9,64.05e9,0,0,0,165.9e9
tbdata,13,0,0,0,79.63e9,0,0
tbdata,19,79.63e9,0,79.63e9
tbtemp,40,
tbdata,1,165.5e9,63.81e9,63.81e9,0,0,0
tbdata,7,165.5e9,63.81e9,0,0,0,165.5e9
tbdata,13,0,0,0,79.50e9,0,0
tbdata,19,79.50e9,0,79.50e9
tbtemp,80,
tbdata,1,165.1e9,63.57e9,63.57e9,0,0,0
tbdata,7,165.1e9,63.57e9,0,0,0,165.1e9
tbdata,13,0,0,0,79.37e9,0,0
tbdata,19,79.37e9,0,79.37e9
tbtemp,125,
tbdata,1,164.7e9,63.30e9,63.30e9,0,0,0
tbdata,7,164.7e9,63.30e9,0,0,0,164.7e9
tbdata,13,0,0,0,79.22e9,0,0
tbdata,19,79.22e9,0,79.22e9

!*
!* 60Sn40Pb (multilinear)
MPLIST,ALL,,,EVLT
MPLIST,ALL,,,EVLT
!*
TB,MKIN,2,3,4, ,
!*
TBMODIF,1,2,0.0005
TBMODIF,1,3,0.0015
TBMODIF,1,4,0.003
TBMODIF,1,5,0.01
TBMODIF,2,1,-40
TBMODIF,2,2,23050000
TBMODIF,2,3,50850000
TBMODIF,2,4,59250000
TBMODIF,2,5,69680000
TBMODIF,3,1,25
TBMODIF,3,2,13850000
TBMODIF,3,3,30050000
```

```
TBMODIF,3,4,37985000
TBMODIF,3,5,38475000
TBMODIF,4,1,125
TBMODIF,4,2,8500000
TBMODIF,4,3,13170000
TBMODIF,4,4,14880000
TBMODIF,4,5,16336000
!Tempearturliste
MPTEMP,1,-40,25,125, , , ,
!REFERENCE TEMPERATURE
MP,REFT,2,tref
!Poisson's Ratio
MPDATA,PRXY,2,1,0.32,0.43,0.43, , , ,
!Thermal expansion coeff
MPDATA,ALPX,2,1,23.9e-6,23.9e-6,23.9e-6, , , ,
!Young's Modulus
MPDATA,EX,2,1,46100e6,27700e6,17000e6, , , ,
!*
!*  Substrate (Al2O3)
UIMP,3,EX, , ,350000e6,
UIMP,3,DENS, , ,3890 ,
UIMP,3,ALPX, , , 6.7e-6,
UIMP,3,REFT, , , tref,
UIMP,3,NUXY, , ,0.25,
UIMP,3,PRXY, , , ,
UIMP,3,GXY, , , ,
UIMP,3,MU, , , ,
UIMP,3,DAMP, , , ,
UIMP,3,KXX, , , ,
UIMP,3,C, , , ,
UIMP,3,ENTH, , , ,
UIMP,3,HF, , , ,
UIMP,3,EMIS, , , ,
UIMP,3,QRATE, , , ,
UIMP,3,RSVX, , , ,
UIMP,3,PERX, , , ,
UIMP,3,VISC, , , ,
UIMP,3,SONC, , , ,

!* Geometry

!*  Die (Points and Lines)
K,1,,,,
K,2,s,,,
K,3,s,h-d,,
K,4,s,h,,
K,5,0,h,,
K,6,0,h-d,,
K,7,s-w,0,,
K,8,s-m,h-d,,
K,9,s-m,h,,
K,10,0.8*s,0,,
K,11,0.8*s,h-d,,
```

```
K,12,0.8*s,h,,
LSTR,     1,    7
LSTR,     7,   10
LSTR,    10,    2
LSTR,     2,    3
LSTR,     3,    4
LSTR,     3,   11
LSTR,    11,   10
LSTR,     4,   12
LSTR,    12,   11
LSTR,    11,    8
LSTR,    12,    9
LSTR,     8,    9
LSTR,     9,    5
LSTR,     5,    6
LSTR,     6,    8
LSTR,     6,    1
LSTR,     7,    8
K,13,0,0,s,
K,14,0,h-d,s,
K,15,0,h,s,
K,16,0,0,s-w,
K,17,0,h-d,s-m,
K,18,0,h,s-m,
K,19,0,0,0.8*s,
K,20,0,h-d,0.8*s,
K,21,0,h,0.8*s,
LSTR,     1,   16
LSTR,    16,   19
LSTR,    19,   13
LSTR,    13,   14
LSTR,    14,   15
LSTR,    14,   20
LSTR,    15,   21
LSTR,    21,   20
LSTR,    20,   19
LSTR,    21,   18
LSTR,    18,   17
LSTR,    17,   20
LSTR,    18,    5
LSTR,     6,   17
LSTR,    16,   17
LSTR,    19,   20
K,22,s-w,0,s,
K,23,s-m,h-d,s,
K,24,s-m,h,s,
K,25,s,h-d,s,
K,26,s,h,s,
K,27,0.8*s,h,s,
K,28,0.8*s,h-d,s,
K,29,0.8*s,h-d,0.8*s,
K,30,0.8*s,h,0.8*s,
K,31,s,h,0.8*s,
```

```
K,32,s,h-d,0.8*s,
K,33,s,h,s-m,
K,34,s,h-d,s-m,
K,35,s,0,s-w,
LSTR,	13,	22
LSTR,	22,	23
LSTR,	23,	24
LSTR,	23,	28
LSTR,	28,	25
LSTR,	25,	32
LSTR,	32,	34
LSTR,	34,	35
LSTR,	35,	2
LSTR,	34,	3
LSTR,	28,	29
LSTR,	29,	32
LSTR,	24,	27
LSTR,	27,	30
LSTR,	30,	31
LSTR,	31,	26
LSTR,	26,	27
LSTR,	31,	33
LSTR,	33,	4
LSTR,	31,	32
LSTR,	26,	25
LSTR,	27,	28
LSTR,	30,	29
LSTR,	23,	14
LSTR,	15,	24
K,36,s-w,0,s-w,
K,37,s-m,h-d,s-m,
K,38,s-m,h,s-m,
K,39,0.8*s,h,s-m,
K,40,0.8*s,h-d,s-m,
K,41,0.8*s,0,s-w,
K,42,s-w,0,0.8*s,
K,43,s-m,h-d,0.8*s,
K,44,s-m,h,0.8*s,
LSTR,	22,	42
LSTR,	42,	36
LSTR,	36,	41
LSTR,	41,	35
LSTR,	41,	10
LSTR,	36,	7
LSTR,	36,	16
LSTR,	42,	19
LSTR,	36,	37
LSTR,	42,	43
LSTR,	23,	43
LSTR,	43,	37
LSTR,	37,	40
LSTR,	40,	34
LSTR,	24,	44
```

```
LSTR,   44,   43
LSTR,   44,   38
LSTR,   38,   37
LSTR,   38,   39
LSTR,   39,   40
LSTR,   39,   33
LSTR,   40,   29
LSTR,   30,   39
LSTR,   30,   44
LSTR,   43,   29
LSTR,   44,   21
LSTR,   20,   43
LSTR,   40,   11
LSTR,   12,   39
LSTR,    8,   37
LSTR,   38,    9
LSTR,   38,   18
LSTR,   17,   37

! Adhesive Layer (Points and Lines)
K,45,0,-adthick,0,
K,46,0,-adthick,s-w,
K,47,0,-adthick,0.8*s,
K,48,0,-adthick,s,
K,49,s-w,-adthick,s,
K,50,s-w,-adthick,0.8*s,
K,51,s-w,-adthick,s-w,
K,52,0.8*s,-adthick,s-w,
K,53,s,-adthick,s-w,
K,54,s,-adthick,0,
K,55,0.8*s,-adthick,0,
K,56,s-w,-adthick,0,
LSTR,   45,   46
LSTR,   46,   47
LSTR,   47,   48
LSTR,   48,   49
LSTR,   49,   50
LSTR,   50,   51
LSTR,   51,   52
LSTR,   52,   53
LSTR,   53,   54
LSTR,   54,   55
LSTR,   55,   56
LSTR,   56,   45

! Substrate (Points and Lines)
K,57,s-headsid,-adthick,s-headsid,
K,58,s-headsid,-adthick,0,
K,59,s-headsid,-adthick,s-w,
K,60,s-headsid,-adthick,0.8*s,
K,61,s-headsid,-adthick,s,
K,62,0,-adthick,s-headsid,
K,63,s-w,-adthick,s-headsid,
```

```
K,64,0.8*s,-adthick,s-headsid,
K,65,s,-adthick,s-headsid,
K,66,s-holerad,-adthick,s,
K,67,s,-adthick,s,
K,68,s,-adthick,s-holerad,
K,69,0,-adthick-headhig,0,
K,70,0,-adthick-headhig,s-w,
K,71,0,-adthick-headhig,0.8*s,
K,72,0,-adthick-headhig,s,
K,73,s-w,-adthick-headhig,s,
K,74,s-w,-adthick-headhig,0.8*s,
K,75,s-w,-adthick-headhig,s-w,
K,76,0.8*s,-adthick-headhig,s-w,
K,77,s,-adthick-headhig,s-w,
K,78,s,-adthick-headhig,0,
K,79,0.8*s,-adthick-headhig,0,
K,80,s-w,-adthick-headhig,0,
K,81,s-headsid,-adthick-headhig,s-headsid,
K,82,s-headsid,-adthick-headhig,0,
K,83,s-headsid,-adthick-headhig,s-w,
K,84,s-headsid,-adthick-headhig,0.8*s,
K,85,s-headsid,-adthick-headhig,s,
K,86,,-adthick-headhig,s-headsid,
K,87,s-w,-adthick-headhig,s-headsid,
K,88,0.8*s,-adthick-headhig,s-headsid,
K,89,s,-adthick-headhig,s-headsid,
K,90,s-holerad,-adthick-headhig,s,
K,91,s,-adthick-headhig,s,
K,92,s,-adthick-headhig,s-holerad,
LSTR,    57,    58
LSTR,    58,    59
LSTR,    59,    60
LSTR,    60,    61
LSTR,    61,    48
LSTR,    57,    62
LSTR,    62,    63
LSTR,    63,    64
LSTR,    64,    65
LSTR,    65,    54
LSTR,    49,    66
LSTR,    57,    62
LSTR,    62,    63
LSTR,    63,    64
LSTR,    64,    65
LSTR,    65,    54
LSTR,    53,    68
LSTR,    69,    70
LSTR,    70,    71
LSTR,    71,    72
LSTR,    72,    73
LSTR,    73,    74
LSTR,    74,    75
LSTR,    75,    76
```

```
LSTR,   76,   77
LSTR,   77,   78
LSTR,   78,   79
LSTR,   79,   80
LSTR,   80,   69
LSTR,   81,   82
LSTR,   82,   83
LSTR,   83,   84
LSTR,   84,   85
LSTR,   85,   72
LSTR,   81,   86
LSTR,   86,   87
LSTR,   87,   88
LSTR,   88,   89
LSTR,   89,   78
LSTR,   57,   81
LSTR,   61,   85
LSTR,   49,   73
LSTR,   50,   74
LSTR,   51,   75
LSTR,   52,   76
LSTR,   53,   77
LSTR,   66,   90
LSTR,   68,   92
LSTR,   65,   89
LSTR,   73,   90
LSTR,   77,   92
LARC,   66,   68,   67,   HOLERAD
LARC,   90,   92,   91,   HOLERAD
! Die (Volumes)
!1
V,1,7,8,6,16,36,37,17
!2
V,6,8,9,5,17,37,38,18
!3
V,16,36,37,17,19,42,43,20
!4
V,17,37,38,18,20,43,44,21
!5
V,19,42,43,20,13,22,23,14
!6
V,20,43,44,21,14,23,24,15
!7
V,7,10,11,8,36,41,40,37
!8
V,8,11,12,9,37,40,39,38
!9
V,10,2,3,11,41,35,34,40
!10
V,11,3,4,12,40,34,33,39
!11
V,37,40,39,38,43,29,30,44
!12
```

```
V,43,29,30,44,23,28,27,24
!13
V,40,34,33,39,29,32,31,30
!14
V,29,32,31,30,28,25,26,27
!*
! Die Attach (Volumes)
!15
V,45,56,7,1,46,51,36,16
!16
V,46,51,36,16,47,50,42,19
!17
V,47,50,42,19,48,49,22,13
!18
V,56,55,10,7,51,52,41,36
!19
V,55,54,2,10,52,53,35,41
!*
! Header (Volumes)
!20
V,81,86,62,57,82,69,45,58
!21
V,82,69,45,58,83,70,46,59
!22
V,83,70,46,59,84,71,47,60
!23
V,84,71,47,60,85,72,48,61
!24
V,86,87,63,62,69,80,56,45
!25
V,87,88,64,63,80,79,55,56
!26
V,88,89,65,64,79,78,54,55
!27
V,69,80,56,45,70,75,51,46
!28
V,70,75,51,46,71,74,50,47
!29
V,71,74,50,47,72,73,49,48
!30
V,80,79,55,56,75,76,52,51
!31
V,79,78,54,55,76,77,53,52

!Inner Volumes
FLST,2,2,4,ORDE,2
FITEM,2,149
FITEM,2,-150
LDIV,P51X,0.25, ,4,0
LSTR,    50,    93
LSTR,    51,    94
LSTR,    52,    95
LSTR,    74,    96
```

```
LSTR,    75,    97
LSTR,    76,    98
FLST,2,4,4
FITEM,2,147
FITEM,2,144
FITEM,2,113
FITEM,2,139
AL,P51X
LSTR,    93,    96
LSTR,    94,    97
LSTR,    95,    98
FLST,2,4,4
FITEM,2,150
FITEM,2,210
FITEM,2,149
FITEM,2,144
AL,P51X
FLST,2,4,4
FITEM,2,207
FITEM,2,210
FITEM,2,204
FITEM,2,140
AL,P51X
FLST,2,4,4
FITEM,2,210
FITEM,2,201
FITEM,2,211
FITEM,2,198
AL,P51X
FLST,2,4,4
FITEM,2,208
FITEM,2,211
FITEM,2,205
FITEM,2,141
AL,P51X
FLST,2,4,4
FITEM,2,202
FITEM,2,212
FITEM,2,199
FITEM,2,211
AL,P51X
FLST,2,4,4
FITEM,2,209
FITEM,2,142
FITEM,2,206
FITEM,2,212
AL,P51X
FLST,2,4,4
FITEM,2,203
FITEM,2,145
FITEM,2,200
FITEM,2,212
AL,P51X
```

```
FLST,2,4,4
FITEM,2,148
FITEM,2,143
FITEM,2,114
FITEM,2,145
AL,P51X
FLST,2,4,4
FITEM,2,113
FITEM,2,149
FITEM,2,204
FITEM,2,95
AL,P51X
FLST,2,4,4
FITEM,2,96
FITEM,2,204
FITEM,2,198
FITEM,2,205
AL,P51X
FLST,2,4,4
FITEM,2,205
FITEM,2,199
FITEM,2,206
FITEM,2,97
AL,P51X
FLST,2,4,4
FITEM,2,98
FITEM,2,206
FITEM,2,200
FITEM,2,114
AL,P51X
FLST,2,4,4
FITEM,2,150
FITEM,2,147
FITEM,2,119
FITEM,2,207
AL,P51X
FLST,2,4,4
FITEM,2,201
FITEM,2,207
FITEM,2,120
FITEM,2,208
AL,P51X
FLST,2,4,4
FITEM,2,202
FITEM,2,208
FITEM,2,121
FITEM,2,209
AL,P51X
FLST,2,4,4
FITEM,2,203
FITEM,2,209
FITEM,2,122
FITEM,2,148
```

```
AL,P51X
FLST,2,6,5,ORDE,5
FITEM,2,128
FITEM,2,136
FITEM,2,-138
FITEM,2,145
FITEM,2,149
VA,P51X
FLST,2,6,5,ORDE,5
FITEM,2,125
FITEM,2,138
FITEM,2,-140
FITEM,2,146
FITEM,2,150
VA,P51X
FLST,2,6,5,ORDE,5
FITEM,2,132
FITEM,2,140
FITEM,2,-142
FITEM,2,147
FITEM,2,151
VA,P51X
FLST,2,6,5,ORDE,5
FITEM,2,135
FITEM,2,142
FITEM,2,-144
FITEM,2,148
FITEM,2,152
VA,P51X
!***********************
!Meshing
!***********************
!Sizing (c=4, n=1/c, o=-c)
!Group 1  Die Cross Section
LESIZE,1, , ,dm,n,
LESIZE,13, , ,dm,c,
LESIZE,15, , ,dm,n,
LESIZE,18, , ,dm,n,
LESIZE,30, , ,dm,c,
LESIZE,31, , ,dm,n,
LESIZE,33, , ,dm,n,
LESIZE,41, , ,dm,c,
LESIZE,42, , ,dm,c,
LESIZE,51, , ,dm,c,
LESIZE,56, , ,dm,c,
LESIZE,57, , ,dm,n,
LESIZE,62, , ,dm,c,
LESIZE,63, , ,dm,c,
LESIZE,64, , ,dm,c,
LESIZE,65, , ,dm,c,
LESIZE,83, , ,dm,c,
LESIZE,84, , ,dm,n,
LESIZE,85, , ,dm,c,
```

```
LESIZE,86, , ,dm,n,
LESIZE,87, , ,dm,n,
LESIZE,88, , ,dm,c,
LESIZE,89, , ,dm,c,
LESIZE,90, , ,dm,n,
LESIZE,91, , ,dm,n,
LESIZE,94, , ,dm,n,
LESIZE,99, , ,dm,c,
LESIZE,102, , ,dm,c,
LESIZE,104, , ,dm,n,
LESIZE,109, , ,dm,n,
LESIZE,115, , ,dm,n,
LESIZE,118, , ,dm,n,
LESIZE,123, , ,dm,c,
LESIZE,126, , ,dm,c,
LESIZE,128, , ,dm,n,
LESIZE,133, , ,dm,n,
LESIZE,155, , ,dm,n,
LESIZE,156, , ,dm,c,
LESIZE,159, , ,dm,c,
LESIZE,165, , ,dm,n,
LESIZE,194, , ,dm,n,
LESIZE,195, , ,dm,c,
LESIZE,196, , ,dm,c,
LESIZE,197, , ,dm,n,
!*
!* Die Height
!*
LESIZE,4, , ,8,o,
LESIZE,7, , ,8,o,
LESIZE,16, , ,8,o,
LESIZE,17, , ,8,o,
LESIZE,21, , ,8,o,
LESIZE,26, , ,8,o,
LESIZE,32, , ,8,o,
LESIZE,34, , ,8,o,
LESIZE,40, , ,8,o,
LESIZE,66, , ,8,o,
LESIZE,67, , ,8,o,
LESIZE,151, , ,8,o,
!*
!group 2 Outer Membrane Segment
!*
FLST,5,36,4,ORDE,34
FITEM,5,3
FITEM,5,6
FITEM,5,8
FITEM,5,20
FITEM,5,23
FITEM,5,-24
FITEM,5,37
FITEM,5,-38
FITEM,5,43
```

```
FITEM,5,-44
FITEM,5,46
FITEM,5,-49
FITEM,5,58
FITEM,5,61
FITEM,5,68
FITEM,5,71
FITEM,5,-72
FITEM,5,78
FITEM,5,93
FITEM,5,95
FITEM,5,98
FITEM,5,100
FITEM,5,106
FITEM,5,111
FITEM,5,117
FITEM,5,119
FITEM,5,122
FITEM,5,124
FITEM,5,130
FITEM,5,135
FITEM,5,149
FITEM,5,-150
FITEM,5,200
FITEM,5,203
CM,_Y,LINE
LSEL, , , ,P51X
!*
CM,_Y1,LINE
CMSEL,,_Y
LESIZE,_Y1, , ,4,3,
CMDEL,_Y
CMDEL,_Y1
FLST,5,19,4,ORDE,19
FITEM,5,3
FITEM,5,20
FITEM,5,37
FITEM,5,44
FITEM,5,47
FITEM,5,-48
FITEM,5,61
FITEM,5,71
FITEM,5,78
FITEM,5,93
FITEM,5,98
FITEM,5,106
FITEM,5,111
FITEM,5,117
FITEM,5,122
FITEM,5,130
FITEM,5,135
FITEM,5,200
FITEM,5,203
```

```
CM,_Y,LINE
LSEL, , , ,P51X
!*
CM,_Y1,LINE
CMSEL,,_Y
!*
CLRMSHLN
LESIZE,_Y1, , ,4,1/3,
CMDEL,_Y
CMDEL,_Y1

!group 3 Inner membrane Segment
!*
FLST,5,30,4,ORDE,30
FITEM,5,2
FITEM,5,10
FITEM,5,-11
FITEM,5,19
FITEM,5,27
FITEM,5,29
FITEM,5,39
FITEM,5,50
FITEM,5,59
FITEM,5,-60
FITEM,5,69
FITEM,5,74
FITEM,5,79
FITEM,5,-80
FITEM,5,92
FITEM,5,96
FITEM,5,-97
FITEM,5,101
FITEM,5,105
FITEM,5,110
FITEM,5,116
FITEM,5,120
FITEM,5,-121
FITEM,5,125
FITEM,5,129
FITEM,5,134
FITEM,5,198
FITEM,5,-199
FITEM,5,201
FITEM,5,-202
CM,_Y,LINE
LSEL, , , ,P51X
!*
CM,_Y1,LINE
CMSEL,,_Y
LESIZE,_Y1, , ,7,1,
CMDEL,_Y
CMDEL,_Y1
!*
```

```
!group 4 Membrane Hight
!*
FLST,5,25,4,ORDE,20
FITEM,5,5
FITEM,5,9
FITEM,5,12
FITEM,5,14
FITEM,5,22
FITEM,5,25
FITEM,5,28
FITEM,5,35
FITEM,5,53
FITEM,5,-55
FITEM,5,73
FITEM,5,75
FITEM,5,77
FITEM,5,152
FITEM,5,154
FITEM,5,157
FITEM,5,160
FITEM,5,-164
FITEM,5,166
FITEM,5,-168
CM,_Y,LINE
LSEL, , , ,P51X
!*
CM,_Y1,LINE
CMSEL,,_Y
FLST,5,15,4,ORDE,13
FITEM,5,5
FITEM,5,9
FITEM,5,12
FITEM,5,14
FITEM,5,22
FITEM,5,25
FITEM,5,28
FITEM,5,35
FITEM,5,52
FITEM,5,-55
FITEM,5,75
FITEM,5,77
FITEM,5,152
CM,_Y,LINE
LSEL, , , ,P51X
!*
CM,_Y1,LINE
CMSEL,,_Y
LESIZE,_Y1, , ,2,1,
CMDEL,_Y
CMDEL,_Y1
!*
!group 5 Die Attach Height
!*
```

```
FLST,5,12,4,ORDE,8
FITEM,5,153
FITEM,5,-154
FITEM,5,157
FITEM,5,-158
FITEM,5,160
FITEM,5,-164
FITEM,5,166
FITEM,5,-168
CM,_Y,LINE
LSEL, , , ,P51X
!*
CM,_Y1,LINE
CMSEL,,_Y
LESIZE,_Y1, , ,2,1,
CMDEL,_Y
CMDEL,_Y1
!*
!group 6 Substrate
!*
FLST,5,4,4,ORDE,4
FITEM,5,36
FITEM,5,45
FITEM,5,81
FITEM,5,-82
CM,_Y,LINE
LSEL, , , ,P51X
!*
CM,_Y1,LINE
CMSEL,,_Y
LESIZE,_Y1, , ,7,1,
CMDEL,_Y
CMDEL,_Y1
!*
FLST,5,16,4,ORDE,14
FITEM,5,10
FITEM,5,-11
FITEM,5,27
FITEM,5,29
FITEM,5,36
FITEM,5,39
FITEM,5,45
FITEM,5,50
FITEM,5,69
FITEM,5,-70
FITEM,5,74
FITEM,5,76
FITEM,5,79
FITEM,5,-82
CM,_Y,LINE
LSEL, , , ,P51X
!*
CM,_Y1,LINE
```

```
CMSEL,,_Y
LESIZE,_Y1, , ,7,4,
CMDEL,_Y
CMDEL,_Y1
!*
FLST,5,9,4,ORDE,9
FITEM,5,10
FITEM,5,-11
FITEM,5,27
FITEM,5,39
FITEM,5,50
FITEM,5,69
FITEM,5,74
FITEM,5,80
FITEM,5,-81
CM,_Y,LINE
LSEL, , , ,P51X
!*
CM,_Y1,LINE
CMSEL,,_Y
LESIZE,_Y1, , ,7,.25,
CMDEL,_Y
CMDEL,_Y1
!*
!*
!group 7 Substrate
FLST,5,30,4,ORDE,25
FITEM,5,103
FITEM,5,107
FITEM,5,-108
FITEM,5,112
FITEM,5,-114
FITEM,5,127
FITEM,5,131
FITEM,5,-132
FITEM,5,136
FITEM,5,147
FITEM,5,-148
FITEM,5,170
FITEM,5,-171
FITEM,5,173
FITEM,5,-174
FITEM,5,176
FITEM,5,178
FITEM,5,180
FITEM,5,182
FITEM,5,186
FITEM,5,188
FITEM,5,190
FITEM,5,192
FITEM,5,204
FITEM,5,-209
CM,_Y,LINE
```

```
LSEL, , , ,P51X
!*
CM,_Y1,LINE
CMSEL,,_Y
LESIZE,_Y1, , ,4,1,
CMDEL,_Y
CMDEL,_Y1
!*
!group 8 Substrate height
!*
FLST,5,26,4,ORDE,16
FITEM,5,137
FITEM,5,-146
FITEM,5,169
FITEM,5,172
FITEM,5,175
FITEM,5,177
FITEM,5,179
FITEM,5,181
FITEM,5,183
FITEM,5,-185
FITEM,5,187
FITEM,5,189
FITEM,5,191
FITEM,5,193
FITEM,5,210
FITEM,5,-212
CM,_Y,LINE
LSEL, , , ,P51X
!*
CM,_Y1,LINE
CMSEL,,_Y
LESIZE,_Y1, , ,4,c,
CMDEL,_Y
CMDEL,_Y1

FLST,5,9,4,ORDE,9
FITEM,5,169
FITEM,5,172
FITEM,5,177
FITEM,5,181
FITEM,5,184
FITEM,5,-185
FITEM,5,187
FITEM,5,189
FITEM,5,193
CM,_Y,LINE
LSEL, , , ,P51X
!*
CM,_Y1,LINE
CMSEL,,_Y
!.25
LESIZE,_Y1, , ,4,n,
```

```
CMDEL,_Y
CMDEL,_Y1
!***
FLST,5,1,4,ORDE,1
FITEM,5,191
CM,_Y,LINE
LSEL, , , ,P51X
!*
CM,_Y1,LINE
CMSEL,,_Y
!0.25
LESIZE,_Y1, , ,4,n,
CMDEL,_Y
CMDEL,_Y1
!*
! Die Mesh
!*
FLST,5,14,6,ORDE,2
FITEM,5,1
FITEM,5,-14
CM,_Y,VOLU
VSEL, , , ,P51X
CM,_Y1,VOLU
CHKMSH,'VOLU'
CMSEL,S,_Y
!*
MSHKEY,1
VMESH,_Y1
MSHKEY,-1
!*
CMDEL,_Y
CMDEL,_Y1
CMDEL,_Y2
!*
! Die Attach Mesh
!*
TYPE,   2
MAT,     2
REAL,
ESYS,     0
!*
FLST,5,5,6,ORDE,2
FITEM,5,15
FITEM,5,-19
CM,_Y,VOLU
VSEL, , , ,P51X
CM,_Y1,VOLU
CHKMSH,'VOLU'
CMSEL,S,_Y
!*
MSHKEY,1
VMESH,_Y1
MSHKEY,0
```

```
!*
CMDEL,_Y
CMDEL,_Y1
CMDEL,_Y2
!*
! Header Mesh
!*
TYPE,   3
MAT,      3
REAL,
ESYS,      0
!*
! VPLOT
ALLSEL,ALL
VSEL,ALL
ASEL,ALL
LSEL,ALL
KSEL,ALL
ESEL,ALL
NSEL,ALL
FLST,5,16,6,ORDE,2
FITEM,5,20
FITEM,5,-35
CM,_Y,VOLU
VSEL, , , ,P51X
CM,_Y1,VOLU
CHKMSH,'VOLU'
CMSEL,S,_Y
!*
MSHKEY,1
VMESH,_Y1
MSHKEY,0
!*
CMDEL,_Y
CMDEL,_Y1
CMDEL,_Y2
ALLSEL,ALL
VSEL,ALL
ASEL,ALL
LSEL,ALL
KSEL,ALL
ESEL,ALL
NSEL,ALL
!*************************
!Uniform Temperature T
!*************************
BFUNIF,TEMP,T
!*************************
FINISH
/SOLU
!*************************
!Boundary Coinditions
!*************************
```

```
! Mounting of the Substrate
FLST,2,596,1,ORDE,58
FITEM,2,4524
FITEM,2,-4528
FITEM,2,4549
FITEM,2,-4568
FITEM,2,4648
FITEM,2,-4692
FITEM,2,4864
FITEM,2,-4898
FITEM,2,5032
FITEM,2,-5051
FITEM,2,5128
FITEM,2,-5136
FITEM,2,5173
FITEM,2,-5208
FITEM,2,5344
FITEM,2,-5350
FITEM,2,5379
FITEM,2,-5406
FITEM,2,5512
FITEM,2,-5515
FITEM,2,5532
FITEM,2,-5547
FITEM,2,5608
FITEM,2,-5688
FITEM,2,5932
FITEM,2,-5994
FITEM,2,6184
FITEM,2,-6219
FITEM,2,6328
FITEM,2,-6390
FITEM,2,6580
FITEM,2,-6615
FITEM,2,6724
FITEM,2,-6727
FITEM,2,6744
FITEM,2,-6747
FITEM,2,6764
FITEM,2,-6766
FITEM,2,6788
FITEM,2,-6796
FITEM,2,6824
FITEM,2,-6830
FITEM,2,6859
FITEM,2,-6861
FITEM,2,6892
FITEM,2,-6909
FITEM,2,6964
FITEM,2,-6970
FITEM,2,6999
FITEM,2,-7001
FITEM,2,7032
```

```
FITEM,2,-7049
FITEM,2,7104
FITEM,2,-7107
FITEM,2,7124
FITEM,2,-7126
FITEM,2,7148
FITEM,2,-7156
D,P51X, , , , , ,UY
!D,P51X, , , , , ,ALL
ALLSEL,ALL
VSEL,ALL
ASEL,ALL
LSEL,ALL
KSEL,ALL
ESEL,ALL
NSEL,ALL
!*
! Symmetry BC
!*
FLST,2,16,5
FITEM,2,118
FITEM,2,134
FITEM,2,144
FITEM,2,41
FITEM,2,45
FITEM,2,83
FITEM,2,57
FITEM,2,61
FITEM,2,105
FITEM,2,129
FITEM,2,136
FITEM,2,25
FITEM,2,76
FITEM,2,29
FITEM,2,55
FITEM,2,63
DA,P51X,SYMM
!**********************
! Pressure
!**********************
*do,i,1,LST
TIME,1
AUTOTS,0
DELTIM,1,0,0,0
KBC,1
!*
ALLSEL,ALL
VSEL,ALL
ASEL,ALL
LSEL,ALL
KSEL,ALL
ESEL,ALL
NSEL,ALL
```

```
FLST,2,20,5,ORDE,18
FITEM,2,13
FITEM,2,22
FITEM,2,34
FITEM,2,43
FITEM,2,48
FITEM,2,52
FITEM,2,56
FITEM,2,60
FITEM,2,70
FITEM,2,74
FITEM,2,80
FITEM,2,84
FITEM,2,137
FITEM,2,139
FITEM,2,141
FITEM,2,143
FITEM,2,145
FITEM,2,-148
SFA,P51X,1,PRES,(i+offset)*0.1*press,
ALLSEL,ALL
VSEL,ALL
ASEL,ALL
LSEL,ALL
KSEL,ALL
ESEL,ALL
NSEL,ALL
LSWRITE,i,
!*
*enddo
finish
```

## Changes in the ANSYS code for the Epoxy

Substitute input data of the Solder with the following lines to change to the Epoxy:

```
!* Epoxy Ablebond 789-3 (multilinear)
MPLIST,ALL,,,EVLT
MPLIST,ALL,,,EVLT
!*
TB,MKIN,2,3,5, ,
!*
TBMODIF,1,2,500e-6
TBMODIF,1,3,2000e-6
TBMODIF,1,4,10000e-6
TBMODIF,1,5,20000e-6
TBMODIF,1,6,30000e-6
TBMODIF,2,1,-40
TBMODIF,2,2,3995000
TBMODIF,2,3,11015000
TBMODIF,2,4,41655000
TBMODIF,2,5,77755000
TBMODIF,2,6,77756000
TBMODIF,3,1,25
TBMODIF,3,2,2965000
TBMODIF,3,3,9505000
TBMODIF,3,4,38465000
TBMODIF,3,5,64965000
TBMODIF,3,6,82865000
TBMODIF,4,1,115
TBMODIF,4,2,100000
TBMODIF,4,3,265000
TBMODIF,4,4,745000
TBMODIF,4,5,1165000
TBMODIF,4,6,1455000
!Tempearturliste
MPTEMP,1,-40,25,115, , , ,
!REFERENCE TEMPERATURE
MP,REFT,2,tref
!Poisson's Ratio
MPDATA,PRXY,2,1,0.42,0.42,0.49, , , ,
!Thermal expansion coeff
MPDATA,ALPX,2,1,63e-6,63e-6,140e-6, , , ,
!Young's Modulus
MPDATA,EX,2,1,7990e6,5930e6,200e6, , , ,
```

## Changes in the ANSYS code for the RTV

Change the element type of the second element (adhesive) from SOLID45 to HYPER86:

```
!*adhesive
ET,2,HYPER86
```

Substitute input data of the Solder with the following lines to change to the RTV:

```
!* RTV - Mooney Rivlin Hypereleastic Element
TB,MOONEY,2,3
TBTEMP,-40
TBDAT,1,  0.330760E+06
TBDAT,2,  -0.183066E+06
TBTEMP,25
TBDAT,1,  0.330760E+06
TBDAT,2,  -0.183066E+06
TBTEMP,125
TBDAT,1,  0.330760E+06
TBDAT,2,  -0.183066E+06

!Tempearturliste
MPTEMP,1,-40,25,125, , , ,
!REFERENCE TEMPERATURE
MP,REFT,2,tref
!Poisson's Ratio
MPDATA,PRXY,2,1,0.49,0.49,0.49, , , ,
!Thermal expansion coeff
MPDATA,ALPX,2,1,370e-6,370e-6,370e-6, , , ,
```

# Appendix D - Results

The output characteristic of the sensor was determined from the stresses that were picked up in the piezoresistive regions. The following data represents the averaged stresses in the region as well as the determined output and the resulting pressure nonlinearity.

The floating die is the ideal case in which the silicon die can expand freely in the x-z-plane. This model is used as a reference for the comparison of the different die attach materials.

Floating Die (2 pages)

Solder (2 pages)

Epoxy (2 pages)

RTV (2 pages)

Table A-4: Stresses in the Floating Die

| | Region 1 | | | | | | Region 1 | | | | | |
|---|---|---|---|---|---|---|---|---|---|---|---|---|
| p in kPa | Sx, T=-40C | Sy, T=-40C | Sz, T=-40C | Sxy, T=-40C | Syz, T=-40C | Sxz, T=-40C | Sx,T=-40C | Sy,T=-40C | Sz, T=-40C | Sxy,T=-40C | Syz,T=-40C | Sxz,T=-40C |
| 0 | -2.75E+03 | -2.75E+03 | -2.75E+03 | -2.05E-05 | 4.67E-06 | 0.00E+00 | -2.75E+03 | -2.75E+03 | -2.75E+03 | 0.00E+00 | -1.00E-05 | 0.00E+00 |
| 3.5 | -6.35E+06 | -3.00E+05 | -1.83E+06 | 1.28E+05 | -9.56E+03 | -1.37E+04 | -1.83E+06 | -3.00E+05 | -6.35E+06 | -9.56E+03 | 1.28E+05 | -1.37E+04 |
| 7 | -1.24E+07 | -5.97E+05 | -3.61E+06 | 2.56E+05 | -1.90E+04 | -2.05E+04 | -3.61E+06 | -5.97E+05 | -1.24E+07 | -1.90E+04 | 2.56E+05 | -2.05E+04 |
| 10.5 | -1.81E+07 | -8.88E+05 | -5.32E+06 | 3.82E+05 | -2.84E+04 | -2.08E+04 | -5.32E+06 | -8.88E+05 | -1.81E+07 | -2.84E+04 | 3.82E+05 | -2.08E+04 |
| 14 | -2.35E+07 | -1.17E+06 | -6.95E+06 | 5.07E+05 | -3.75E+04 | -1.54E+04 | -6.95E+06 | -1.17E+06 | -2.35E+07 | -3.75E+04 | 5.07E+05 | -1.54E+04 |
| 17.5 | -2.86E+07 | -1.45E+06 | -8.50E+06 | 6.30E+05 | -4.65E+04 | -5.27E+03 | -8.50E+06 | -1.45E+06 | -2.86E+07 | -4.65E+04 | 6.30E+05 | -5.27E+03 |
| 21 | -3.33E+07 | -1.71E+06 | -9.96E+06 | 7.52E+05 | -5.54E+04 | 8.68E+03 | -9.96E+06 | -1.71E+06 | -3.33E+07 | -5.54E+04 | 7.52E+05 | 8.68E+03 |
| 24.5 | -3.77E+07 | -1.97E+06 | -1.14E+07 | 8.72E+05 | -6.40E+04 | 2.57E+04 | -1.14E+07 | -1.97E+06 | -3.77E+07 | -6.40E+04 | 8.72E+05 | 2.57E+04 |
| 28 | -4.18E+07 | -2.22E+06 | -1.27E+07 | 9.91E+05 | -7.25E+04 | 4.50E+04 | -1.27E+07 | -2.22E+06 | -4.18E+07 | -7.25E+04 | 9.91E+05 | 4.50E+04 |
| 31.5 | -4.57E+07 | -2.46E+06 | -1.39E+07 | 1.11E+06 | -8.08E+04 | 6.61E+04 | -1.39E+07 | -2.46E+06 | -4.57E+07 | -8.08E+04 | 1.11E+06 | 6.61E+04 |
| 35 | -4.93E+07 | -2.70E+06 | -1.51E+07 | 1.23E+06 | -8.90E+04 | 8.85E+04 | -1.51E+07 | -2.70E+06 | -4.93E+07 | -8.90E+04 | 1.23E+06 | 8.85E+04 |

| | Region 1 | | | | | | Region 1 | | | | | |
|---|---|---|---|---|---|---|---|---|---|---|---|---|
| p in kPa | Sx,T=25C | Sy,T=25C | Sz,T=25C | Sxy,T=25C | Syz,T=25C | Sxz,T=25C | Sx,T=25C | Sy,T=25C | Sz,T=25C | Sxy,T=25C | Syz,T=25C | Sxz,T=25C |
| 0 | 0.00E+00 | 0.00E+00 | 0.00E+00 | 0.00E+00 | 0.00E+00 | 0.00E+00 | 0.00E+00 | 0.00E+00 | 0.00E+00 | 0.00E+00 | 0.00E+00 | 0.00E+00 |
| 3.5 | -6.35E+06 | -2.99E+05 | -1.83E+06 | 1.28E+05 | -9.57E+03 | -1.37E+04 | -1.83E+06 | -2.99E+05 | -6.35E+06 | -9.57E+03 | 1.28E+05 | -1.37E+04 |
| 7 | -1.24E+07 | -5.96E+05 | -3.61E+06 | 2.56E+05 | -1.91E+04 | -2.04E+04 | -3.61E+06 | -5.96E+05 | -1.24E+07 | -1.91E+04 | 2.56E+05 | -2.04E+04 |
| 10.5 | -1.81E+07 | -8.87E+05 | -5.31E+06 | 3.82E+05 | -2.84E+04 | -2.07E+04 | -5.31E+06 | -8.87E+05 | -1.81E+07 | -2.84E+04 | 3.82E+05 | -2.07E+04 |
| 14 | -2.35E+07 | -1.17E+06 | -6.94E+06 | 5.07E+05 | -3.76E+04 | -1.52E+04 | -6.94E+06 | -1.17E+06 | -2.35E+07 | -3.76E+04 | 5.07E+05 | -1.52E+04 |
| 17.5 | -2.85E+07 | -1.44E+06 | -8.49E+06 | 6.30E+05 | -4.66E+04 | -5.04E+03 | -8.49E+06 | -1.44E+06 | -2.85E+07 | -4.66E+04 | 6.30E+05 | -5.04E+03 |
| 21 | -3.32E+07 | -1.71E+06 | -9.95E+06 | 7.52E+05 | -5.54E+04 | 8.99E+03 | -9.95E+06 | -1.71E+06 | -3.32E+07 | -5.54E+04 | 7.52E+05 | 8.99E+03 |
| 24.5 | -3.76E+07 | -1.97E+06 | -1.13E+07 | 8.72E+05 | -6.41E+04 | 2.60E+04 | -1.13E+07 | -1.97E+06 | -3.76E+07 | -6.41E+04 | 8.72E+05 | 2.60E+04 |
| 28 | -4.17E+07 | -2.22E+06 | -1.26E+07 | 9.91E+05 | -7.26E+04 | 4.54E+04 | -1.26E+07 | -2.22E+06 | -4.17E+07 | -7.26E+04 | 9.91E+05 | 4.54E+04 |
| 31.5 | -4.56E+07 | -2.46E+06 | -1.39E+07 | 1.11E+06 | -8.09E+04 | 6.66E+04 | -1.39E+07 | -2.46E+06 | -4.56E+07 | -8.09E+04 | 1.11E+06 | 6.66E+04 |
| 35 | -4.93E+07 | -2.69E+06 | -1.51E+07 | 1.23E+06 | -8.91E+04 | 8.91E+04 | -1.51E+07 | -2.69E+06 | -4.93E+07 | -8.91E+04 | 1.23E+06 | 8.91E+04 |

Table A-4: Stresses in the Floating Die

| | Region 1 | | | | | | Region 1 | | | | | |
|---|---|---|---|---|---|---|---|---|---|---|---|---|
| p in kPa | Sx,T=125C | Sy,T=125C | Sz,T=125C | Sxy,T=125C | Syz,T=125C | Sxz,T=125C | Sx,T=125C | Sy,T=125C | Sz,T=125C | Sxy,T=125C | Syz,T=125C | Sxz,T=125C |
| 0 | -1.63E-03 | -1.63E-03 | -1.63E-03 | 1.63E-07 | -4.09E-08 | 3.59E-08 | -1.63E-03 | -1.63E-03 | -1.63E-03 | 2.55E-07 | 2.03E-07 | -5.35E-08 |
| 3.5 | -6.35E+06 | -2.98E+05 | -1.82E+06 | 1.28E+05 | -9.57E+03 | -1.37E+04 | -1.82E+06 | -2.98E+05 | -6.35E+06 | -9.57E+03 | 1.28E+05 | -1.37E+04 |
| 7 | -1.24E+07 | -5.93E+05 | -3.60E+06 | 2.56E+05 | -1.91E+04 | -2.04E+04 | -3.60E+06 | -5.93E+05 | -1.24E+07 | -1.91E+04 | 2.56E+05 | -2.04E+04 |
| 10.5 | -1.81E+07 | -8.82E+05 | -5.30E+06 | 3.82E+05 | -2.84E+04 | -2.05E+04 | -5.30E+06 | -8.82E+05 | -1.81E+07 | -2.84E+04 | 3.82E+05 | -2.05E+04 |
| 14 | -2.35E+07 | -1.16E+06 | -6.92E+06 | 5.07E+05 | -3.76E+04 | -1.50E+04 | -6.92E+06 | -1.16E+06 | -2.35E+07 | -3.76E+04 | 5.07E+05 | -1.50E+04 |
| 17.5 | -2.85E+07 | -1.44E+06 | -8.46E+06 | 6.30E+05 | -4.66E+04 | -4.76E+03 | -8.46E+06 | -1.44E+06 | -2.85E+07 | -4.66E+04 | 6.30E+05 | -4.76E+03 |
| 21 | -3.32E+07 | -1.70E+06 | -9.91E+06 | 7.52E+05 | -5.54E+04 | 9.35E+03 | -9.91E+06 | -1.70E+06 | -3.32E+07 | -5.54E+04 | 7.52E+05 | 9.35E+03 |
| 24.5 | -3.76E+07 | -1.96E+06 | -1.13E+07 | 8.72E+05 | -6.41E+04 | 2.65E+04 | -1.13E+07 | -1.96E+06 | -3.76E+07 | -6.41E+04 | 8.72E+05 | 2.65E+04 |
| 28 | -4.17E+07 | -2.21E+06 | -1.26E+07 | 9.91E+05 | -7.25E+04 | 4.59E+04 | -1.26E+07 | -2.21E+06 | -4.17E+07 | -7.25E+04 | 9.91E+05 | 4.59E+04 |
| 31.5 | -4.56E+07 | -2.45E+06 | -1.38E+07 | 1.11E+06 | -8.09E+04 | 6.71E+04 | -1.38E+07 | -2.45E+06 | -4.56E+07 | -8.09E+04 | 1.11E+06 | 6.71E+04 |
| 35 | -4.92E+07 | -2.68E+06 | -1.50E+07 | 1.23E+06 | -8.91E+04 | 8.97E+04 | -1.50E+07 | -2.68E+06 | -4.92E+07 | -8.91E+04 | 1.23E+06 | 8.97E+04 |

Table A-5: Uncompensated Output and Relative Nonlinearity of the Floating Die at DifferentTemperatures

| | Output in mV/V | | | Nonlinearity | | |
|---|---|---|---|---|---|---|
| p in kPa | -40 | 25 | 125 | -40 | 25 | 125 |
| 0 | -0.0001758 | 0 | -6.417E-11 | 0 | 0 | 0 |
| 3.5 | -3.8862747 | -3.3447861 | -2.3988705 | 0.03165427 | 0.03177563 | 0.03193565 |
| 7 | -7.5735686 | -6.517687 | -4.6738216 | 0.05657337 | 0.05677944 | 0.05705585 |
| 10.5 | -11.03732 | -9.497405 | -6.8095482 | 0.07391923 | 0.07417237 | 0.07451884 |
| 14 | -14.269843 | -12.277573 | -8.8012859 | 0.0834315 | 0.08370355 | 0.08406256 |
| 17.5 | -17.276848 | -14.863005 | -10.65298 | 0.0853036 | 0.08556265 | 0.08590403 |
| 21 | -20.072656 | -17.266418 | -12.37369 | 0.08002071 | 0.0802507 | 0.08054147 |
| 24.5 | -22.675982 | -19.503792 | -13.975252 | 0.06821687 | 0.06839728 | 0.06862588 |
| 28 | -25.105847 | -21.591719 | -15.469553 | 0.05053644 | 0.05065599 | 0.05081109 |
| 31.5 | -27.380864 | -23.546309 | -16.868052 | 0.02761006 | 0.02766165 | 0.0277272 |
| 35 | -29.51763 | -25.382433 | -18.182125 | 0 | 0 | 0 |

Table A-6: Stresses in the Die with Solder

| | Region 1 | | | | | | Region 2 | | | | | |
|---|---|---|---|---|---|---|---|---|---|---|---|---|
| p in kPa | Sx,T=-40C | Sy,T=-40C | Sz,T=-40C | Sxy,T=-40C | Syz,T=-40C | Sxz,T=-40C | Sx,T=-40C | Sy,T=-40C | Sz,T=-40C | Sxy,T=-40C | Syz,T=-40C | Sxz,T=-40C |
| 0 | -4.15E+07 | -3.97E+05 | -1.01E+07 | 1.95E+05 | 1.11E+05 | 1.01E+06 | -1.01E+07 | -3.97E+05 | -4.15E+07 | 1.11E+05 | 1.95E+05 | 1.01E+06 |
| 3.5 | -5.06E+07 | -8.32E+05 | -1.28E+07 | 3.07E+05 | 9.74E+04 | 1.02E+06 | -1.28E+07 | -8.32E+05 | -5.06E+07 | 9.74E+04 | 3.07E+05 | 1.02E+06 |
| 7 | -5.77E+07 | -1.19E+06 | -1.49E+07 | 4.23E+05 | 8.60E+04 | 1.04E+06 | -1.49E+07 | -1.19E+06 | -5.77E+07 | 8.60E+04 | 4.23E+05 | 1.04E+06 |
| 10.5 | -6.46E+07 | -1.56E+06 | -1.71E+07 | 5.30E+05 | 7.42E+04 | 1.07E+06 | -1.71E+07 | -1.56E+06 | -6.46E+07 | 7.42E+04 | 5.30E+05 | 1.07E+06 |
| 14 | -7.05E+07 | -1.90E+06 | -1.90E+07 | 6.35E+05 | 6.31E+04 | 1.10E+06 | -1.90E+07 | -1.90E+06 | -7.05E+07 | 6.31E+04 | 6.35E+05 | 1.10E+06 |
| 17.5 | -7.57E+07 | -2.21E+06 | -2.07E+07 | 7.38E+05 | 5.26E+04 | 1.14E+06 | -2.07E+07 | -2.21E+06 | -7.57E+07 | 5.26E+04 | 7.38E+05 | 1.14E+06 |
| 21 | -8.03E+07 | -2.50E+06 | -2.23E+07 | 8.42E+05 | 4.25E+04 | 1.18E+06 | -2.23E+07 | -2.50E+06 | -8.03E+07 | 4.25E+04 | 8.42E+05 | 1.18E+06 |
| 24.5 | -8.44E+07 | -2.77E+06 | -2.36E+07 | 9.45E+05 | 3.29E+04 | 1.22E+06 | -2.36E+07 | -2.77E+06 | -8.44E+07 | 3.29E+04 | 9.45E+05 | 1.22E+06 |
| 28 | -8.82E+07 | -3.03E+06 | -2.49E+07 | 1.05E+06 | 2.35E+04 | 1.26E+06 | -2.49E+07 | -3.03E+06 | -8.82E+07 | 2.35E+04 | 1.05E+06 | 1.26E+06 |
| 31.5 | -9.17E+07 | -3.28E+06 | -2.61E+07 | 1.15E+06 | 1.44E+04 | 1.30E+06 | -2.61E+07 | -3.28E+06 | -9.17E+07 | 1.44E+04 | 1.15E+06 | 1.30E+06 |
| 35 | -9.49E+07 | -3.51E+06 | -2.72E+07 | 1.25E+06 | 5.49E+03 | 1.34E+06 | -2.72E+07 | -3.51E+06 | -9.49E+07 | 5.49E+03 | 1.25E+06 | 1.34E+06 |

| | Region 1 | | | | | | Region 2 | | | | | |
|---|---|---|---|---|---|---|---|---|---|---|---|---|
| p in kPa | Sx,T=25C | Sy,T=25C | Sz,T=25C | Sxy,T=25C | Syz,T=25C | Sxz,T=25C | Sx,T=25C | Sy,T=25C | Sz,T=25C | Sxy,T=25C | Syz,T=25C | Sxz,T=25C |
| 0 | -2.22E+07 | -1.77E+05 | -4.10E+06 | 1.00E+05 | 6.31E+04 | 6.13E+05 | -4.10E+06 | -1.77E+05 | -2.22E+07 | 6.31E+04 | 1.00E+05 | 6.13E+05 |
| 3.5 | -2.95E+07 | -5.20E+05 | -6.23E+06 | 2.23E+05 | 5.22E+04 | 6.05E+05 | -6.23E+06 | -5.20E+05 | -2.95E+07 | 5.22E+04 | 2.23E+05 | 6.05E+05 |
| 7 | -3.65E+07 | -8.66E+05 | -8.33E+06 | 3.42E+05 | 4.12E+04 | 6.09E+05 | -8.33E+06 | -8.66E+05 | -3.65E+07 | 4.12E+04 | 3.42E+05 | 6.09E+05 |
| 10.5 | -4.29E+07 | -1.20E+06 | -1.03E+07 | 4.59E+05 | 3.06E+04 | 6.22E+05 | -1.03E+07 | -1.20E+06 | -4.29E+07 | 3.06E+04 | 4.59E+05 | 6.22E+05 |
| 14 | -4.86E+07 | -1.51E+06 | -1.21E+07 | 5.74E+05 | 2.03E+04 | 6.41E+05 | -1.21E+07 | -1.51E+06 | -4.86E+07 | 2.03E+04 | 5.74E+05 | 6.41E+05 |
| 17.5 | -5.39E+07 | -1.81E+06 | -1.38E+07 | 6.87E+05 | 1.04E+04 | 6.67E+05 | -1.38E+07 | -1.81E+06 | -5.39E+07 | 1.04E+04 | 6.87E+05 | 6.67E+05 |
| 21 | -5.86E+07 | -2.09E+06 | -1.53E+07 | 8.00E+05 | 9.43E+02 | 6.94E+05 | -1.53E+07 | -2.09E+06 | -5.86E+07 | 9.43E+02 | 8.00E+05 | 6.94E+05 |
| 24.5 | -6.30E+07 | -2.36E+06 | -1.67E+07 | 9.10E+05 | -8.36E+03 | 7.23E+05 | -1.67E+07 | -2.36E+06 | -6.30E+07 | -8.36E+03 | 9.10E+05 | 7.23E+05 |
| 28 | -6.70E+07 | -2.61E+06 | -1.80E+07 | 1.02E+06 | -1.74E+04 | 7.53E+05 | -1.80E+07 | -2.61E+06 | -6.70E+07 | -1.74E+04 | 1.02E+06 | 7.53E+05 |
| 31.5 | -7.07E+07 | -2.86E+06 | -1.92E+07 | 1.13E+06 | -2.62E+04 | 7.83E+05 | -1.92E+07 | -2.86E+06 | -7.07E+07 | -2.62E+04 | 1.13E+06 | 7.83E+05 |
| 35 | -7.42E+07 | -3.10E+06 | -2.04E+07 | 1.24E+06 | -3.49E+04 | 8.14E+05 | -2.04E+07 | -3.10E+06 | -7.42E+07 | -3.49E+04 | 1.24E+06 | 8.14E+05 |

Table A-6: Stresses in the Die with Solder

| | Region 1 | | | | | | Region 2 | | | | | |
|---|---|---|---|---|---|---|---|---|---|---|---|---|
| p in kPa | Sx,T=125C | Sy,T=125C | Sz,T=125C | Sxy,T=125C | Syz,T=125C | Sxz,T=125C | Sx,T=125C | Sy,T=125C | Sz,T=125C | Sxy,T=125C | Syz,T=125C | Sxz,T=125C |
| 0 | -7.05E+06 | -4.87E+04 | -1.42E+06 | 2.99E+04 | 2.08E+04 | 1.94E+05 | -1.42E+06 | -4.87E+04 | -7.05E+06 | 20769.8833 | 2.08E+04 | 1.94E+05 |
| 3.5 | -1.37E+07 | -3.63E+05 | -3.35E+06 | 1.56E+05 | 1.07E+04 | 1.82E+05 | -3.35E+06 | -3.63E+05 | -1.37E+07 | 1.07E+04 | 1.07E+04 | 1.82E+05 |
| 7 | -2.01E+07 | -6.72E+05 | -5.21E+06 | 2.82E+05 | 7.30E+02 | 1.78E+05 | -5.21E+06 | -6.72E+05 | -2.01E+07 | 7.30E+02 | 7.30E+02 | 1.78E+05 |
| 10.5 | -2.60E+07 | -9.73E+05 | -6.98E+06 | 4.06E+05 | -9.05E+03 | 1.81E+05 | -6.98E+06 | -9.73E+05 | -2.60E+07 | -9.05E+03 | -9.05E+03 | 1.81E+05 |
| 14 | -3.15E+07 | -1.27E+06 | -8.66E+06 | 5.28E+05 | -1.86E+04 | 1.90E+05 | -8.66E+06 | -1.27E+06 | -3.15E+07 | -1.86E+04 | -1.86E+04 | 1.90E+05 |
| 17.5 | -3.66E+07 | -1.55E+06 | -1.02E+07 | 6.48E+05 | -2.79E+04 | 2.04E+05 | -1.02E+07 | -1.55E+06 | -3.66E+07 | -2.79E+04 | -2.79E+04 | 2.04E+05 |
| 21 | -4.13E+07 | -1.82E+06 | -1.17E+07 | 7.67E+05 | -3.70E+04 | 2.22E+05 | -1.17E+07 | -1.82E+06 | -4.13E+07 | -3.70E+04 | -3.70E+04 | 2.22E+05 |
| 24.5 | -4.57E+07 | -2.08E+06 | -1.31E+07 | 8.85E+05 | -4.59E+04 | 2.42E+05 | -1.31E+07 | -2.08E+06 | -4.57E+07 | -4.59E+04 | -4.59E+04 | 2.42E+05 |
| 28 | -4.98E+07 | -2.33E+06 | -1.44E+07 | 1.00E+06 | -5.46E+04 | 2.65E+05 | -1.44E+07 | -2.33E+06 | -4.98E+07 | -5.46E+04 | -5.46E+04 | 2.65E+05 |
| 31.5 | -5.36E+07 | -2.57E+06 | -1.57E+07 | 1.12E+06 | -6.31E+04 | 2.89E+05 | -1.57E+07 | -2.57E+06 | -5.36E+07 | -6.31E+04 | -6.31E+04 | 2.89E+05 |
| 35 | -5.72E+07 | -2.80E+06 | -1.68E+07 | 1.23E+06 | -7.15E+04 | 3.14E+05 | -1.68E+07 | -2.80E+06 | -5.72E+07 | -7.15E+04 | -7.15E+04 | 3.14E+05 |

Table A-7: Uncompensated Output and Relative Nonlinearity of the Die with Solder at DifferentTemperatures

| | Output in mV/V | | | Nonlinearity | | |
|---|---|---|---|---|---|---|
| p in kPa | -40 | 25 | 125 | -40 | 20 | 125 |
| 0 | -26.865395 | -13.190199 | -2.9521665 | 0 | 0 | 0 |
| 3.5 | -32.376203 | -17.017887 | -5.4799142 | 0.07569015 | 0.04422072 | 0.03691047 |
| 7 | -36.604628 | -20.672676 | -7.847758 | 0.11049662 | 0.08192684 | 0.06516007 |
| 10.5 | -40.678844 | -23.967172 | -10.053905 | 0.14038672 | 0.1060578 | 0.08465169 |
| 14 | -44.170712 | -26.915253 | -12.087779 | 0.15171101 | 0.11713641 | 0.09481246 |
| 17.5 | -47.181677 | -29.608489 | -13.958842 | 0.14770363 | 0.11861288 | 0.09615487 |
| 21 | -49.836586 | -31.981671 | -15.681993 | 0.13234481 | 0.10803028 | 0.08948595 |
| 24.5 | -52.218114 | -34.159394 | -17.274142 | 0.10827033 | 0.09008315 | 0.07572159 |
| 28 | -54.384928 | -36.157976 | -18.751238 | 0.07735055 | 0.06538627 | 0.05572558 |
| 31.5 | -56.379554 | -38.008431 | -20.127578 | 0.04094124 | 0.03510822 | 0.03027235 |
| 35 | -58.232028 | -39.730691 | -21.414944 | 0 | 0 | 0 |

Table A-8: Stresses in the Die with Epoxy

| | Region 1 | | | | | | Region 1 | | | | | |
|---|---|---|---|---|---|---|---|---|---|---|---|---|
| p in kPa | Sx,T=-40C | Sy,T=-40C | Sz,T=-40C | Sxy,T=-40C | Syz,T=-40C | Sxz,T=-40C | Sx,T=-40C | Sy,T=-40C | Sz,T=-40C | Sxy,T=-40C | Syz,T=-40C | Sxz,T=-40C |
| 0 | -1.57E+07 | -1.17E+05 | 2.04E+05 | 7.30E+04 | 4.03E+04 | 5.51E+05 | 2.04E+05 | -1.17E+05 | -1.57E+07 | 4.03E+04 | 7.30E+04 | 5.51E+05 |
| 3.5 | -2.24E+07 | -4.38E+05 | -1.76E+06 | 1.94E+05 | 2.99E+04 | 5.42E+05 | -1.76E+06 | -4.38E+05 | -2.24E+07 | 2.99E+04 | 1.94E+05 | 5.42E+05 |
| 7 | -2.89E+07 | -7.56E+05 | -3.68E+06 | 3.12E+05 | 1.96E+04 | 5.43E+05 | -3.68E+06 | -7.56E+05 | -2.89E+07 | 1.96E+04 | 3.12E+05 | 5.43E+05 |
| 10.5 | -3.49E+07 | -1.06E+06 | -5.48E+06 | 4.29E+05 | 9.48E+03 | 5.52E+05 | -5.48E+06 | -1.06E+06 | -3.49E+07 | 9.48E+03 | 4.29E+05 | 5.52E+05 |
| 14 | -4.04E+07 | -1.36E+06 | -7.18E+06 | 5.44E+05 | -3.39E+02 | 5.66E+05 | -7.18E+06 | -1.36E+06 | -4.04E+07 | -3.39E+02 | 5.44E+05 | 5.66E+05 |
| 17.5 | -4.54E+07 | -1.64E+06 | -8.77E+06 | 6.58E+05 | -9.88E+03 | 5.84E+05 | -8.77E+06 | -1.64E+06 | -4.54E+07 | -9.88E+03 | 6.58E+05 | 5.84E+05 |
| 21 | -5.01E+07 | -1.92E+06 | -1.03E+07 | 7.70E+05 | -1.92E+04 | 6.06E+05 | -1.03E+07 | -1.92E+06 | -5.01E+07 | -1.92E+04 | 7.70E+05 | 6.06E+05 |
| 24.5 | -5.44E+07 | -2.18E+06 | -1.17E+07 | 8.82E+05 | -2.82E+04 | 6.31E+05 | -1.17E+07 | -2.18E+06 | -5.44E+07 | -2.82E+04 | 8.82E+05 | 6.31E+05 |
| 28 | -5.85E+07 | -2.43E+06 | -1.30E+07 | 9.93E+05 | -3.71E+04 | 6.57E+05 | -1.30E+07 | -2.43E+06 | -5.85E+07 | -3.71E+04 | 9.93E+05 | 6.57E+05 |
| 31.5 | -6.22E+07 | -2.67E+06 | -1.42E+07 | 1.10E+06 | -4.57E+04 | 6.83E+05 | -1.42E+07 | -2.67E+06 | -6.22E+07 | -4.57E+04 | 1.10E+06 | 6.83E+05 |
| 35 | -6.58E+07 | -2.90E+06 | -1.54E+07 | 1.21E+06 | -5.42E+04 | 7.11E+05 | -1.54E+07 | -2.90E+06 | -6.58E+07 | -5.42E+04 | 1.21E+06 | 7.11E+05 |

| | Region 1 | | | | | | Region 1 | | | | | |
|---|---|---|---|---|---|---|---|---|---|---|---|---|
| p in kPa | Sx,T=25C | Sy,T=25C | Sz,T=25C | Sxy,T=25C | Syz,T=25C | Sxz,T=25C | Sx,T=25C | Sy,T=25C | Sz,T=25C | Sxy,T=25C | Syz,T=25C | Sxz,T=25C |
| 0 | -7.24E+06 | -4.89E+04 | 1.16E+06 | 3.31E+04 | 1.80E+04 | 2.96E+05 | 1.16E+06 | -4.89E+04 | -7.24E+06 | 1.80E+04 | 3.31E+04 | 2.96E+05 |
| 3.5 | -1.37E+07 | -3.55E+05 | -7.11E+05 | 1.57E+05 | 8.04E+03 | 2.85E+05 | -7.11E+05 | -3.55E+05 | -1.37E+07 | 8.04E+03 | 1.57E+05 | 2.85E+05 |
| 7 | -1.99E+07 | -6.57E+05 | -2.52E+06 | 2.79E+05 | -1.83E+03 | 2.81E+05 | -2.52E+06 | -6.57E+05 | -1.99E+07 | -1.83E+03 | 2.79E+05 | 2.81E+05 |
| 10.5 | -2.56E+07 | -9.52E+05 | -4.25E+06 | 4.00E+05 | -1.15E+04 | 2.85E+05 | -4.25E+06 | -9.52E+05 | -2.56E+07 | -1.15E+04 | 4.00E+05 | 2.85E+05 |
| 14 | -3.10E+07 | -1.24E+06 | -5.89E+06 | 5.19E+05 | -2.10E+04 | 2.94E+05 | -5.89E+06 | -1.24E+06 | -3.10E+07 | -2.10E+04 | 5.19E+05 | 2.94E+05 |
| 17.5 | -3.60E+07 | -1.52E+06 | -7.45E+06 | 6.38E+05 | -3.02E+04 | 3.08E+05 | -7.45E+06 | -1.52E+06 | -3.60E+07 | -3.02E+04 | 6.38E+05 | 3.08E+05 |
| 21 | -4.07E+07 | -1.78E+06 | -8.91E+06 | 7.54E+05 | -3.93E+04 | 3.25E+05 | -8.91E+06 | -1.78E+06 | -4.07E+07 | -3.93E+04 | 7.54E+05 | 3.25E+05 |
| 24.5 | -4.50E+07 | -2.04E+06 | -1.03E+07 | 8.70E+05 | -4.81E+04 | 3.45E+05 | -1.03E+07 | -2.04E+06 | -4.50E+07 | -4.81E+04 | 8.70E+05 | 3.45E+05 |
| 28 | -4.91E+07 | -2.29E+06 | -1.16E+07 | 9.85E+05 | -5.68E+04 | 3.67E+05 | -1.16E+07 | -2.29E+06 | -4.91E+07 | -5.68E+04 | 9.85E+05 | 3.67E+05 |
| 31.5 | -5.29E+07 | -2.53E+06 | -1.28E+07 | 1.10E+06 | -6.53E+04 | 3.90E+05 | -1.28E+07 | -2.53E+06 | -5.29E+07 | -6.53E+04 | 1.10E+06 | 3.90E+05 |
| 35 | -5.65E+07 | -2.76E+06 | -1.40E+07 | 1.21E+06 | -7.36E+04 | 4.15E+05 | -1.40E+07 | -2.76E+06 | -5.65E+07 | -7.36E+04 | 1.21E+06 | 4.15E+05 |

Table A-8: Stresses in the Die with Epoxy

| | Region 1 | | | | | | Region 1 | | | | | |
|---|---|---|---|---|---|---|---|---|---|---|---|---|
| p in kPa | Sx,T=125C | Sy,T=125C | Sz,T=125C | Sxy,T=125C | Syz,T=125C | Sxz,T=125C | Sx,T=125C | Sy,T=125C | Sz,T=125C | Sxy,T=125C | Syz,T=125C | Sxz,T=125C |
| 0 | 9.73E+03 | 6.36E+01 | 2.00E+04 | -2.76E+01 | -3.48E+01 | 3.90E+02 | 2.00E+04 | 6.36E+01 | 9.73E+03 | -3.48E+01 | -2.76E+01 | 3.90E+02 |
| 3.5 | -6.29E+06 | -2.97E+05 | -1.77E+06 | 1.28E+05 | -9.75E+03 | -1.34E+04 | -1.77E+06 | -2.97E+05 | -6.29E+06 | -9.75E+03 | 1.28E+05 | -1.34E+04 |
| 7 | -1.23E+07 | -5.92E+05 | -3.51E+06 | 2.55E+05 | -1.93E+04 | -2.02E+04 | -3.51E+06 | -5.92E+05 | -1.23E+07 | -1.93E+04 | 2.55E+05 | -2.02E+04 |
| 10.5 | -1.80E+07 | -8.80E+05 | -5.19E+06 | 3.81E+05 | -2.88E+04 | -2.05E+04 | -5.19E+06 | -8.80E+05 | -1.80E+07 | -2.88E+04 | 3.81E+05 | -2.05E+04 |
| 14 | -2.33E+07 | -1.16E+06 | -6.79E+06 | 5.06E+05 | -3.80E+04 | -1.51E+04 | -6.79E+06 | -1.16E+06 | -2.33E+07 | -3.80E+04 | 5.06E+05 | -1.51E+04 |
| 17.5 | -2.83E+07 | -1.43E+06 | -8.32E+06 | 6.29E+05 | -4.70E+04 | -5.06E+03 | -8.32E+06 | -1.43E+06 | -2.83E+07 | -4.70E+04 | 6.29E+05 | -5.06E+03 |
| 21 | -3.30E+07 | -1.70E+06 | -9.77E+06 | 7.51E+05 | -5.59E+04 | 8.85E+03 | -9.77E+06 | -1.70E+06 | -3.30E+07 | -5.59E+04 | 7.51E+05 | 8.85E+03 |
| 24.5 | -3.74E+07 | -1.95E+06 | -1.12E+07 | 8.71E+05 | -6.45E+04 | 2.58E+04 | -1.12E+07 | -1.95E+06 | -3.74E+07 | -6.45E+04 | 8.71E+05 | 2.58E+04 |
| 28 | -4.15E+07 | -2.20E+06 | -1.25E+07 | 9.90E+05 | -7.30E+04 | 4.51E+04 | -1.25E+07 | -2.20E+06 | -4.15E+07 | -7.30E+04 | 9.90E+05 | 4.51E+04 |
| 31.5 | -4.54E+07 | -2.44E+06 | -1.37E+07 | 1.11E+06 | -8.13E+04 | 6.61E+04 | -1.37E+07 | -2.44E+06 | -4.54E+07 | -8.13E+04 | 1.11E+06 | 6.61E+04 |
| 35 | -4.90E+07 | -2.68E+06 | -1.49E+07 | 1.22E+06 | -8.95E+04 | 8.85E+04 | -1.49E+07 | -2.68E+06 | -4.90E+07 | -8.95E+04 | 1.22E+06 | 8.85E+04 |

Table A-9: Uncompensated Output and Relative Nonlinearity of the Die with Epoxy at DifferentTemperatures

| | Output in mV/V | | | Nonlinearity | | |
|---|---|---|---|---|---|---|
| p in kPa | -40 | 25 | 125 | -40 | 25 | 125 |
| 0 | -13.229333 | -5.9659652 | -0.0044715 | 0 | 0 | 0 |
| 3.5 | -17.369112 | -9.372804 | -2.3973647 | 0.03886743 | 0.0346065 | 0.03186318 |
| 7 | -21.269868 | -12.586986 | -4.6651493 | 0.06971694 | 0.061601 | 0.05683211 |
| 10.5 | -24.860506 | -15.583803 | -6.793901 | 0.09016361 | 0.08000727 | 0.07413947 |
| 14 | -28.146771 | -18.361066 | -8.7798382 | 0.10040021 | 0.0897388 | 0.08357687 |
| 17.5 | -31.153038 | -20.929318 | -10.627336 | 0.10124438 | 0.0912122 | 0.08538542 |
| 21 | -33.91066 | -23.305745 | -12.345148 | 0.09374784 | 0.0851064 | 0.08004747 |
| 24.5 | -36.450704 | -25.50999 | -13.944966 | 0.07895272 | 0.07219763 | 0.06820729 |
| 28 | -38.80406 | -27.561493 | -15.438516 | 0.05789522 | 0.0532539 | 0.05051114 |
| 31.5 | -40.991589 | -29.478792 | -16.837255 | 0.03127512 | 0.02900765 | 0.02759028 |
| 35 | -43.040348 | -31.275581 | -18.151259 | 1.1917E-16 | 0 | 0 |

Table A-10: Stresses in the Die with RTV

| | Region 1 | | | | | | Region 2 | | | | | |
|---|---|---|---|---|---|---|---|---|---|---|---|---|
| p in kPa | Sx,T=-40C | Sy,T=-40C | Sz,T=-40C | Sxy,T=-40C | Syz,T=-40C | Sxz,T=-40C | Sx,T=-40C | Sy,T=-40C | Sz,T=-40C | Sxy,T=-40C | Syz,T=-40C | Sxz,T=-40C |
| 0 | 8.16E+03 | 5.42E+01 | 1.27E+04 | -2.60E+01 | -2.67E+01 | 1.78E+02 | 1.27E+04 | 5.42E+01 | 8.16E+03 | -2.67E+01 | -2.60E+01 | 1.78E+02 |
| 3.5 | -6.28E+06 | -2.99E+05 | -1.76E+06 | 1.28E+05 | -9.77E+03 | -1.35E+04 | -1.76E+06 | -2.99E+05 | -6.28E+06 | -9.77E+03 | 1.28E+05 | -1.35E+04 |
| 7 | -1.23E+07 | -5.95E+05 | -3.50E+06 | 2.55E+05 | -1.94E+04 | -2.03E+04 | -3.50E+06 | -5.95E+05 | -1.23E+07 | -1.94E+04 | 2.55E+05 | -2.03E+04 |
| 10.5 | -1.80E+07 | -8.85E+05 | -5.17E+06 | 3.81E+05 | -2.88E+04 | -2.07E+04 | -5.17E+06 | -8.85E+05 | -1.80E+07 | -2.88E+04 | 3.81E+05 | -2.07E+04 |
| 14 | -2.33E+07 | -1.17E+06 | -6.78E+06 | 5.06E+05 | -3.81E+04 | -1.55E+04 | -6.78E+06 | -1.17E+06 | -2.33E+07 | -3.81E+04 | 5.06E+05 | -1.55E+04 |
| 17.5 | -2.83E+07 | -1.44E+06 | -8.31E+06 | 6.29E+05 | -4.71E+04 | -5.52E+03 | -8.31E+06 | -1.44E+06 | -2.83E+07 | -4.71E+04 | 6.29E+05 | -5.52E+03 |
| 21 | -3.30E+07 | -1.71E+06 | -9.77E+06 | 7.51E+05 | -5.59E+04 | 8.24E+03 | -9.77E+06 | -1.71E+06 | -3.30E+07 | -5.59E+04 | 7.51E+05 | 8.24E+03 |
| 24.5 | -3.74E+07 | -1.97E+06 | -1.12E+07 | 8.71E+05 | -6.46E+04 | 2.50E+04 | -1.12E+07 | -1.97E+06 | -3.74E+07 | -6.46E+04 | 8.71E+05 | 2.50E+04 |
| 28 | -4.15E+07 | -2.22E+06 | -1.25E+07 | 9.90E+05 | -7.31E+04 | 4.42E+04 | -1.25E+07 | -2.22E+06 | -4.15E+07 | -7.31E+04 | 9.90E+05 | 4.42E+04 |
| 31.5 | -4.54E+07 | -2.46E+06 | -1.37E+07 | 1.11E+06 | -8.14E+04 | 6.51E+04 | -1.37E+07 | -2.46E+06 | -4.54E+07 | -8.14E+04 | 1.11E+06 | 6.51E+04 |
| 35 | -4.91E+07 | -2.69E+06 | -1.49E+07 | 1.22E+06 | -8.95E+04 | 8.74E+04 | -1.49E+07 | -2.69E+06 | -4.91E+07 | -8.95E+04 | 1.22E+06 | 8.74E+04 |

| | Region 1 | | | | | | Region 2 | | | | | |
|---|---|---|---|---|---|---|---|---|---|---|---|---|
| p in kPa | Sx,T=25C | Sy,T=25C | Sz,T=25C | Sxy,T=25C | Syz,T=25C | Sxz,T=25C | Sx,T=25C | Sy,T=25C | Sz,T=25C | Sxy,T=25C | Syz,T=25C | Sxz,T=25C |
| 0 | 0.00E+00 | 0.00E+00 | 0.00E+00 | 0.00E+00 | 0.00E+00 | 0.00E+00 | 0.00E+00 | 0.00E+00 | 0.00E+00 | 0.00E+00 | 0.00E+00 | 0.00E+00 |
| 3.5 | -6.29E+06 | -2.99E+05 | -1.77E+06 | 1.28E+05 | -9.76E+03 | -1.37E+04 | -1.77E+06 | -2.99E+05 | -6.29E+06 | -9.76E+03 | 1.28E+05 | -1.37E+04 |
| 7 | -1.23E+07 | -5.94E+05 | -3.50E+06 | 2.55E+05 | -1.94E+04 | -2.04E+04 | -3.50E+06 | -5.94E+05 | -1.23E+07 | -1.94E+04 | 2.55E+05 | -2.04E+04 |
| 10.5 | -1.80E+07 | -8.84E+05 | -5.18E+06 | 3.81E+05 | -2.88E+04 | -2.08E+04 | -5.18E+06 | -8.84E+05 | -1.80E+07 | -2.88E+04 | 3.81E+05 | -2.08E+04 |
| 14 | -2.33E+07 | -1.17E+06 | -6.78E+06 | 5.06E+05 | -3.81E+04 | -1.55E+04 | -6.78E+06 | -1.17E+06 | -2.33E+07 | -3.81E+04 | 5.06E+05 | -1.55E+04 |
| 17.5 | -2.83E+07 | -1.44E+06 | -8.31E+06 | 6.29E+05 | -4.71E+04 | -5.44E+03 | -8.31E+06 | -1.44E+06 | -2.83E+07 | -4.71E+04 | 6.29E+05 | -5.44E+03 |
| 21 | -3.30E+07 | -1.71E+06 | -9.77E+06 | 7.51E+05 | -5.60E+04 | 8.39E+03 | -9.77E+06 | -1.71E+06 | -3.30E+07 | -5.60E+04 | 7.51E+05 | 8.39E+03 |
| 24.5 | -3.74E+07 | -1.96E+06 | -1.12E+07 | 8.71E+05 | -6.46E+04 | 2.53E+04 | -1.12E+07 | -1.96E+06 | -3.74E+07 | -6.46E+04 | 8.71E+05 | 2.53E+04 |
| 28 | -4.15E+07 | -2.21E+06 | -1.25E+07 | 9.90E+05 | -7.31E+04 | 4.45E+04 | -1.25E+07 | -2.21E+06 | -4.15E+07 | -7.31E+04 | 9.90E+05 | 4.45E+04 |
| 31.5 | -4.54E+07 | -2.45E+06 | -1.37E+07 | 1.11E+06 | -8.14E+04 | 6.55E+04 | -1.37E+07 | -2.45E+06 | -4.54E+07 | -8.14E+04 | 1.11E+06 | 6.55E+04 |
| 35 | -4.91E+07 | -2.69E+06 | -1.49E+07 | 1.22E+06 | -8.96E+04 | 8.78E+04 | -1.49E+07 | -2.69E+06 | -4.91E+07 | -8.96E+04 | 1.22E+06 | 8.78E+04 |

Table A-10: Stresses in the Die with RTV

| | Region 1 | | | | | | Region 2 | | | | | |
|---|---|---|---|---|---|---|---|---|---|---|---|---|
| p in kPa | Sx,T=125C | Sy,T=125C | Sz,T=125C | Sxy,T=125C | Syz,T=125C | Sxz,T=125C | Sx,T=125C | Sy,T=125C | Sz,T=125C | Sxy,T=125C | Syz,T=125C | Sxz,T=125C |
| 0 | -9.61E+03 | -6.35E+01 | -1.50E+04 | 3.05E+01 | 3.15E+01 | -2.11E+02 | -1.50E+04 | -6.35E+01 | -9.61E+03 | 3.15E+01 | 3.05E+01 | -2.11E+02 |
| 3.5 | -6.30E+06 | -2.97E+05 | -1.78E+06 | 1.28E+05 | -9.73E+03 | -1.39E+04 | -1.78E+06 | -2.97E+05 | -6.30E+06 | -9.73E+03 | 1.28E+05 | -1.39E+04 |
| 7 | -1.23E+07 | -5.92E+05 | -3.51E+06 | 2.55E+05 | -1.94E+04 | -2.06E+04 | -3.51E+06 | -5.92E+05 | -1.23E+07 | -1.94E+04 | 2.55E+05 | -2.06E+04 |
| 10.5 | -1.80E+07 | -8.80E+05 | -5.18E+06 | 3.81E+05 | -2.88E+04 | -2.09E+04 | -5.18E+06 | -8.80E+05 | -1.80E+07 | -2.88E+04 | 3.81E+05 | -2.09E+04 |
| 14 | -2.33E+07 | -1.16E+06 | -6.77E+06 | 5.06E+05 | -3.80E+04 | -1.55E+04 | -6.77E+06 | -1.16E+06 | -2.33E+07 | -3.80E+04 | 5.06E+05 | -1.55E+04 |
| 17.5 | -2.83E+07 | -1.43E+06 | -8.30E+06 | 6.29E+05 | -4.71E+04 | -5.38E+03 | -8.30E+06 | -1.43E+06 | -2.83E+07 | -4.71E+04 | 6.29E+05 | -5.38E+03 |
| 21 | -3.30E+07 | -1.70E+06 | -9.75E+06 | 7.51E+05 | -5.59E+04 | 8.54E+03 | -9.75E+06 | -1.70E+06 | -3.30E+07 | -5.59E+04 | 7.51E+05 | 8.54E+03 |
| 24.5 | -3.74E+07 | -1.95E+06 | -1.11E+07 | 8.71E+05 | -6.46E+04 | 2.55E+04 | -1.11E+07 | -1.95E+06 | -3.74E+07 | -6.46E+04 | 8.71E+05 | 2.55E+04 |
| 28 | -4.15E+07 | -2.20E+06 | -1.24E+07 | 9.90E+05 | -7.31E+04 | 4.48E+04 | -1.24E+07 | -2.20E+06 | -4.15E+07 | -7.31E+04 | 9.90E+05 | 4.48E+04 |
| 31.5 | -4.54E+07 | -2.44E+06 | -1.37E+07 | 1.11E+06 | -8.14E+04 | 6.58E+04 | -1.37E+07 | -2.44E+06 | -4.54E+07 | -8.14E+04 | 1.11E+06 | 6.58E+04 |
| 35 | -4.90E+07 | -2.68E+06 | -1.49E+07 | 1.22E+06 | -8.95E+04 | 8.82E+04 | -1.49E+07 | -2.68E+06 | -4.90E+07 | -8.95E+04 | 1.22E+06 | 8.82E+04 |

Table A-11: Uncompensated Output and Relative Nonlinearity of the Die with Solder at DifferentTemperatures

| | Output in mV/V | | | Nonlinearity | | |
|---|---|---|---|---|---|---|
| p in kPa | -40 | 25 | 125 | -40 | 25 | 125 |
| 0 | -0.0030023 | 0 | 0.0021755 | 0 | 0 | 0 |
| 3.5 | -3.9245043 | -3.3370908 | -2.3915406 | 0.03159941 | 0.03173531 | 0.03190194 |
| 7 | -7.6412186 | -6.4991372 | -4.6591812 | 0.05632648 | 0.05656055 | 0.0568567 |
| 10.5 | -11.131769 | -9.4679433 | -6.7873506 | 0.07346384 | 0.07375743 | 0.07412611 |
| 14 | -14.390216 | -12.238616 | -8.7727235 | 0.08281218 | 0.08313277 | 0.08352695 |
| 17.5 | -17.423928 | -14.817019 | -10.619665 | 0.08461878 | 0.08491803 | 0.08529977 |
| 21 | -20.246906 | -17.215795 | -12.337431 | 0.07935346 | 0.07961236 | 0.07995452 |
| 24.5 | -22.877607 | -19.450911 | -13.937399 | 0.06763563 | 0.06784599 | 0.06811822 |
| 28 | -25.335029 | -21.53825 | -15.431362 | 0.05010283 | 0.050246 | 0.05044069 |
| 31.5 | -27.637625 | -23.493523 | -16.830501 | 0.02737432 | 0.02743253 | 0.02753807 |
| 35 | -29.801782 | -25.331786 | -18.145518 | 1.1922E-16 | 0 | 0 |

**MOTOROLA**

September 21, 1998

Volker Schulze
289 Bluefield Drive
San Jose, CA 95136

Dear Volker,

This is in response to your email on September 16, 1998 requesting permission to reproduce certain Motorola material. Permission is hereby granted for you to reproduce the following documents for which Motorola Semiconductor Products Sector holds the copyright:

**BR121/D Pressure Sensors Rev. 5, 1991 (page 13)--**
**Differential Porting Option (Exploded View)**
**MPX Differential Pressure Sensor Element Cross Section**
**BR121/D Pressure Sensors Rev. 6, 1992 (cover)--**
**On Chip Signal Conditioned Sensor (cover picture)**

We understand that copies of this will be reproduced for use in your Master's Thesis and future publications resulting from the thesis.

This permission conveys to you non-exclusive North American and world rights in the English language, to reprint this material in the current and future editions of this work. We also grant permission for reproduction in Braille, large print, and in recorded form for the blind and handicapped. This permission extends to usage in the associated study guide, instructors manual, and transparency masters. With each usage of this material, please include the following source attribution statement:

"Copyright of Motorola,
Used by Permission"

Thank you for your interest in Motorola products and technology.

Regards,

Karen Bosco
Manager, Technical Publications
(602) 244-6584
(602) 244-6560 (FAX)

**Motorola, Semiconductor Products Sector**
**Technical Publications Department, MD A201**
**5005 East McDowell Road, Phoenix, Arizona 85008**

Volker Schulze
289 Bluefield Dr.
San Jose, CA-95136
Tel: (408) 360-0651
Fax: (510) 770-0645
vschulze@hotmail.com
09/30/1998

Florian Koss
Institut für Mikrotechnik Mainz GmbH
Postfach 42 13 64
D-55071 Mainz
Germany
Tel: (01149) 6131-990-164
Fax: (01149) 6131-990-205

Dear Mr. Koss:

This letter will confirm your approval for the use of pictures that you sent me.
I am a graduate student at San Jose University. I would like your permission to include the following photos and drawings of products of your company in my Master's Thesis and future publications resulting from the thesis. Due acknowledgment will be given to your company in the thesis and publications.

All pictures from the sources listed below:

LIGA Technology
Electro-Magnetic Micro-Geared Motor
Fibre-Optic Switches
Optical Backplane based on integrated-optical Star Coupler for Computer Applications

Please indicate your approval of this permission by signing below and return it to me as soon as possible. Your signing of this letter will also confirm that your company owns the copyright to the above-described material.
Thank you very much.

Sincerely,

Volker Schulze

Permission granted for the use requested above:

---

Prof. Dr. W. Ehrfeld
Managing Director
Date: 10/08/1998

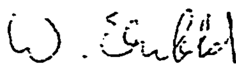

AUG-18-98 TUE 10:26 AM FAX NO. 953856 P. 01

Volker Schulze
289 Bluefield Dr.
San Jose, CA-95136
Fax: (510) 770-0645
08/18/1998

Carol Noethe
Druck Incorporated
4 Dunham Dr.
New Fairfield, CT-06812

Dear Mrs. Noethe:

This letter will confirm your approval for the use of a picture.
I'm a graduate student at San Jose University. I would like your permission to include a drawing of the PTX 600 Series Pressure Sensor of your company in my Master's Thesis and future publications resulting from the thesis. Due acknowledgment will be given to your company in the thesis and publications

Source: Druck PTX 600 Series 6/91

PTX 600 Series (Cutaway Diagram) on the second page

Please indicate your approval of this permission by signing below and return it to me as soon as possible. Your signing of this letter will also confirm that your company owns the copyright to the above described material.

Thank you very much

Sincerely,

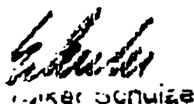

Volker Schulze

Permission granted for the use requested above:

Date 8-20-98

Volker Schulze
289 Bluefield Dr.
San Jose, CA-95136
Tel: (408) 360-0651
vschulze@hotmail.com
11/17/1998

Bill Michaels
Lucas NovaSensor
1055Mission Court
Fremont, CA-94539
Tel: (510) 661-6103

Dear Mr. Michaels:

This letter will confirm your approval for the use of pictures that were supplied by Lucas NovaSensor. I would like your permission to include the following photos and drawings of products of your company in my Master's Thesis and future publications resulting from the thesis. Due acknowledgment will be given to your company in the thesis and publications.

NPC - series (Silicon pressure sensors in ceramic packages)
DRIE - lag (SEM)
DRIE - notching (SEM)
Picture of die with contacts
Silicon fusion bonding (SEM)
TO8 - header (Schematic drawing)
Wirebond on die (SEM)
NPI - series (All media compatible sensor)
Oil isolated pressure sensor (Schematic drawing)
Exploded drawing of the NPI package components
NPH - series (Silicon pressure sensors in TO packages on wafer)
NPP - series (Silicon sensors in plastic package)
P4100 - series (Silicon pressure transducer advanced digitally compensated)

Please indicate your approval of this permission by signing below and return it to me as soon as possible. Your signing of this letter will also confirm that your company owns the copyright to the above-described material. Thank you very much.

Sincerely,

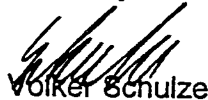

Volker Schulze

Permission granted for the use requested above:

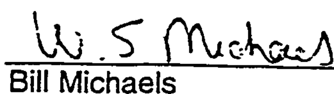

Bill Michaels

Date: 11 / 17 / 98

# IMAGE EVALUATION TEST TARGET (QA-3)

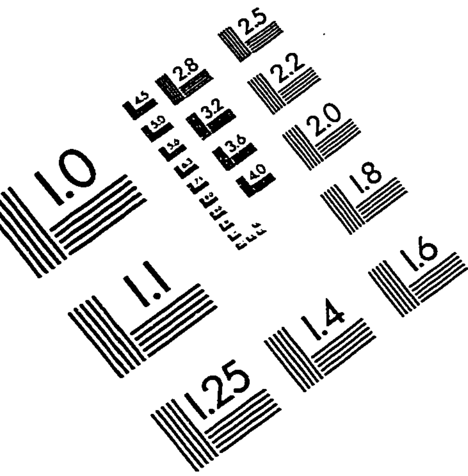

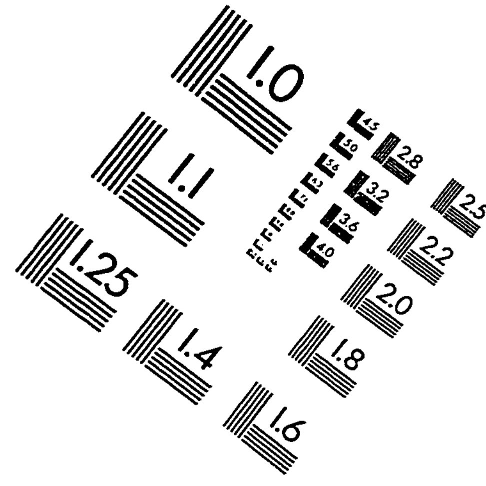

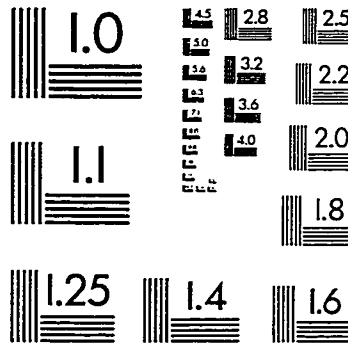


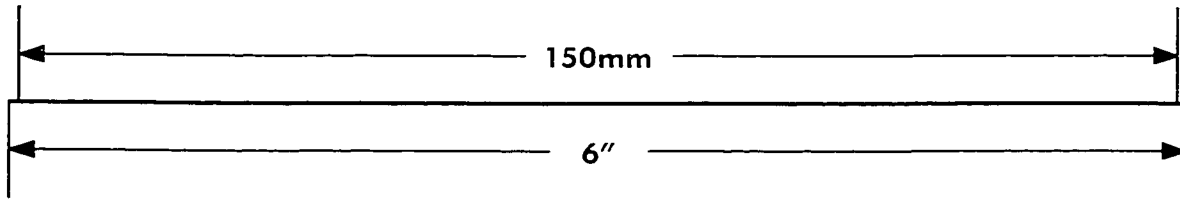


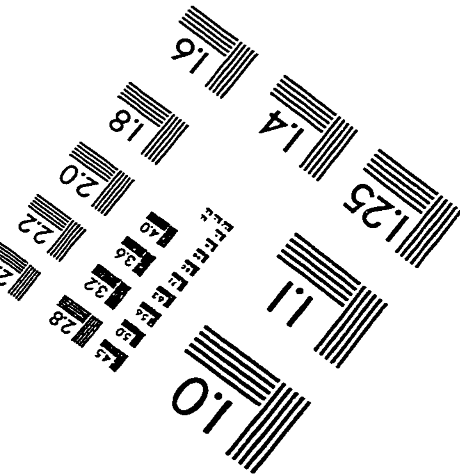

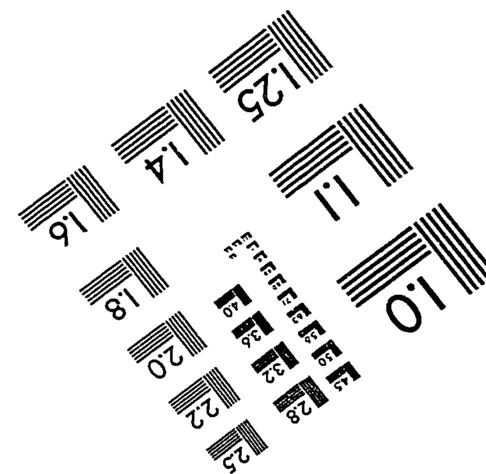

APPLIED IMAGE . Inc
1653 East Main Street
Rochester, NY 14609 USA
Phone: 716/482-0300
Fax: 716/288-5989

© 1993, Applied Image, Inc., All Rights Reserved